The Influence of Chemical Structure of Model Epoxy Networks on Chemical Resistance

DIDSBURY, MATTHEW,PAUL

Department of Chemistry

The Influence of Chemical Structure of Model Epoxy Networks on Chemical Resistance

Matthew Paul Didsbury

A thesis submitted for the degree of Doctor of Philosophy

2014

Declaration

The work described in this thesis was carried out in the Department of Chemistry at the University of Durham between October 2010 and December 2013. All of the work is my own, except where specifically stated otherwise. No part has previously been submitted for a degree at this or any other university.

Statement of Copyright

Abstract

Structural differences in cross-linked epoxy networks from the use of different isomers (*ortho-, meta-* and *para-*) of disubstituted aromatic diglycidyl ethers can have a dramatic effect on the polymer properties. By changing the disubstitution from *meta-* to *para-* it has been shown that there is a direct correlation between the diffusion of gasses and the symmetry of related polymers. The aim of this work is to investigate the influence of the chemical structure of aromatic diglycidyl ethers on the ability of the resulting amine-cured epoxy polymer networks to adsorb organic solvents. Pure diglycidyl ethers based on hydroquinone and catechol, have been synthesised in high purity and good yields using a process previously developed at Durham University which utilise elemental fluorine to produce hypofluorous acid. The diglycidyl ether of resorcinol is commercially available and readily purified via vacuum distillation. Using the pure epoxides model networks have been produced by reacting the diglycidyl ethers with the diamine 4,4'-methylenebis(cyclohexylamine) to produce highly cross-linked films. Analytical techniques including DSC, DMTA, TGA, FTIR, solid state NMR, thermodynamic testing, PALs and density measurements have been used to investigate the influence of polymer structure on the network properties. With these materials we are determining the effect of the different epoxide isomers on the chemical resistance of the polymers. The results obtained for the polymers shows consistency with those suggested by the literature which is that the *meta-* polymer has the best chemical resistance with the other isomers having similar results.

Acknowledgements

I would like to acknowledge several people and groups for their assistance and help throughout my Ph.D and have helped make the thesis possible.

I would first like to thank my supervisors Professor Neil R. Cameron and Professor Graham Sandford, for their guidance and advice throughout my Ph.D.

I would like to thank the NRC group and the GS group for their help and ideas from group meetings and for the friendly atmosphere created in the lab. I would like to give special thanks to Chris McPake for his training and assistance with using the fluorine rig. I would like to Dan, Sarah, Lauren, Scott, David, Ross, Mike, Adam, Artur, Caitlin, Ffion, Tony, Rob and the rest of office 235 and the tough rugby team for their friendship throughout my period in Durham and for not leaving me to prop the bar up on my own.

I would also like to thank all of the technical staff for their help in running analysis with special mention to Dr Allen Kenwright for assistance with solution state NMR. Dr David Apperley and Dr Eric Hughes for their assistance with solid state NMR spectroscopy, Dr Jackie Mosley for her assistance with mass spectrometry, Dr Richard Thompson and Doug Carswell for their help with thermal analysis, Neil Holmes and the lads in the mechanical workshop and the guys down in stores for their help and assistance.

Acknowledgements paid also to my industrial supervisors Dr. Colin Cameron and Dr. Anthony Wright from International Paint Ltd, AkzoNobel.

Finally I would like to thank all of the people that I have had the pleasure in meeting in and around Durham University that have made my time in Durham enjoyable.

I would like to give special thanks to my family who have helped and supported me throughout my life and have pushed to me achieve more than I

thought possible. Without them none of this would have been possible so I thank them for their love and care by dedicating this thesis to them.

Glossary of Terms

P	Permeability coefficient
D	Diffusion coefficient
S	Sorption equilibrium
J	Diffusion flux
c	Concentration
x	Distance
M_i	Initial mass of the polymer
M_t	Mass of the swollen polymer as a certain time
M_∞	Mass of the swollen polymer at equilibrium
k	Constant
t	Time
n	Exponent of determining the diffusion mechanism
Q(t)	Percentage weight gain of solvent at equilibrium
h	Initial sample thickness
Ø	Initial slope of linear section of a plot of Q(t) versus $t^{1/2}$
A	Constant for determining the Permachor factor
s	Constant for determining the Permachor factor
Pf	Permachor factor
M_c	Molecular weight between cross-links
ϑ_e	Cross-link density
A	Fitting constant for equation 1.10
B	Fitting constant for equation 1.10
C	Fitting constant for equation 1.10
Log P	Hydrophobicity of a polymer
T_g	Glass transition temperature
EEW	Epoxide equivalent weight
Mw	Molecular weight
E’	Storage modulus
E’’	Loss modulus
tan δ	Tan delta

R	Gas constant
T	Temperature
P	Density
C_p	Heat capacity
c_o	Segment mobility of uncross-linked polymer
c_∞	Segment mobility of cross-linked polymer
ε	Lattice energy
M_s	Mass of solvent uptake
AHEW	Active hydrogen equivalent weight

Table of contents

Chapter 1 – Introduction

1.1 – Chemical Resistance

The chemical resistance of a coating or a polymer is its ability to withstand absorption and retention of a chemical media[1]. These chemicals can come in many forms for example solids, liquids or gases; they can be acidic, basic or neutral; hot or cold and with different chemistries[2, 3]. When the polymer comes under attack from the media it undergoes possible swelling and/ or plasticisation which causes softening of the polymers. This occurs when a solvent which is chemically "good" for the polymer in question, diffuses into the polymer which causes a change in the free volume. Upon swelling there is the possibility of the solvent to ingress further in to the polymer causing further swelling of the polymer which becomes a big problem with a large amount of stress being put upon the polymer causing failure[4].

There are two main types of chemical resistance, which differ according to the exposure time to the chemical. The first is where the substrate is only occasionally exposed to chemicals wherein the coating is not constantly under attack but still needs to hold up to its functionality. The other is when the substrates are exposed over a lengthier period of time towards chemicals[2]. Each of these types of chemical resistance is important for industrial applications as the protective polymer properties can change making the polymers involved redundant to their intended purpose. There are several cases where the effect of the chemical resistance plays a role for application for example: gloves[5,6]; tubing[7]; membranes[8,9] and coatings[10,11]. These areas need to maintain their functionality like food and non-fizzy drink containers have in some cases mild conditions affecting the chemical resistance[12]; containers made from metals, such as steel, need to have some form of coating to protect the contents from contamination[13, 14] or corrosion[15]; protective coatings for aerospace use need to be able to maintain durability of the components[16]. Plastic containers however, have potential protection, depending on the polymers used,[17] arising from the material themselves. If the area is under constant exposure to different chemicals, for example transporting crude oil, then, a greater amount of protection is required for the container walls[11, 18] due to possible cross contamination[4].

The main factors that affect the chemical resistance of a substance are the diffusion of the medium, permeability of the medium, the sorption and the solubility of the polymer. This is due to the relationship between each of the parameters with equation (1.1) showing how each of the parameters relies on the other[19]. This is due to permeability being a three stage process with the initial stage being the absorption of the media into the polymer (S). Second is the diffusion of the medium through the film (D) and then desorption and surface removal.

$$P = D.S \tag{1.1}$$

where *P* is the permeability coefficient, *D* is the diffusion coefficient and *S* is the sorption equilibrium parameter obtained by gram of liquid adsorbed per gram of polymer[20]. This is a simplified equation assuming that the diffusion coefficient is constant.

The diffusion coefficient can be described by the use of Fick's first law of diffusion (1.2) where the flux is proportional to the concentration gradient which is non-changing[21-23].

$$J = -D\left(\frac{\delta c}{\delta x}\right) \tag{1.2}$$

where *J* is the diffusion flux, c is the concentration of solute and x is the distance which gives $\left(\frac{\delta c}{\delta x}\right)$ as the concentration gradient. Fick's first law describes the transport process where the penetrant concentration difference or chemical potential between the phases separated by the solid in a steady state process[21]. If however the diffusion is in a non-steady state process then Fick's second law of diffusion follows, with the change in concentration of penetrant. This law takes into account the rate of change of the penetrant at a point in the solid[22].

$$\left(\frac{\delta c}{\delta x}\right) = D\left(\frac{\delta c^2}{\delta x^2}\right) \tag{1.3}$$

The sorption parameter can be used to determine the Fickian state of the diffusion transport properties. This parameter is the amount of permeant that has been absorbed and retained in the polymer at the maximum uptake. This can determine the amount of swelling and sorption of the polymer by measuring changes in the mass of polymer sample over a period of time until equilibrium is reached. Equation (1.4) can be used to determine the diffusion mechanism using experimental sorption data[24, 19].

$$\frac{M_t}{M_\infty} = kt^n \tag{1.4}$$

where M_t is the mass of swollen polymer at a certain time and M_∞ is the mass of the polymer at equilibrium, k is a constant, t is time and n is an exponent which determines the diffusion mechanism. If n is 0.5 then it is potentially Fickian diffusion whereas if n is 1.0 this suggests that the diffusion mechanism moves away from Fickian. Intermediate values suggest that the results deviate between the two systems. By transforming equation (1.4) into its logarithmic form (1.5) it is possible to obtain k and n from a plot of the data. Using least-squares estimates can then be used to determine the constant k and diffusion mechanism n from the slope and intercept respectively.

$$\log \frac{M_t}{M_\infty} = \log k + n \log t \tag{1.5}$$

The swelling of the polymer can also be used to determine the diffusion coefficient. Again by using the experimental sorption data, equation (1.6) can be used to determine percentage weight gain (Q(t)) of a polymer[24].

$$Q(t) = \frac{M_t - M_i}{M_i} 100 \tag{1.6}$$

with M_i being the initial mass of the polymer. The value for Q(t) can then be put into equation (1.7) which when a plot of Q(t) versus $t^{1/2}$ is used gives a curve with the initial section being linear.

$$\frac{Q(t)}{Q(\infty)} = \frac{4}{\pi^2}\frac{[Dt]^{1/2}}{h^2} \quad (1.7)$$

where Q(∞) is the percentage weight gain at equilibrium, t is time and h is the initial sample thickness[19, 25].

Taking the initial slope of the plot of Q(t) versus $t^{1/2}$, the initial slope of the linear section (Ø) can be obtained. By rearranging equation (1.7) it is possible to determine the diffusion coefficient as shown in equation (1.8)[24, 26].

$$D = \pi\left(\frac{h\emptyset}{4Q_\infty}\right)^2 \quad (1.8)$$

There are also considerations for other factors in these measurements such as temperature, size of penetrant, size of polymer free volume, polymer-solvent interaction, composition of the polymer (linear, branched or cross-linked) and pressure[27].

1.2 – Factors Affecting Chemical Resistance

1.2.1 – Effects of polymer structure

There are several different parameters to take into account when discussing polymeric structure: the nature of the repeating units; the end group functionality; composition of potential branches and or cross-links and any structural defects that occur[28]. As can be seen in (Figure 1.1) the structure of a homo-polymer can have three main configurations depending on the type of polymerisation or monomers used[29]. There are inter- and intramolecular forces to be taken into consideration as these have a major impact on the chemical properties of polymers[30]. In this section however the molecular structure of the mer units, effects of cross-linking and the effect of free volume will be discussed.

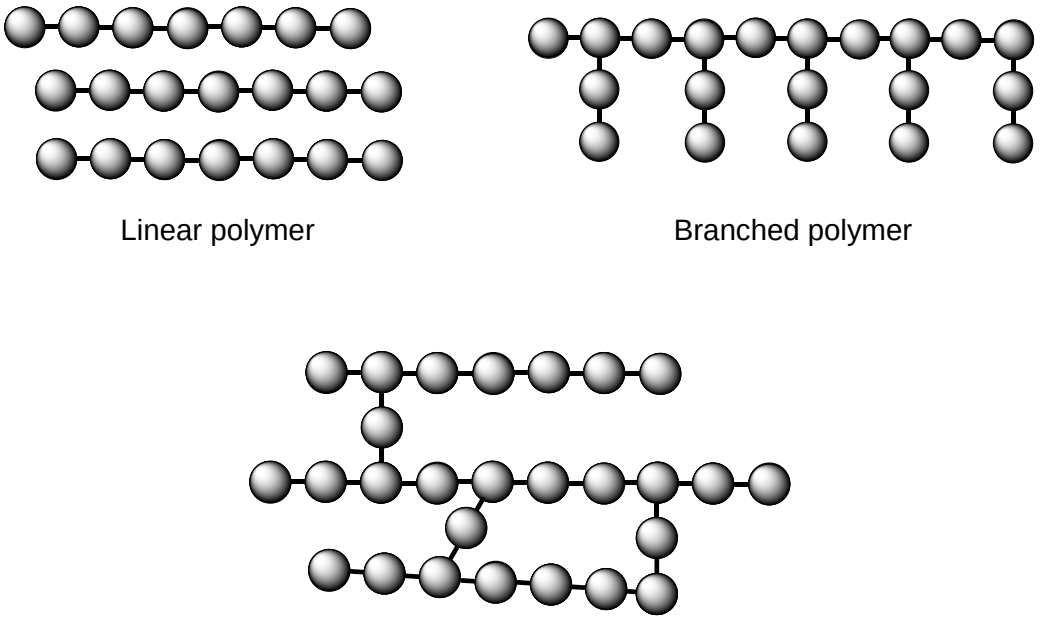

Figure 1.1 – Schematic representation of polymer structures, each circle represents individual units

1.2.2 – Polymer molecular structure

When considering the molecular structure of a polymer the main effect is the molecular structure of the initial starting materials. Factors include aromatic ring structure with mono, di, etc. substitutions and their patterns i.e. *ortho, meta* or *para*, varying the R groups on a hydrocarbon backbone or several other possibilities. Several papers have been published dealing with the use of aromatic polymers and the effect of structure on the gas barrier properties[31-35]. Aitken *et al*[31] discuss how different aromatic linkages affect the permeability and selectivity coefficients for polysulfones. The research uses different pairs of *para*- or *meta*- linked aromatic bisphenol monomers and their barrier properties against a range of gasses. They show that there is a decrease in permeability from *para* to *meta* in most of the pairs that they show, for example a polymer based on 4,4'-isopropylidenediphenol has a permeability coefficient that is between three to four times higher than that of the 3,4'-isopropylidenediphenol based polysulfones. They show similar results with the use of 4,4'-(1,3-phenylenediisopropylidene)bisphenol as the monomeric linkage having a lower permeability but higher selectivity than that based on 4,4'-(1,4-phenylenediisopropylidene)bisphenol. This is related to the fractional free volume of the samples as there is a higher density in the unsymmetrical polymers (*meta*) than those that have the *para* linkages. Wang *et al*[32] utilised the results gathered by Aitken and co-workers to develop a simulation technique to determine the gas diffusivity of neon through the polymer systems. They also used this simulation technique to determine the fractional cavity volume and the cavity size which can be shown to decrease from the *para* substituted polymer to the *meta* substituted. They determined that the gas diffusion decreases in the *meta* isomer compared to the *para*. This is due to the change in the free volume of the polymers which they show has an exponential relationship with the diffusion. They suggest that larger cavities in the polymers produce the difference in the diffusion coefficients with their results being consistent with previous experimental results. Alventev *et al*.[33] show a range of polyimides with varying structures (aromatic isomerism, functional groups and chain length), and the effect on the barrier properties and the fractional free volume. Again there is evidence that the more structurally unsymmetrical the polymer chains the better the barrier to gasses. They also increase the chain length while varying

the isomers of *para, para; meta, para* and *meta, meta* connections of the ring which relate to the initial polymer series with symmetry having a major effect on the barrier to gasses. Pavel and Shanks[34] attempt to explain how structural symmetry affects and gas barrier properties through work done on poly(ethylene terephthalate) (a), poly(ethylene isophthalate) (b) and poly(ethylene phthalate) (c) to determine the diffusion coefficients in relation to the free volume and density.

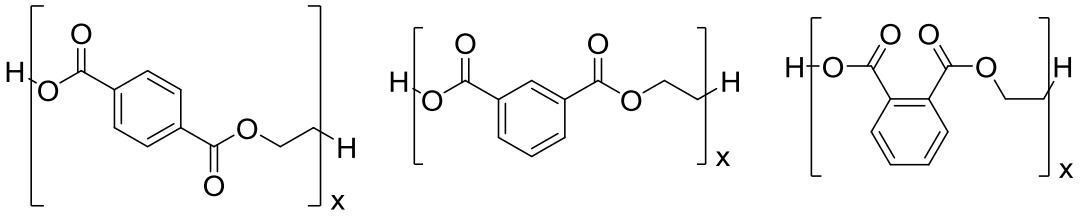

Figure 1.2 – Different polymers used to determine the effects of structural symmetry on the gas barrier properties

They describe how the diffusion of O_2 in the *para* polymer is the highest due to the symmetrical linear geometry which slightly increases the free volume. This they ascribe to the rotational freedom of the aromatic rings which can rotate readily for the symmetrical isomer whereas in the bent (*ortho*) and slightly bent isomers (*meta*) are restricted from rotations around the aromatic ring. They also show that the number of aromatic rings in the system affects the diffusion coefficient, with increasing the number of aromatic rings (benzene to naphthalene to anthracene) decreasing the diffusion coefficient. With the same symmetry they show that there is a decrease in the diffusion coefficient of over one hundred fold from benzene to anthracene. Tanaka *et al.*[35] use a mixture of homo and co-polymers of *meta* and *para* diaminodiphenylsulfones to show the difference in the permeability coefficients of the polymer films. Using different ratios of the *para* monomer to the *meta* monomer of 10:0; 7:3; 1:1 and 0:10 they show that the T_g and free volume decrease but the density increases decreases with the decrease of *para* monomer. They show consistently the increase in the *meta* ratio decreases the permeability coefficient for a range of gasses: H_2, CO_2, CO and CH_4. Their explanation for this is that there is lower segmental mobility in the *meta* material compared to that of the *meta*, which restricts the rotational mobility decreasing the diffusivity of the polymer.

As has already been stated, changing the side groups in a polymer chain have also been shown to change the barrier properties, for example the addition of a phenyl side group increases the barrier properties of some polyimides[33]. Salame[36] has measured the oxygen permeability of a wide range of polymers with a plethora of side groups and compared this to the calculated polymer "Permachor" of each polymer. The "Permachor" is a method used to estimate the permeability coefficients in polymers developed by Salame. A method was devised to determine the "Permachor" of the polymer from its individual segments and side groups which can then be added together and divided by the number of segments in the chain. By showing that there is a linear relationship between log permeability obtained experimentally against the calculated "Permachor". It is possible to predict the permeability of oxygen of any polymer using equation (1.9):

$$P = Ae^{sPf} \tag{1.9}$$

where *A* and *s* are gas constants and *Pf* being the "Permachor" factor as calculated empirically from the determined "Permachor" values for different atoms and functional groups provided by Salame.

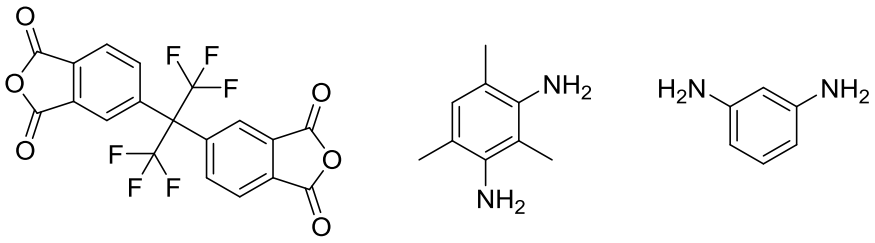

Figure 1.3 – Structure of 6-FDA (left), DAM (middle) and *m*-PDA (right)

Cui *et al.*[37] show that the introduction of methyl side groups changes the gas permeability of a polymer. By using polymers based on 2,2'-Bis-(3,4-dicarboxyphenyl) hexafluoropropane dianhydride (6-FDA) with ether 2,4-diaminomesitylene (DAM) or *m*-phenylenediamine (*m*-PDA) (figure 1.3) they show that 6-FDA-DAM has a consistently higher permeability that those that have no methyl side groups. This they suggest is due to the differences in chain packing and free volume effects. With even the incorporation of just two methyl groups Nagel *et*

al[38] show that there is a dramatic effect on the permeability of polymers. By introducing these methyl groups to the aromatic ring of poly(amide *meta*-imide)s there is a four-fold increase in the permeability of both oxygen and carbon dioxide. Pixton and Paul[39] show the differences in the permeability barrier for different side groups on polyacrylates based on bisphenol A. They use various R groups on the bisphenol A rings utilizing H, CH_3 and Br groups. They show that increasing the number of methyl groups (four instead of two) there is a dramatic increase in the barrier properties. They also show that if there are no methyls then there is a slight detrimental effect on the barrier properties and that utilizing bromine does not have a significant effect on the barrier properties. Changing the linkage between the oligomers has an effect on the permeability coefficients[40, 41]. Ronova *et al*[40] show that there is a large decrease in the permeability from methylene groups to ethers with a drop of roughly half with (a) having a permeability coefficient of 37.1 cm cm^{-2} s^{-1} and (b) having one of 14.8 cm cm^{-2} s^{-1}. Changing the benzyl group as well decreases the permeability again by a lower degree with (c) having 11.4 cm cm^{-2} s^{-1} (figure 1.4).

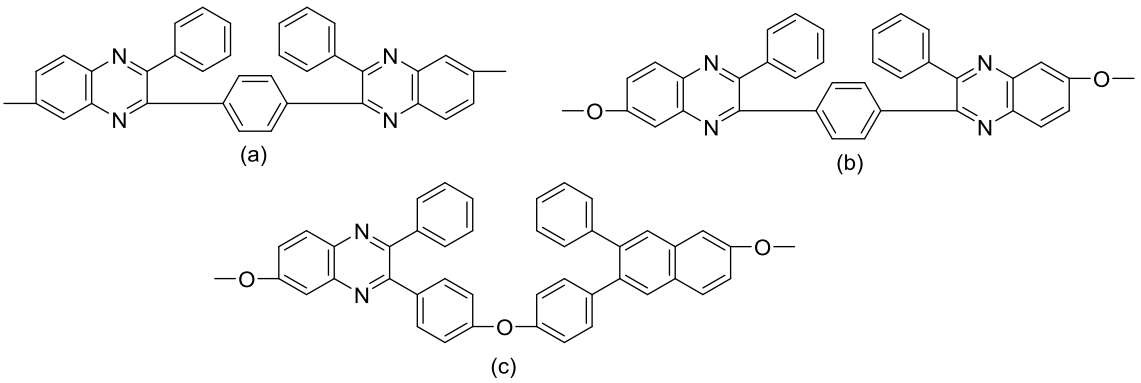

Figure 1.4 – Different linkers of phenylquinoxaline monomer unit[40].

1.2.3 – Cross-linking

Cross-links are covalent or physical bonds (Van der Waals, hydrogen bonding etc.) that are formed between each macromolecule to create a network of interconnected polymer chains. These can be formed using several different methods which can be put into three main groups: thermal, chemical and radiation.[42] There are different types of thermal cross-linking possible: be this at ambient

temperature[43] or elevated temperatures, there is a plethora of chemistry to do with each. Using elevated temperatures can produce cross-linked systems either with use of an additional cross-linking agent or the use of multifunctional monomers. Epoxy amine networks are formed from the use of multifunctional monomers at elevated temperatures. For example bisepoxides and a diamine can form highly cross-linked polymer networks depending on the temperature of the curing (which controls the degree of polymerisastion).[44] Using both multifunctional epoxides and amines Fu *et al.*[45] have shown that the introduction of phenyl-trisilanol polyhedral silsesquioxane (POSS-triol) promotes cross-linking of their epoxy-amine polymers dur to the ring opening of the epoxides by the acidity of the silanol groups attached to the POSS-triol. The post-vitrification stage that show that there is an increase in the T_g which has been attributed to the effect of increased cross-link density.[46-48]

Polymers that are used in chemical cross-linking need to have sites along the polymer that can be reacted with the chemical agent to induce a reaction that interconnects the polymeric chains.[49] There are four main types of cross-linking agents (Figure 1.5): (A) bridging agents, where the chemical agent becomes a bridge between two polymer chains;[50] (B) agents that can initiate cross-linking producing radical functionalities on the polymer chains;[51] (C) those that can catalyse the cross-linking reaction[52] and (D) agents that can generate reactive functionalities along the polymer.

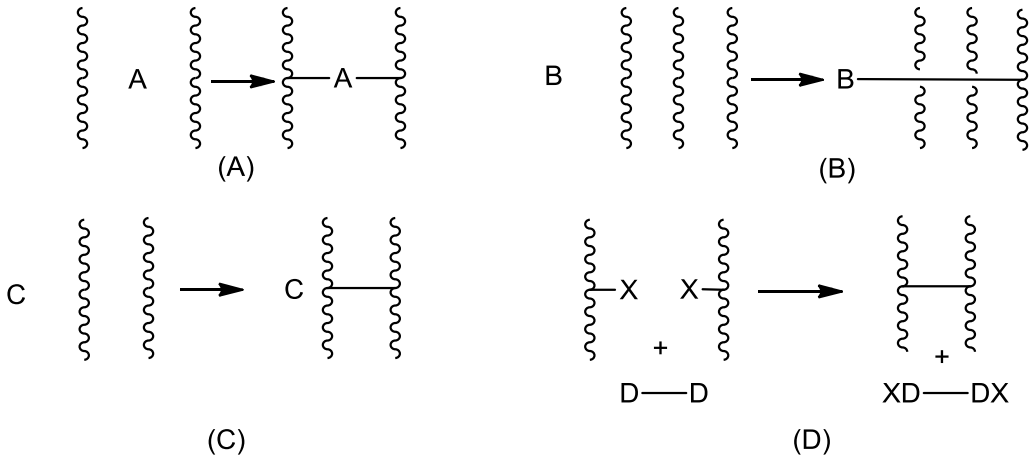

Figure 1.5 – Different cross-linking agents (A) bridging agents; (B) initiating agents; (C) catalyst agents and (D) functionality generators

Bridging cross-linkers are usually formed when there are two polymer chains that contain two different functional groups along the polymer chain, which can react together. An example of this is using carboxylic acid moieties with carbodiimide functionality[53] which react to form *N*-acetylurea. By utilizing this chemistry Hung *et al*[50] have shown that different annealing times with different carbodiimidies decrease the swell ratio of latex polymer films, based on acrylates. This could correspond with the increase in the cross-link ratio over time which they show is consistent with the decrease in the –NCN- reactive groups remaining.

One of the most common initiating agents used are peroxides which can be used to initiate the cross-linking of polymers containing double bonds and some saturated polymers[54-56]. Work by Han *et al.*[57] shows that there is a decrease in the swelling of poly(*ε*-caprolactone) with increased content of benzoyl peroxide. The benzoyl peroxide acts as a cross-linking agent which initiates cross-linking of the poly(*ε*-caprolactone) and such a higher content of the peroxide will increase the cross-link density of the polymer network. They however find that there is a decrease in the T_g of the networks with an increase in cross-link density which is contradictory to what is expected. This they ascribe to the decrease in the crystalline regions in the polymer network, as the incorporation of cross-links at an elevated temperature will produce a more amorphous polymer. Using a peroxide as the cross-linking initiator Mironi-Harpaz *et al.*[58] show that incorporating more of the peroxide into a styrene-free unsaturated polyester alkyd, decreases the amount of swelling in the polymer. This is also indicative of a larger cross-link density as there will be a lower molecular weight between cross-links (M_c) that are able to swell, with 1% peroxide in the polymer mixture the M_c is 13700 g/g mol, whereas with 6% peroxide content this decreases to 3300 g/g mol. The initiation reaction for the cross-linking by utilizing peroxides follows the reaction method shown in Figure 1.5.

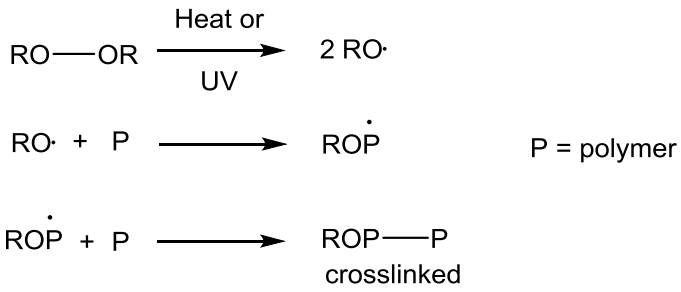

Figure 1.6 – Free radical cross-linking via initiation by peroxide.

Catalytic curing agents are formed by using a small amount of a cross-linking agent which induces homopolymerisation of polymeric chains. Examples of this are: acid catalysed cross-linking of phenolic resins[59]; the reactions of epoxides with imidazoles[60], tertiary amines[61] or Lewis acids[62]. Liu *et al.*[63] have shown that changing the amount of formaldehyde and hydrochloric acid concentration in cross-linking of phenolic fibres changes the cross-link density. They show that the ideal concentration of the acidic catalyst is 12% by weight as this gives the highest tensile strength. Above this concentration there is a decrease in the tensile strength which they attribute to cross-linking on the outer shell of the phenolic fibres being increased which decreases the ability of the formaldehyde molecules to diffuse into the centre of the fibres. This would decrease the cross-linking on the inside of the fibres and reduce the strength of the fibres. With a decrease in the catalyst percentage there is less of the formaldehyde formed which decreases the degree of cross-linking. Tertiary amines catalysts have been widely used industrially, mainly in the cases of being used to catalyse the reactions of epoxides with other hardeners[64-66], although some work has used tertiary amines as a curing agent in its own right. Fernandez-francoz *et al.*[67] have used diglycidyl ethers of bisphenol A with different molecular weights with 4-(N,N-dimethylamino)pyridine as the initiator. They have shown that the larger the molecular weight of the epoxy oligomer the higher the conversion of epoxide groups and a higher heat of reaction. The reason they give for this is that there are more hydroxyl groups in the higher molecular weight oligomer that react with the initiated epoxide rings.

Radiation curing is similar to that of using peroxides to initiate the cross-linking reaction (as described previously). Different radiation sources produce energy that can create free radicals that can be used in the same method as

peroxide initiation of polymers.[68] Using monomers and oligomers that contain acrylates it is possible to cure and cross-link using UV radiation.[69-73] By using an array of methacrylates, Safranski and Gall[71] have shown that there is a dependence of the cross-linking of the polymer on the thermo-mechanical properties of monomers with different functional side groups on the backbone. They show that by having the side functionalities closer to the back bone they have less of an impact on the thermo-mechanical properties compared to those close to the methacrylate. Parthasarath *et al.*[72] research the diffusivity of water and subsequent leachables through polymers based on methacrylates. By using a set of different length methacrylates cured using the same visible light photo-initiators they show that the increase in chain length decreases the cross-link density of the polymer networks formed. This then inhibits the diffusion of water through the polymer; however the subsequent leachables appear to not be affected by the cross-link density. They show that there is generally an exponential decrease in the diffusion coefficient with relation to cross-link density. They attribute this to the difference in cross-link density (as mol cm^{-3}) and hydrophobicity of the polymers (log *P,* referring to the partition-coefficient) on the variation of diffusion coefficients using the following equation:

$$D = Ce^{A\vartheta + B \log P} \tag{1.10}$$

where ϑ is cross-link density; log *P* is the hydrophobicity of the polymers and *A, B* and *C* are fitting constants.

As has already been alluded to the chemical resistance of a polymer has been shown to be affected by the level of cross-linking in the sample.[74-78] Increasing the cross-link density can improve the chemical resistance, as an increase of cross-link density will reduce the molecular freedom of polymer chains and limit the amount of free volume that is available.[47, 79] The T_g of a polymer is also affected by the free volume and the cross-link density, which can be used as a way to show the reason why some polymers with higher T_g's have better chemcial resistance than those with lower T_g's. This is due to there being more specific volume above the T_g as show in Figure 1.7.

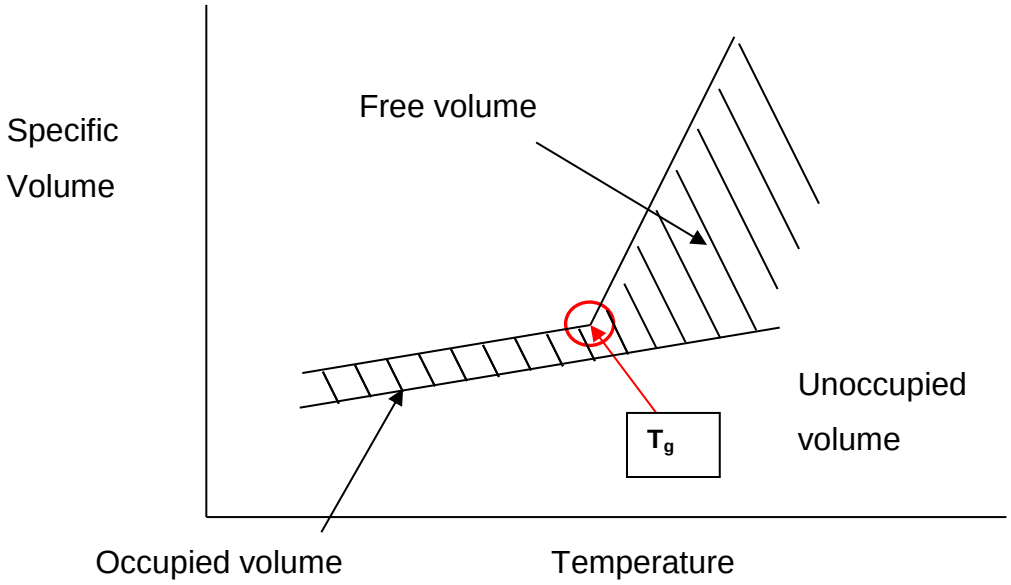

Figure 1.7 – Effect of the T_g on the specific volume

1.2.4 – Free Volume

Free volume is the amount of volume within a polymer sample that is not actually occupied by polymer molecules. It is the volume where there are "holes" that are needed for movement of polymer chains within a liquid or an amorphous solid (Figure 1.8).[80] These "holes" or areas of free volume allow molecular motion to occur (Figure 1.9), this in turn moves the areas of free volume through the polymeric material. This can then be utilised by small molecules to permeate and diffuse through the polymeric material by a mass transport process.[81]

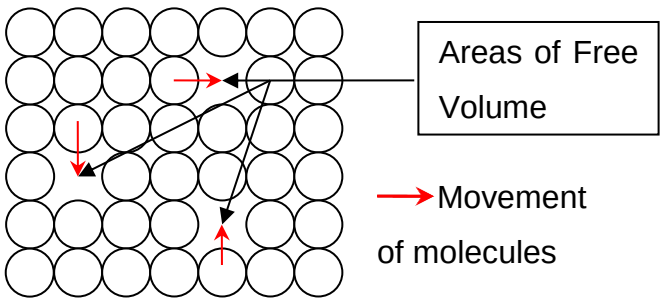

Figure 1.8 – Visualisation of movement of occupied volume into areas of free volume

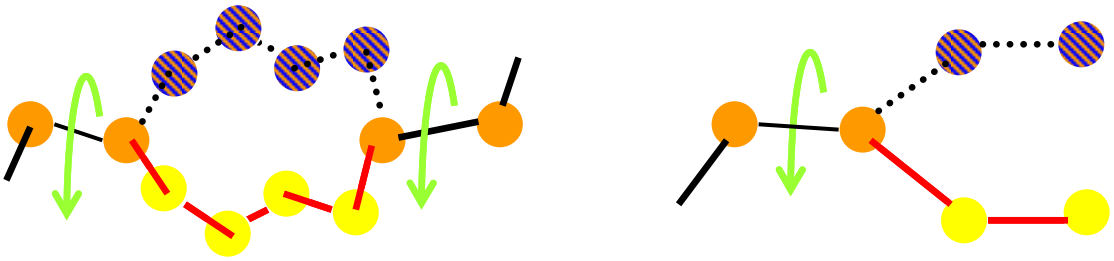

(i) (ii)

Figure 1.9 – Molecular motion of (i) polymer chain and (ii) polymer end

The change of permeability with regards to free volume has been shown by Kobayashi *et al*[82], who researched the effect of co-polymers of poly(ethyleneterephthate)(PET)-co-poly(1,4-cyclohexylenedimethyleneterephthate) (PCT) with changing compositions on the free volume and the gas permeability of the different polymers. By using positron annihilation lifetime spectroscopy (PALS) they have shown that increasing the amount of PCT from 0 – 100% the free volume concentration based on the intensity measurement I_3, increases. This shows that there is an increase in the amount of free volume areas throughout the polymer as the intensity measurement can be related to the relative free volume concentration since the I_3 is indicative of the relative number of annihilations that take place in the lifetime. They also show that there is a logarithmic increase in the diffusion coefficient of oxygen and carbon dioxide with an increase in the PCT%. Jackson *et al.*[83] show that there is a restriction in the ability of some fluids to permeate into certain glassy epoxy networks. By using PALS they determined the free volume sizes of a set of different epoxy amine polymers, in this case those based on either diglycidyl ether of bisphenol A (DGEBA) or tertaglycidyl-4,4'-diaminodiphenyl methane (TGDDM), using either 3,3'- or 4,4'-diaminodiphenyl sulfone (3,3'DDS and 4,4'DDS respectively). They found that the different polymer systems contained different free volume sizes, with the 4,4'DDS mixed with DGEBA having 82 Å^3, that with 3,3'DDS having 77 Å^3 and the mixture of TGDDM with 4,4'DDS having 59 Å^3. They then go on to show that the differences in size restrict the uptake of methyl isobutyl ketone which has a van der Waals volume of 81 Å^3. Their results show that there is rapid uptake of the MEK through 4,4'DDS DGEBA polymer which is to be expected as the free volume size is higher than that of MEK. They do go on to show

however that the 3,3'DDS equivalent also uptakes MEK albeit at a slower rate it reaches the same equilibrium level as the 4,4'DDS polymer. This they ascribe to the polymer swelling which increases the chain mobility which expands the polymer and allows diffusion through the polymer. Y.-J. Fu *et al.*[84] have shown that the difference in free volume in the same polymer system has an effect on the properties of the polymers. By casting the same molecular weight poly(methyl methacrylate)s with different solvents they are able to produce membranes that have different densities, fractional free volumes and free volume sizes. The volume of the holes ranges from 95 to 114 $Å^3$ which will affect the barrier properties of these membranes as the molecules will be able to pass through the bigger holes more readily as shown in the results of the study. With a higher free volume hole size there is a greater permeability coefficient of oxygen, helium and nitrogen through the membranes.

1.3 – Polymeric Materials used to Achieve Chemical Resistance

As has been previously stated there have been a plethora of different methodologies used to achieve chemical resistance. Therefore the focus will be on those of a polymeric nature, providing an in-depth guide to the numerous polymeric materials used to create chemically resistant coatings.

1.3.1 – High Performance Polymers

One type of polymeric material used for chemical resistance are those of "high performance polymers", which are a group of polymers that show high thermal resistance, have good mechanical properties and possess a high glass transition temperature.[85] These polymers come in several different categories for example: poly(phenylene sulphides); poly(aryl ether ketone); poly(oxadiazoles); poly(naphthalates); different polyimides and liquid crystal polymers[86] to name a few. The chemical resistance of high performance polymers is often high and has been utilised in many commercial applications including: electronics (for use as protective coatings for semiconductors); structural materials for aerospace[87]; fuel cell membranes and as coatings[88]. Several papers have been published in which the gas transport properties and the diffusion of gasses through these polymers have been investigated[34, 36, 37, 89]. Cui *et al.*[37] studied the effect of aging and annealing temperature on different polymers with regards to their gas barrier properties. They have found that using polymers made from 2,4-diaminomesitylene are more permeable than those that are from *m*-phenylenediamine. The gas barrier properties could possibly be related to the chemical resistance due to the relationship between the gas diffusion and fractional free volume.[38, 90, 91] Using the "Permachor" factor as described in equation (1.9) Salame[36] has calculated the permeability of several known high performance polymers and copolymers. The diffusion coefficient and solubility coefficient can then be estimated from these results using equation (1.1). The resistance of these polymers to chemical media such as alkalis[92]; acids[41] and organic solvents[93] has been shown to be relatively high, work done by Wang *et al.*[94] have shown that the addition of rigid aromatic

groups into high performance polymers can be used to increase the chemical resistance.

1.3.2 – Fluorinated Polymers

A subclass of high performance polymers is that of fluorinated polymers. These polymers have been found to have advantageous properties such as good thermal stability, excellent chemical resistance and weatherability[95, 96]. These are enhanced partly due to their low surface energy[97] and the unsurpassed electronegativity of fluorine[95]. The properties also increased due in part to the low wettability, low adhesion and low coefficient of friction[98] but high stability of the carbon fluorine bond which when covalently bonded causes a small polarization of the bond[99]. There are several applications that these materials have been used for: gas diffusion layers in proton exchange membranes[100]; protective coatings for historical monuments[99]; improving the hydrophobicity of other polymeric materials by co-polymerisation; functionalisation[97] and several others. By incorporation of fluorine containing polymers Miyamoto *et al.*[101] show that the critical micelle concentration increases with the increase in fluorine and the surface tension decreases. Kim *et al.*[102] have also shown that incorporating perfluoro acrylates into copolymers increases the contact angle following increased fluoro acrylate wt.%. Yang *et al.*[103] have shown that incorporating dodecafluoroheptyl methacrylate into a latex based core shell in a poly(urethane) blended film increases the contact angle with the more PFA-CS that is incorporated. This relates to the hydrophobic nature of fluorine at the surface and will affect the diffusion into the polymeric material which directly corresponds to the chemical resistance[104]. Zeng *et al.*[105] have patented a range of formulations that make use of polyvinylidene fluoride as the main component with adhesive promoters of acrylic resins and polyepoxide resins. They show that below 75% of polyvinylidene there is a decrease in the chemical resistance of the coatings towards chemicals used in break fluids. The fluorination has been shown to increase the chemical resistance of some polymers that initially have very low chemical resistance due to the high phobicity of fluorine within the polymer[106]. Kharitonov and Kharitonova[107] show that direct fluorination of polymers is possible over a sufficient amount of time, converting the C-H bonds to C-F bonds. This has

positive effects on the properties of the samples that they have evaluated. They show that there is an improvement in the barrier properties of high density polyethylene that is treated with fluorine by a factor of 6-7 orders of magnitude compared to that of untreated polyethylene.

1.3.3 – Additives

Additives play an important role in coating technologies and have been used for over 60 000 years[108], with pigments such as ochre and hematite being used as basic paint colours. However additives play a far bigger role than just that of colouring[109-113]. Kalendova *et al.*[113] show that pigments in an organic coating have an effect on the coefficient of diffusion depending on the pigment volume concentration. The work shows that pigments such as TiO_2 show a linear increase in the diffusion coefficient with increasing pigment volume concentration. However pigments such as $MgFe_2O_4$ decrease exponentially until 30% where the diffusion coefficient levels out. Jana and Jain[111] show that polymers based on poly(ethersulphone)s utilizing additives of nanoparticles and a low molecular weight epoxy resin as a dispersion agent resulted in the formation of a high performance polymers. The silica nanoparticles have a positive effect on the swellability of the polymer mixture with 10% weight of the fumed silica having a dramatic improvement on the weight gain of the polymer. The applicability of additives to enhance chemical resistance ranges from the use of co-polymers[114, 115] to nanoparticles[116]. Orlicki[117] showed in a patent, a polymer additive based on a hyper-branched AB_2 polymer system in a solvent borne chemical agent resistant coating creates a system where the additive is “self-cleaning” towards materials used in chemical warfare. Simone *et al.*[118] have shown evidence that the use of small molecules as additives to improve processability might also have an effect on the chemical resistance.

1.3.4 – Composites

Composite materials possessing different properties arising from their individual components[119] have been around for millennia, with many composites appearing in nature. For example, wood and bone are forms of composites that

contain a variety of constituents to produce strong materials[120]. Examples of man-made composites are that of concrete bonded fibreboards[121] and more recently polymer-matrix composites[122]. Polymer-matrix composites use a polymeric material such as an epoxy thermoset[123] with the addition of in(organic) materials such as fibres[124], (nano)-particles[125-127] and carbon nanotubes[128] to name but a few. Patel *et al*.[123] show that using an oligoamide-epoxy composite in different ratios affects the percentage weight change. Work done by Rahgu *et al*.[129] used surface-treated fibres (from the Sisal plant) in a polyester/ styrene based polymer matrix. The washing of the fibres using different concentrations of sodium hydroxide produced different chemical resistant properties. Work by Guduri *et al.*[130] (using natural fibres for reinforcement of epoxy polymers) showed that treatment of the fibre with a higher concentration of sodium hydroxide led to a higher mass gain of the composites.

1.3.5 – Epoxides

One of the main polymeric materials used for achieving chemical resistance in coatings are epoxy resins. These are produced from monomers that contain more than one epoxide (oxirane) rings that ring-open to form thermoset polymeric materials. Epoxy resins formed by reacting olefins with peroxybenzoic acid were first discovered in 1909[131]. An application for these resins was not developed until thirty years later when the most widely used epoxy resin to date, bisphenol A diglycidyl ether (Figure 1.10), was synthesised. The first use of epoxy resins was as a dental adhesive but this was unsuccessful due to the sensitising nature of the epoxide group[132]. These materials have since been used in applications as coatings, adhesives, floorings and composites.[133, 134]

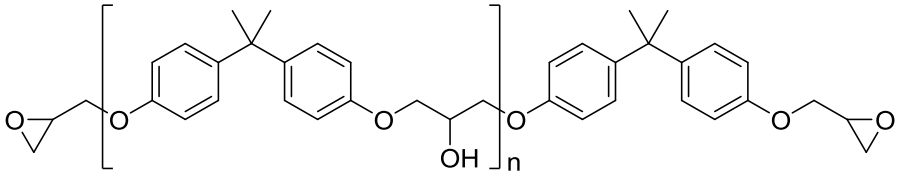

Figure 1.10 – Diglycidyl ether of bisphenol A[135]

Epoxy resins are widely used because of their advantageous material properties, which include: high tensile strength; high adhesion and high chemical

resistance. As monomers epoxides are reactive towards a wide range of curing agents. A few examples of these different co-monomers are: polyamines (such as polyethylene polyamine[136], poly(propylene glycol) bis(2-aminopropyl)ether[137]), aromatic amines[138] (4,4'-methylenedianiline[139], 4,4'-diaminobiphenyl[140]), thiols[141] (3,6-dioxa-1,8-octanedithiol[142]) and anhydrides[143] (maleic anhydride[144]). There is also homopolymerisation that can occur using different hardeners for example: catalytic amounts of imidazole[60]; tertiary amines and Lewis acids and bases.[145] The different hardeners can also contribute to the properties of the final polymer.

The main hardeners that are used are diamines as they have versatility with their properties with different parameters being used to change functionality. By using different backbones Santiago *et al.*[77] have been able to increase the storage modulus of an epoxy polymer by changing the backbone of the amine from a small molecule diethylenetriamine (DETA), to a hyper-branched polymeric amine (HBpei). They relate this to the hyper-branched polymeric amine having a higher cross-link density due to there being more functional amines available. By changing the polarity of the curing agents, Wang *et al.*[139] have shown that altering one functional group on the amine has a dramatic effect on the water absorption. Wang *et al.*[140] have shown that by changing the chain length of the amines has an effect on the activation energy needed to initiate curing. Also, they show that there is a severe drop off with regards to the glass transition temperature, due to the longer chains having more flexibility. Several patents have been published incorporating the use of different amines bearing different properties. For example Williams' patent describes numerous different amines that can be used as water-based polymers, by using different polyalkyleneamine adducts.[146] For lower cure temperatures Dimopoulos *et al.* have utilised polyoxypropylene diamine (Aradur HY5922) as the curing agent to determine the cure kinetics.[44] Their measurements show that the rate of reaction and heat of the reaction slightly change, when different heating rates are applied via dynamic DSC. Sato *et al.* describe the use of mixtures of amine curing agents to also give low curing temperature performance with excellent chemical resistance.[147] The patent describes the use of polyamide compounds from fatty acids with phenalkamine compounds as a mixture giving high solids content and low viscosity. Nakka *et al.*[78] show that changing the chain length of the amine curing agent has an

effect on the properties of the network polymer formed. Using a homologous series of diamines with 2-8 methylene groups with bisphenol A diglycidyl ether, they show that increasing the length of the amine decreases the T_g; the cross-link density; rubbery and glassy modulus but causes an increase in the fractional free volume.

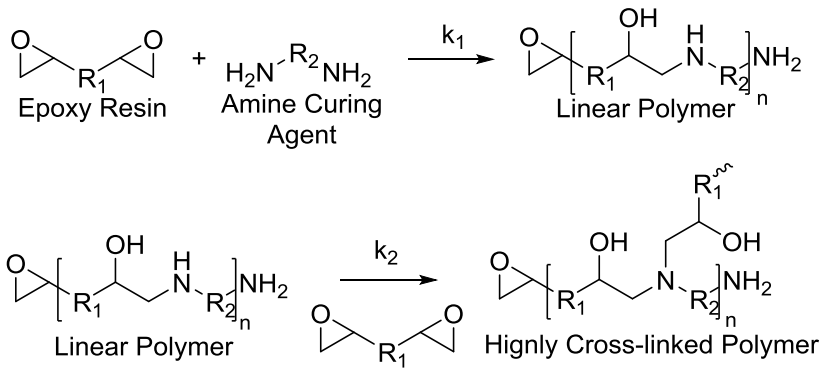

Figure 1.11 – Diepoxide/ diamine reaction

There have been several articles and patents published on the chemistry involved in the epoxy-amine reaction. Pascault and Williams[148] cover a wide range of reactions that epoxy resins can undertake. The main reaction of interest for this thesis is the reaction between di-epoxides and di-amines as shown in Figure 1.11. As previously stated there is also a potential for homopolymerisation even when there is a stoichiometric amount of amine functionality relative to the epoxide.[149] This can occur via two methods: the ring opening of the epoxide via the hydroxyl group; or via etherification of two or more epoxide groups as can be seen in Figure 1.12.[150, 151] Rozenberg[152] has reported a multitude of different systems that contain different epoxides and amines to determine the mechanisms and kinetics of various systems. The work revealed that there are two main different mechanisms that the reactions: catalytic, where there is autocatalysis from the OH groups present during the cure which produce ionic homopolymerisation, and a non-catalytic reaction which can occur with stoichiometric amount of pure starting materials and completely dry reaction vessels, decreasing the amount of hydroxyl containing impurities to less than 10^{-6} mol L^{-1}. This reduces the probability of the ionic homopolymerisation by limiting the initiator levels.

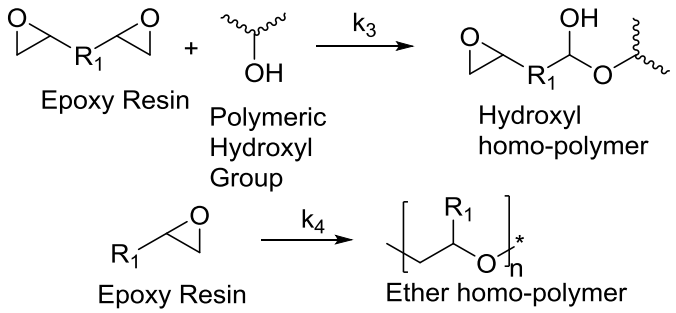

Figure 1.12- homopolymerisation reactions of epoxides

When an epoxy resin is mixed with a diamine a cross-linked network is formed (Figure 1.13) which, (depending on the cross-link density[74, 75] amongst other factors) has the ability to resist absorption and permeation of small molecules through the system that is described earlier in this chapter. Many different methods have been used to attempt to increase the chemical resistance of epoxy resins. These have ranged from changing the molecular structure associated with the epoxide such as using a bisphenol A epoxy resin compared to one that is based on bisphenol F[83], to those that are based on aromatic systems.[153] There have been studies and patents published using different glycidyl ethers[154-158] and their effect on the properties of the polymers formed. Shinkareva *et al.*[155] show that using different analogues of epoxy resins based on 4,4'-isopropylidenediphenol produce polymers that have different properties when emulsified using the same curing agents and surfactants. By using different functional epoxides based on the same backbone Dai *et al.*[156] deduce that a tri-functional epoxide has a higher thermal stability than a di-functionalised epoxide. White *et al.*[158] have patented many examples of different epoxy resins and the effect of the incorporation of different moieties. For example they show that the addition of 4,4'-α-methylstilbene decreases the oxygen transmission rates compared to those of similar polymers derived from conventional epoxides. Work done by Brennan *et al.*[159] has shown that the amorphous polymers formed by epoxy resins can have barrier properties to oxygen that are equivalent to crystalline polymers such as polyvinylidene chloride and poly(ethylene-co-vinyl alcohol). Wegmann[154] compared the chemical resistance of both waterborne and solvent based epoxy amine polymers. The work suggests that the main parameters that have an effect on the chemical resistance are: the choice of the hardener (in this case the amine); stoichiometry; film thickness; curing times and coalescence. Epoxy

amine polymers will be the main focus of this thesis and will therefore be the only polymeric material referred to.

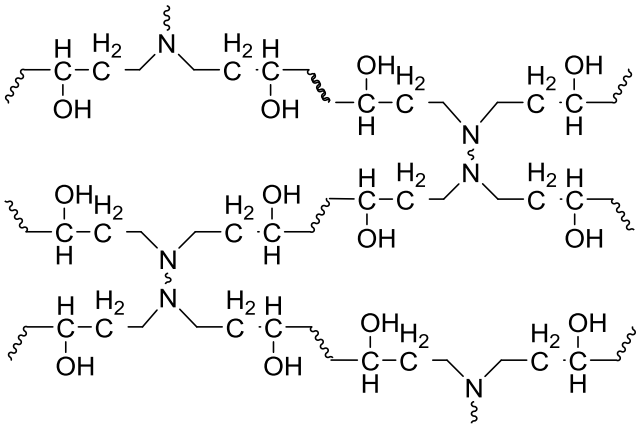

Figure 1.13 – Cross-linked polymer network of epoxy amines

1.4 – Conventional Synthesis of Epoxides

There are several ways in which these resins can be made with one of the main methods used in industry utilizing epichlorohydrin. This method is the nucleophilic addition of epichlorohydrin to an alcohol to form a chlorohydrin which, in the presence of sodium hydroxide undergoes dehydrochlorination (Scheme 1.1) giving the epoxide.

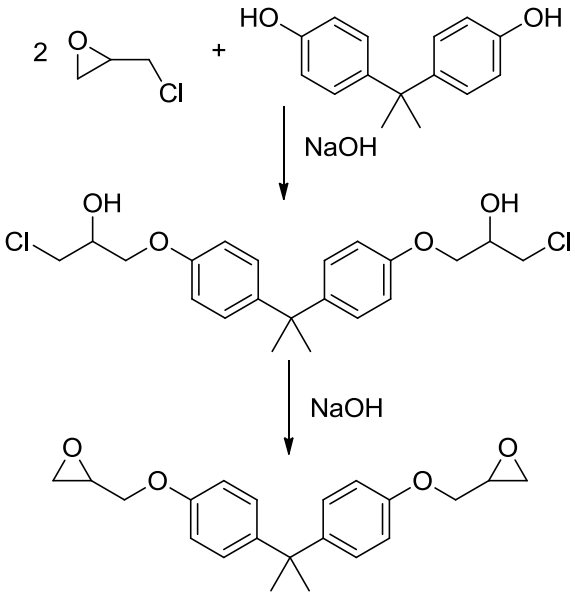

Scheme 1.1 – The production of Bisphenol A Epoxy[160]

There are also some health and safety issues with the use of epichlorohydrin as there is the possibility of acute toxicity from exposure and also the possibility of carcinogenicity. There have been, therefore, several papers which have looked at other approaches towards the synthesis of epoxides.

1.4.1 – Via Halohydrin Intermediates

Instead of using epichlorohydrin and attacking the alcohol group, there are methods that produce the halohydrin utilizing different starting materials. There have been several papers published on the synthesis of different halohydrins using several different methods using a variety of synthetic steps.

Kolb *et al.*[161] provide a synthetic approach that utilizes a cyclic acetoxonium intermediate to synthesise the chlorohydrin and then using a weak base in methanol to ring-close the epoxide as show in Scheme 1.2.

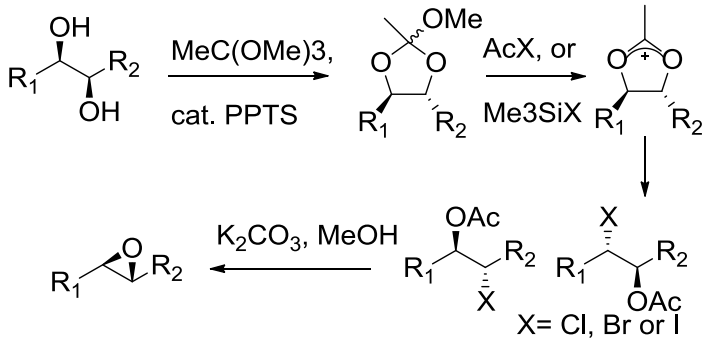

Scheme 1.2 – Synthesis of epoxides using halohydrins as developed by Kolb *et al*

They show that this method is successful with a wide range of functionalities which contain a 1,2-diol. The research shows that there is a high yield in the multi-step one-pot procedure using enatiomerically enriched diols. They show that all three of the halogens can produce epoxides with similar yields on cyclohexylpropane-1,2-diol with the exception of iodine, which only produces the halide.

Another method of producing chlorohydrins is the direct attack of chlorine onto the olefin by bubbling chlorine gas through water in the presence of the olefin. Bentley *et al.*[162] have published a patent that describes the synthesis of glycidyl ethers from allylpolypropylene glycols. The method requires dissolving the allylpolypropylene glycols in water and adding a flow of chlorine gas at a specific flow rate for the synthesis of the chlorohydrin, which is then followed by being treated with sodium hydroxide solution to form the epoxide as shown in Scheme1.3.

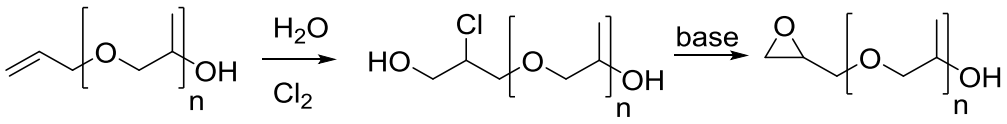

Scheme 1.3 – Synthesis of allylpropylene

There are several other methods that are available to synthesise chlorohydrins which do not require the use of elemental chlorine for example: Prilezhaev reaction[163]; Baeyer-Villiger reaction[164]; "turbo Grignard" reaction[165]; using HCl and carboxylic acids[166] and utilizing trichloroisocyanuric acid[167].

1.4.2 – Prilezhaev Reaction

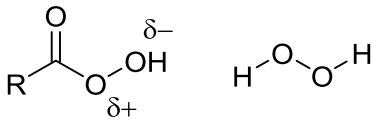

Figure 1.14 – Molecular structure of peroxy acids and hydrogen peroxide.

Another route in the synthesis for epoxides from olefins is the use of peroxy acids or hydrogen peroxide (Figure 1.14). These contain a peroxy group (-OOH) which gives a delta positive oxygen that can readily be used in oxidations. The most popular of these peroxy acids is *m*-chloroperbenzoic acid (MCPBA) which when reacted with an alkene can form an epoxide. Bach *et al.*[168] have researched the effect of different acidic catalysts on the rate of epoxidation and decomposition on both 1-nonene (Scheme 1.4) and (Z)-cyclooctene (Scheme 1.5). The two catalysts that they have researched are trichloro- and trifluoro-acetic acid. They show that trifluoroacetic acid has a greater effect on the reaction rate at higher concentrations than that of trichloroacetic acid.

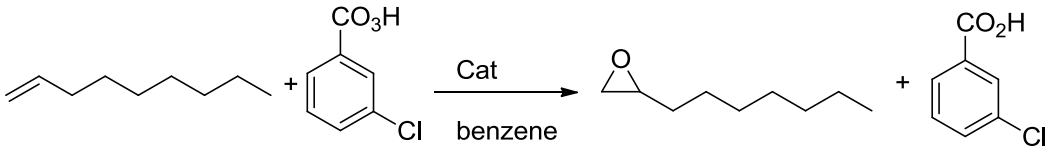

Scheme 1.4 – epoxidation of 1-nonene with *m*-chloroperbenzoic acid

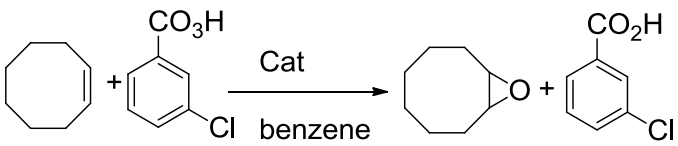

Scheme 1.5 – Epoxidation of (Z)-cyclooctene with *m*-chloroperbenzoic acid

Hoveyda *et al.*[169] research the effect of different substituents have on the selectivity and rate of the epoxidation of different olefins utilizing *m*-CPBA. They show that the geometry of cis and trans-5-tert-butyl-2-cyclohexen-1-ol have different effects on the selectivity and rate. The cis isomer has a higher syn:anti stereoselectivity with a ratio of 24:1 whereas the trans isomer has a ratio of 5:1. The rate is also heavily reduced from the cis isomer to the trans isomer with the cis having a rate of 0.75 and trans of 0.10 compared to the rate of cyclohexene. They surmise that this is due to the heteroatom functionality having a direct effect on the oxidation with the reaction progressing more efficiently from the pseudoequatorial orientation.

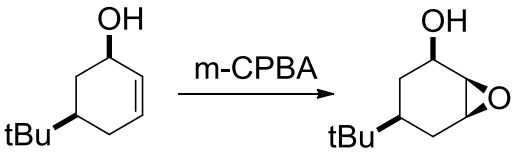

cis-5-tert-butyl-2-cyclohexen-1-ol: stereoselectivity 24:1, rate 0.75

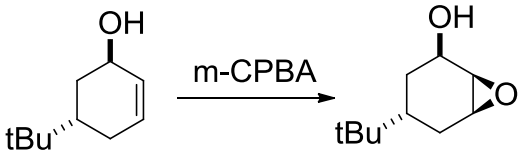

trans-5-tert-butyl-2-cyclohexen-1-ol: stereoselectivity 5:1, rate 0.10

Scheme 1.6 – Reactions of cis and trans-5-tert-butyl-2-cyclohexen-1-ol with *m*-CPBA

1.5 – Epoxidation using HOF.MeCN

Fluorine has a higher electronegativity than that of oxygen, therefore a molecule with one oxygen-fluorine atom that will have both a negative dipole on the fluorine and a positive dipole on the oxygen as seen in Figure 1.15. Indeed by flowing fluorine gas through water it is possible to create hypofluorous acid.

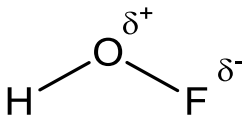

Figure 1.15 – Molecular structure of hypofluorous acid

1.5.1 – a brief history of fluorine

Elemental fluorine has had a long, exciting and colourful history. The first successful attempt to prepare and isolate elemental fluorine is accredited to Henri Moissan in 1886[170], although fluorine appears much earlier in history. The first mention of elemental fluorine occurred as early as 1670 where calcium fluoride was used to etch glassware. Carl Wilhelm Scheele is thought to have been the first person to "discover" elemental fluorine in 1771 but due to its reactive nature he was unable to isolate and identify it correctly. One of several other chemists that attempted to isolate elemental fluorine was George Core in 1869 who managed to produce a small amount using electrolytic processes. This, however, did not end in success due to the hydrogen produced at the other electrode which resulted in his equipment exploding.[171]

Despite the high reactivity of fluorine, it has found use in several applications in synthetic chemistry. Organofluorine compounds have been studied before the isolation of elemental fluorine by Moissan, with work on synthesising fluoroaromatic derivatives beginning in the 1850's. However, it was not until just before the Second World War that organofluorine molecules were produced on an industrial scale, due to the production of anhydrous hydrofluorus acid in commercial quantities[172]. Since the 1950's there has been great interest in the incorporation of fluorine into organic compounds due to the unique properties that fluorine bestows on organic molecules

following the discovery of the increased bioactivity of 2α-fluorohydrocortisone compared to activity of the initial parent compound.[173, 174]

Although there are thousands of publications describing organofluorine compounds, only a small fraction of these utilize elemental fluorine for their synthesis. The main source of fluorine for most organofluorine reactions is anhydrous hydrofluorus acid (HF)[175, 176] and metal fluorides[177]. The reason that there was little use of elemental fluorine as a reagent is in part due to the high toxicity of fluorine and the sometimes uncontrolled reactions that occur. However, there is growing interest in the use of fluorine gas as a reagent in synthetic reactions. One of the pioneers in this area is Shlomo Rozen who has developed several reactions utilizing elemental fluorine including the synthesis of fluorine containing compounds. One of the reactions he has developed is a method to produce the oxidising agent HOF.MeCN[178] which can be used to as a very powerful oxidising agent.

1.5.2 – Epoxidation using HOF.MeCN

It is possible to perform reactions in a safe manner using fluorine gas as with any other corrosive gas by using a closed system and taking care with the reactants that are used and ensuring that the reaction equipment is appropriate.

There have been several publications that deal with oxidation reactions that can be performed by utilizing HOF.MeCN which produces highly pure, clean products with relatively high yields as compared to conventional oxidation methods. Rozen *et al*[179, 180] show that it is possible to oxidise olefins that contain either alcohol groups or free acid groups without signs of simultaneous oxidation of the hydroxyl groups. Scheme 1.7 shows just a selection of reactants and their subsequent epoxidised products after treatment with HOF.MeCN. They show that a range of alcohols, even those that have low nucleophilic olefins such as dihydrocarveol, can be epoxidised. Rozen shows that oleic acid, which has previously been epoxidised using conventional methods but only reaching 65% yield at elevated temperatures, gave a yield of 90% in approximately 10 minutes using HOF.MeCN. Even

bisepoxides of linoleic acid can be synthesised using a two-fold excess of HOF.MeCN giving a 90% yield after 3 minutes compared to other methods using peracids which yield only 35% yield after several hours.

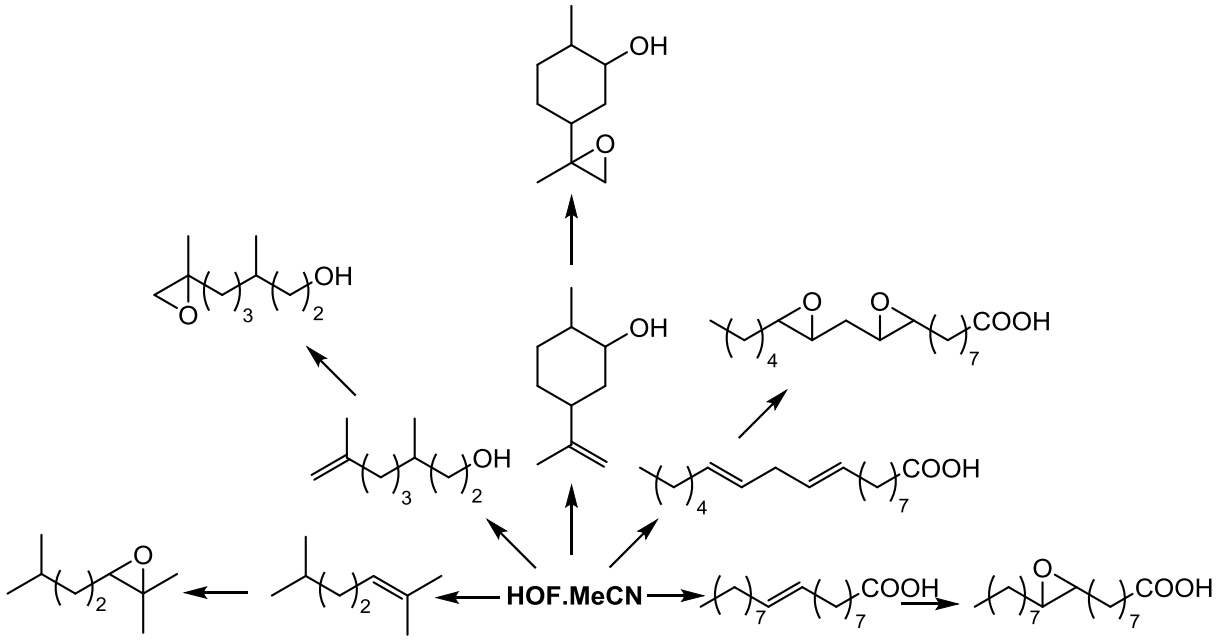

Scheme 1.7 – Reactions of alcohols and free acids containing olefins with HOF.MeCN

Even deactivated and sterically hindered olefins can be epoxidised using HOF.MeCN (Scheme 1.8). Even electron deficient olefins such as diethyl maleate and fumarate that with a large excess of HOF.MeCN to give the corresponding epoxides with good yields[181, 182]. 2,6-Dimethylbenzoquinone has also been shown to be epoxidised utilizing HOF.MeCN in a high yield in under 5 minutes although only one of the double bonds undergo epoxidation. Using the less electron-deficient, but sterically hindered, pentaphenylcyclopentadiene it is possible to produce the epoxide using HOF.MeCN in 70% yield in 15 minutes. Even the oxygen rich bicylco[2.2.2]oct-7-ene-2,3,5,6-tetracarboxylate can be epoxidised to 80% yield despite it being weakly nuclephilic[183].

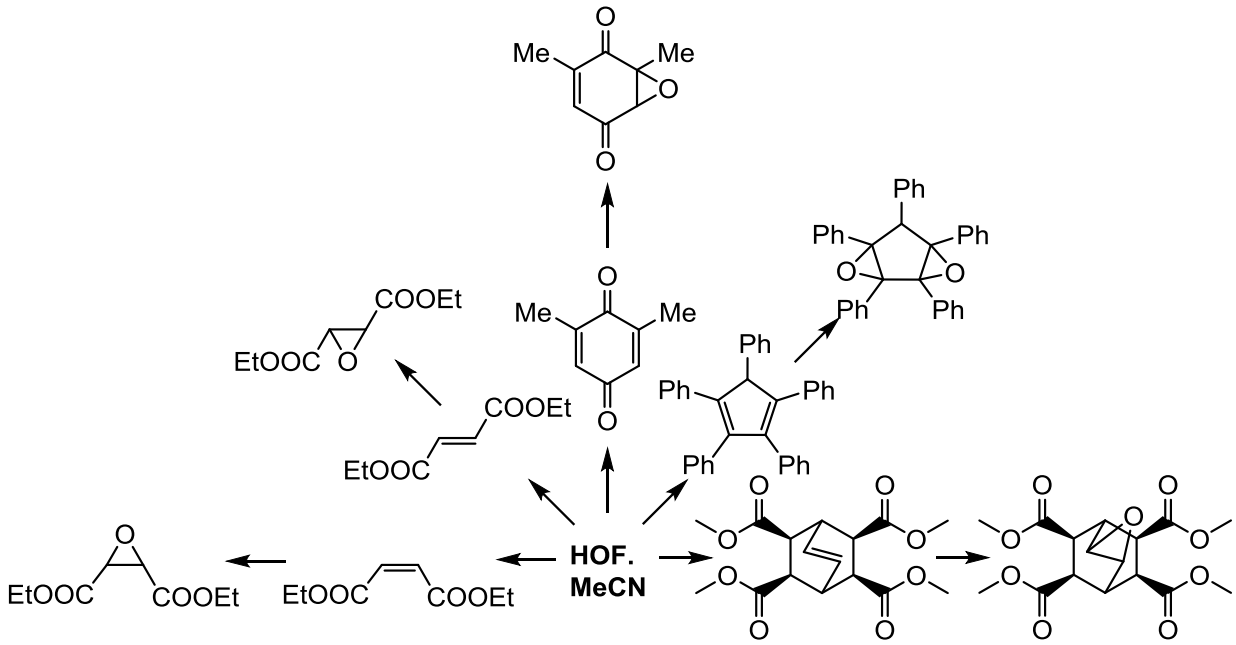

Scheme 1.8 – Reactions of electron deficient and sterically hindered olefins using HOF.MeCN.

Polyaromatic substrates have been shown to be selectively epoxidised using HOF.MeCN (Scheme 1.9) in good yields compared to those that have been previously obtained using conventional methods. Using phenanthrene Rozen shows that after a reaction of 10 seconds at -15°C the corresponding epoxide was produced in 97% yield but with only 45% conversion. However, by increasing the reaction time to 30 seconds the conversion can be increased to 90% but with a detrimental effect to the yield, decreasing it to 77%. Pyrene can also be epoxidised by this method to a higher yield and conversion to conventional methods with the epoxide being produced in 5 seconds with a yield of 80% and conversion of 65%[184].

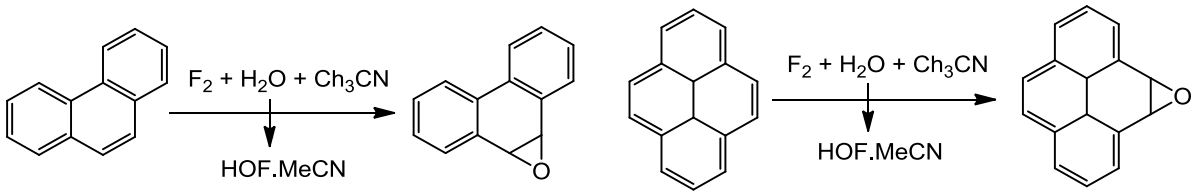

Scheme 1.9 – Epoxidation of polyaromatics using HOF.MeCN.

1.5.3 – Concluding Remarks

Although there are several conventional methods that are available for epoxidation of alkenes there are several difficulties:

- Complicated multi-step reactions
- Dangerous reagents
- Extensive reactions times
- Non-selectivity
- High temperature reactions

However with the use of Rozen's strong oxidising complex, HOF.MeCN, it is possible to produce pure epoxides in a selective manner in a short time period at low temperatures. However, there is a drawback with this method because the creation of HOF.MeCN can only be performed at low concentrations due to the instability of HOF.MeCN which restrict the amount of product that can be synthesised.

Chapter 2 – Conventional synthesis of diglycidyl ethers

2.1 – Aims and approach

The ability of a material to resist absorption when exposed to chemical media is a highly important property in the coatings industry, for example, in the marine industry when the coating forms the inside layer of a cargo tank that will be transporting a variety of different liquid media. It is of vital importance that there is no adsorption from each liquid cargos as this can lead to cross-contamination and resulting in the loss of the cargo. While there have been several publications on the effect that coating structure has on the barrier properties of polymers with regards to gases[27, 33, 37-39, 89], our aim is to explore the effects that different isomeric aromatic polymers have on barrier properties with respect to various liquid media.

The polymers that will studied in this thesis are based on polymer networks derived from bisepoxides and diamines, as these are known for having good barrier properties[154, 159]. They are also widely used in the coatings industry as they are readily available on a large scale and can have tuneable properties depending on the monomers used. Therefore, a series of isometric aromatic bisepoxides will be synthesised to determine the effect the structure of these bisepoxides has on the thermal, mechanical and thermodynamic properties of the resulting polymers and how the microstructures formed by the different isomers affects the network properties. The monomers to be used in this study are a series of bisepoxides based on catechol, resorcinol and hydroquinone, (Figure 2.1 (a)) and the diamine 4,4'-methylenebis(cyclohexylamine) (Figure 2.1 (b)) as these are of significant commercial interest in the coatings industry.

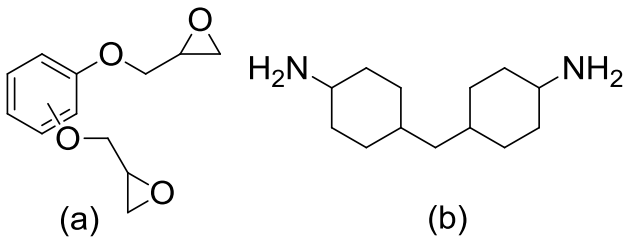

Figure 2.1 – Monomers targeted for the synthesis of model polymer networks

As the aim of this thesis is to determine the effect of polymer network structure on liquid barrier properties, model polymer systems are required. Therefore, pure epoxides are needed, which must be prepared from different isomeric aromatic diols materials by multistep synthesis routes. The synthetic plan for this thesis consists of two main stages: Scheme 2.1 is the proposed synthesis of monomers and Scheme 2.2 is the proposed formation of the polymer networks for subsequent analysis.

The first stage in the synthesis of monomers from the bisepoxides will be allylation of bisalcohols using Williamson ether reactions. For the synthesis of the epoxides, two routes will be explored: conventional epoxidation utilizing trichloroisocyanuric acid (TCA) in the presence of a base (Route 1) and novel epoxidation with the oxidising agent HOF.MeCN (Route 2). These will be compared to determine which of the methodologies is ideal for the synthesis of the target bisepoxide systems.

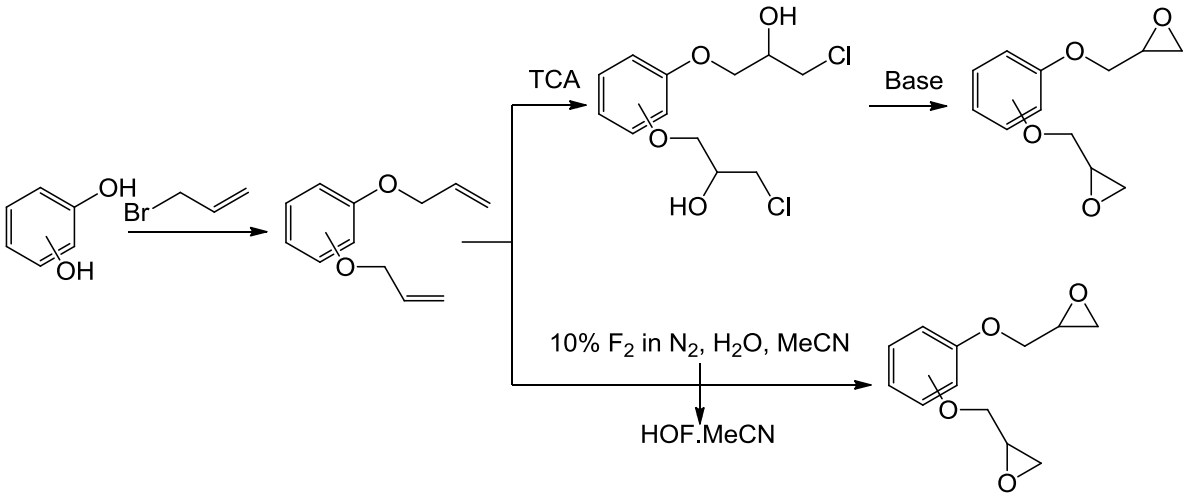

Scheme 2.1 – Synthetic routes to synthesise bisepoxides from diols using allylation and both conventional and novel epoxidation techniques.

Upon establishing ideal parameters on the small scale, scale up of the reactions will be performed to produce the required amount of bisepoxide for production of the polymer networks for further characterisation.

Once there is a sufficient amount of epoxide, a method to produce polymer films will be developed using a variety of substrates and different temperatures. The method will require the polymer films to be fully cured (as measured by DSC), easily removed so that analysis can be performed and be either readily shaped or moulded for analysis. The polymer films will be produced by mixing the monomers in a 100% stoichiometric ratio so that model networks will be produced with limited possible side reactions. As can be seen in Scheme 2.2 the monomers will, in principle, make a highly cross-linked polymer network which should consist of only ether linkages derived from the epoxide to the amine, with no competing homopolymerisation.

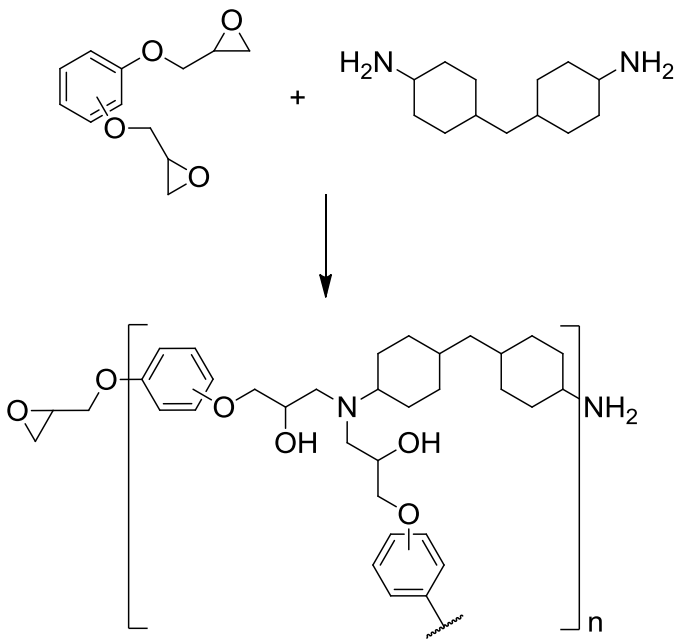

Scheme 2.2 – Production of epoxy amine polymer networks.

The polymer films will then be fully characterised to assess their thermal, mechanical, structural and thermodynamic properties and the effect of structure on the chemical barrier resistance to liquids.

The aim of this chapter is to develop methods to synthesise, firstly, the bisallyl ethers of each of the aromatic diols and, then, subsequent epoxidation as shown Scheme 2.1.

2.2 – Synthesis of allyl ethers

The bisepoxide monomers required for polymerisation studies will be synthesised by epoxidation of appropriate bis-alkene derivatives which were prepared by Williamson ether synthesis of the corresponding diols and allyl bromide as described below.

2.2.1 – Williamson ether reaction

2.2.1.1 Hydroquinone 1.a

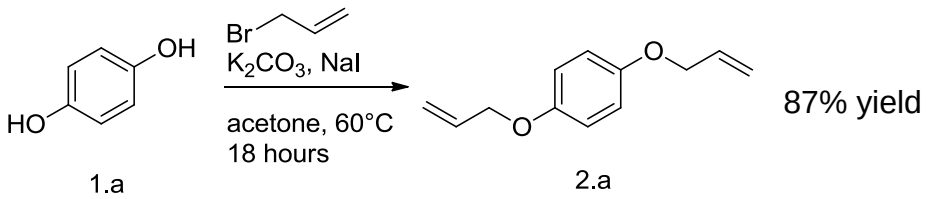

Scheme 2.3 – Reaction of hydroquinone with allyl bromide to form hydroquinone diallyl ether.

The reaction of hydroquinone with allyl bromide was carried out at 55 °C in acetone and under nitrogen for eighteen hours. The extent of the reaction was measured by ^{1}H NMR spectroscopy after one hour and 18 hours using the method described by Sanford *et al*[185]. As can be seen from the ^{1}H NMR spectrum (Figure 2.2) it was possible to determine the percentage conversion to diallyl product by the intensities of the resonances in the aromatic region. A singlet at 6.77 ppm relates to the aromatic C-H resonance of the desired diallyl species (1), a multiplet at 6.69 ppm to the monoallyl species (2) aromatic region and a singlet at 6.62 ppm to the starting material (3). After one hour, the reaction mixture was comprised of 19.8% diallyl product and 74.8% monoallyl species with 5.4% starting material remaining. After eighteen hours, the desired product was observed to be 90.3% with monoallyl (9.3%) and starting material remaining (0.4%) making up the rest of the mixture.

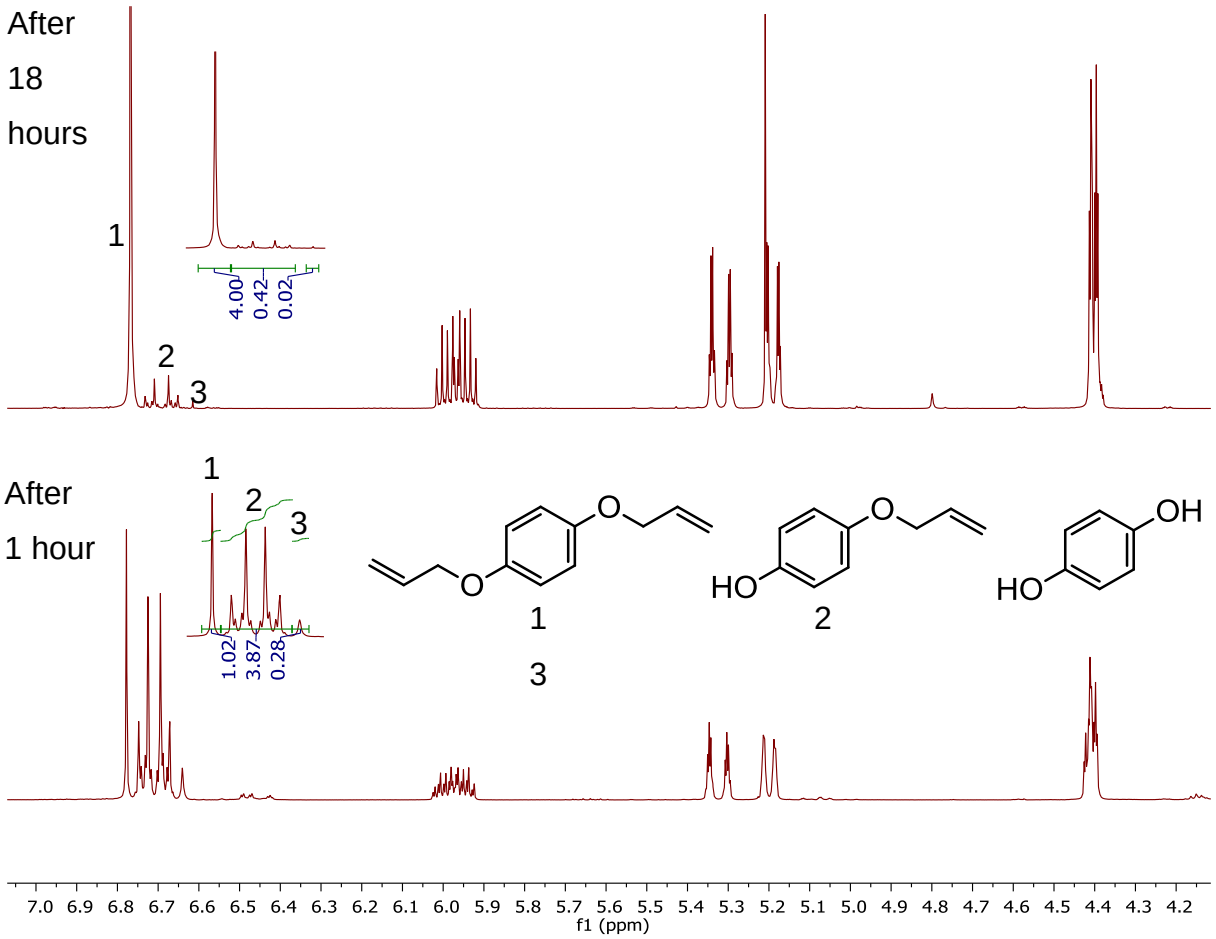

Figure. 2.2 – ^{1}H NMR spectra of reaction of hydroquinone diallyl ether with allyl bromide. 1 refers to the peak from the aromatic protons of the diallyl product; 2 refers to the aromatic protons from the monoallylated product and 3 refers to resonance due to the starting material.

Following workup, involving washing the reaction mixture with 2 M sodium hydroxide the desired bisallyl product was isolated in 87% yield and the NMR analysis shows that the product was 99% pure which was confirmed by GC-MS analysis. The singlet peak at 6.86 ppm (4H) in the ^{1}H NMR spectrum of the pure diallyl system (Figure 2.3) correlates to the aromatic region (1) of the molecule as each of the four hydrogens are equivalent. The doublet of doublet of triplets resonance at 6.06 ppm (2H, *J*=17.2, 10.6, 5.3Hz) corresponds to the CH_2–<u>CH</u>=CH_2 resonance (3). The doublet of quartets 5.42 ppm (2H, *J*=17.3, 1.6Hz) relates to the trans CH of the double bond (4'), which shows a larger $^{3}J_{HH\ trans}$ coupling. The other doublet of quartets at 5.29 ppm (2H, *J*=10.5, 1.4Hz) is assigned to the cis (4) CH which shows a smaller $^{3}J_{HH\ cis}$ coupling constant. Finally, the doublet of triplets at

4.49 ppm (4H, *J*=5.3, 1.5Hz) corresponds to the OCH_2 (2/2'). The 1.5 Hz coupling value is due to coupling between the two hydrogens in this environment.

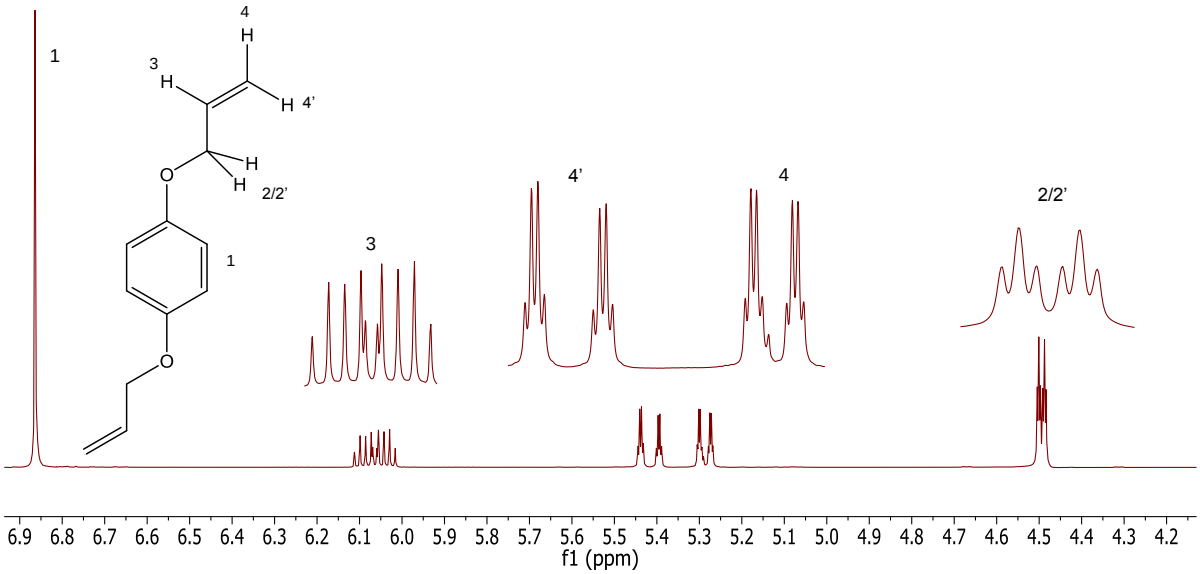

Figure 2.3 – ^{1}H NMR spectra of pure hydroquinone diallyl ether.

In the ^{13}C NMR and DEPT spectrum shown in Figure 2.4 (with the blue overlay being the DEPT spectra), the peak at 152.91 ppm correlates to the quaternary carbon of the aromatic ring (2); the vinylic CH (4) appears at 133.63 ppm; 117.49 ppm arises from the $=CH_2$ group (5); 115.66 ppm are due to the aromatic carbons bonded to hydrogen (1) and 69.46 ppm is the ether $O\text{-}CH_2$ group (3).

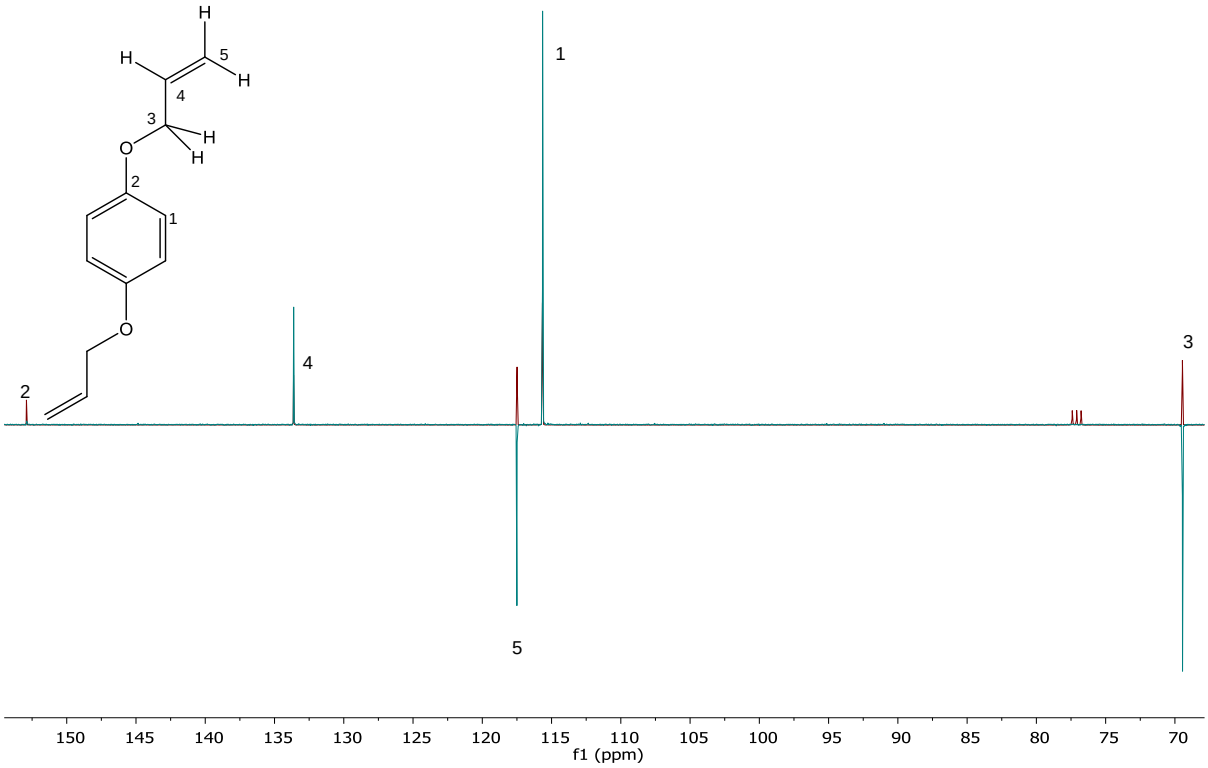

Figure 2.4 – ^{13}C NMR spectra of hydroquinone diallyl ether

2.2.1.2 Catechol 1.b

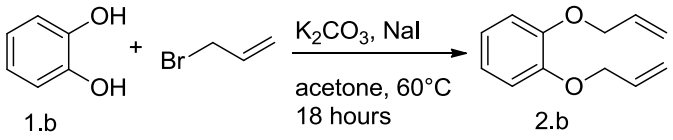

1.b 2.b

82% Yield

Scheme 2.4 - Reaction of catechol with allyl bromide to form catechol diallyl ether.

By a similar allylation method, catechol was used to synthesise the corresponding 1,2-diallylphenyl ether. Following workup, the ^{1}H NMR spectrum shows the product to be pure as compared to the literature data[186] (Figure 2.5). The multiplet that appears at 6.92ppm (4H) correlates to hydrogens attached to the aromatic ring (1 and 2). The doublet of doublet of triplets peak at 6.10ppm (2H, *J*=17.2, 10.5, 5.3Hz) corresponds to the CH on the double bond of the allyl (4). The doublet of quartets 5.45 ppm (2H, *J*=17.3, 1.6Hz) relates to the trans CH_2 for the double bond of the allyl (5). The doublet of doublets of doublets at 5.30 ppm (2H, *J*=10.5, 2.9, 1.4Hz) relates to the cis CH_2 for the double bond of the allyl group (5').

Finally the doublet of triplets at 4.64 ppm (4H, *J*=5.3, 1.5Hz) corresponds to the OCH_2 group (3 and 3').

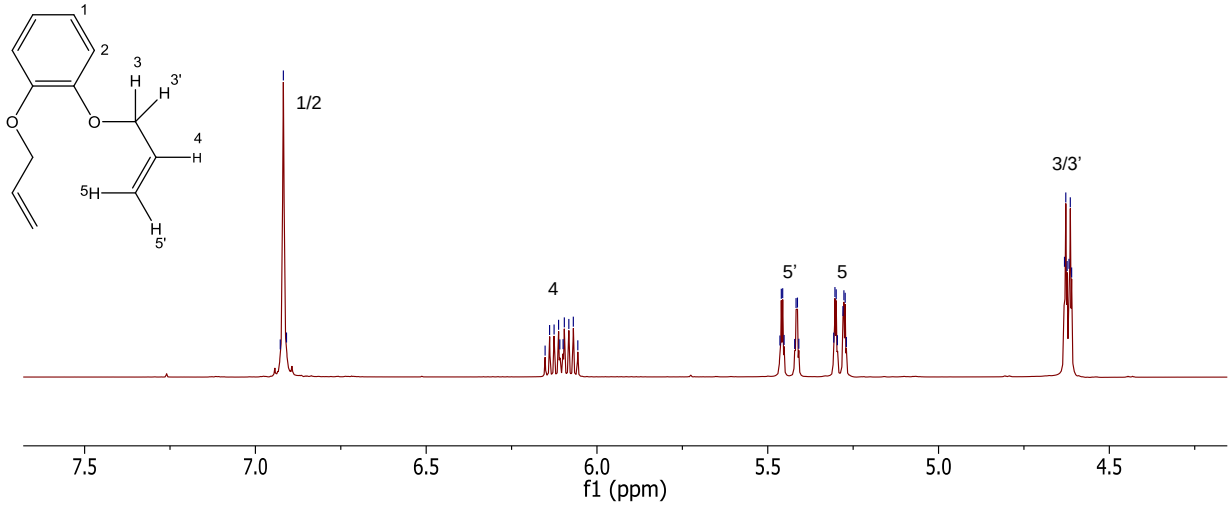

Figure 2.5 – ^{1}H NMR spectrum of catechol diallyl ether.

In the ^{13}C NMR spectrum (Figure 2.6), the peak at 148.62ppm correlates to the quaternary carbon of the aromatic ring (3); 133.61 ppm is the CH for the vinyl (5); 121.29 ppm are the CH on the aromatic ring at the 1 and 1' position; 117.50 ppm is the CH_2 on the double bond for the allyl (6); 114.34 ppm are the CH on the aromatic ring at the 2 and 2' position and 69.93 ppm is the OCH_2 (4) resonance.

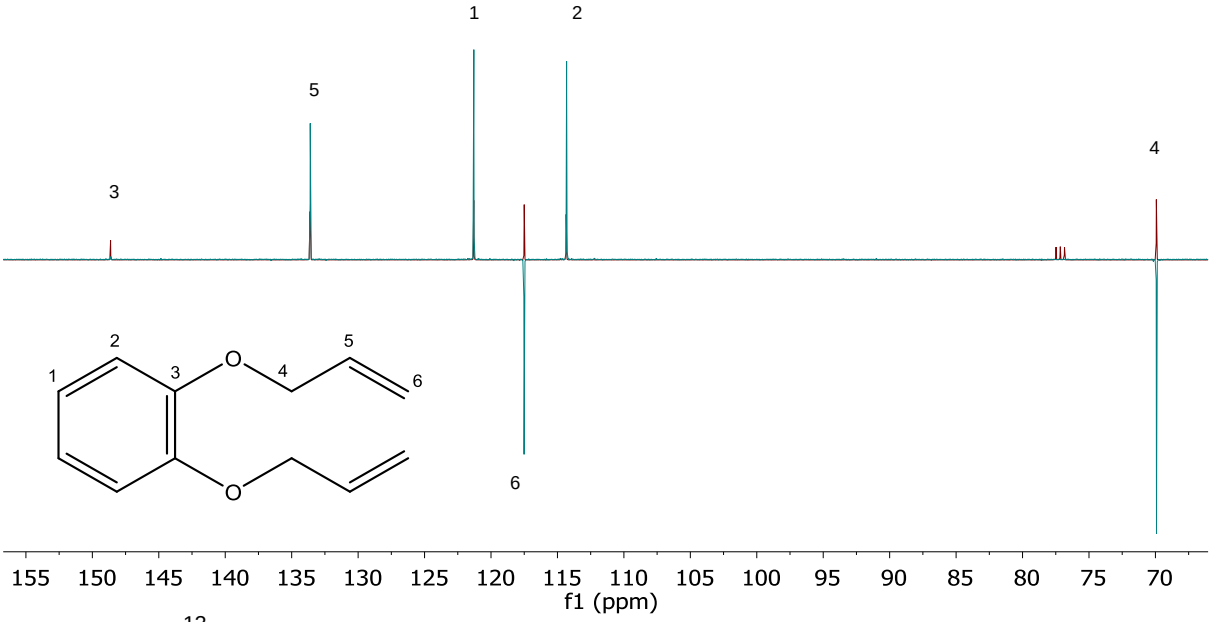

Figure 2.6 – ^{13}C NMR spectrum of catechol diallyl ether

2.2.1.3 Resorcinol 1.c

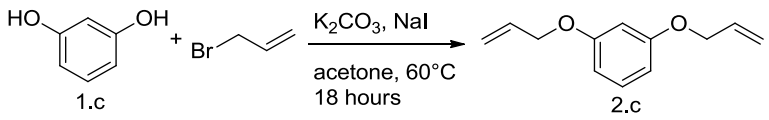

Scheme 2.5 – Synthesis of resorcinol diallyl ether using the Williamson ether reaction.

Similarly, diallylation of 1,3-dihydroxybenzene was performed using the same procedure but, the results obtained for this reaction show that the product obtained was a mixture of two compounds. Before work up, the impure product was analysed using NMR spectroscopy to determine the degree of conversion. This proved to be difficult as many unexpected peaks were present due to the presence of one or more by-products.

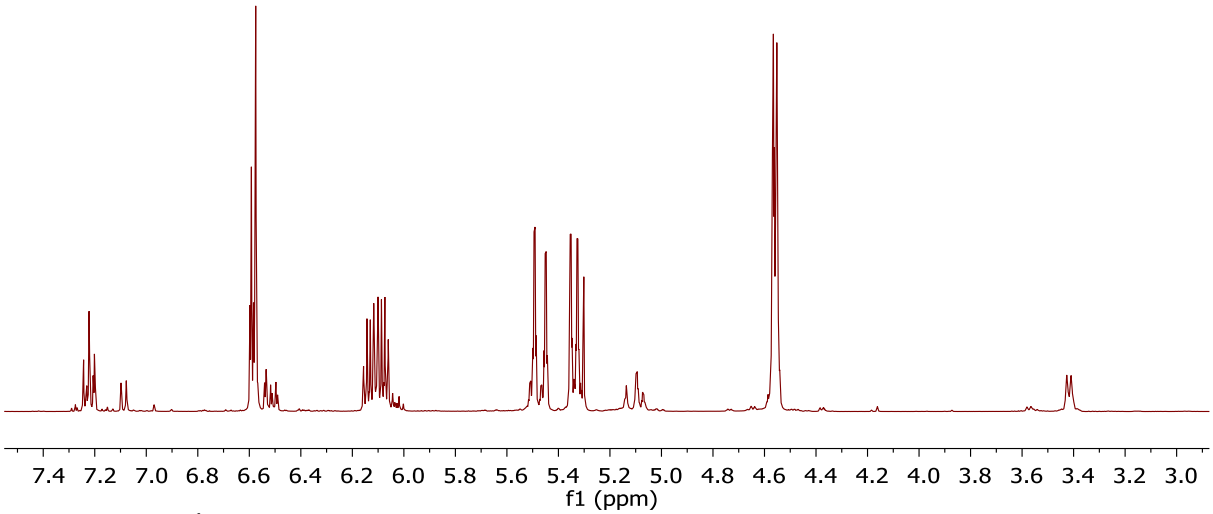

Figure 2.7 – ^{1}H NMR spectra of crude resorcinol diallyl ether

After work up, the sample was again analysed by ^{1}H NMR spectroscopy (Figure 2.7) with the spectrum again showing peaks that are in addition to the peaks derived from the desired product. We propose that by-product (3) has a similar structure to the desired product (2.b) with the only difference being C allylation as shown in Figure 2.8. An attempt to purify this mixture was performed using column chromatography and recrystallization but neither was successful.

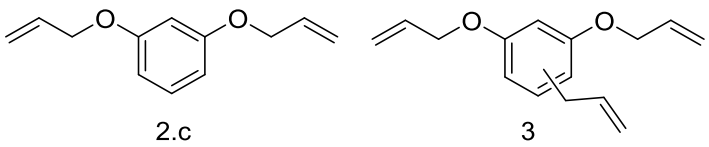

2.c 3

Figure 2.8 Desired product (O-allylated 2.c) and proposed by-product (C/O-allylated 3)[187]

2.2.1.4 – Allylation of resorcinol 2.b using potassium tert-butoxide[188-190]

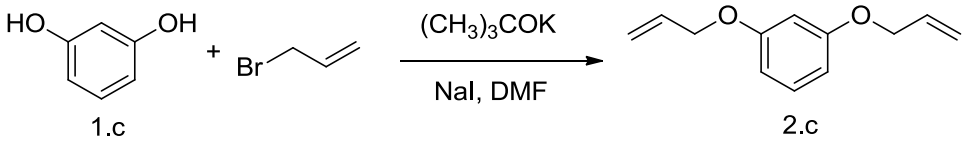

1.c 2.c

Scheme 2.6 – Allylation using potassium *tert*-butoxide

As the synthesis of resorcinol diallyl ether, described above, was not fully successful and the desired product difficult to purify, a different base was used. Astruc *et al.*[189] have shown that potassium *tert*-butoxide is a softer base that may be used to mediate nucleophilic substitution. The reaction was carried out with the hope that less C-allylated by-product would form in the mixture. However, the ^{1}H NMR spectrum (Figure 2.9) of the crude product shows that there is by-product is formed at a similar level to that of previous experiments.

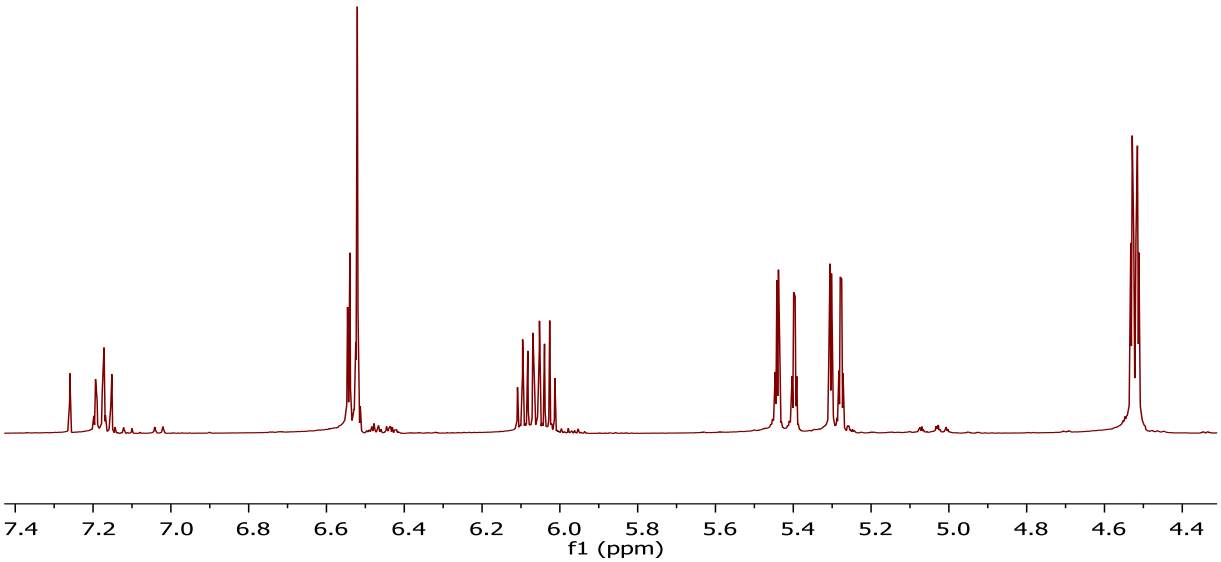

Figure 2.9 – NMR spectrum for the attempted synthesis of resorcinol diallyl ether using potassium *tert*-butoxide as the base.

GC-MS confirms the formation of desired product and the by-product formed with two peaks in the retention time at 14.26 minutes and at 16.59 minutes. The peak at 14.26 min has a mass of 190.1 m/z relating to the desired product and at 16.59 min the mass is 230.2 m/z that corresponds with the by-product. They could not be separated, however, using conventional methods.

There are two possible reasons for the formation of by-product (3). The first is due to electrophilic substitution at the 2, 4 or 6 positions of the aromatic ring that are activated by the hydroxyl groups (as shown in Figure 2.10). Following literature reports[191], resorcinol reacts with formaldehyde to give substitution at the 2, 4 or 6 positions of the aromatic ring. This would explain why there is the appearance of the C-allylated product as well as the O-allylated product as shown in Figure 2.10.

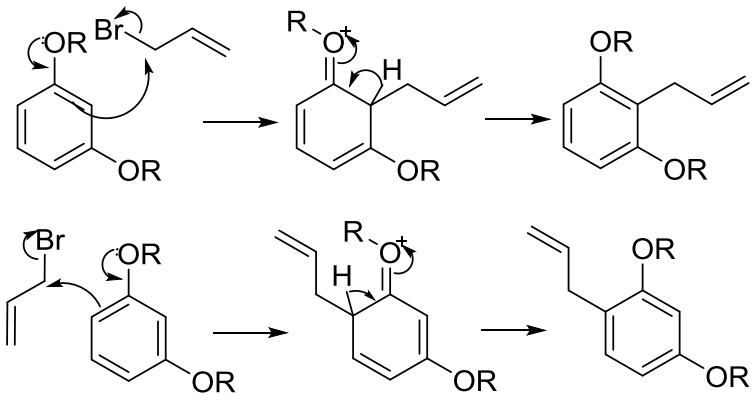

Figure 2.10 – Possible reaction of allyl bromide with resorcinol with the activation of the *ortho* and *para* positions for electrophilic substitution[191]. R= H or $CH_2CH=CH_2$

Another possible reaction mechanism for C-allylation could be Claisen rearrangement (Figure 2.11) of the initial O-allylated product. The rearranged product has been reported before by Hurd *et al.*[187] although a higher temperature for the rearrangement of resorcinol diallyl ether of 210°C[187] was required.

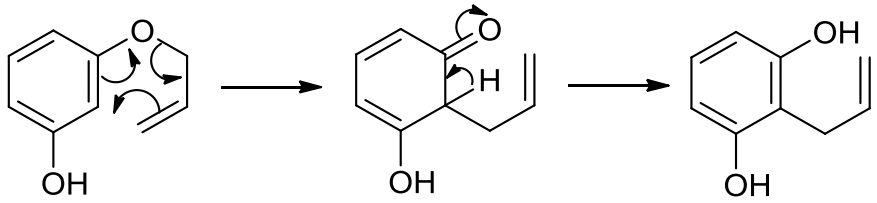

Figure 2.11 – Claisen rearrangement process

Van Rijin has shown that there is the possibility of the C-allylated product being formed from allyl phenol ether where the O-allylated product being the kinetic product and the C-allylated being the thermodynamic product[192]. Therefore, after an increased amount of reaction time there should be an increase of C-allylated product as the kinetic product is converted to the more stable thermodynamic product.

As there is a possibility that the longer reaction times could lead to the C-allylation of resorcinol, a method utilizing a microwave reactor was used to determine which of the two mechanisms (Figure 2.10 or 2.11) is more probable. This was performed using several different solvents and temperatures based on reaction and times reported by Moseley[193]. The synthesis of diallyl ethers of hydroquinone and resorcinol were accomplished by Williamson ether synthesis using microwave irradiation. By changing the solvent and temperatures the best reaction conditions were determined, with results recorded in Table 2.1. The procedure used was similar to those described above in section 2.1.1 with only the solvent and heating method changing. All the NMR spectroscopy data showed products that are consistent to those that were previously obtained. For hydroquinone diallyl ether, NMR spectroscopy shows that the sample produced by microwave heating was pure. As can be seen in Table 2.1 the most suitable parameters were acetone at 55°C as this produced the highest yield of the desired product.

As can be seen for the resorcinol each of the reactions produced the desired product but with the by-product being present, apart for the reaction with NMP, which gave no desired product or by-product. The best system for this reaction appeared to be acetone at 70°C, which will be the conditions used for all future reactions.

Table 2.1 – The effect of different solvents and temperatures on the yields of bisallylated products against the yield of C-allylated by-product

Diol	Solvent	Time (min)	Temperature (°C)	Yield Product (%)	Yield By-product (%)
Hydroquinone	DMA	20	150	96	-
	NMP	20	150	79	-
	Acetone	20	55	99	-
Resorcinol	DMA	15	150	66	34
	NMP	15	150	-	-
	DMF	20	150	65	35
	DMF	40	70	79	21
	Acetone	40	100	79	21
	Acetone	40	70	81	19

Since the reaction time is believed to be a factor in producing the C-allylated by-product, therefore changing the reaction time was performed to determine the effect on the ratio of the products obtained. The three reaction times that were studied were 15 minutes, 30 minutes and 60 minutes. However, the NMR spectra for each of the reaction mixtures were similar to those obtained previously, with exactly the same peaks occurring in the same ratios. This seems to show that there is no influence of the reaction time on the amount of by-product made and, therefore, shows that the Claisen rearrangement is less likely. It was found by changing the reaction times there was an increase in the sample yield, with 15 minutes obtaining 36% overall product whereas 30 minutes yielded 62% and for 60 minutes 63%.

Previous experiments were carried out using 2.2 equivalents of allyl bromide to resorcinol, to ensure that there was full allylation occurring. By changing the number of equivalents to 1.5 and 4 it was hoped that there would be a change in the amount of by-product formed. However, no significant change in product composition was observed under the reaction conditions used.

2.2.2 – Conclusion

Bisallyl ethers of hydroquinone and catechol were synthesised and purified using conventional Williamson ether synthesis utilizing allyl bromide as the electrophile. However, a similar process for the resorcinol isomer gave a mixture of bisallyl systems and by-product(s). From the reactions performed, by-products are most probably formed by an electrophilic substitution process. This method of synthesising the resorcinol derivative was abandoned as the end product, resorcinol diglycidyl ether, is commercially available and can be readily purified. All three bisallyl systems were now available in high purity and quantities which were suitable for subsequent epoxidation studies.

2.3 – Epoxidation using trichloroisocyanuric acid

The conventional method for the synthesis of epoxides is to use epichlorohydrin as described in Chapter 1 but this leads to the formation of oligomers, which is undesirable. Therefore, a more selective method was assessed utilizing research by Wengert *et al.*[167] which involves reaction of alkenes with trichloroisocyanuric acid. They claim to have developed a method that produces pure epoxides in good yields using simple, cheap and safe reagents. This method is a two-step process which first involves synthesising chlorohydrins, followed by the ring-closing of the chlorohydrin to produce the epoxide, as shown in Scheme 2.7.

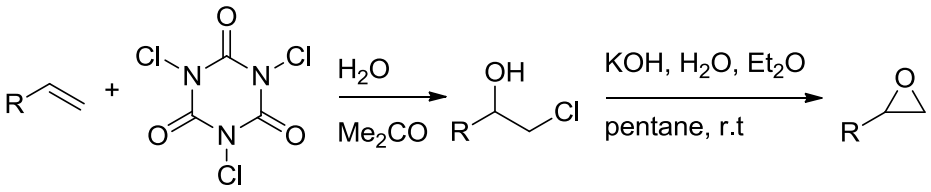

Scheme 2.7 – Synthesis of epoxides using trichloroisocyanuric acid

The process occurs by the hydrolysis of trichloroisocyanuric acid to give both hypochlorous acid and cyanuric acid. The hypochlorous acid can then react with the double bond of the alkene giving the chlorohydrin by electrophilic addition.

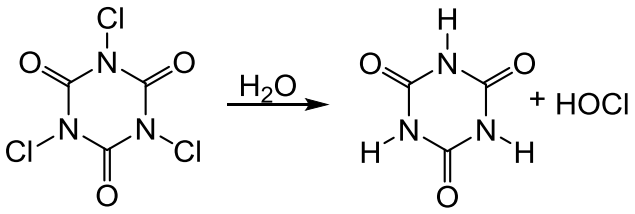

Scheme 2.8 – Hydrolysis of trichloroisocyanuric acid and synthesis of hypochlorous acid[194]

Once the chlorohydrin has been synthesised this, ring closure via an S_N2 process in the presence of a base, gives the desired epoxide.

2.3.1 – Synthesis of chlorohydrins

The diallyl products prepared from hydroquinone and catechol as described in section 2.1 were the substrates for epoxidation.

2.3.1.1 – Synthesis of hydroquinone dichlorohydrin ether

Diallyl system 2a and trichloroisocyanuric acid were stirred in acetone at 0°C to room temperature over-night and, after standard work up, a crude product was obtained.

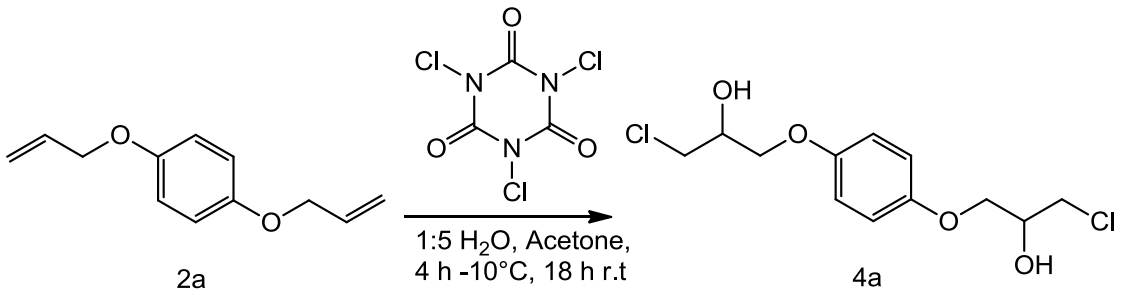

Scheme 2.9 – Formation of hydroquinone dichlorohydrin ether

The ^{1}H NMR analysis of the crude chlorohydrin was difficult to interpret due to the presence of two chiral centres in the product. There are several possible diastereoisomers, as shown in Figure 2.13, which could be the reason for the complicated ^{1}H NMR spectra in Figure 2.14. However, it is possible by using both 2D NMR spectroscopy and prediction software to assign the resonances. GC-MS (Figure 2.15) of the crude product shows that there are three main components which all have a mass of 294.0 m/z, which is consistent with the mass of dichlorohydrin at 294.0. Therefore the presence of the three components in the GC trace supports the hypothesis that there are different orientations (S,R'; S,S' and R,R').

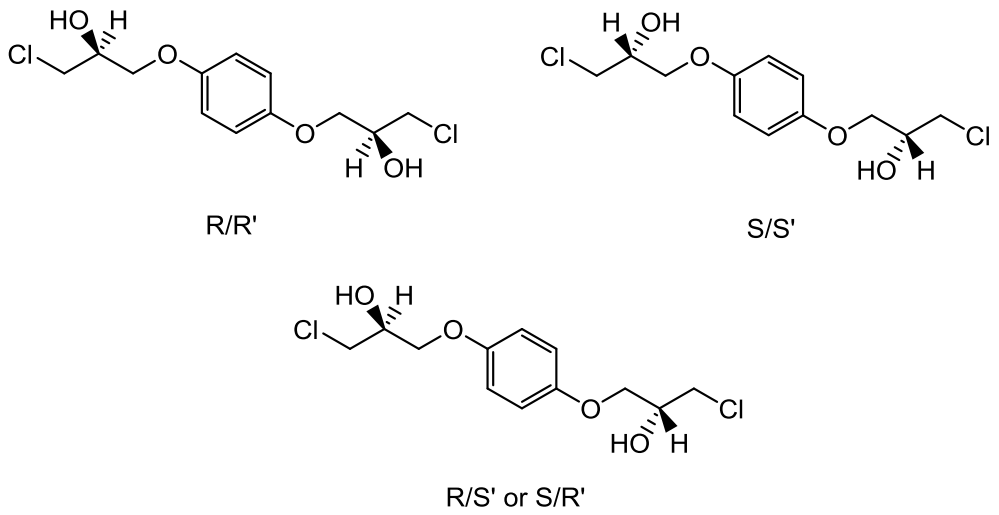

Figure. 2.13 – Structural orientation around the chiral centre.

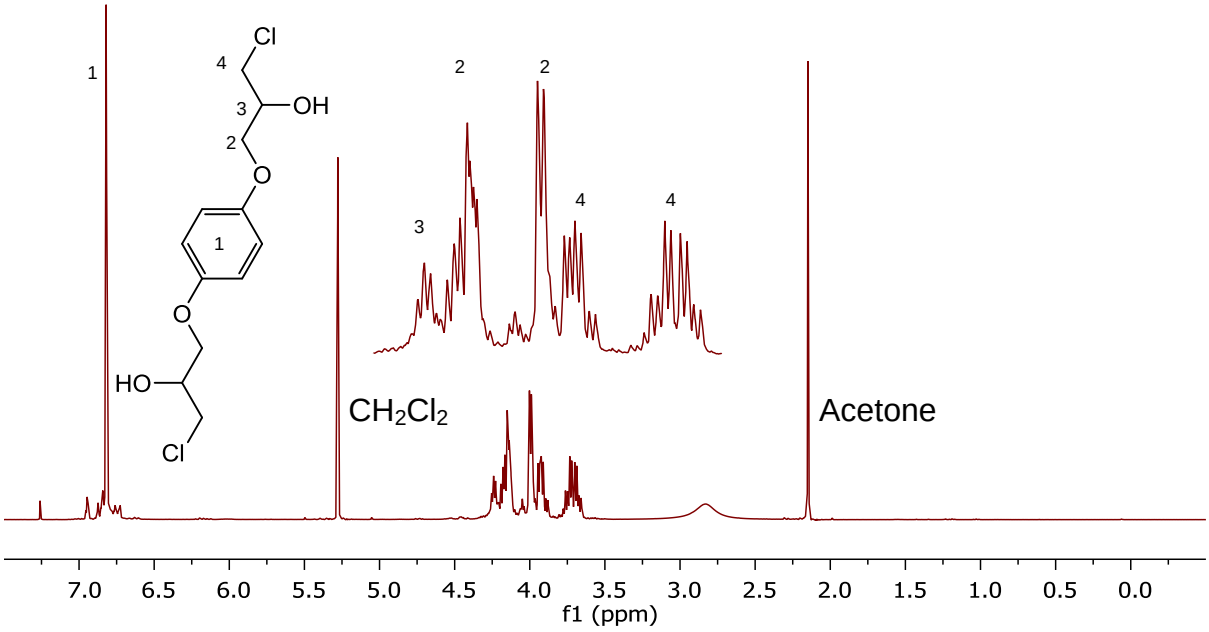

Figure 2.14 – ^{1}H NMR spectrum for hydroquinone dichlorohydrin ether.

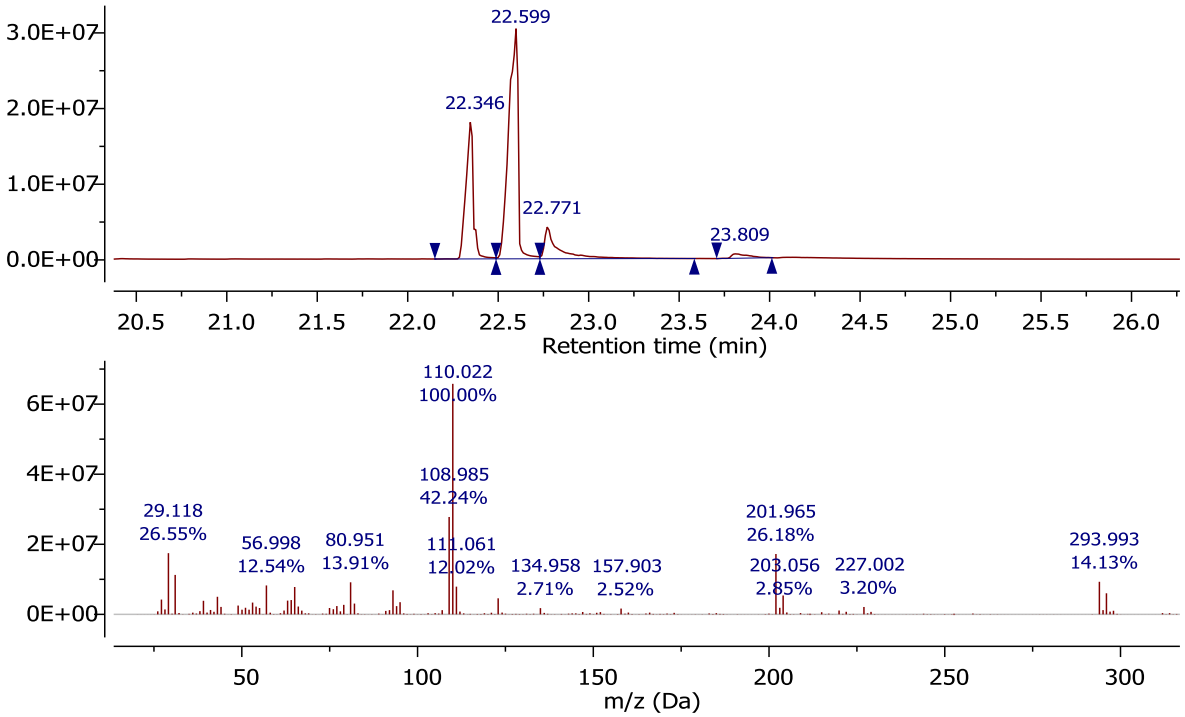

Figure 2.15 – GC-MS spectrum for hydroquinone dichlorohydrin ether. The selected mass spectrum is for peaks 22.35; 22.60 and 22.77 min which relate to the mass of the desired product. The mass peak of 110.0 m/z relates to hydroquinone which occurs due to fragmentation.

2.3.1.2 – Synthesis of catechol dichlorohydrin ether

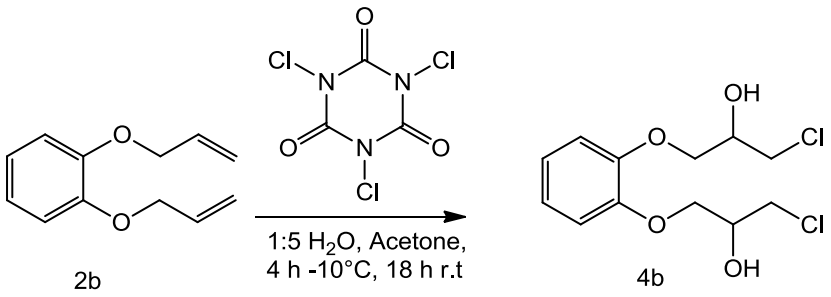

Scheme 2.10 – Formation of catechol dichlorohydrin ether

As the synthesis method used for hydroquinone was a success the same method was applied to the bisallyl catechol derivative. GC-MS analysis of the crude product (Figure 2.17) shows two sets of components. Three peaks (54% of the sample) having the same mass of 294.0 m/z which is expected of the desired

product (4.b) are observed and also a second set of three peaks (46%) of the sample that have a higher mass of 328.0 m/z (Figure 2.17) consistent with an additional chlorine atom attached to the aromatic ring. Work by Silva *et al*[195] reports ring chlorination using trichloroisocyanuric acid with an isatin, that has the nitrogen species protected, in acetone at room temperature after only two hours (Scheme 2.11) and so competing chlorination of catechol derivatives is reasonable.

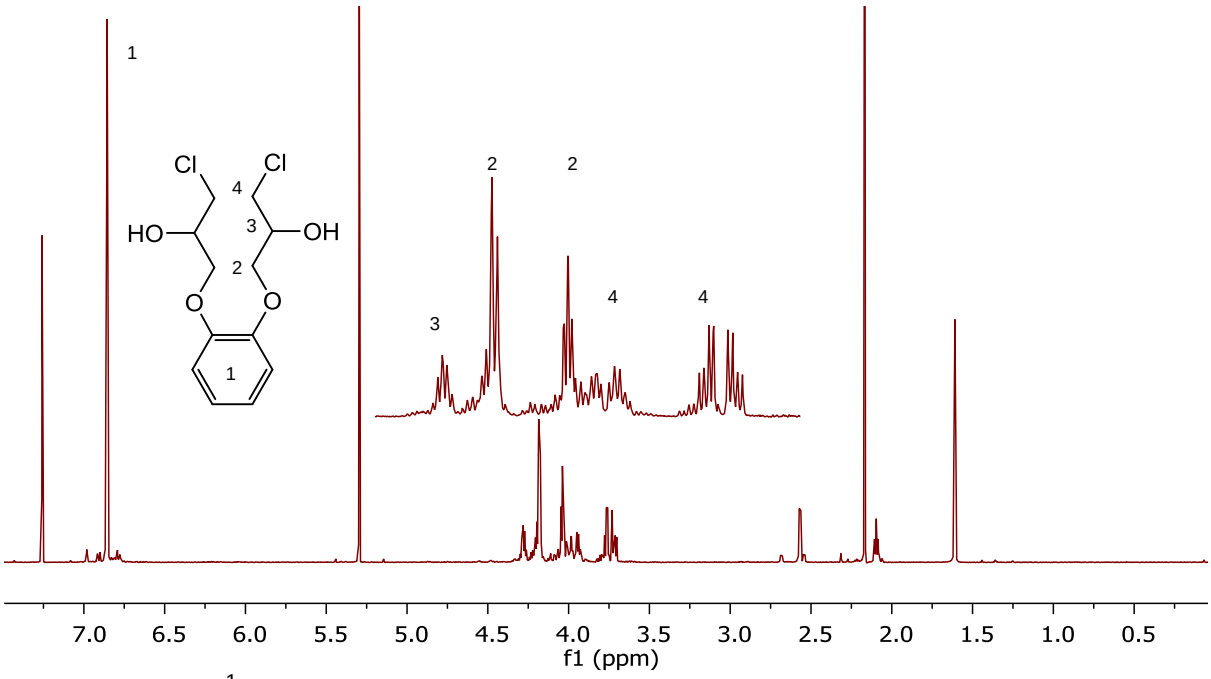

Figure 2.16 – ^{1}H NMR spectrum for catechol dichlorohydrin ether. The peaks at 1.61, 2.15 and 5.28 ppm correspond to water, acetone and dichloromethane respectively.

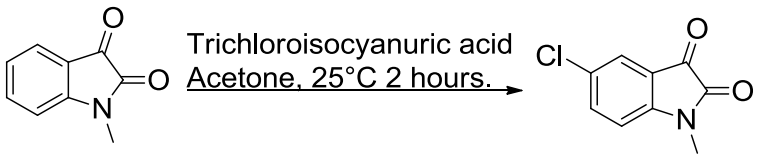

Scheme 2.11 – Aromatic chlorination of isatin using trichloroisocyanuric acid in acetone[195].

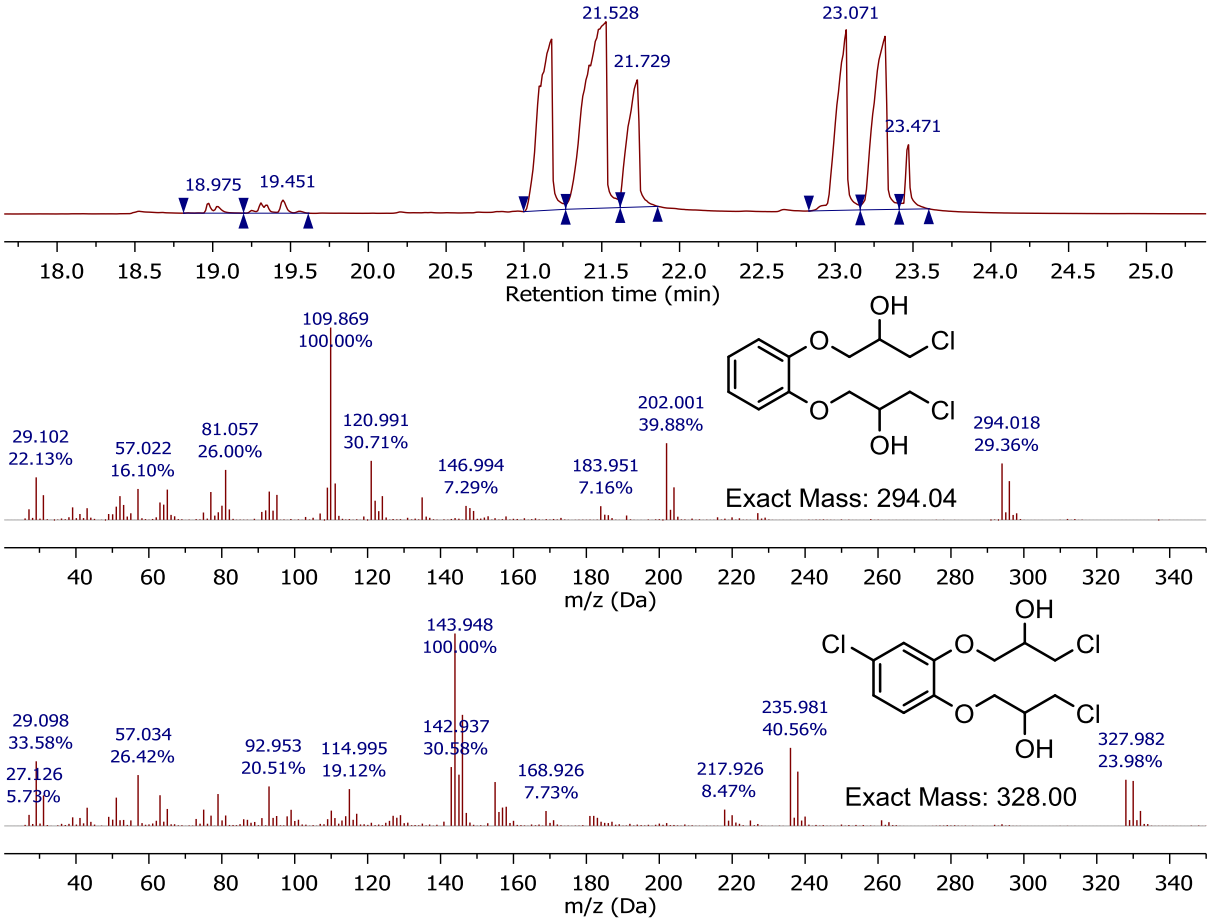

Figure 2.17 – GC-MS spectrum of crude product of hydrochlorination of catechol. The selected mass spectrum is for peaks 21.21, 21.53 and 21.73 min which relate to the mass of the desired product. The mass peak of 110 m/z relates to catechol which occurs due to fragmentation. The peaks at 23.07, 23.32 and 23.47 min, relates to a mass of 328 m/z which is indicative of another chlorine atom attached to the molecule.

With these results in mind, reactions to limit the production of the ring chlorinated species by either reducing the reaction time or by decreasing the equivalents of trichloroisocyanuric acid were attempted.

2.3.1.2.1 – Reducing reaction time to 1 hour

By reducing the reaction time to 1 hour consistent with conditions given in Wengert *et al.*'s paper[167], it was hoped that there would be a limit to the amount of ring chlorination occurring. GC-MS (Figure 2.18) shows that several products are

formed, with the same two sets of three products as previously discussed but with also a second set of 2 and 3 products with lower retention time. The main set of three products occurring at 5.83 to 5.99 min relate to the desired product of the chlorohydrin, with the other three products at 6.52 to 6.73 min relating to the ring chlorinated species. However the lower products at 4.90 to 4.95 min appear to have a mass of 242.1 which relates to a monochlorohydrin species that shows that the reaction time is not sufficient for all alkene functional groups to react with the TCA. There was, however, another set of products at 5.33 to 5.43 min which have a mass of 276.1 which relate to a monochlorohydrin with ring chlorination. From GC analysis it is possible to determine that there is only a 52% conversion to the desired product, 23% conversion to the dichlorohydrin ring chlorinated product, 12% of the monochlorohydrin and 13% of the monochlorohydrin with ring chlorination. This suggests that the ring chlorination does not occur after synthesis of the chlorohydrin but is a competitive process.

By reducing the number of equivalents of TCA, a similar number of products were found which could not be separated. By using a lower reaction time and lower equivalents of TCA also led to a mixture of chlorinated products which could not be separated by various techniques such as, recrystallization, vacuum distillation and TLC. The reaction mixtures were used without purification in subsequent reactions.

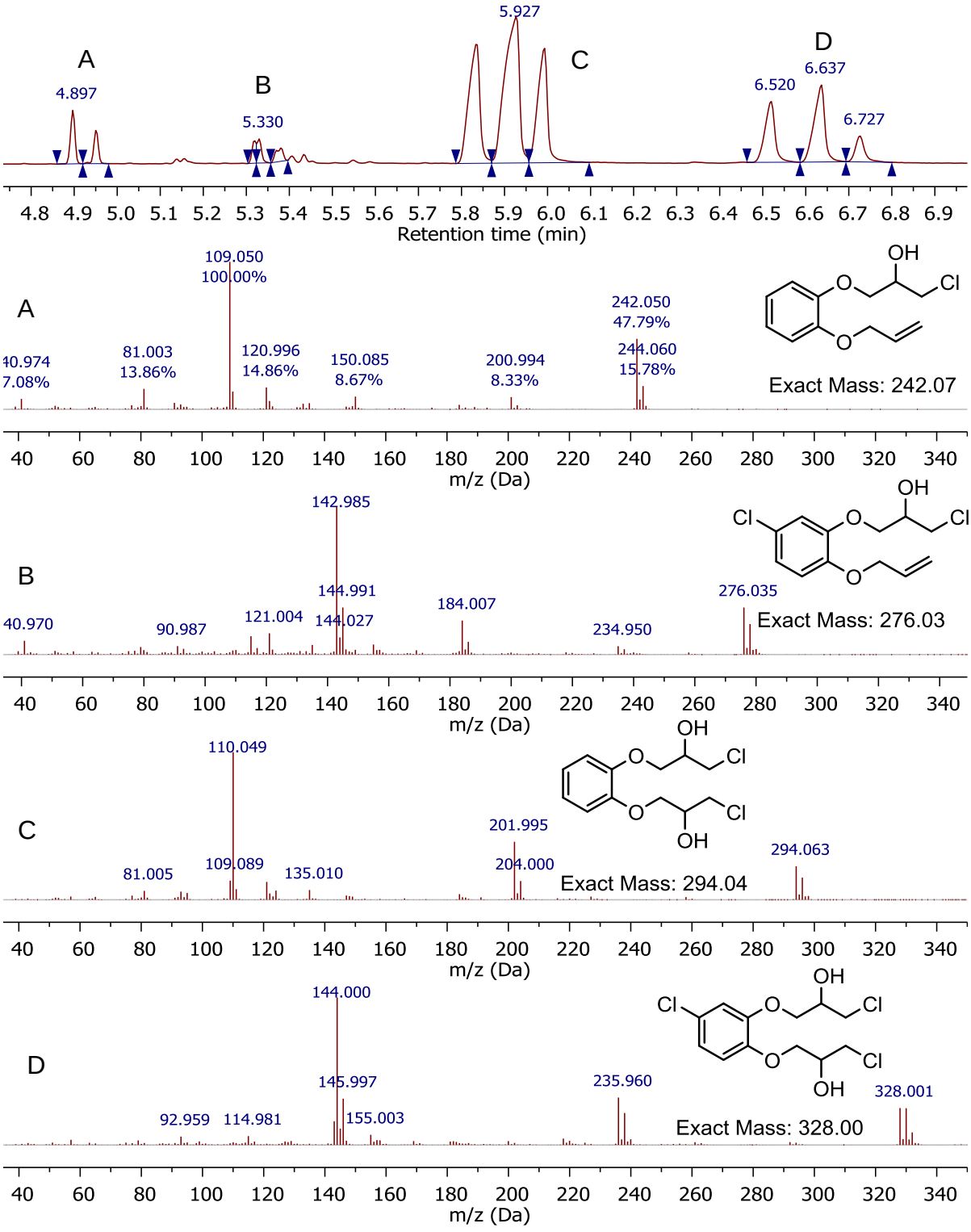

Figure 2.18 – GC-MS spectrum for reaction of catechol diallyl ether with TCA after 1 hour.

2.3.2 – Dechlorination and epoxide formation

Once the chlorohydrin substrates had been prepared epoxide formation was studied.

2.3.2.1 – Epoxidation of hydroquinone dichlorohydrin ether

Dichlorohydrin was stirred with potassium hydroxide in water, ether and pentane mixture at room temperature and a precipitate formed. This was isolated by filtration and analysed.

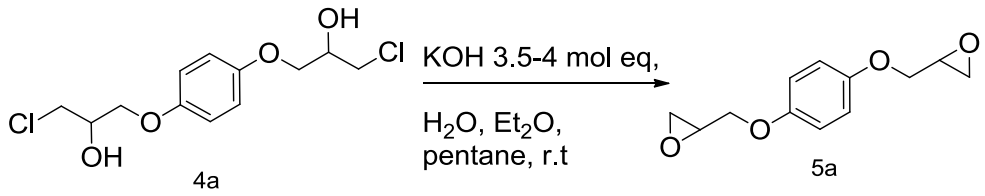

Scheme 2.12 – Ring closing of hydroquinone dichlorohydrin ether to create hydroquinone diglycidyl ether.

Analysis of the product by ^{1}H NMR spectroscopy (Figure 2.20) suggests that there is 89% conversion of the chlorohydrin to the epoxide. As can be seen by GC-MS analysis (Figure 2.21) there is one major product present which has a retention time of 18.74 relating to the desired product which has a mass of 222 Daltons.

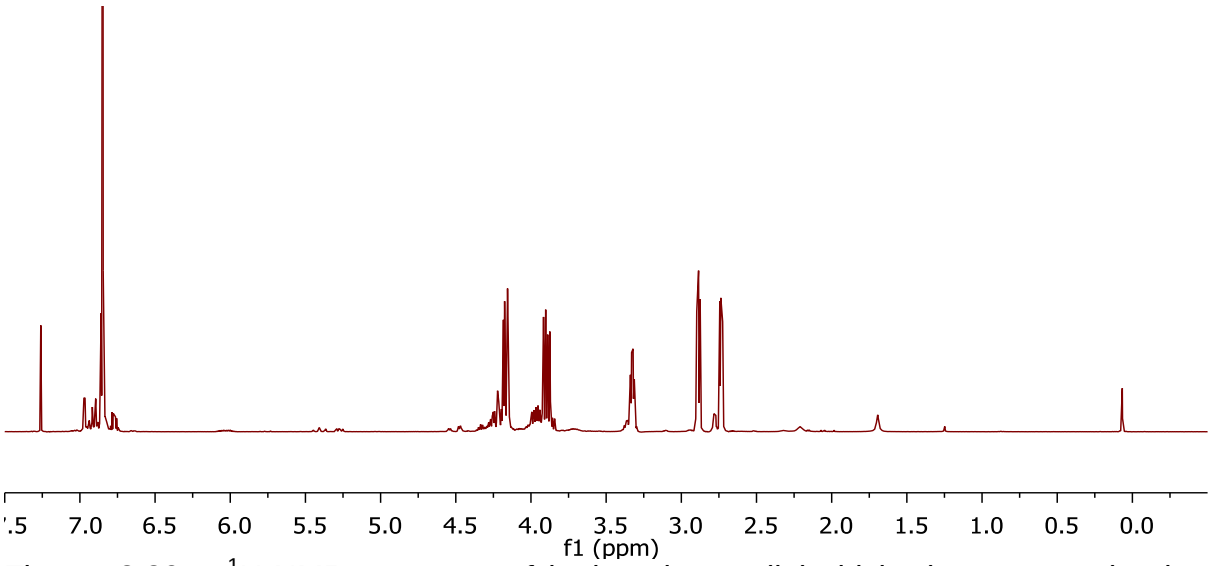

Figure. 2.20 – ^{1}H NMR spectrum of hydroquinone diglycidyl ether prepared using trichloroisocyanuric acid.

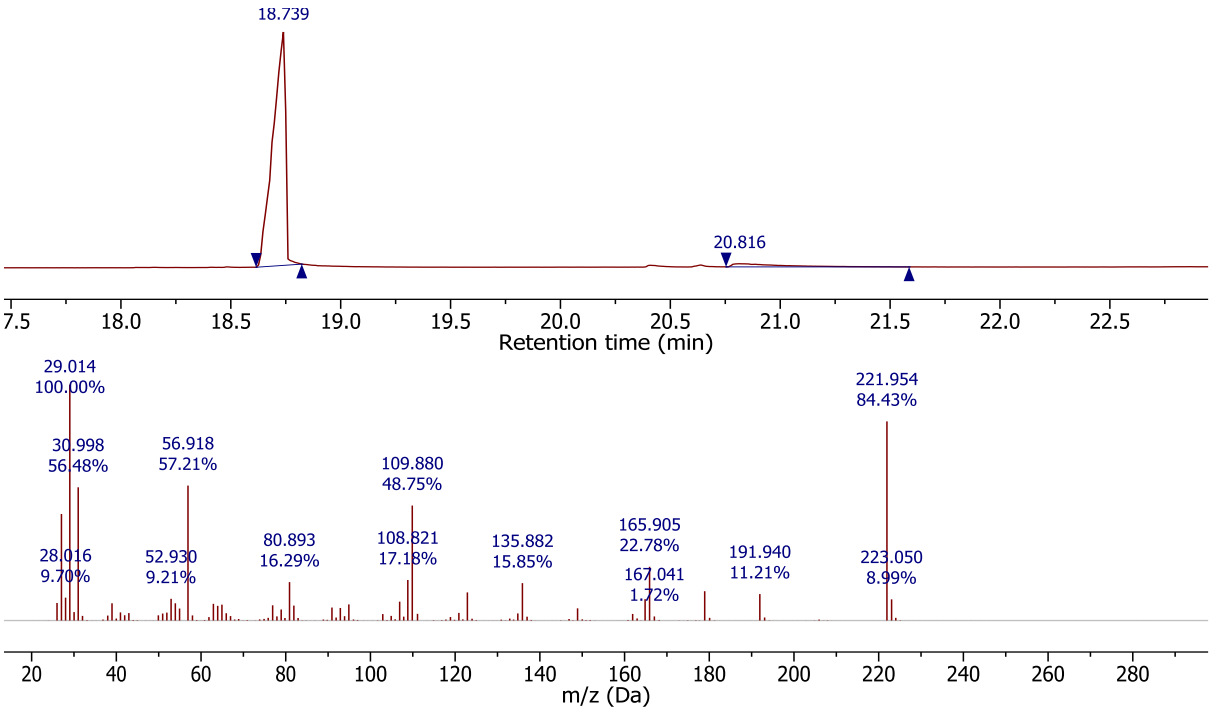

Figure 2.21 – GC-MS for hydroquinone diglycidyl ether prepared by trichloroisocyanuric acid

2.3.2.2 – Epoxidation of catechol dichlorohydrin ether

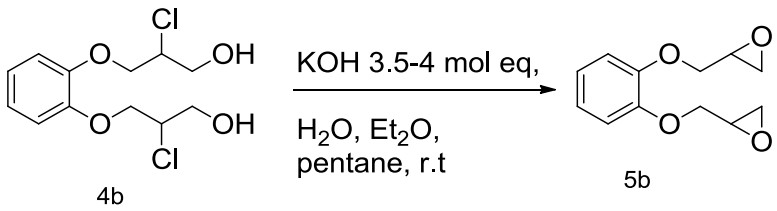

4b 5b

Scheme 2.13 – Ring closing of catechol dichlorohydrin ether to create catechol diglycidyl ether.

Using the same reaction conditions as described for hydroquinone, an attempt was made to ring close the bisallyl catechol derivative. As can be seen in the ^{1}H NMR spectrum (Figure. 2.22) there is still evidence of several other products. GC-MS analysis shows that (Figure 2.23) it is possible to identify the impurities in the sample, with 27% of the desired product at peak 5.06 mins (222 m/z); 14% ring chlorinated product (256 m/z) and 22% monoepoxide (258 m/z). There is also evidence of dichlorohydrin at peak 5.97 mins with 26% of this occurring and 11% of the ring chlorinated dichlorohydrin at 6.17 mins. Even with the production of the bisepoxide it was still impossible to separate the products by several different purification techniques (re-crystallization, distillation and TLC column) and, therefore, this method was deemed unsuitable for the synthesis of catechol diglycidyl ether.

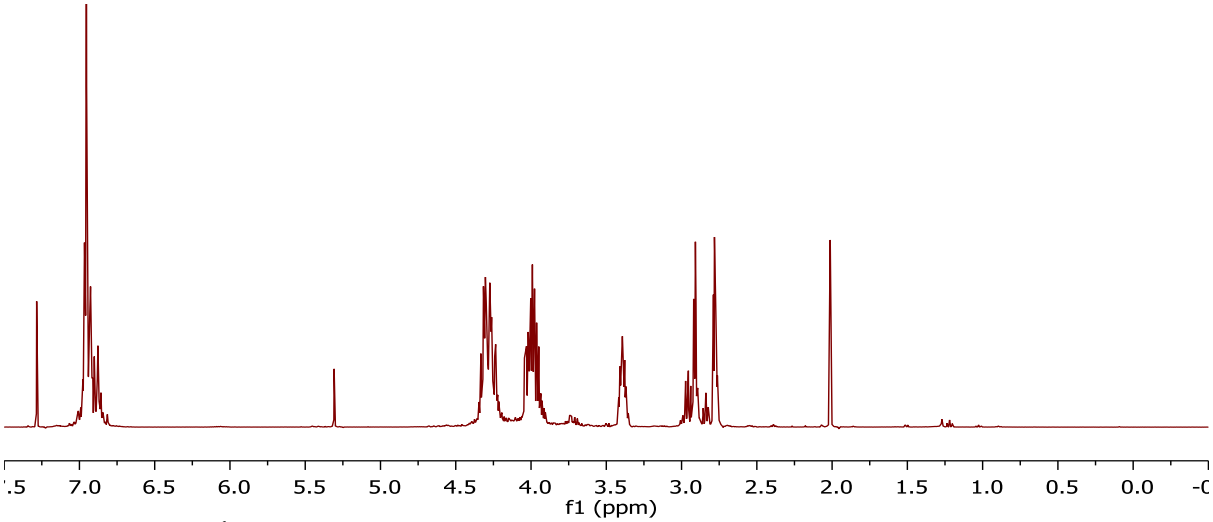

Figure 2.22 – ^{1}H NMR for catechol diglycidyl ether after 3.5 molar equivalents of potassium hydroxide. The peaks at 2.16 and 5.29 ppm correspond to acetone and dichloromethane respectively.

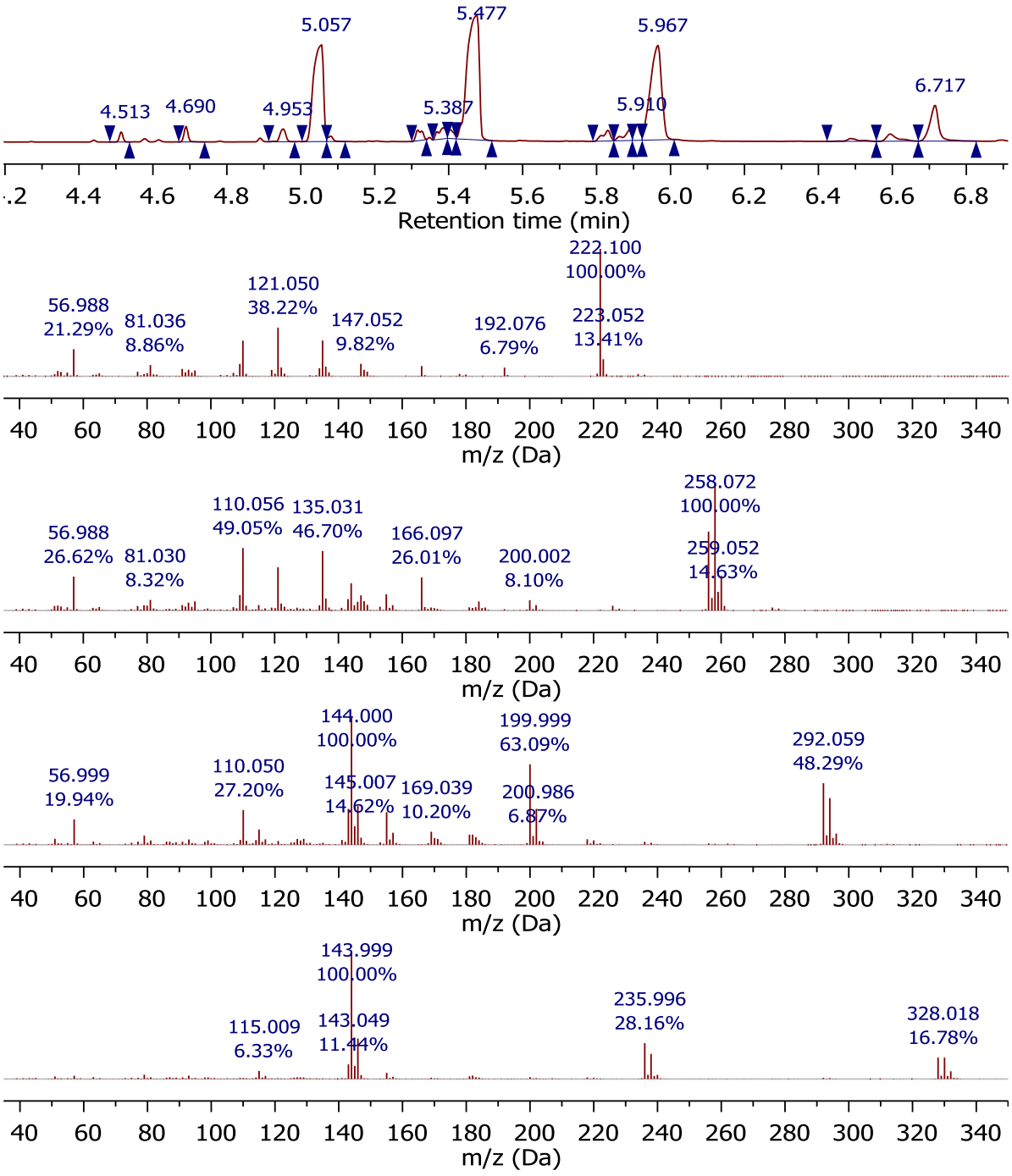

Figure 2.23 – GC-MS for catechol diglycidyl ether after 3 equivalents of potassium hydroxide.

2.3.3 – Conclusion

Formulation of the hydroquinone bisepoxide derivative was successful. The readiness for the hydroquinone diglycidyl ether to precipitate out of the reaction solution is useful as it is easier to purify. Therefore, for hydroquinone glycidyl ether, this method of synthesis was successful.

With the catechol derivative, however, there are several problems that arise from using the chlorohydrin/ epoxide method of synthesis. Firstly there is significant competing ring chlorination that occurs during the synthesis of the chlorohydrin which appears to occur even at lower reaction times and lower equivalents of trichloroisocyanuric acid. Consequently, this method is not a viable method for the synthesis of catechol diglycidyl ether.

2.4 – Conclusions

In this chapter we have successfully shown the synthesis and purification of both hydroquinone and catechol bisallyl ethers using the Williamson ether reaction. For these systems it was possible to produce highly pure bisallyl derivatives in suitable quantities for subsequent studies. The resorcinol derivative, however, produced by-products formed by an electrophilic substitution process. This was shown to form due to activation of the 2, 4 and 6 positions on the aromatic ring and subsequent electrophilic substitution reaction with allyl bromide. Changing several parameters showed no change in the ratio of the desired product to by-product. Therefore, this method of synthesis was unsuitable for the synthesis of the bisallyl derivative of resorcinol, however, this is commercially available (as prepared by addition of epichlorohydrin to resorcinol in the presence of sodium hydroxide) and readily purified as discussed in Chapter 4.

Conventional methods of epoxidation using trichloroisocyanuric acid show mixed results with the hydrochlorination of the bisallyl hydroquinone derivative showing 96% conversion whereas the hydrochlorination of the bisallyl catechol system gives a mixture of products due to ring chlorination.

Subsequent formation of the epoxide for the bisallyl hydroquinone system shows that there is formation of the desired product containing a slight amount of either the monoepoxide or a possible ring chlorinated product, possibly carried over from the hydrochlorination. However, catechol formed several products of containing monoepoxides which created a complex mixture which could not be separated.

This shows that the conventional synthesis of hydroquinone diglycidyl ether was possible with good yields and is possible to scale up, whereas for the catechol derivative the synthesis is not possible due to the ring chlorination.

Chapter 3 – Epoxidation using HOF.MeCN

3.1 – Aims and approach

When fluorine is reacted with water in acetonitrile, a HOF.MeCN complex is formed. This discovery was made by a pioneer in the field of fluorine chemistry, Professor Shlomo Rozen. Whilst hypofluorous acid had been known for several years it was too unstable to be useful for synthesis but a complex of HOF with acetonitrile makes the HOF reagent more stable with an estimated half-life of approximately 30 minutes at room temperature. HOF.MeCN is considered to be the most effective oxygen transfer agent available to date with reaction times of seconds being recorded to give full conversion in some oxidation reactions[181]. For example the oxidation of pyrene occurs within 5 seconds upon reaction with this powerful oxidising reagent[180, 182].

We planned to develop a method for the epoxidation of alkenes using HOF.MeCN based on previous work by McPake et al.[196] as a method to make pure epoxides without some of the usual impurities that we found in the "conventional" methods as discussed in Chapter 2.

The aim of this chapter was to produce pure, fully characterised bisepoxides which can be used to produce model polymer systems by utilizing route 2 (Scheme 2.1). To obtain pure products, ideal reaction parameters would need to be established to ensure that maximum conversion and yield were obtained, including fluorine flow rate, equipment and solvent quantities, which would then be scaled up because large amounts of bisepoxides are required.

Upon completion of the synthesis, this HOF.MeCN method will be compared to the method described in section 2.3 which utilizes trichloroisocyanuric acid.

3.2 – Safe use of elemental fluorine

3.2.1. – Health and safety

Due to the high reactivity of elemental fluorine, exposure to high concentrations of F_2 is toxic and corrosive to human tissues. Therefore, there is an EEL (emergency exposure limit) of 15 ppm over a period of 10 minutes which is equal to 150 ppm per minute as suggested by the National Research Council[197]. Extensive studies to determine the toxicological effects of fluorine have been carried out with Keplinger and Sussia reporting a median lethal concentration limit (LC_{50}) of 700 ppm per 5 minutes.[198] However, it is possible to reduce the associated hazards and toxicity of fluorine by dilution using nitrogen. The supplied cylinder at Durham has a concentration of 20% by volume of fluorine in nitrogen, which is then further diluted in most cases to a 10% mixture with N_2. This reduces the reactivity of the F_2 mixture but also limits the risks associated, as it is possible to detect fluorine at levels of as low as 35 ppb due to its distinctive odour[199].

With the production of HOF.MeCN from F_2 and water there is also one equivalent of HF produced, and so the hazards associated with using HF need to be taken into account. Hydrofluoric acid (aqueous HF) can cause a variety of problems when exposed to the skin and eyes. When in contact with the skin HF has the ability to penetrate deep into the tissue and cause necrosis of the soft tissue and even decalcification of bone. This is due to the fluoride ions' ability to migrate through cell membranes and attack enzymes in the body leading to severe burns. Concentrated solutions of HF (70%) have been reported to cause pulmonary edema and death within 2 hours of exposure. Therefore, Durham University requires all personnel using HF, which may be generated as side-products in reactions, to attend a safety course and have an antidote gel (calcium gluconate) available. As an added precaution saturated sodium bicarbonate solution was added to reactions after collection to neutralise any HF present.

3.2.2 – Equipment set up for handling fluorine gas

The set-up for the fluorine apparatus shown in Figure 3.1 is based on a previous design already developed at Durham University[200]. The rig was purposely built for the safe use of elemental fluorine in continuous flow reactor apparatus. Although there have been minor variations to the design with regards to this project, the apparatus is essentially described as below.

The permanent storage cylinder (A) is connected to both nitrogen and a 20% fluorine in nitrogen cylinder[i], and has an analogue pressure gauge attached. This is operated by the valve control board (B) which controls the flow of fluorine and nitrogen into a separate storage cylinder. Flow out of the storage cylinder is controlled by valve board (C) which is connected to both the reaction set up (D-F) and also the soda lime 'scrubber' (G). The mass flow controller (D) is used to control the gas flow through the reaction apparatus at a maximum flow rate of 100 mL min^{-1} which is calibrated for the use of fluorine. This is operated by the flow control box (E) which is used to set the gas flow rates. The desired reaction set up can vary but generally consists of a micro reactor, collection pot and a set of syringe or HPLC pumps. Any excess fluorine from the reaction will then pass into a soda lime scrubber (G) which is a metal cylinder containing 75% calcium hydroxide which will react with the remaining fluorine and any HF product. This can also be accessed through both of the valve control boards so that any excess fluorine in any part of the rig can be removed safely.

All valves and connectors used are made from Alloy 400 as supplied by Swagelok® with the metallic tubing being made of stainless steel. Teflon tubing is used for the reaction apparatus (F) as these parts are frequently moved and changed. The tubing is all connected by Swagelok® Alloy 400 connectors.

i – The 20% fluorine cylinder is housed in its own vented container which unless used is locked when not in use.

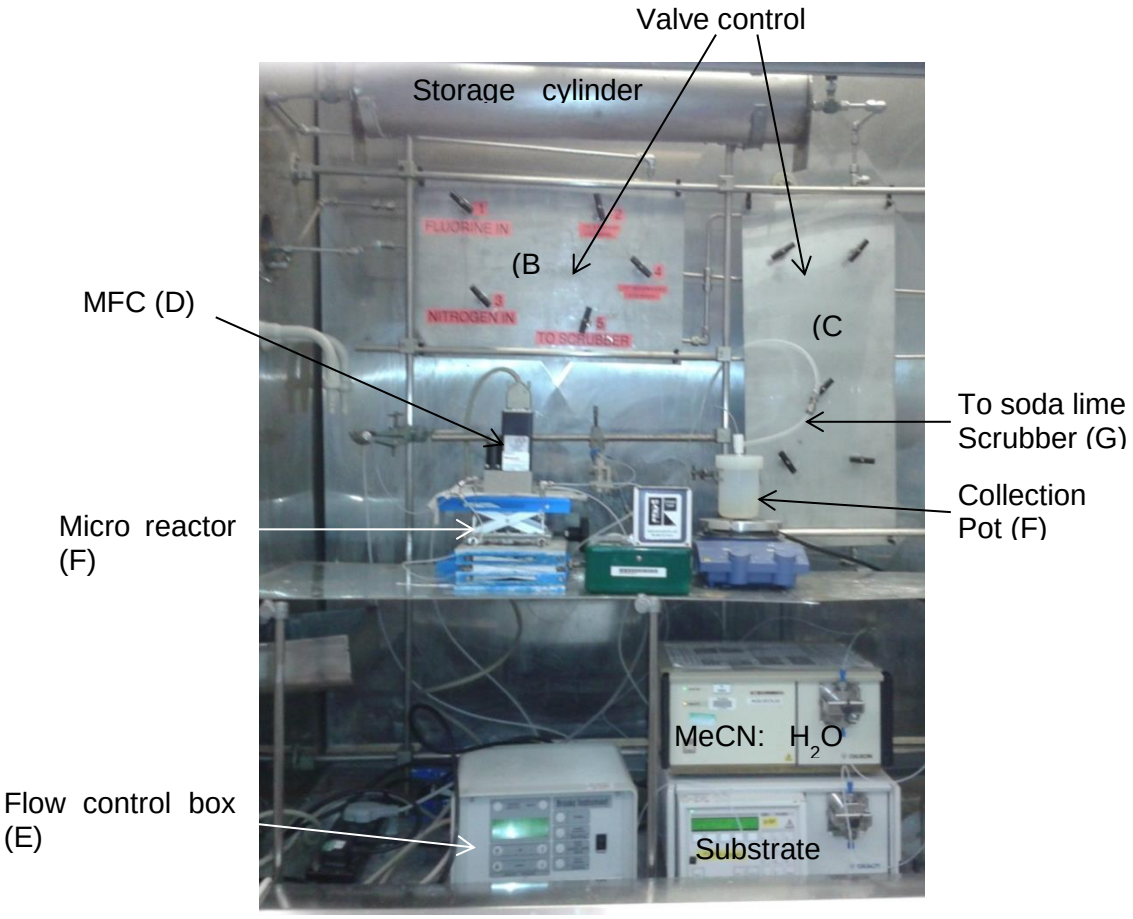

Figure 3.1 – Apparatus for the fluorine rig for HOF.MeCN reactions.

3.2.3 – Passivation of the apparatus

Before the rig in Figure 3.1 could be used, all of the components had to be passivated using different concentrations of fluorine in nitrogen, to protect the metallic components of the apparatus from corrosion. The way in which passivation protects the metal components is by coating the metal substrate with a metal fluoride surface which helps to prevent corrosion and subsequent leaking. Using initial low concentrations of fluorine allows the build-up of the metal fluoride on the metal components over the period of exposure. Every time a metal component is either introduced or replaced, this procedure has to be performed.

3.3 – Batch Epoxidation using HOF.MeCN

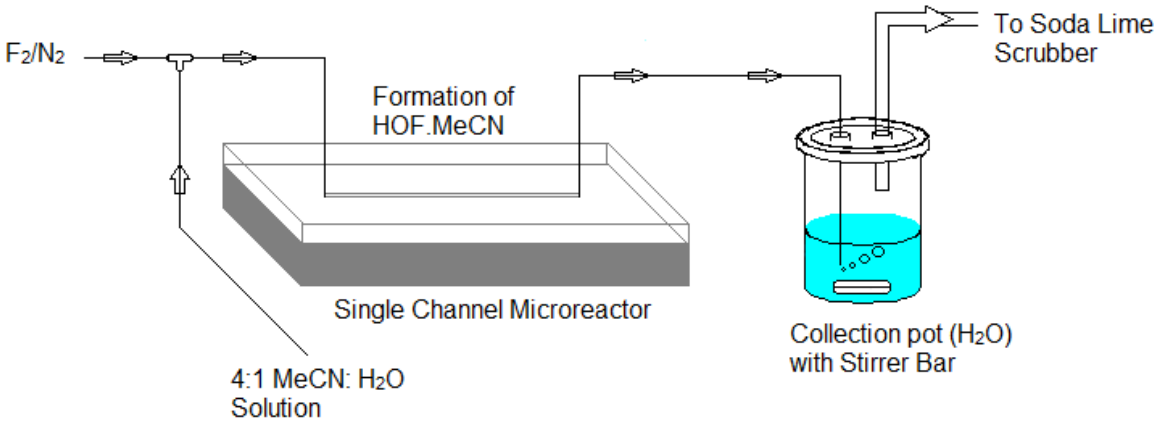

Figure 3.2 – Experimental set up for batch epoxidation using HOF.MeCN

Epoxidation was first tested on a small scale using a 'batch' process (Figure 3.2) which produces the HOF.MeCN in the single channel micro reactor and passed into a collection pot, to which the allyl substrate is added and the mixture is then stirred for two minutes.

With any reaction system the rig first needed to be calibrated and this was achieved using dodec-1-ene and phenol allyl ether. Dodec-1-ene was used as it reacts instantaneously with HOF.MeCN, as stated by Rozen in his original paper[178] and phenol allyl ether was also used as a model substrate to the target bisallyl derivatives.

3.3.1 – Calibration using dodec-1-ene

Calibration of the apparatus was performed to determine the flow rate of F_2 that should be required to produce a specific concentration of HOF.MeCN required for the conversion of the alkene. Also by calculating the theoretical concentration using ideal gas laws it is possible to postulate the theoretical concentration of HOF.MeCN created assuming that all of the fluorine is used.

We calculated that using 7 mL min^{-1} (1.7 mmol h^{-1} of F_2) of 10% F_2 in N_2 equates to approximately 0.86 mmol h^{-1} of HOF.MeCN generated and 14 mL min^{-1} (3.4 mmol h^{-1} F_2) equates to 1.72 mmol h^{-1} of HOF.MeCN.

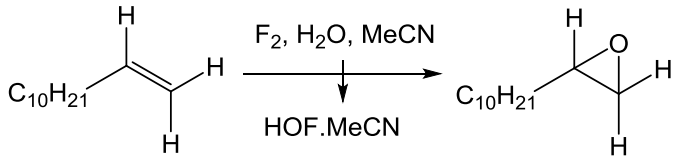

Scheme 3.1 – Conversion of dodcec-1-ene to the epoxide using HOF.MeCN prepared in 'batch'.

Using a flow rate of 7 mL min^{-1} (1.7 mmol h^{-1} F_2) the conversion for dodec-1-ene to epoxide derivative was 35% as measured by the ratio of the integrals of the ^{1}H NMR spectrum. The peaks at 5.74, 4.92 and 4.85 ppm relate to the alkene bond on the starting material and the peaks at 2.83, 2.67 and 2.39 ppm relate to the epoxy group on the product. This proves that the reaction does proceed but a higher flow rate is required to create enough HOF.MeCN.

As there was only a low degree of conversion with using 7 mL min^{-1} (1.7 mmol h^{-1} F_2) the fluorine flow rate was increased to 14 mL min^{-1} (3.4 mmol h^{-1} F_2). ^{1}H NMR analysis again shows that there is conversion of the alkene to the epoxy but conversion was higher at 91% of starting material to desired product (Figure 3.3).

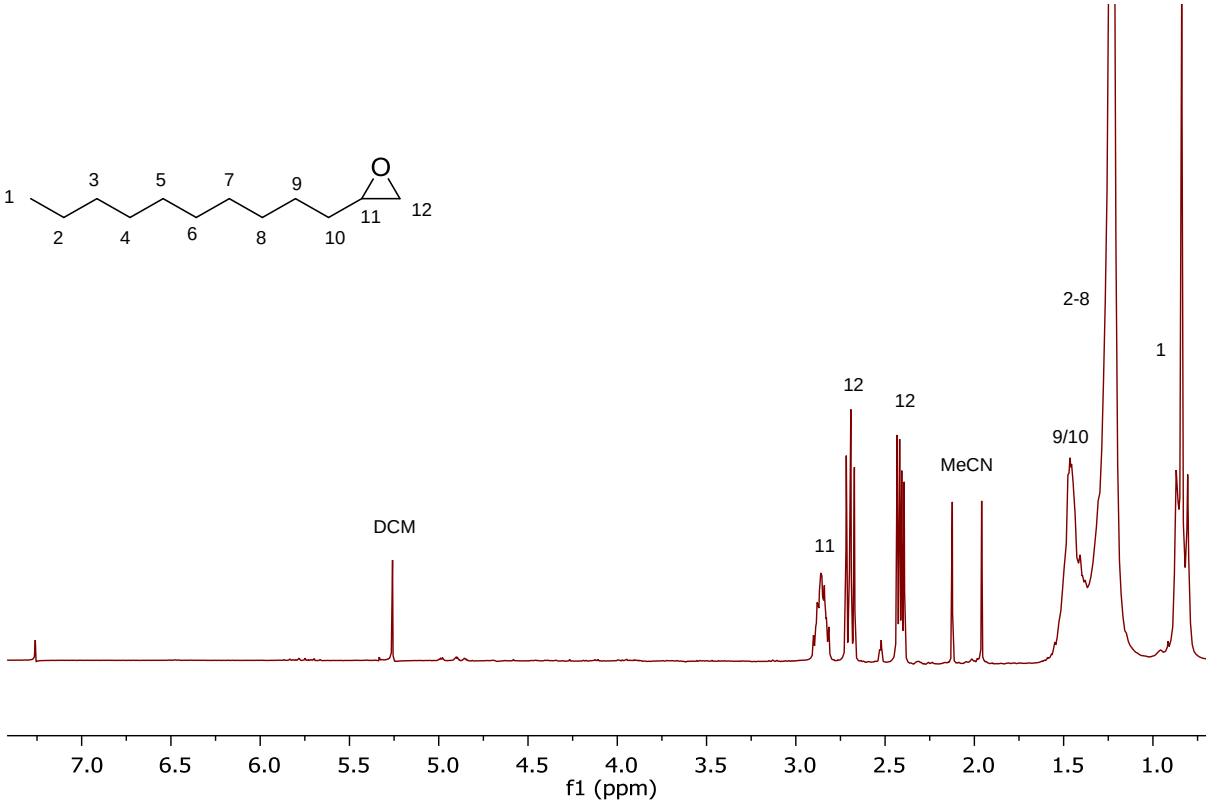

Figure 3.3 – ^{1}H NMR spectrum for the reaction of dodec-1-ene with HOF.MeCN using 14 mL min^{-1} (3.4 mmol h^{-1}) flow of fluorine

3.3.2 – Epoxidation of allyl phenol ether

Allyl phenol ether was epoxidised using HOF.MeCN complex in a similar 'batch' process as a model system for the bisallyl ethers.

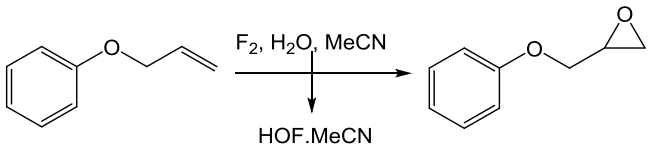

Scheme 3.2 – Conversion of phenol allyl ether to the epoxide using HOF.MeCN prepared in 'batch'.

A flow rate of 15 mL min^{-1} (3.7 mmol h^{-1} F_2) gave a conversion of 97% of alkene to epoxide by ^{1}H NMR analysis (Figure 3.4).

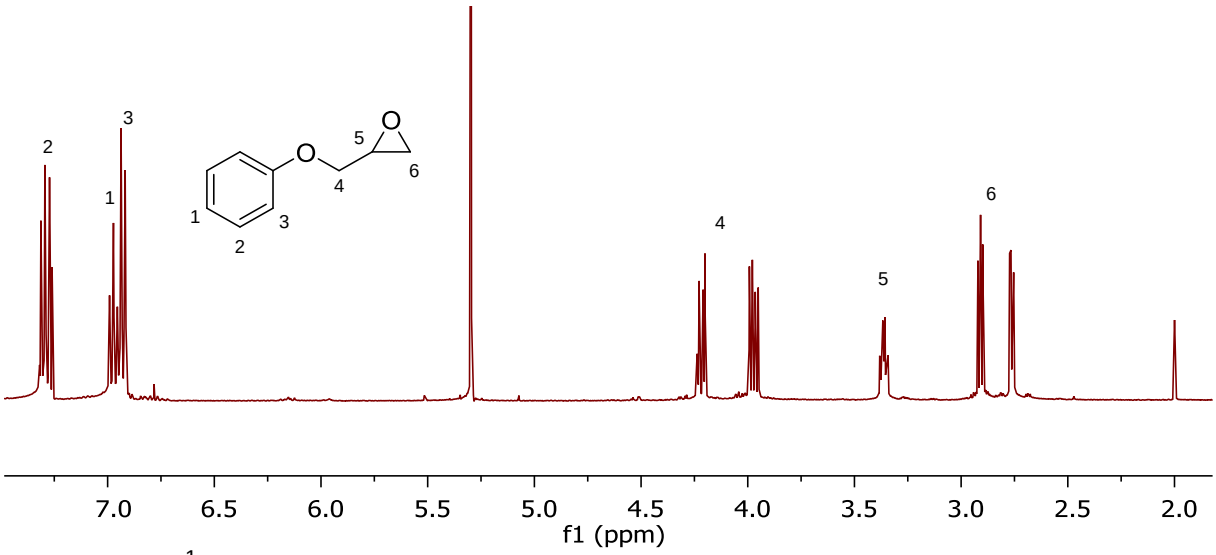

Figure 3.4 – ^{1}H NMR spectrum for synthesis of phenol allyl from HOF.MeCN ether at 15 ml min^{-1} (3.7 mmol h^{-1} F_2) flow of fluorine.

3.3.3 – Epoxidation of hydroquinone diallyl ether

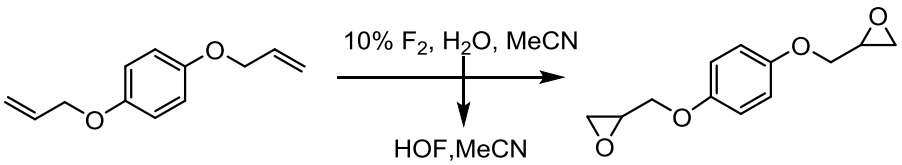

Scheme 3.3 – Conversion of hydroquinone diallyl ether to the epoxide using HOF.MeCN prepared in 'batch'.

Hydroquinone diallyl ether was chosen as the substrate for initial HOF.MeCN 'batch' epoxidation reactions. Reactions were carried out at a flow rate of 15 mL min^{-1} (3.7 mmol h^{-1} F_2) following the calibration reactions above, after which ^{1}H NMR analysis (Figure 3.5) was used to determine the conversion of alkene to epoxide. It is possible to use the integrals of resonances in the aromatic region as there are two peaks which occur at 6.85 ppm which correspond to the desired product (a) and the mono epoxidised product (b) (Figure 3.6). Analysis of these integrals gives a conversion of 91%. A small amount of mono epoxidised product (approx. 9%) is visible at 6.85 ppm when using GSD-based multiplet analysis of the peaks in Mestranova.

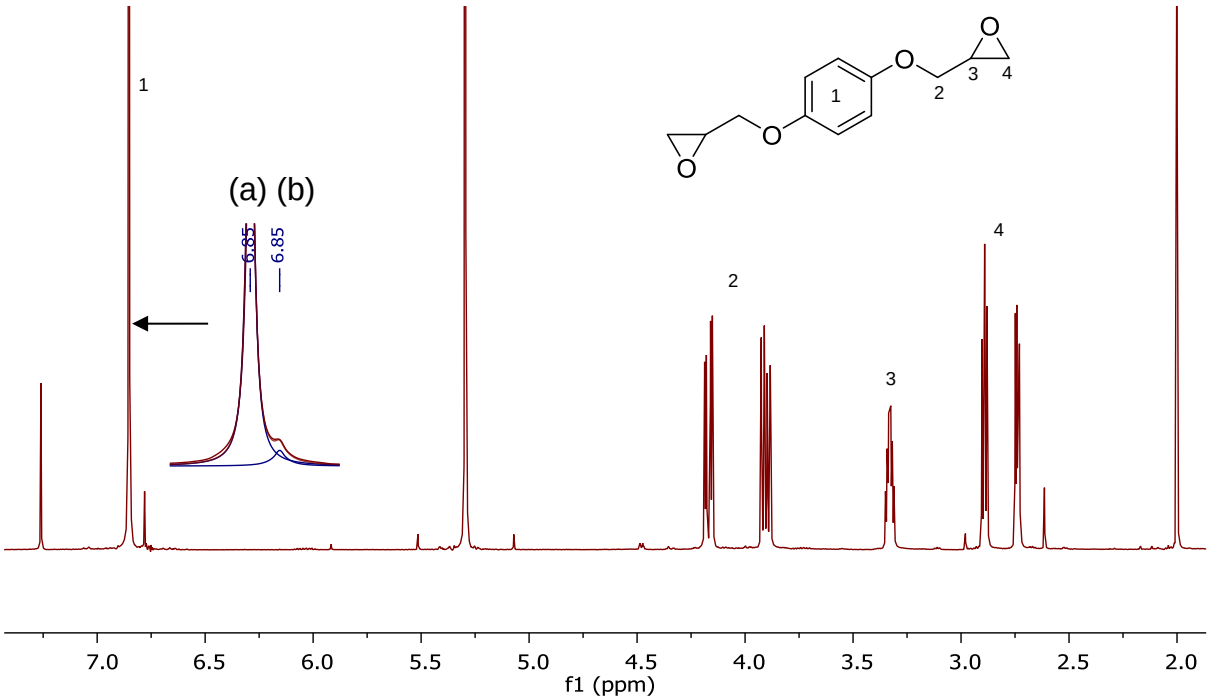

Figure 3.5 – ^{1}H NMR spectrum for hydroquinone diglycidyl ether after 30 mins collection of HOF.MeCN

In a bid to scale up the reaction and create more desired bisepoxide product, the reaction was carried out for a longer time in an attempt to produce more HOF.MeCN. However, when HOF.MeCN was collected over a period of an hour there was a significant decrease in the conversion of the allyl ether to epoxide. ^{1}H NMR analysis gives a conversion of 55% desired product of; 35% mono epoxidised product and 10% unreacted starting material. This is probably due to the degradation of HOF.MeCN as it has been reported that HOF readily degrades into HF and O_2[201, 202]. It has been shown that HOF has a half-life of decomposition of 30 minutes at 298.15K and 0.1 atm[203-205].

In an attempt to combat degradation of HOF.MeCN in batch, the substrate was added to the collection pot before production of the HOF.MeCN in the hopes that the HOF.MeCN formed would react with the alkene *in situ* but ^{1}H NMR analysis showed no conversion. This could be due acid catalysed hydrolysis as explained later on in this chapter.

3.3.4 – Epoxidation of catechol diallyl ether

Due to the successful synthesis of hydroquinone diglycidyl ether using HOF.MeCN the same parameters were used to epoxidise catechol diglycidyl ether in batch. After the reaction was completed and worked up, the product was a pale brown viscous liquid. However, from the ^{1}H NMR spectra (Figure 3.6) it can be seen that there is a conversion of 62% alkene to epoxide. This indicates that the catechol derivative has a lower reactivity than that of the hydroquinone due to higher steric hindrance. ^{1}H NMR analysis gives conversions of 48% desired product (a), 30% mono epoxidised product (b) (Figure. 3.7) and 22% starting material (c).

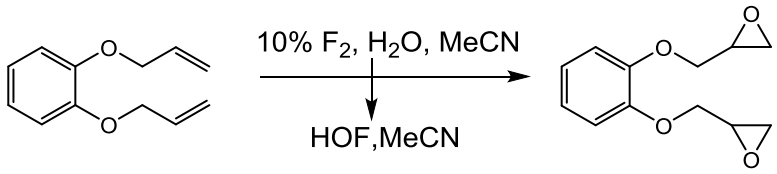

Scheme 3.4 – Conversion of catechol diallyl ether to the epoxide using HOF.MeCN prepared in 'batch'.

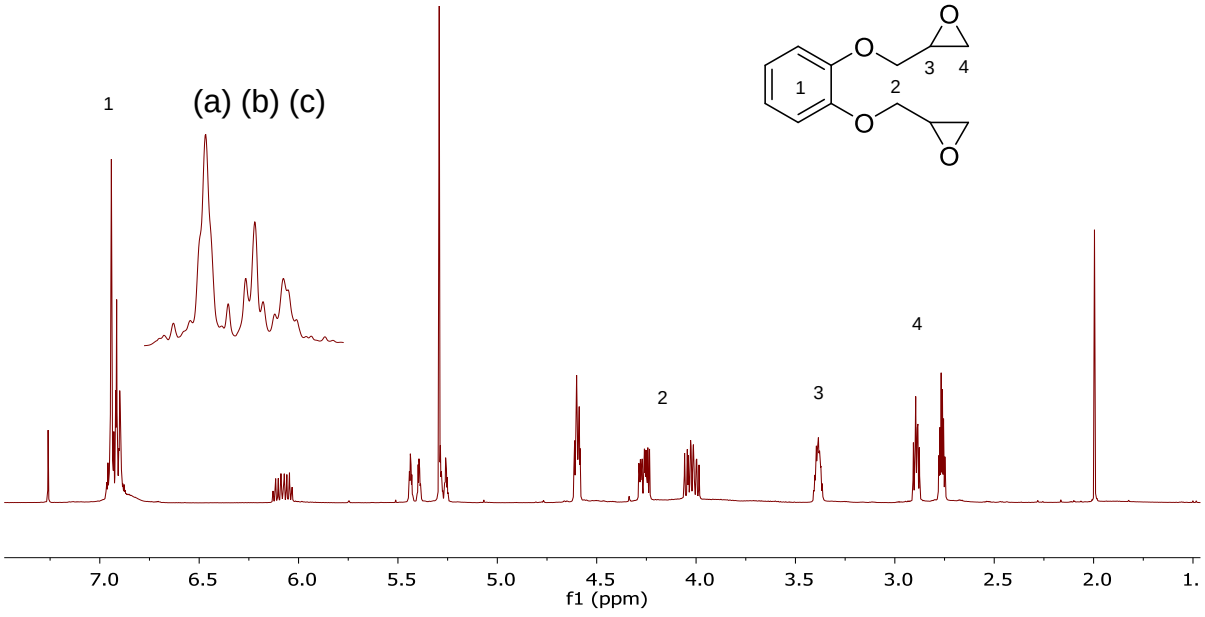

Figure 3.6 – ^{1}H NMR for epoxidation of catechol diallyl ether using HOF.MeCN at 15 mL min^{-1} (3.7 mmol h^{-1} F_2) for 30 minutes

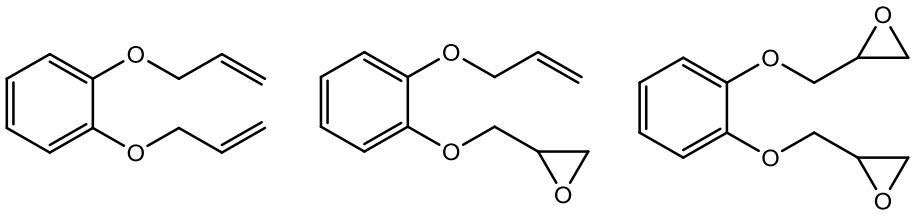

(a) (b) (c)

Figure 3.7 – Reaction products from the HOF.MeCN reaction of catechol diallyl ether (a) starting material, (b) mono epoxidised product and (c) desired product

Utilizing HOF.MeCN in small scale batch processes is successful for the synthesis of hydroquinone diglycidyl ether as there appears to be a high conversion and high purity of the product. However, for catechol diglycidyl ether incomplete conversion is observed.

3.4 – Continuous flow Epoxidation using HOF.MeCN

The model small scale batch process described above showed that epoxidations of the bisallyl ethers was possible using HOF.MeCN and we were required to make larger quantities of the bisepoxides using this reagent system.

The use of continuous flow reactions has been developed at Durham University over the course of several years[206, 207] and has ultimately been used to oxidise compounds using HOF.MeCN in continuous flow[200, 208] which can potentially be used for large scale synthesis. It uses the gas flow micro reactor set up as shown in batch epoxidation but instead of collecting the HOF.MeCN and subsequent addition of the alkene to the mixture, the alkene is added into the flow steam at a set flow rate.

Figure 3.8 shows that the formation of the HOF.MeCN occurs within the micro reactor and, to this flow path, the alkene is injected using a KEL-F (polychlorotrifluoroethylene) T-piece as a micro-mixing station[200]. This is then flowed down 1 m of PTFE tubing to help ensure that the reaction is complete. This reaction set up can be used for an extended period of time depending on the method of injection of the alkene and acetonitrile: water solution.

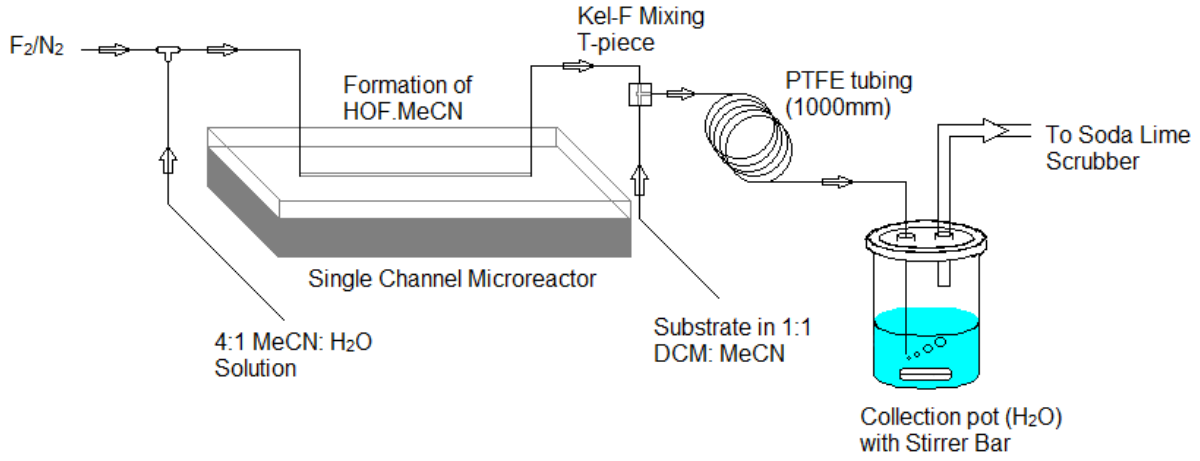

Figure 3.8 – Continuous flow experimental set-up

3.4.2 – Calibration of continuous flow process of epoxidation of phenol allyl ether by HOF.MeCN

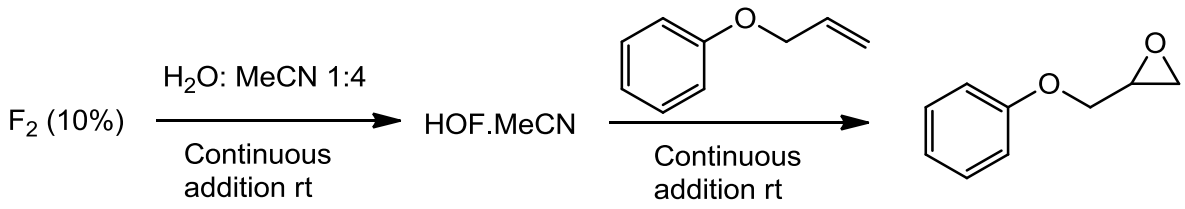

Scheme 3.5 – Continuous flow epoxidation of phenol allyl ether at room temperature

As the flow experimental set up differs from the batch process a new set of calibration experiments were required to determine the flow rate required for the production of 2 mmol of HOF.MeCN. After ensuring that the system was working with the flow of gas and liquid with no build up of pressure or blockages, calibration was performed. By using the continuous flow reaction set-up shown in Figure 3.8 phenol allyl ether was reacted *in-situ* with HOF.MeCN. As can be seen in Table 3.1 the flow rates used were able to finely tune the yield of the reactions. At 20 mL min^{-1} (4.9 mmol h^{-1} F_2) the conversion that was observed was 93% while at 25 mL min^{-1} (6.1 mmol h^{-1} F_2) there was an increase to 97% conversion by ^1H NMR analysis (Figure 3.9).

Table 3.1 – Calibration of HOF.MeCN using phenol allyl ether for 30 minutes

Flow rate of F_2 mL min^{-1} (mmol h^{-1})	MeCN: H_2O flow rate (mL h^{-1})	Phenol allyl ether		NMR Yields %	
		mmol	Flow rate (mL h^{-1})	Alkene	Epoxide
20 (4.9)	10	2	10	7	93
25 (6.1)	10	2	10	3	97

These experiments showed that a flow rate of 25 mL min^{-1} of 10% fluorine in nitrogen could generate ~ 2 mmol of HOF.MeCN per hour.

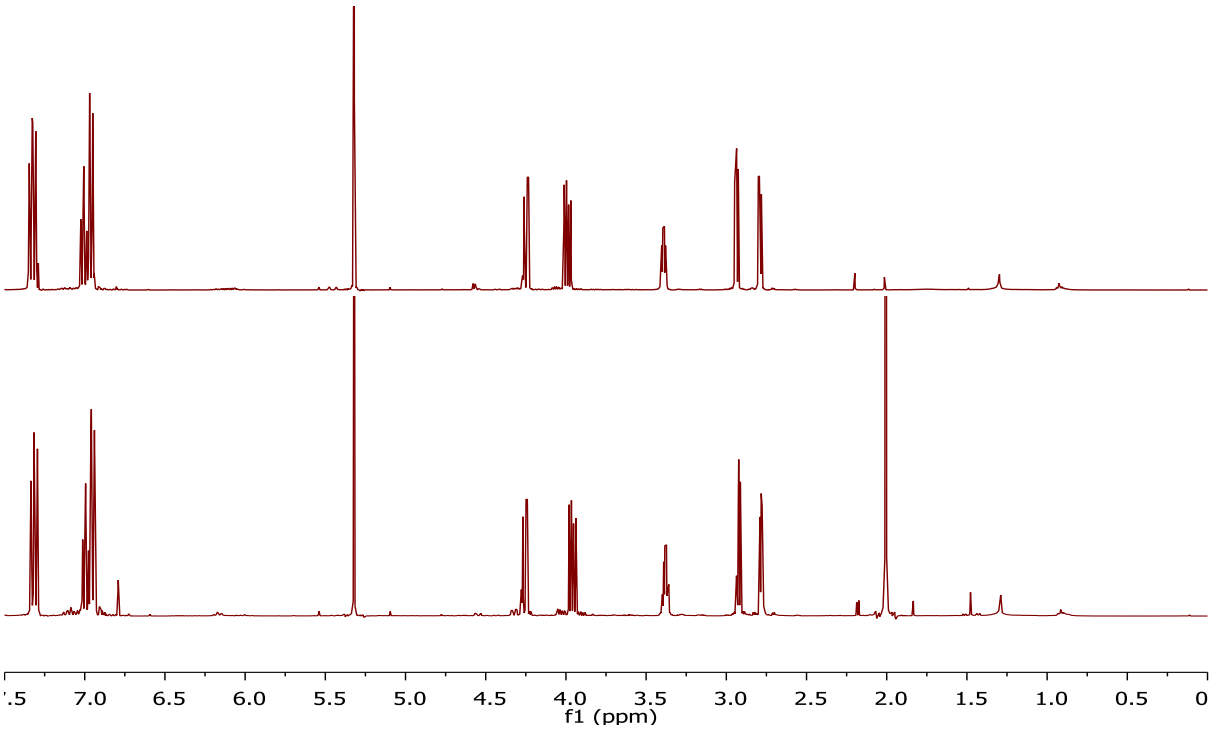

Figure 3.9 – Calibration of phenol allyl ether using continuous flow for 30 mins at: top – 20 mL min^{-1} flow of F_2 (4.9 mmol h^{-1} F_2), bottom – 25 mL min^{-1} flow of F_2 (6.1 mmol h^{-1} F_2)

3.4.3 – Synthesis of hydroquinone diglycidyl ether

With the calibration experiments completed, we studied the epoxidation of bisallyl ether target compounds.

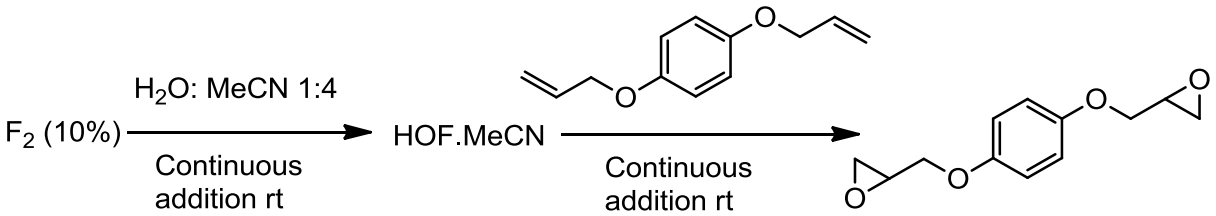

Scheme 3.6 – Continuous flow epoxidation of hydroquinone diglycidyl ether

There are several other factors that have an effect on the synthesis which will have an effect on the scale up of the synthesis such as, collection-pot solute, substrate solvent, and flow rates of fluorine and acetonitrile: water mixture

Therefore, to be able to produce pure bisepoxides in adequate quantities, ideal parameters needed to be determined. The conversions of the reactions will be assessed by the ratios of the three resonances observed in the aromatic region in Figure 3.10.

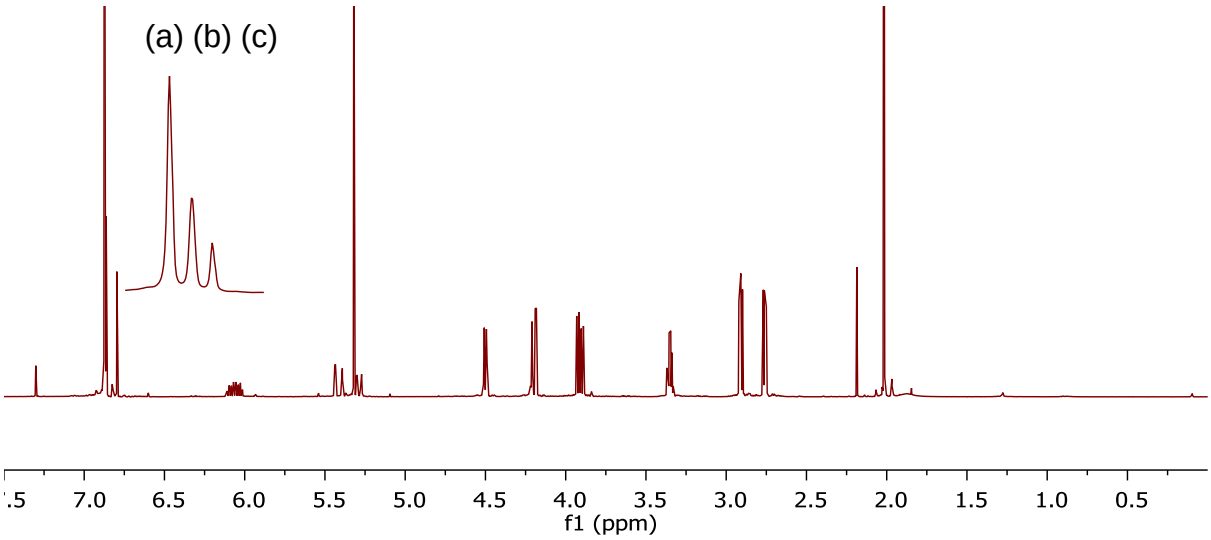

Figure 3.10 – Typical ^{1}H NMR of crude hydroquinone diglycidyl ether using elemental fluorine in continuous flow. (a) bisepoxide, (b) monoepoxide and (c) starting material as taken from the aromatic region at 6.79 ppm.

3.4.3.1 – Changing collection solvents

To determine the effect solvent in the collection vessel has on the conversion of the bisallyl substrate to the bisepoxide product, water, acetonitrile and saturated sodium bicarbonate solution were assessed. The data in Table 3.2 shows that water gives the highest conversion towards the bisepoxide. Acetonitrile leads to a decrease of 5% in conversion of the bisepoxide while sodium bicarbonate solution again shows a lower conversion to bisepoxide but a higher conversion to the monoepoxide than the other two solvents. These experiments show that there is not much difference in yield of bisepoxides obtained when changing collection vessel medium with water being slightly preferable.

Table 3.2 – Comparison of changing collection solvent on product yields

Flow rate of F_2 mL min^{-1} (mmol h^{-1})	Collection solvent	NMR Yields %		
		Starting Material	Mono epoxidised	Desired product
25 (6.1)	H_2O	12	27	61
25 (6.1)	MeCN	17	27	56
25 (6.1)	$NaHCO_3$*	15	33	51

*saturated solution

3.4.3.2 – Changing substrate solvent mixture

Previous work has shown that using a solution of 1:1 acetonitrile to dichloromethane gave good mixing of substrate with HOF.MeCN and produced high conversion[200]. So DCM with MeCN mixtures were assessed in the formation of bisepoxides.

Indeed, as can be seen in Table 3.3, there is an increase in the conversions with the use of the MeCN and DCM solvent mixture. At a flow rate of F_2 of 20 mL min^{-1} (4.9 mmol h^{-1} F_2) the conversion to desired product was 77%; at 25 mL min^{-1} (6.1 mmol h^{-1} F_2) this was 92% and at 30 mL min^{-1} (7.3 mmol h^{-1} F_2) this was 92%.

Table 3.3 – Changing the flow rate of F_2 with a substrate solution of 1:1 DCM: MeCN on product yields

Flow rate of F_2 mL min^{-1} (mmol h^{-1})	Collection solvent	Substrate solvent solution	NMR Yields %		
			Starting Material	Mono epoxidised	Desired product
20 (4.9)	H_2O	1:1 DCM:MeCN	5	16	79
25 (6.1)	H_2O	1:1 DCM:MeCN	2	6	92
30 (7.3)	H_2O	1:1 DCM:MeCN	2	6	92

3.4.3.3 – Changing flow rate of acetonitrile: water mixture and 10% F_2 in N_2

+As seen previously the flow rate of F_2 has a large effect on the conversions of bisallyl substrate to bisepoxides products. Therefore, the effect of changing the flow rate of both F_2 and MeCN and water mixture was assessed to determine the effect this has on the production of HOF.MeCN. As seen in Table 3.4, by changing MeCN. H_2O flow from 10 mL h^{-1} to 15 mL h^{-1} shows an increase in the conversion. Consequently, to achieve higher conversions, the optimal parameters are a flow rate of 25 mL min^{-1} (6.1 mmol h^{-1} F_2) of F_2 and 20 mL h^{-1} (4.9 mmol h^{-1} F_2) of MeCN. H_2O.

Table 3.4 – Effect of changing the flow rate of F_2 with changing flow rate of MeCN. H_2O on the yields of products

Flow rate of F_2 mL min^{-1} (mmol h^{-1})	MeCN: H_2O flow rate (mL h^{-1})	Time (min)	NMR Yields %		
			Starting material	Mono epoxidised	Desired product
20 (4.9)	10	30	14	14	72
20 (4.9)	15	30	13	13	74
25 (6.1)	10	30	9	11	80
25 (6.1)	15	30	6	11	83
25 (6.1)	10	60	8	15	77
25 (6.1)	15	60	4	10	86
25 (6.1)	20	60	5	7	88

3.4.3.4 – Test for hydrolysis product in HDGE

As can be seen from the NMR analysis an extra peak occurs at 6.71 ppm in all instances. This appears to increase with an increased fluorine flow rate which suggests that the resonance is due to a by-product of the reaction, possibly hydroquinone which has a chemical shift of 6.66 ppm. An experiment was performed replacing water with D_2O and collecting in acetonitrile. To determine if the by-product was hydroquinone, a few drops of sodium deuteroxide were added to the mixture before separation. The aqueous phase was then analysed via ^1H NMR spectroscopy with and without doping of hydroquinone to determine if there is an

increase in the peak with addition of hydroquinone. As can be seen in Figure 3.11 there is an increase in the intensity of the peak at 6.36 ppm demonstrating that hydroquinone is the relative by-product. One explanation for the formation of the side product is acid catalysed hydrolysis by HF. This by-product is roughly half the yield of the overall synthesis and as over half of the fluorine in the reaction is converted to HF, this is possible.

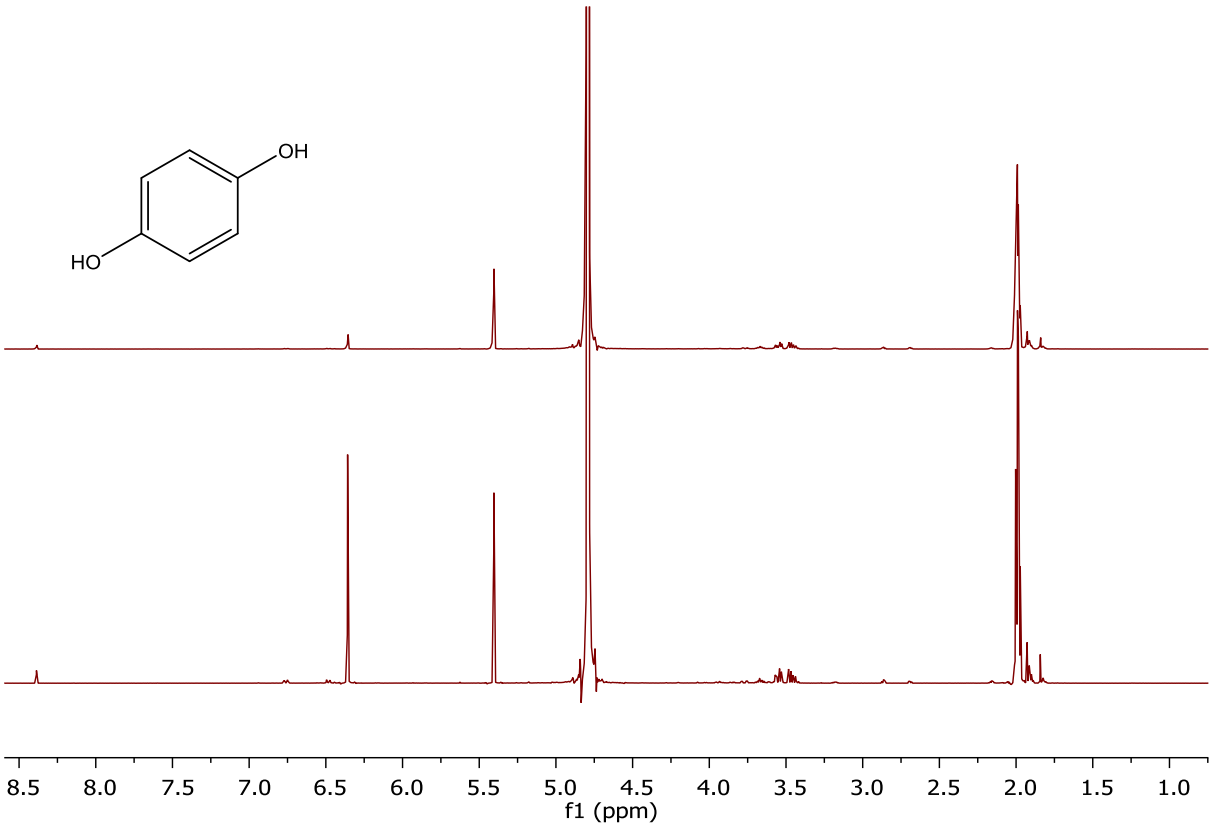

Figure 3.11 – ^{1}H NMR spectra of the aqueous layer after collection with D_2O and NaOD. Top spectrum is un-doped and bottom spectrum is doped with hydroquinone.

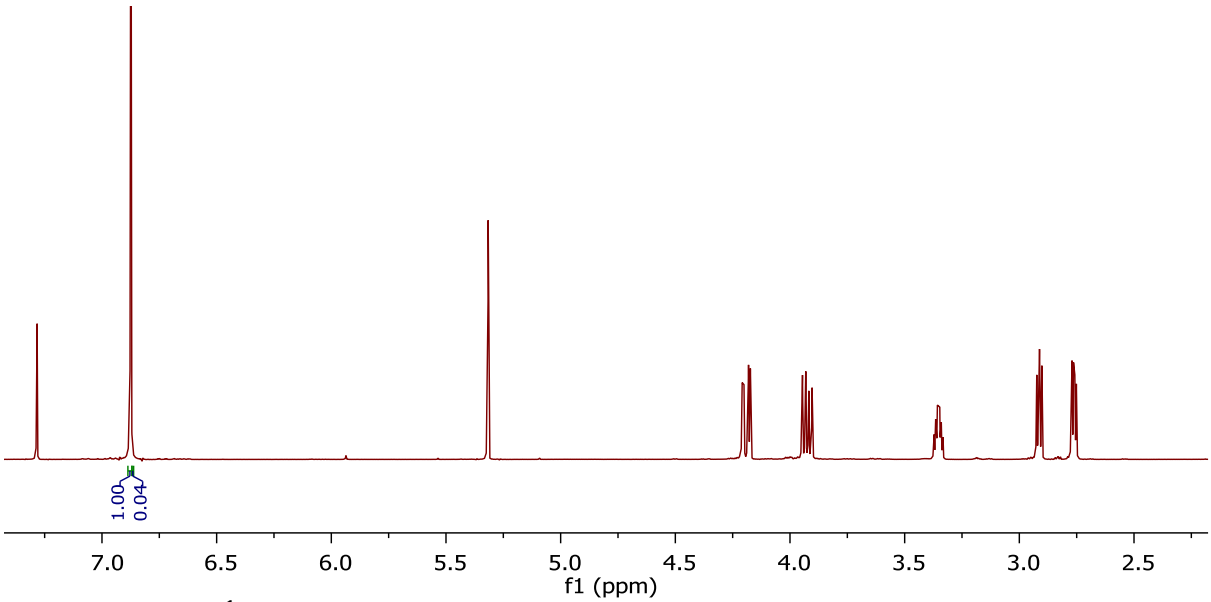

Figure 3.12 – ^{1}H NMR analysis of the organic layer after collection with D_2O and NaOD.

Using the parameters that were developed previously and washing with sodium hydroxide gave a conversion of 99% and only 1% of the mono epoxide. The yield, however, was low at only 37% which suggests that there is a large amount of the hydroquinone by-product formed.

3.4.3.5 – Conclusion for continuous flow of HDGE

This method appears to be successful as there is a higher conversion towards the desired product. However, with an increased flow rate of F_2 there is more evidence of the formation of hydroquinone by acid catalysed hydrolysis[209]. The best parameters obtained for the synthesis of hydroquinone diglycidyl ether were: an F_2 flow rate of 25 mL min^{-1} (6.1 mmol h^{-1} F_2); collecting in water; with a substrate solvent mixture of 1:1 acetonitrile to dichloromethane; a flow rate ratio of 20:10 mL h^{-1} of acetonitrile/ water mix to substrate and then working the reaction up with 2 M sodium hydroxide.

3.4.4 – Synthesis of catechol diglycidyl ether

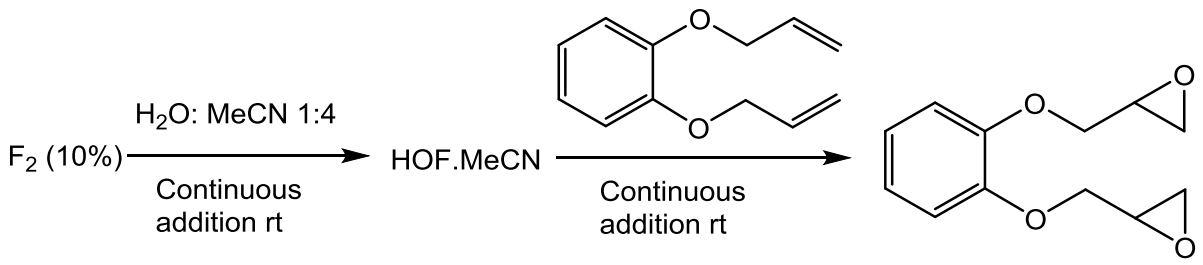

Scheme 3.7 – Continuous flow epoxidation of catechol diglycidyl ether

Ideal flow rates were determined to produce the highest conversion of catechol diallyl ether to the bisepoxide.

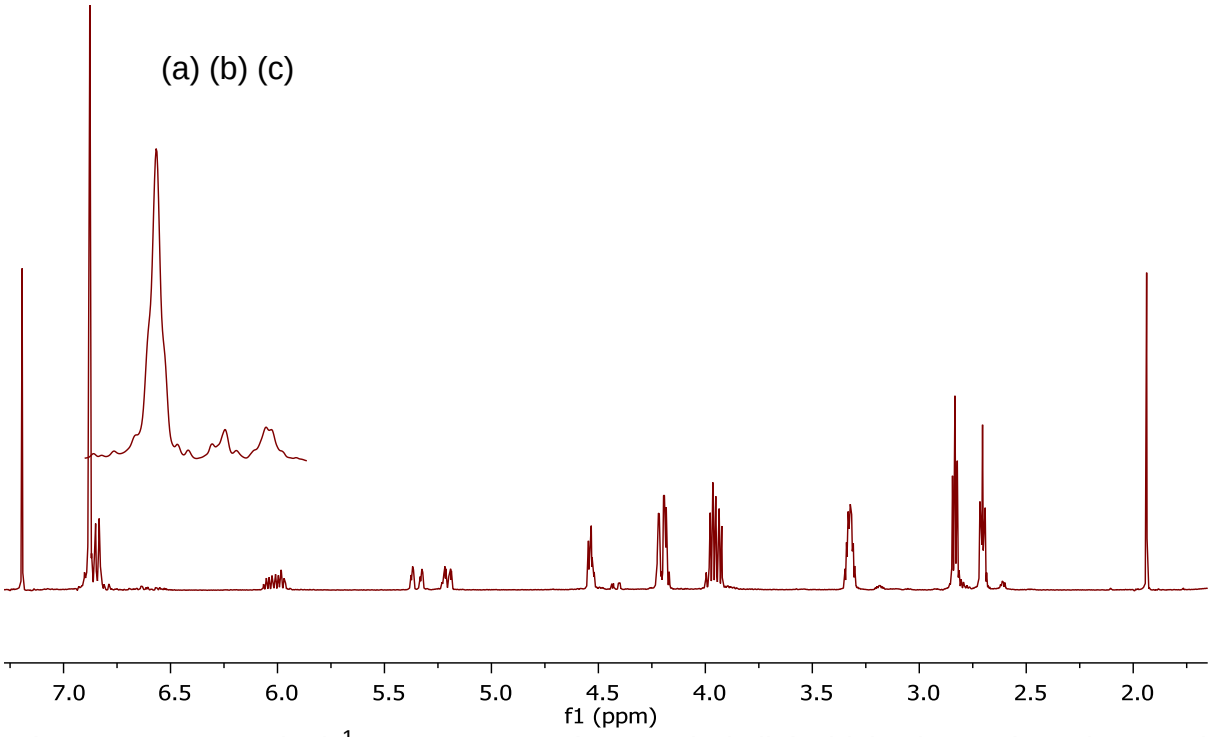

Figure 3.13 – Typical ^{1}H NMR of crude catechol diglycidyl ether using elemental fluorine in continuous flow. (a) bisepoxide, (b) monoepoxide and (c) starting material (Figure 3.24)

Table 3.5 shows that at 20 mL min^{-1} (4.9 mmol h^{-1} F_2) of F_2 in nitrogen there is a low conversion of 79% which is dramatically increased to 90% when 25 mL min^{-1} (6.1 mmol h^{-1} F_2) was used. Additionally with a flow rate of 30 mL min^{-1} (7.1 mmol

h^{-1} F_2) there appears to be almost complete conversion (98%) to the desired product with no side products appearing in the NMR spectrum.

Table 3.5 – Changing the flow rate of 10% fluorine on the yields of products

Flow rate of F_2 mL min^{-1} (mmol h^{-1})	MeCN: H_2O flow rate (mL h^{-1})	NMR Yields %		
		Starting material	Mono epoxidised	Desired product
20 (4.9)	20	8	13	79
25 (6.1)	20	4	6	90
30 (7.3)	20	0	2	98

3.4.5 – Conclusion for continuous flow epoxidation

Bisepoxidation of catechol diglycidyl ether is very successful giving a high conversion of desired product and a high yield with no competitive hydrolysis. The best parameters obtained for the synthesis of the diglycidyl ethers were: a F_2 flow rate of 25 mL min^{-1} (6.1 mmol h^{-1} F_2) for the hydroquinone derivative and 30 mL min^{-1} (7.3 mmol h^{-1} F_2) for the catechol derivative; collecting in water; with a substrate solvent mixture of 1:1 acetonitrile to dichloromethane; a flow rate ratio of 20:10 mL h^{-1} of acetonitrile/ water mix to substrate and then working the reaction up with 2 M sodium hydroxide.

3.5 – Scaling up continuous flow epoxidation using HOF.MeCN

Although synthesis of diglycidyl ethers using HOF.MeCN produces good conversion and yields, so far only small amounts of product were obtained. This is due to the limit in the capacity of the micro reactor and the amount of HOF.MeCN that can be produced using this method since even using a 2 mmol concentration for a 1 hour reaction there is only (assuming 100% conversion and yield) 0.44g of product formed per hour. However, there are several parameters that can be used to increase the production of bisepoxides using flow reactions which include:

1. Increasing reaction time
2. Increasing concentration of fluorine and substrate
3. Type and capacity of pump
4. Size of micro-reactor

Most of these parameters are interlinked because an increase of reaction time there needs to be a change in the capacity of the pump. For example, as all the previous experiments were carried out using single syringe pumps there is the limitation of the size of the syringe that is used (50 mL) which gives the limit of 2.5 hours using 20 mL h^{-1} flow rate of acetonitrile and water. However by using a continuous flow pump (such as a HPLC pump) it is possible to increase the reaction time significantly. By changing the substrate concentration it is also theoretically possible to synthesise more product. In this study the type of reactor used is a single channel reactor, but there is the possibility of using throughout a multichannel reactor which, again, would increase the amount of product formed.

Table 3.6 – Effect of changing the parameters for the scale up of epoxidation with HOF.MeCN on mass of product formed

HOF.MeCN and substrate conc. (mmol h^{-1})	F_2 %gas	Flow F_2 (mL min^{-1})	Flow of H_2O MeCN: substrate (mL h^{-1})	Time (h)	Theoretical Mass (g)
1	10	20 (4.9)	20:10	1	~0.22
				2	~0.44
2	10	25 (6.1)	20:10	1	~0.44
				2	~0.89
4	20	25 (12.2)	40:10	1	~0.89
				2	~1.78
8	20	50 (24.5)	80:10	1	~1.78
				2	~3.56

3.5.1 – Test and calibration of HPLC pumps using HDGE

The use of HPLC pumps for MeCN. H_2O and substrate flow control were assessed. As can be seen in table 3.7 a slightly higher flow rate is needed for the water and acetonitrile mixture to give the best conversion. At the ratio of 10:20 mL h^{-1}, flow rate of substrate to water: acetonitrile mixture the conversion was 91% with a 47% yield. By using a slight excess of 0.3 mL h^{-1} this increases the yield to 58% and the conversion to desired product of 97%.

Table 3.7 – Test for the use of HPLC pumps in epoxidation using HOF.MeCN

Flow of substrate: H_2O MeCN (mL h^{-1})	Time (h)	Yield (%)	NMR Yields %		
			Starting material	Mono epoxidised	Desired product
10:20	5	47	3	6	91
10:20.3	5	58	0	3	97

As expected, HPLC pumps were effective in controlling the introduction of substrate and MeCN. H_2O into the flow reactor.

3.5.2 – Effect of time

3.5.2.1 – Effect of time on hydroquinone diglycidyl ether

By increasing the reaction time to over 20 hours using HPLC pumps, we were able to synthesise more product with consistent results, as shown in Table 3.8. There is little difference in the conversion to bisepoxide with a reaction time of 21 hours producing a conversion to desired product of 95% and an isolated yield of 44%. Overall this method allowed production of approximately 10 g of hydroquinone diglycidyl ether in each overnight reaction.

Table 3.8 – Effect of time on the conversion of hydroquinone diglycidyl ether

Flow of substrate: H_2O MeCN (mL h^{-1})	Time (h)	Yield (%)	NMR Yields %		
			Starting material	Mono epoxidised	Desired product
10:20.3	2.5	44	2	3	95
10:20.3	21	44	0	5	95
10:20.3	23	33	0	9	91

3.5.2.2 – Effect of time on catechol diglycidyl ether

Similarly there is little difference in amounts of product obtained for reaction of the catechol bisepoxide. As can be seen in Table 3.9 there is little difference in the conversion with increasing the reaction to 24 hours compared to 2 hours.

Table 3.9 – Effect of time on the conversion of catechol diglycidyl ether

Flow rate of F_2 mL min^{-1} (mmol h^{-1})	Flow of substrate: H_2O MeCN (mL h^{-1})	Time (h)	NMR Yields %		
			Starting material	Mono epoxidised	Desired product
30 (7.3)	10:20.3	2	0	2	98
30 (7.3)	10:20.3	18	2	4	94
30 (7.3)	10:20.3	24	2	6	92

3.5.3 – Effect of fluorine and substrate concentration

3.5.3.1 – Effect of concentration on hydroquinone diglycidyl ether

The concentrations of HOF.MeCN that were assessed in reaction with hydroquinone diallyl ether were 1, 2, 4 and 8 mmol h^{-1}. Table 3.10 shows that when exposed to higher concentrations of HOF.MeCN the predominant reaction that occurs when hydroquinone diallyl ether is the substrate is hydrolysis.

Table 3.10 – Effect of changing HOF.MeCN concentration on hydroquinone diglycidyl ether

HOF.MeCN and substrate conc. (mmol h^{-1})	F_2 %gas	Flow F_2 mL min^{-1} (mmol)	Flow of H_2O MeCN: substrate (mL h^{-1})	Yield (%)	Conversion (%)		
					SM	ME	DP
1	10	20 (4.9)	10:10	62	0	11	89
2	10	25 (6.1)	20:10	49	0	3	97
4	20	25 (12.2)	40:10	0	0	0	0
8	20	50 (24.5)	80:10	0	0	0	0

3.5.3.2 – Effect of concentration on catechol diglycidyl ether

As shown previously, catechol diallyl ether does not appear to undergo hydrolysis upon reaction with HOF.MeCN so therefore the increase in concentration should not have a detrimental effect. However, when there is an increase in

concentration from 2 mmol to 4 mmol there is a dramatic drop in the yield from and a decrease in the conversion. When the concentration is increased from 4 mmol to 8 mmol there is no change in the conversion and only a slight change in the crude yield and this experiment gave 1.62 g of product over 2 hours.

Table 3.11 – Effect of changing HOF.MeCN concentration on catechol diglycidyl ether for 2 hours

HOF.MeCN and substrate conc. (mmol h^{-1})	F_2 %gas	Flow F_2 mL min^{-1} (mmol)	Flow of H_2O MeCN: substrate (mL h^{-1})	Yield (%)	Conversion (%)		
					SM	ME	DP
2	10	30 (7.3)	20:10	93	0	3	97
4	20	30 (14.7)	40:10	61	5	9	86
8	20	60 (29.4)	80:10	53	5	9	86

3.5.4 – Conclusions for scaling up of HOF.MeCN continuous flow reaction

For hydroquinone diglycidyl ether the best procedure for scaling up the process is though increasing the reaction time. Increase in the concentration of HOF.MeCN led to predominant hydrolysis.

With catechol diglycidyl ether however both of the methods appear to be effective with good yields and good conversions and a combination of these methods was used to produce the required amount of bisepoxide product. This could be due to the steric hindrance of the catechol structure.

3.6 – Conclusion and comparisons

Synthesis of the bis epoxides using HOF.MeCN was possible for both hydroquinone and catechol isomers. With the hydroquinone substrate, acid catalysed hydrolysis is a competing process and this reduces the yield and the possibility of using higher concentrations of HOF.MeCN. With the catechol derivative, there appears to be no hydrolysis or other by-products being formed, enabling the production of large quantities of bisepoxide using HOF.MeCN in flow.

The use of trichloroisocyanuric acid as a batch method (as described in Chapter 2.2) appears to be more successful for the synthesis of the hydroquinone bisepoxide derivative compared to that of HOF.MeCN method. However, for the catechol derivative the use of HOF.MeCN is a useful process.

Chapter 4 – Polymerisation

4.1 – Aims and approach

The aim of the work described in this chapter is to produce polymer films from the epoxides produced previously with 4,4'-methylenebis(cyclohexyl) amine (PACM). These films need to be readily removed from the substrate and form at different thicknesses. To produce usable polymers the networks need to be fully cured, therefore several temperatures and substrates were researched to determine which gives the best films. These polymers will be prepared with no additives or solvents to produce model systems that should be fully cross-linked.

Using PACM in stoichiometric quantities of 1:1 should produce a polymer that has little homopolymerisation as the rate of reaction for the reactions between the amines and hydroxyl groups formed as discussed in Chapter 1 section 1.3.5. By limiting the homopolymerisation, the system should become cross-linked via the amine reaction as shown in Scheme 4.1. These reactions occur via a step growth polymerisation in which the amine ring opens the epoxy group. This then undergoes polyaddition via nucleophilic addition using the diamine which creates an amine linkage between the different polymers chains.

With this reaction being carried out at a stoichiometric level it is important to know the epoxide equivalent weight for the epoxy resin. This is the ratio of the mass of the epoxy functional groups against the rest of the molecule and determines the amount of amine hardener that is required to polymerise the resin. It is defined as the weight of the resin in grams that contains 1 mole equivalent of epoxy groups[210].

To determine the cure of the polymers each temperature and substrate was analysed using differential scanning calourimetry (DSC) which was used to note the change in the glass transition temperature (T_g) at these different temperatures. Once an ideal system was found for all of the polymers, a model polymerisation was performed to determine if all of the polymers can be formed using the same temperatures, with no detrimental effects on the films.

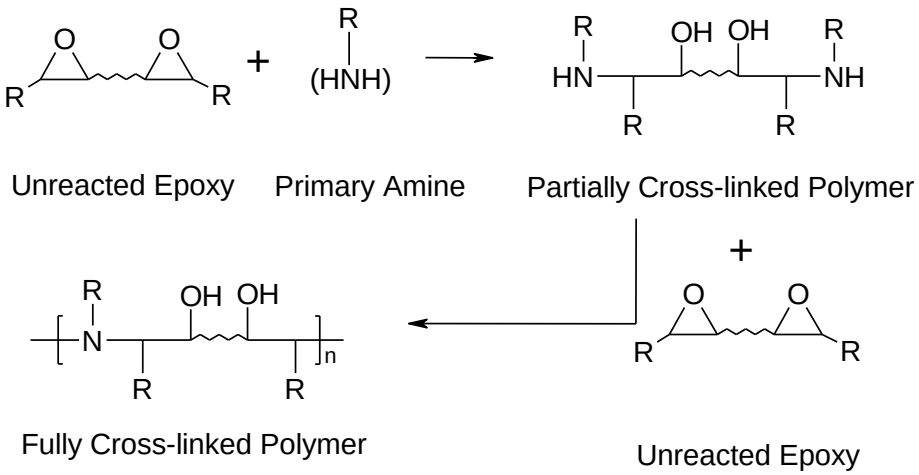

Scheme 4.1 – Reactions between bisepoxides and diamines to give fully cured highly cross-linked polymer networks

As this project aims to create model systems, the monomers used need to be purified and characterised. For the synthesised epoxides only those prepared by HOF.MeCN were used as they were determined to be the purest. The resorcinol diglycidyl ether needed to be purified as it was prepared using conventional methods and so contains oligomers. To determine that the diglycidyl ethers were pure, NMR spectroscopy was used to determine the epoxide equivalent weight. Also GC-MS was used to determine if there were any other impurities in the samples.

4,4’-methylenebis(cyclohexyl) amine was also analysed as two different samples were used. This determined the differences in the samples used, and this information was used to explain the effects the different samples have on their subsequent polymer films.

4.2 – Purification of epoxides

The epoxide equivalent weight (EEW) is the most important parameter to determine the stoichiometry of the polymerisation reaction as it determines the grams of epoxy functional groups to 1 g of monomer. This is used to then calculate the amount of epoxy monomer needed to react with the activated hydrogen sites (AHEW) on the amine which can then be used to determine the mass of amine needed. The epoxide equivalent weight can be determined via ^{1}H NMR spectroscopy[210, 211] by comparing the integral ratios of the epoxy peaks to the aromatic peaks as developed by *Garcia et al.*[211]. This has been done on the impure resorcinol diglycidyl ether (RDGE) as the epoxide equivalent weight should be 111 g/equiv. but is quoted by the suppliers as 120-135 g/equiv. which shows that there was more components in the mixture.

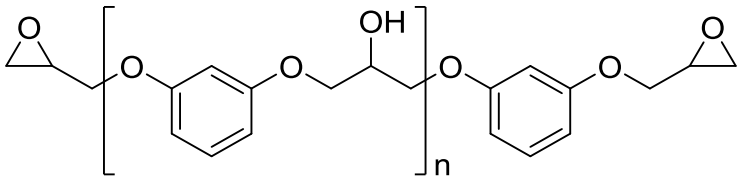

Figure 4.1 – Structure of resorcinol diglycidyl ether where n is a range between 0 and 0.2 as an average for the whole sample.

From the ^{1}H NMR spectrum (Figure 4.2) the relative ratios of the epoxy groups, peaks 3.31, 2.87 and 2.72 ppm is 5.11 and for the aromatic groups it is 4.08. Dividing the aromatic integrals by the epoxy integrals gives 0.7984. This can then be applied to equation 4.1

$$n = \frac{(\text{ratio actual} - \text{ratio theoretical})}{\text{ratio theoretical}} \qquad (4.1)$$

Using the theoretical ratio of 4/6 which is what would be expected in the pure product gives a value of n of 0.1977 substituting this into equation 4.2.

$$EEW = \tfrac{1}{2}Mw_{repeat\,unit} \times n + \tfrac{1}{2}Mw_{polymer\,(n=0)} \qquad (4.2)$$

The ½ Mw of the repeat unit for RDGE is 83 and the ½ Mw of the polymer is 111 therefore substituting the values obtained previously gives an EEW of 118 g/equiv. which is close to the value that is given by the suppliers.

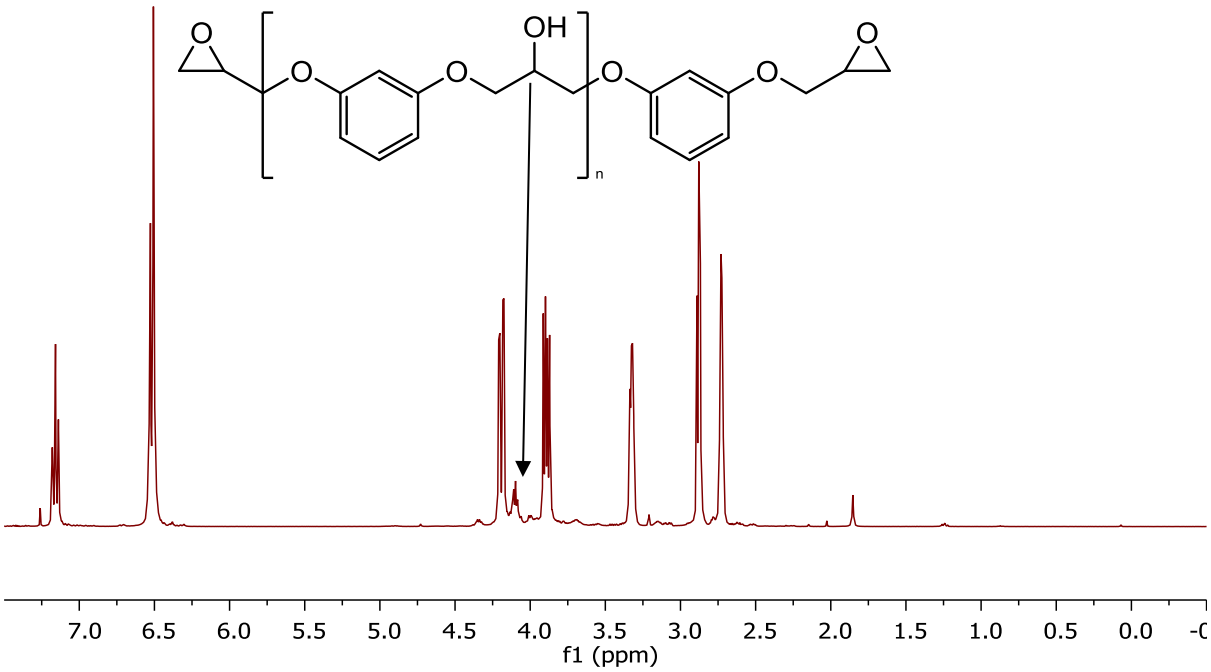

Figure 4.2 – ^{1}H NMR spectrum for impure resorcinol diglycidyl ether

4.2.1 – Purification of resorcinol diglycidyl ether

After attempting to re-crystallise the RDGE sample the ^{1}H NMR spectrum looked identical to the impure RDGE sample spectrum (Figure 4.2) with the peak at 4.14-4.06 ppm which corresponds to the R_2-C**H**-OH (as shown by the arrow in Figure 4.2) of the oligomer. Vacuum distillation (at circa 150°C) was therefore carried out with ultimately better results. The ^{1}H NMR spectrum (Figure 4.3) obtained from the sample that was distilled shows by the integrals and the lack of a peak at 4.14-4.06 ppm that the sample is pure. From these integrals obtained the same data can be used in equation 4.1 and then 4.2 to determine the EEW. The actual ratio that is obtained from the ^{1}H NMR spectrum is now 0.6683 which when input into the equation 4.1 gives a value for n of 0.0025. Using this data in equation 4.2 gives an

EEW of 111.2804 g/equiv. which is what is expected from the pure product. GC-MS also confirms that there is only one product obtained from the vacuum distillation which suggests that the product has been purified.

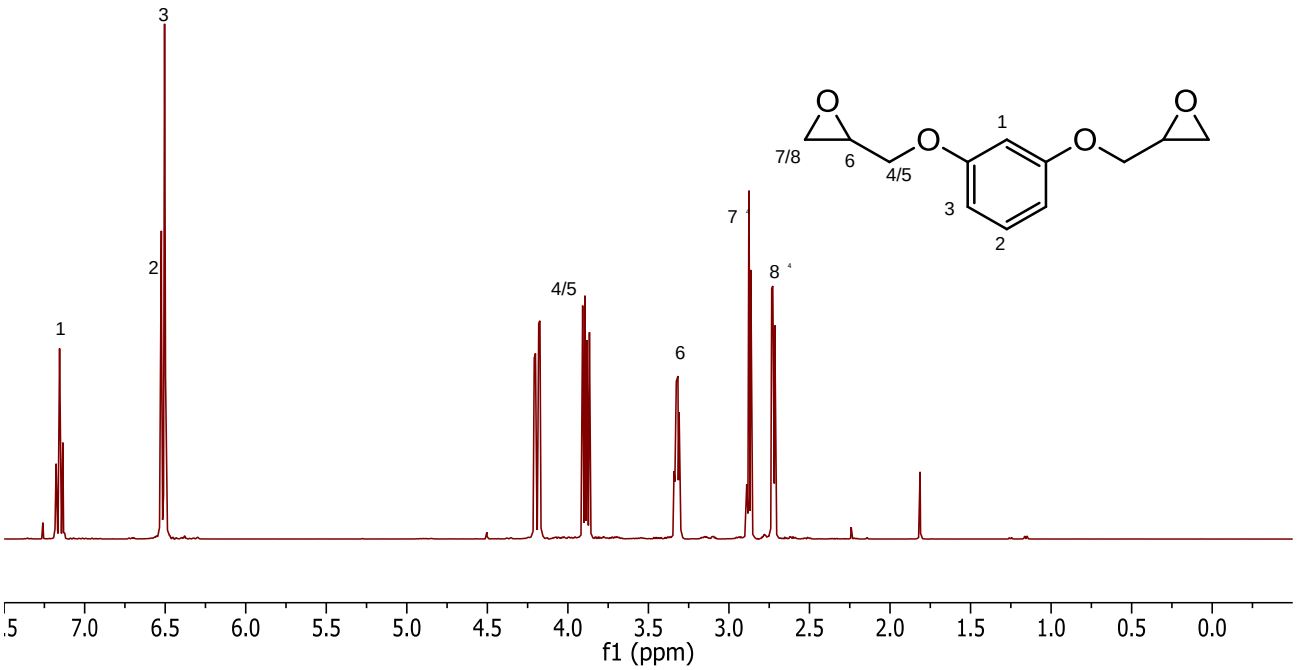

Figure 4.3 – ^{1}H NMR spectrum of resorcinol diglycidyl ether purified by vacuum distillation.

The GC-MS trace shows the exact mass of the purified product to be 222.2 m/z taken from the single peak in the GC of 19.245 mins.

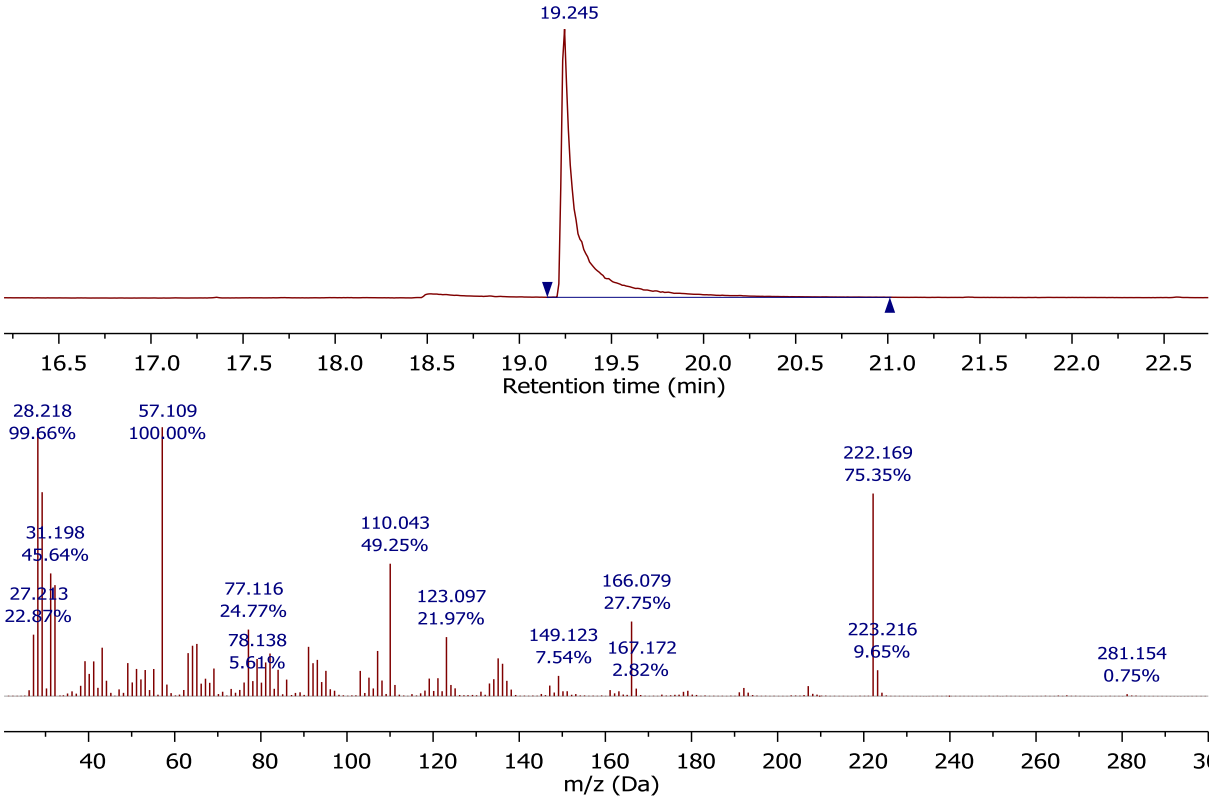

Figure 4.4 – GC-MS trace for resorcinol diglycidyl ether prepared by vacuum distillation

4.2.2 – Purification of hydroquinone diglycidyl ether

Although the synthesis of hydroquinone diglycidyl ether from HOF.MeCN and TCA were made with high purity (See Chapter 2), it was decided to attempt to increase the purity of the samples with recrystallization. Utilizing hexane as the solvent as suggested by Oshima *et al.*[212] gave a purity of over 93% as can be seen in the ^{1}H NMR spectrum (Figure 4.5) but with a recovered yield of less than 10%. Using equation 4.2 the EEW was estimated as 111.1393 g/equiv Therefore, 2-ethoxyethyl ether and methyl isobutyl ketone as a mixed solvent system was used as described by Marand *et al*[213]. As can be seen in the ^{1}H NMR spectrum (Figure 4.6) the product is over 97% pure which is acceptable due to the difficulty in determining 100% purity. The yield for this was also much better than that of the previous method with a recovery of 79% of the pure product. There was also residual product mixed with the by-products remaining in the filtrate which could be recovered to increase the yield.

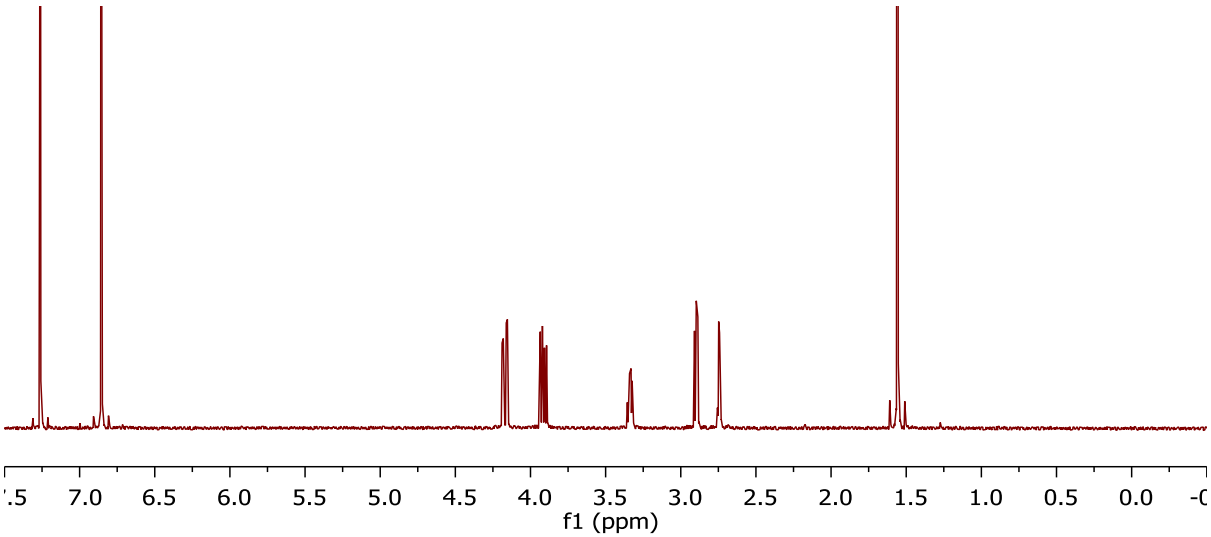

Figure 4.5 – ^{1}H NMR spectrum for hydroquinone diglycidyl ether recrystallized from hexane

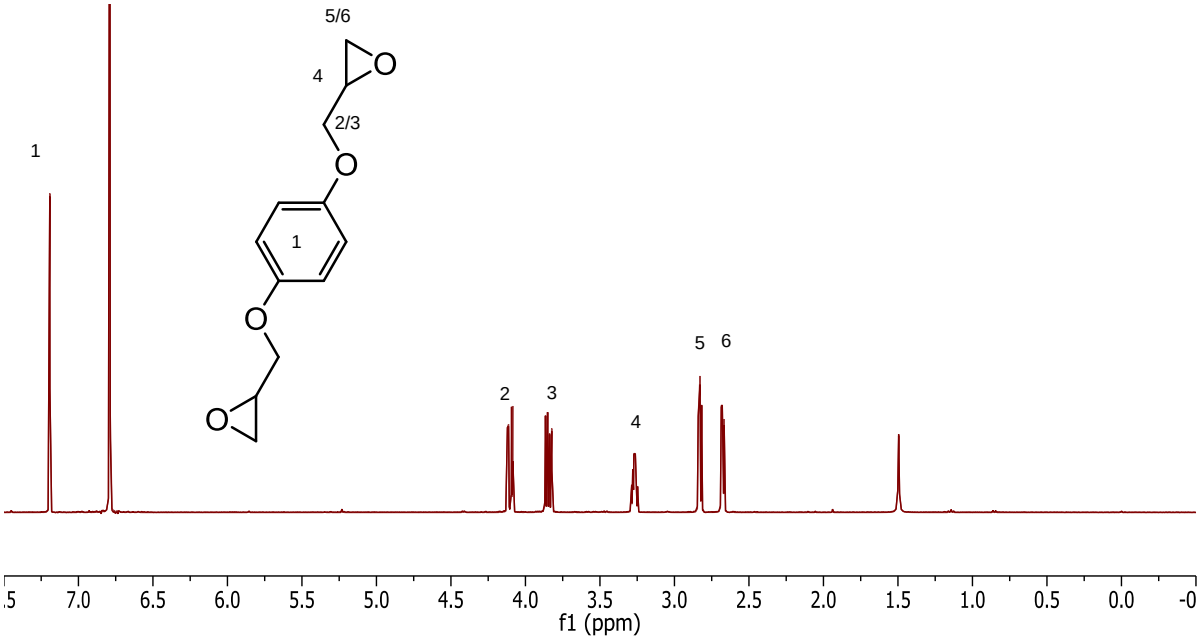

Figure 4.6 – ^{1}H NMR spectrum for hydroquinone diglycidyl ether recrystallized from 2-ethoxyethyl ether and methyl isobutyl ketone (1:1)

The GC-MS trace also shows that there is one product in the sample with a mass of 222.017 Daltons from the single peak at 19.62 minutes as shown in Figure 4.7.

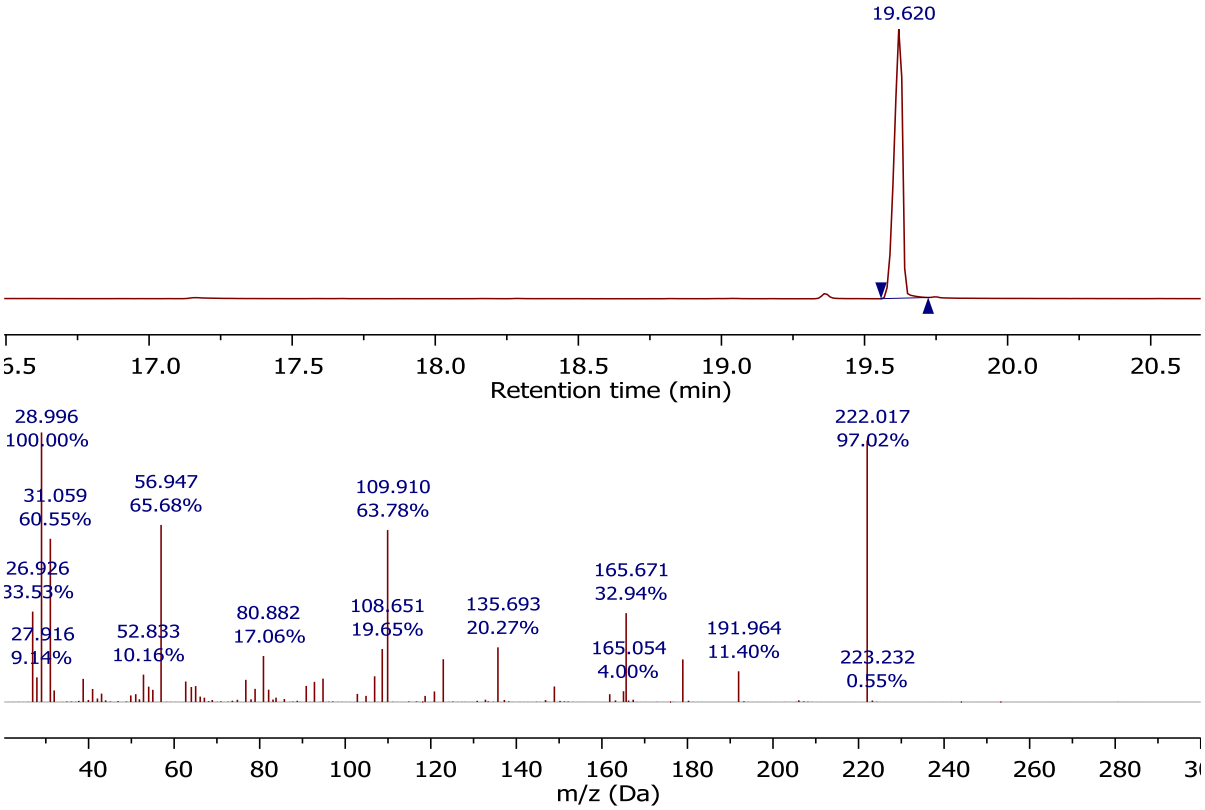

Figure 4.7 – GC-MS trace for hydroquinone diglycidyl ether recrystallized from 2-ethoxyethyl ether and methyl isobutyl ketone (1:1)

4.2.3 – Purification of catechol diglycidyl ether

Utilizing the recrystallization mixture 2-ethoxyethyl ether and methyl isobutyl ketone, catechol diglycidyl ether was purified using freeze recrystallization. As can be seen in the ^{1}H NMR spectrum (Figure 4.8) the product appears to be over 96% pure taken from the aromatic region. As taken from the NMR spectrum it is possible to estimate the EEW from equation 4.2 which equates to 111.2804 g/equiv. GC-MS also suggests that there is one pure product with a single peak at 5.023 min showing a mass of 222.099 Daltons. The sample before recrystallization was a viscous liquid. However, after purification the product was in the form of off-white crystals. As can be seen in the ^{1}H NMR spectrum there is still evidence of the solvents that were used with the peaks at 1.14, 3.46 and 3.56 ppm relating to 2-ethoxyethyl ether.

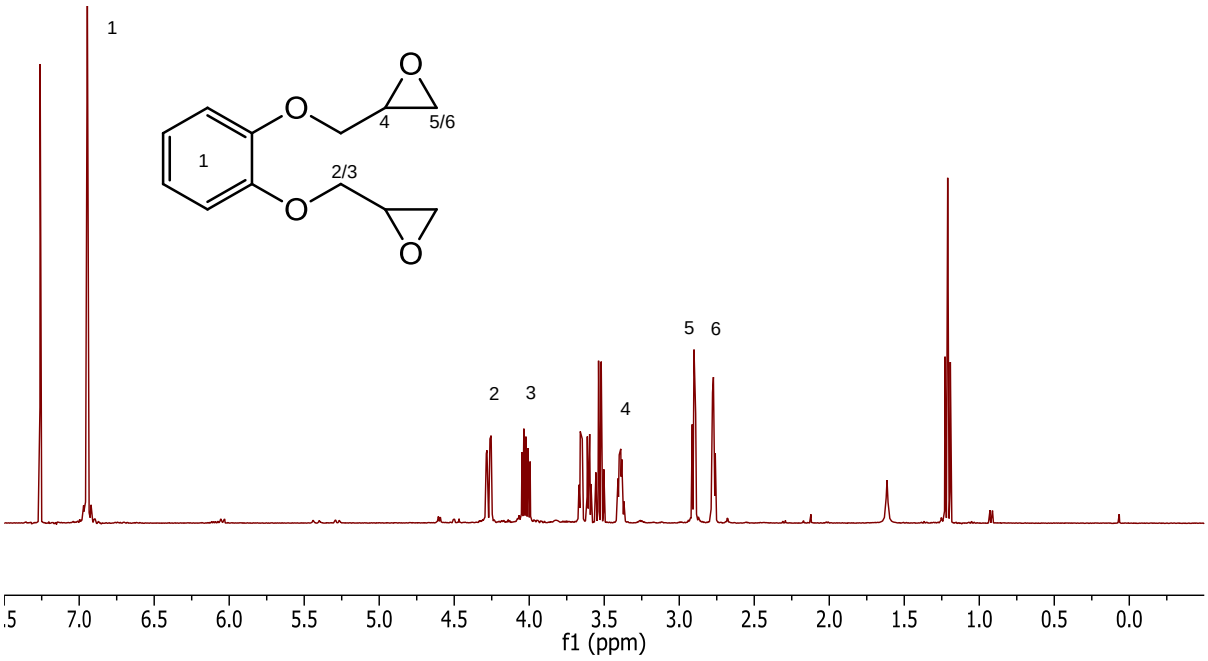

Figure 4.8 – ^{1}H NMR spectrum for catechol diglycidyl ether recrystallized from 2-ethoxyethyl ether and methyl isobutyl ketone (1:1)

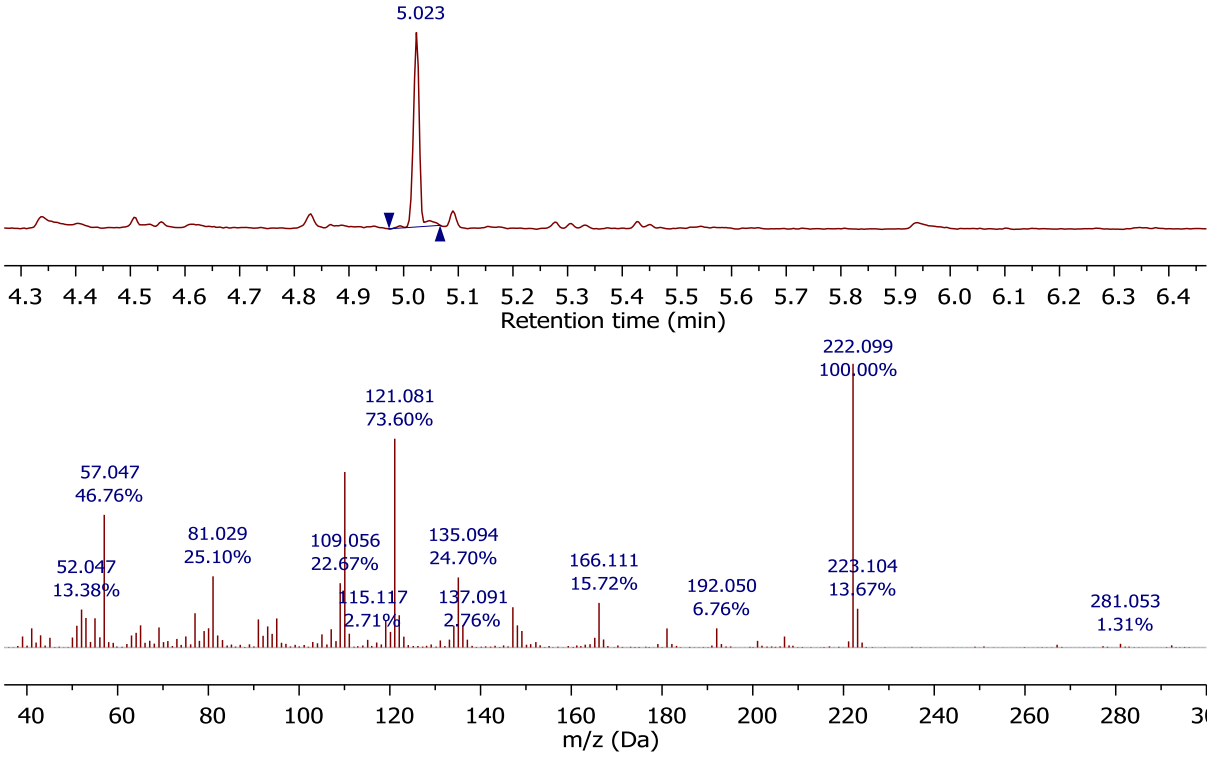

Figure 4.7 – GC-MS trace for recrystallized catechol diglycidyl ether.

4.3– Characterisation of 4,4'-methylenebiscyclohexyl amine

The structure of PACM gives rise to different configurations due to the two cyclohexane functional groups that are present in the molecule. This could affect the way in which the polymer is formed and change the properties obtained[214]. The different isomer configurations can be trans-trans, cis-cis and cis-trans as can be seen in Figure 4.8. If the ratio of the products are the same, twice as much of the trans-cis would be expected due to the two different configurations that this can have of trans-cis and cis-trans. As there were two types of PACM used both were analysed to determine if there is a change in the ratios of the isomers. The first is a solid wax from Sigma Aldrich and the second a liquid sample from Air Products under the name of "Amicure PACM".

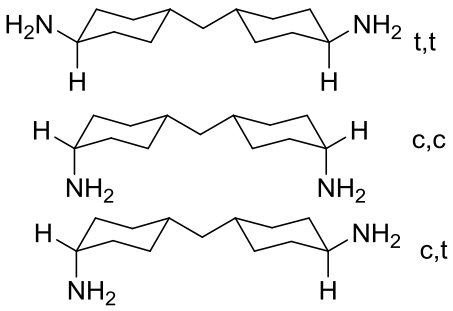

Figure 4.8 – Different possible isomers for PACM[215, 216]

4.3.1 – Characterisation of Sigma Aldrich PACM

The ^{1}H NMR spectrum (Figure 4.9) that was obtained is complicated due to the isomeric effects therefore different NMR spectroscopy methods were used to determine the main isomeric product. ^{13}C NMR spectroscopy (Figure 4.10) shows that there are multiple peaks that are expected with large intensities but there are also several peaks that have lower intensities that are for the different isomers. All of the larger peaks are split into doublets which could be due to isomers that have similar environments. With these splits in the ^{13}C NMR spectrum there are 15 different environments which suggests that there are three isomeric positions. HSQC NMR spectroscopy was used to attempt to determine the relationship of the

^{1}H peaks to the carbon environments that are present. COSY NMR spectroscopy was also used. The spectra show that there are most probably three components in the mixture as can be shown in both the ^{13}C NMR and HSQC NMR spectra. Utilizing 2D NMR spectroscopy it is possible to determine which peaks on the ^{1}H NMR spectrum relate to which species. Using this it is possible to get a rough estimate of how much of each are present. From peaks $1/1^{1}$ and 1^{2} it is possible to determine a mixture of 67% trans and 33% cis. GC-MS trace (Figure 4.11) also confirms this as there are three peaks observed at 18.16 mins, 18.24 mins and 18.30 mins. The relative intensities for these mixtures have been used to determine the relative ratios of each. For the peak at 18.16 the relative ratio is 50%, at 18.24 it is 47% and at 18.30 the ratio is 3%. This can then be compared to work done by Prince *et al*.[214] to determine the most likely probability of each of the isomers. The peak at 18.16 is most probably trans-trans, at 18.24 is most probably cis-trans and at 18.30 is most probably cis-cis. Therefore the most abundant isomer in the sample is the trans-trans isomer as it is more crystalline than the other two as suggested by Prince due to a higher degree of symmetry. They also suggest that the t-t isomers are more stable than the c-t isomer which in turn is more stable that the c-c isomer which would support the results that there is a larger amount of the t-t and c-t isomers.

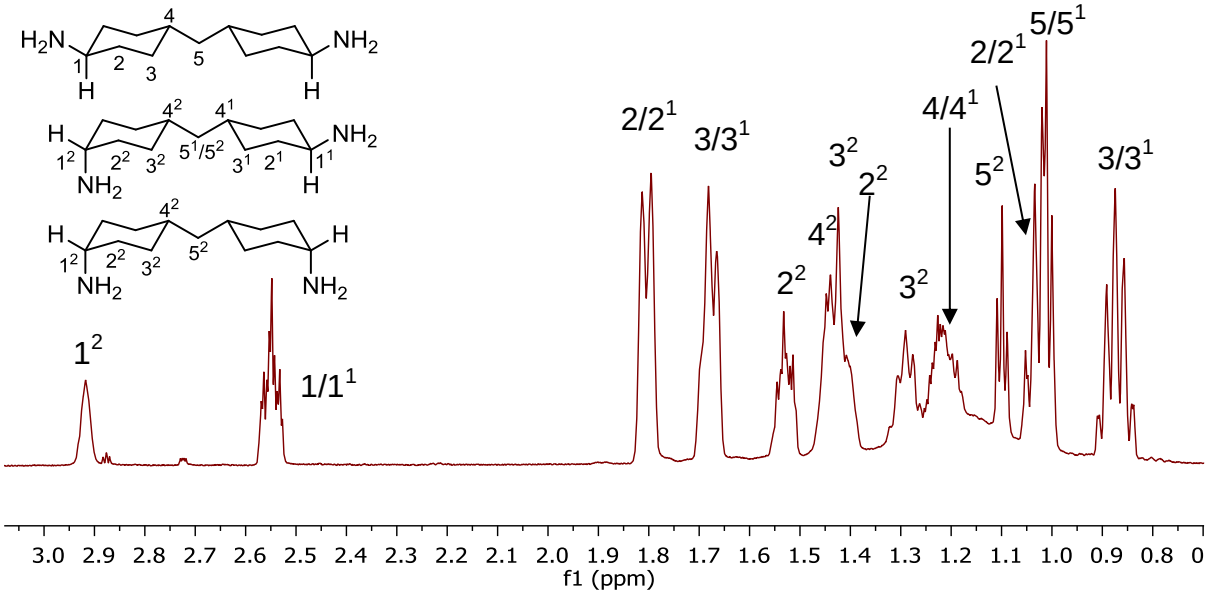

Figure 4.9 – ^{1}H NMR spectrum for Sigma Aldrich PACM. Peaks marked as $1/1^{1}$ and equivalent relate to the axial hydrogens on the trans section of the molecule in the t-t or the t-c. The peaks marked 1^{2} and equivalent relate to the cis section.

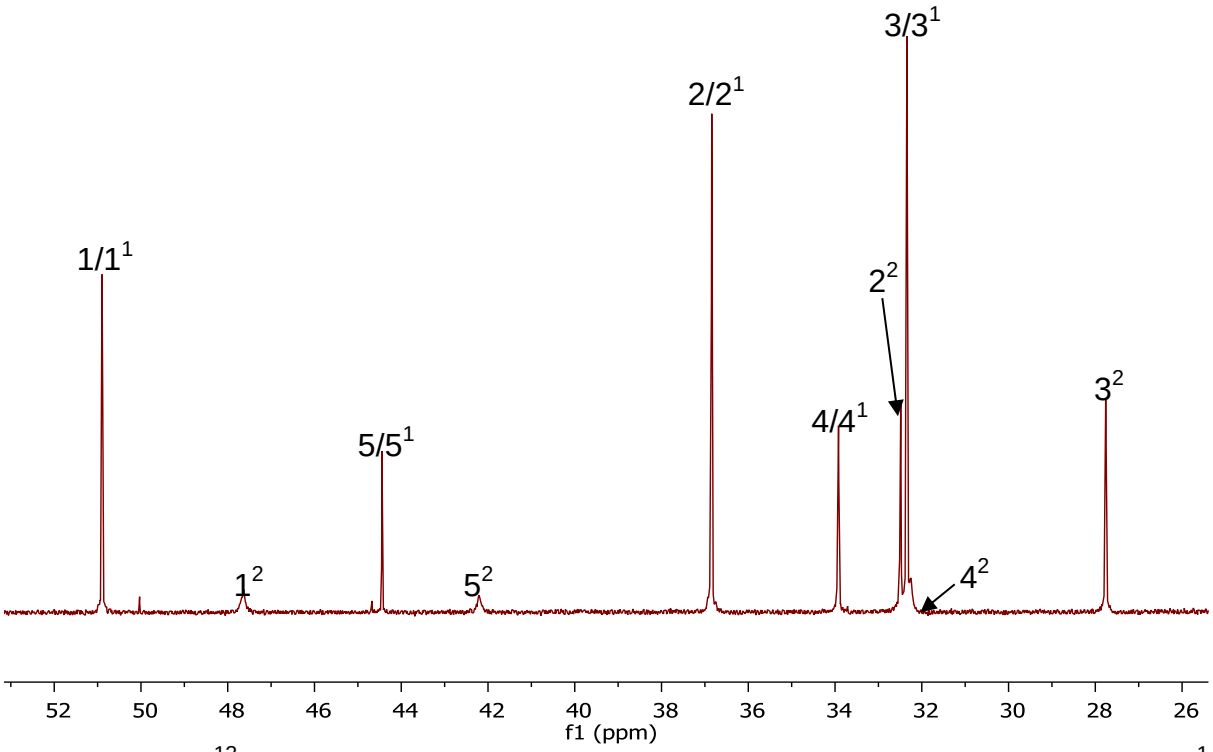

Figure 4.10 – ^{13}C NMR spectrum for Sigma Aldrich PACM. Peaks marked as $1/1^1$ and equivalent relate to the axial hydrogens on the trans section of the molecule be it the t-t or the t-c. The peaks marked 1^2 and equivalent relate to the cis section of the molecule.

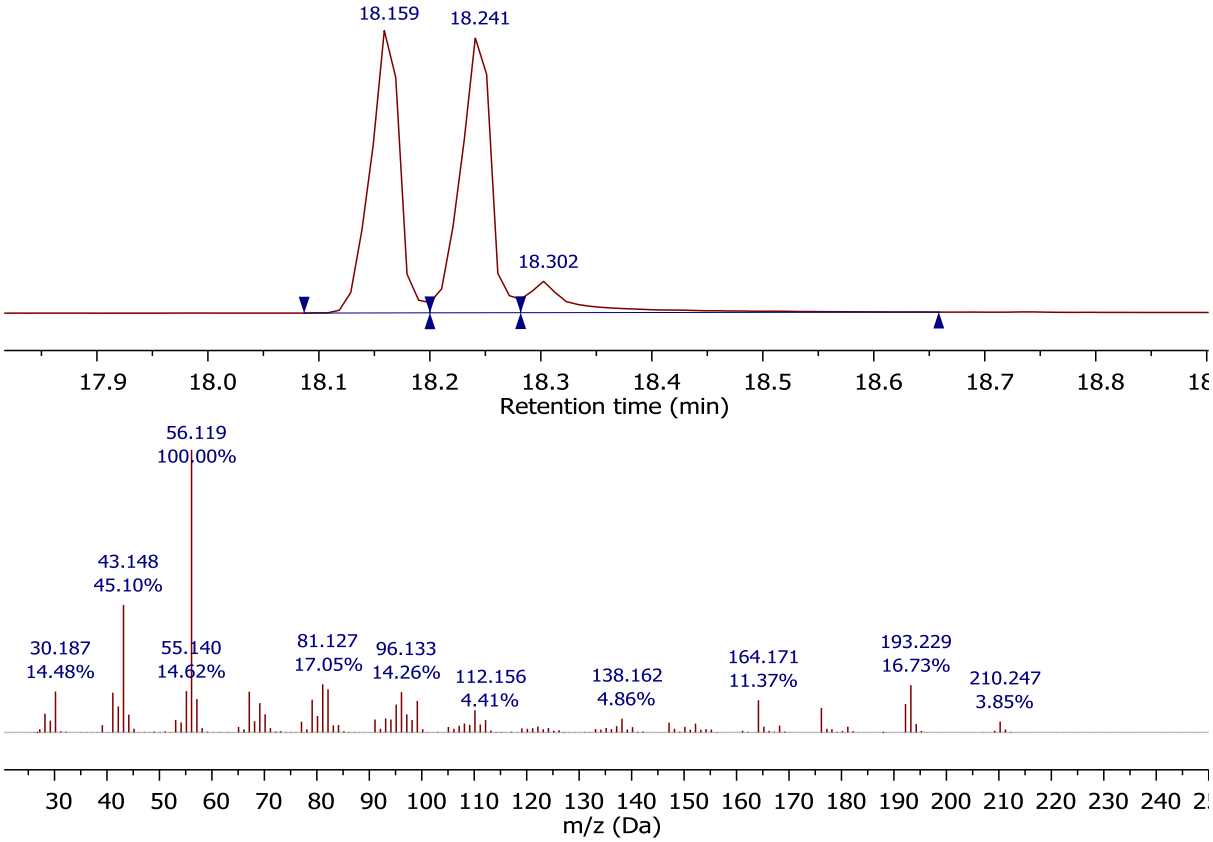

Figure 4.11 – GC-MS trace for Sigma Aldrich PACM. 18.159 = t-t, 18.241 = c-t, 18.302 = c-c

4.3.2 – Characterisation of Air Products PACM (L-PACM)

As can be seen the ^{1}H NMR spectrum was very similar to that of the Sigma Aldrich PACM due to there being all of the possible isomer configurations present. However this sample is in a liquid form which according to van Brederode[217] suggests that there is a lower amount of trans-trans and a varying amount of cis-trans and cis-cis. From the analysis of the ^{1}H NMR spectrum (Figure 4.12) it is possible to see that there is a drop in the intensity of the peaks that relate to those of the trans species. This can be seen from the peaks relating to $1/1^{1}$ and 1^{2} with the intensity of the cis species rising, this now gives a 46% of trans species and 54% cis species. This is also present in the ^{13}C NMR spectrum (Figure 4.13) as well where especially for the peaks of 2 and 2^{2} where there is a dramatic increase in peak 2^{2} compared to that of the Sigma Aldrich PACM. This suggests that there is less t-t species in the sample with it being a liquid due to the t-t species being more crystalline as discussed previously. However, if all of the trans peaks relate to a the

c-t isomer then there would be approximately 8% of the cis isomer. After analysis using GC-MS (Figure 4.14) it is impossible to determine how many species are present as the GC peak is a non-Gaussian peak containing more than one of the species.

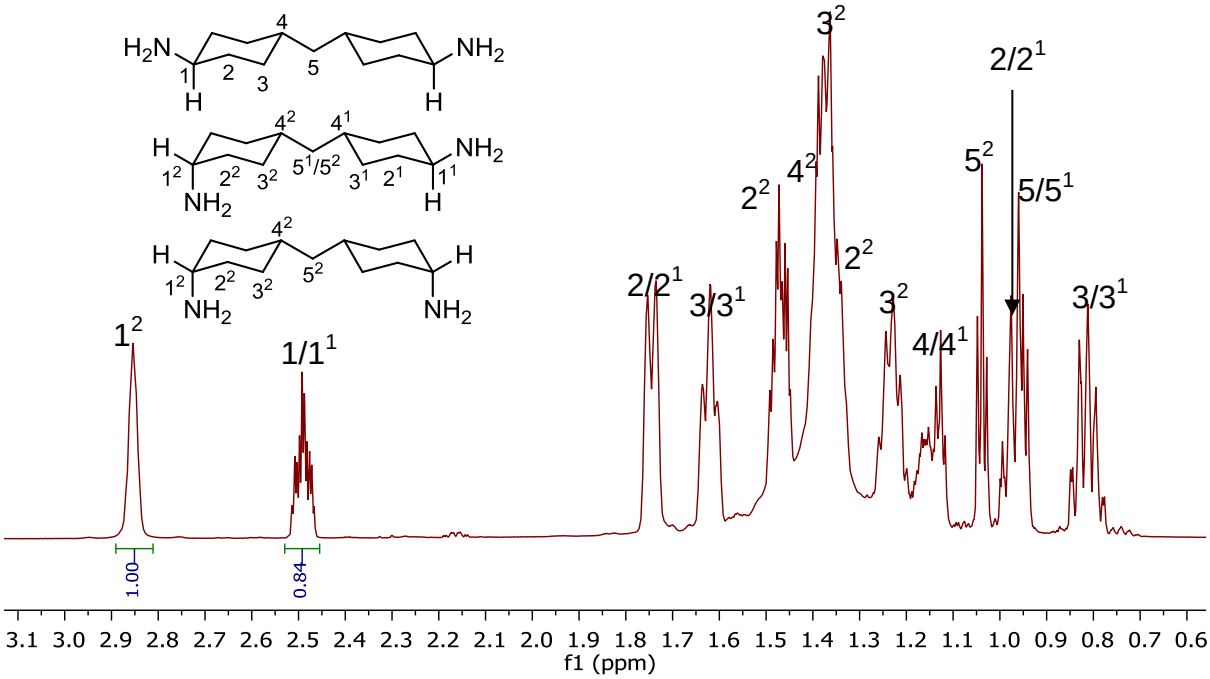

Figure 4.12 – ^{1}H NMR spectrum for Air Products PACM. Peaks marked as $1/1^{1}$ and equivalent relate to the axial hydrogens on the trans section of the molecule be it the t-t or more probably the t-c. The peaks marked 1^{2} and equivalent relate to the cis section of the molecule.

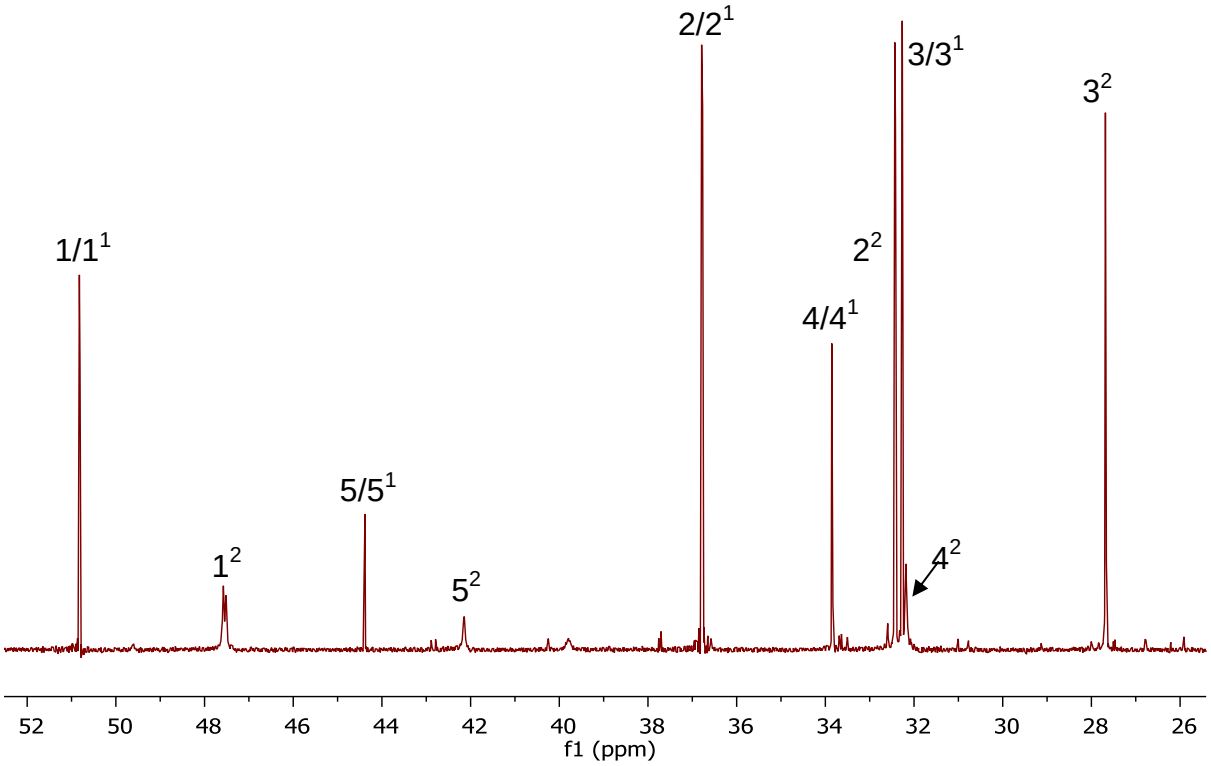

Fig 4.13 – ^{13}C NMR spectrum for Air Products PACM. Peaks marked as $1/1^1$ and equivalent relate to the axial hydrogens on the trans section of the molecule be it the t-t or most likely the t-c. The peaks marked 1^2 and equivalent relate to the cis section of the molecule.

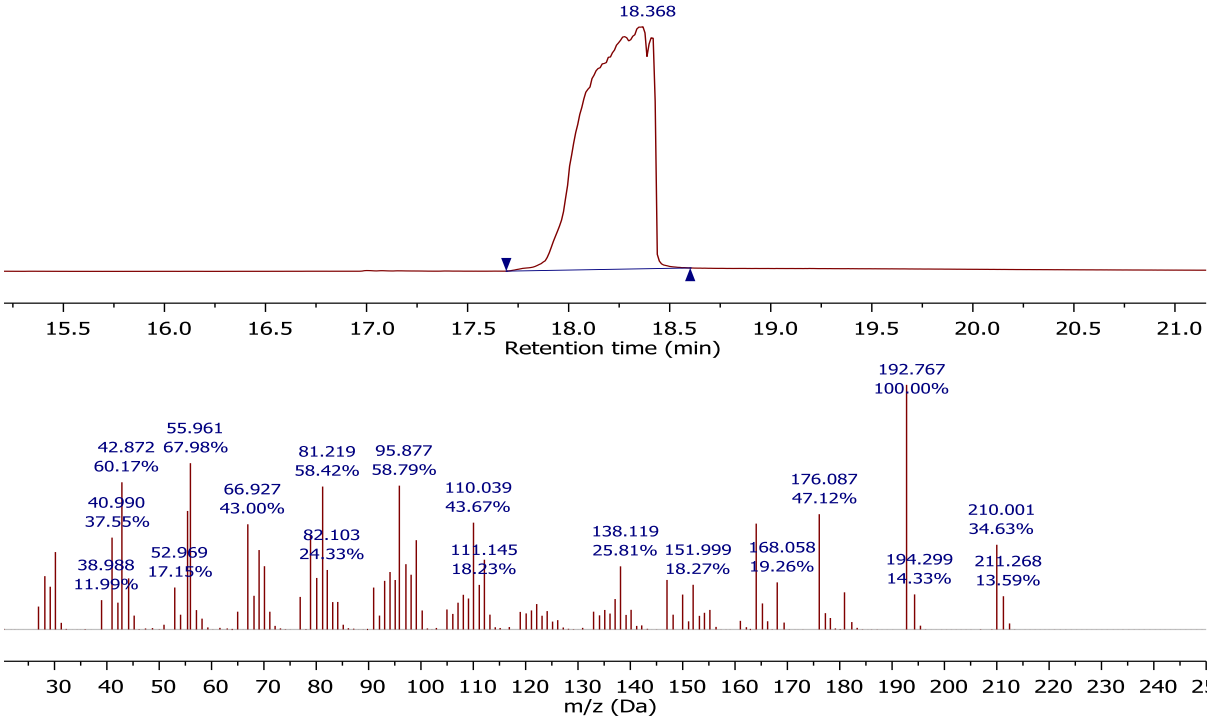

Fig 4.14 – GC-MS trace for Air Products L-PACM.

Over time this sample appeared to form crystals suggesting that there is the possibility of the trans-trans isomer crystallising out into the mixture. This can be seen in the GC-MS (Figure 4.15) for the sample which contains a small amount of crystals with the appearance of a second peak in the GC trace lower in retention time than the main peak. Comparing this to the Sigma Aldrich sample suggests that the appearance of this peak could be due to the trans-trans isomer.

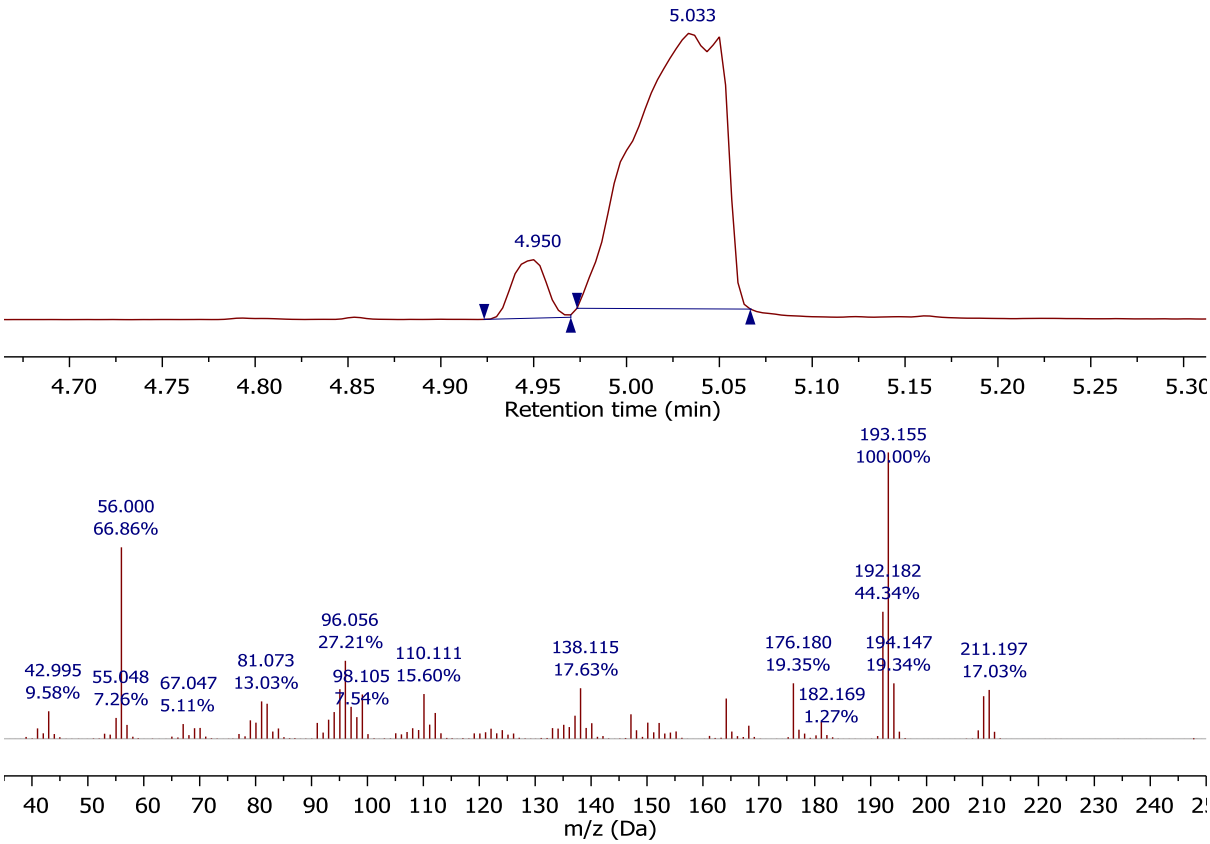

Figure 4.15 – GC-MS for Air Products L-PACM after time.

4.4 – Development of polymerisation technique

To determine the extent of curing of the polymer films, Differential Scanning Calorimetry (DSC) was utilized to see the change in the T_g after two heating runs. By using multiple heating cycles it is possible to determine what reversible and non-reversible transitions are present in the DSC. The T_g of a polymer is a reversible transition as it is the kinetic transition from the glassy state to a rubbery state. However for this polymer system there are several results that are non-reversible such as, aging and curing of the polymer. With the cross-linked nature of the polymer networks, after the first heating cycle the polymer cannot melt. DSC measures the heat flow in the sample and can give information on the heat capacity, the heat of reaction, the crystallinity and the purity of the sample.

4.4.1 – Development of curing method for RDGE

As RDGE was the most abundant epoxide available this was the starting point to determine the best method for curing the polymer networks. The variables that were to be studied are:

- The effect of curing at different temperatures
- The nature of the substrate (clean or coated)
- The effect of the different isomeric forms of PACM on the system

As the curing would need to be done at a temperature close to that of the glass transition temperature (T_g) this would need to be determined first. This is required to ensure that all of the chains have enough mobility to allow the functional groups to react.

4.4.1.1 – Kinetic study to determine T_g

To carry out this study differential scanning calorimetry was utilized. The DSC results (Figure 4.18) show that there is an endotherm on the first heating run at 74°C

which could be due to an initial melt of the system. After this there is an exotherm at that starts at 77°C and finishes at approximately 170°C. This could be due to the cure reaction that takes place with this polymer as it is highly exothermic as the energy emitted from this exotherm is 32.03 J g^{-1}. On the second heating run there is a phase transition that begins at 118°C and finishes at 132°C with a mid-point of 128°C which relates to the glass transition temperature. This shows that a final cure temperature close to 125°C is needed to produce a model system as this will

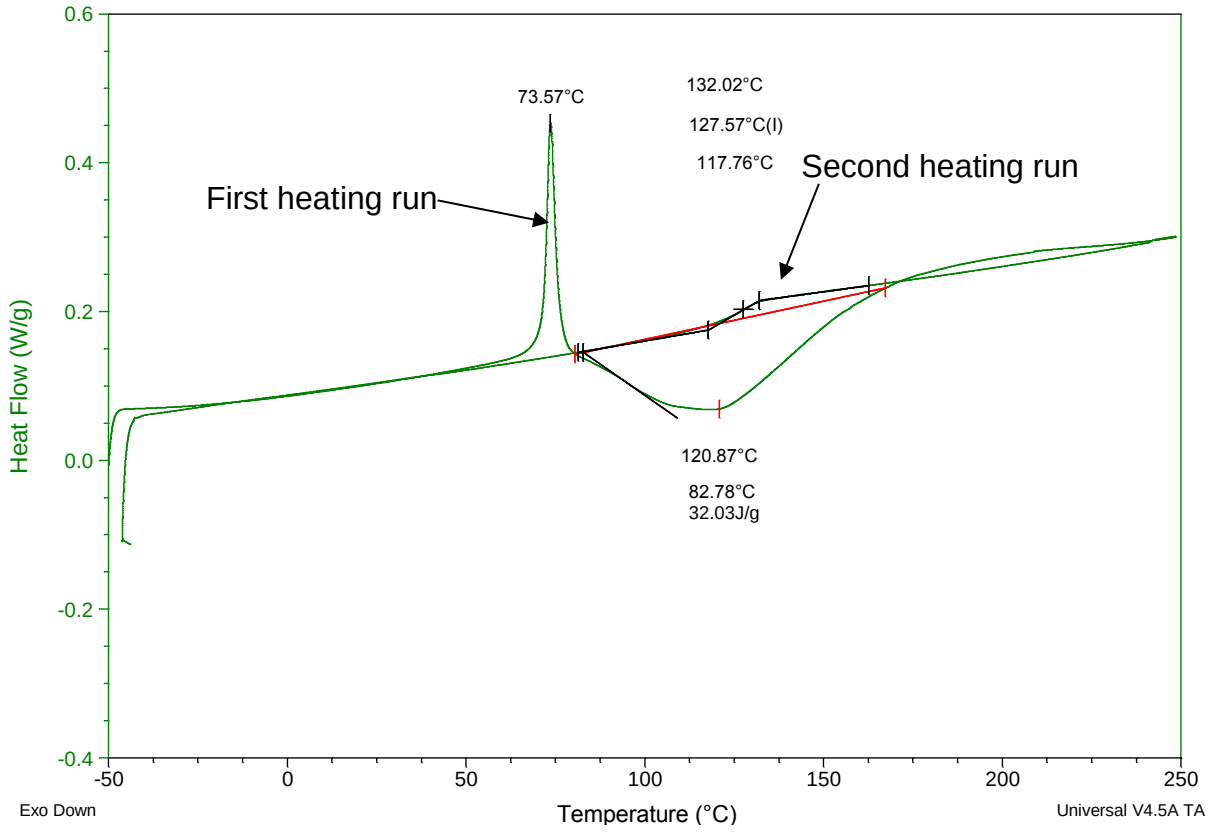

Figure 4.18 – DSC graph for a kinetic study of RDGE with Sigma Aldrich PACM

4.4.1.2 – Model system polymerisation on glass substrates

Using the T_g from the kinetic study the system was applied to a glass substrate and reacted at 120°C, as this was within 10°C of the T_g obtained. After 2 hours DSC data collected for the system shows that there is an increase in the T_g of about 6°C between the heating runs with the first being 93°C and the second being 99°C. However, both of these are lower than obtained from the kinetic study of approximately 30°C. After reacting for 72 hours the system was hardened and

relatively brittle and difficult to remove from the substrate as a film. The DSC results for this system show that the T_g in the first heating run is approximately 127°C whereas in the second heating run the T_g was 137°C which shows there is an increase of 10°C between the two runs meaning that not all of the polymer was cured as there would be no increase in T_g for a fully cured system as discussed in chapter 1.

4.4.1.3 – Curing at 140°C

Curing the polymer on a glass substrate at 140°C as the initial cure temperature appears to have a detrimental effect on the T_g of the polymeric system as can be seen in Table 4.1 with the T_g of both heating runs being lower than the kinetic study. The film is also difficult to remove when using this higher temperature with only shavings of the film being able to be removed which are not significant enough for this project. The T_g also appears to be lower than what is expected with it only reaching 103°C after 3 hours as previously the T_g had reached 137°C. As using clean glass substrate is difficult to obtain a good film and remove a sample, it is difficult to have good contact with the pan. This could affect the heat transfer between the polymer and the pan which could give a lower reading. Therefore changing the initial cure temperature could help to remove the sample before it is fully cured and then post cure the removed film

4.4.1.4 – Curing at 60°C and post curing at 140°C

Curing at 60°C overnight still made the film hard and brittle and also made it difficult to remove from the substrate, which again reduced the ability of the sample to have good contact with the pan. Post curing at 140°C gave inconsistent results as seen in Table 4.1.

Table 4.1 – Glass transition temperatures for different cure temperatures and times using Sigma Aldrich PACM

Experiment	Cure Temp (°C)	Time (h)	T_g 1st run (°C)	T_g 2nd run (°C)
4.4.1.3	140	1	71	91
		2	76	94
		3	88	103
4.4.1.4	60	18	70	80
	140	1	76	89
		2	84	89
		3	78	93
		24	113	122
		48	101	110

4.4.1.5 – Curing using liquid PACM on different substrates

Using the liquid PACM gave more consistent results with the film being noticeably less brittle and easier to handle. On the spray panel (left hand side of Figure 4.19) there was a good film that was easy to remove after curing at 60°C. The tape however (right hand side of Figure 4.19) did not form a good film with the polymer appearing to de-wet from the substrate. However, the DSC data for each of these was very similar.

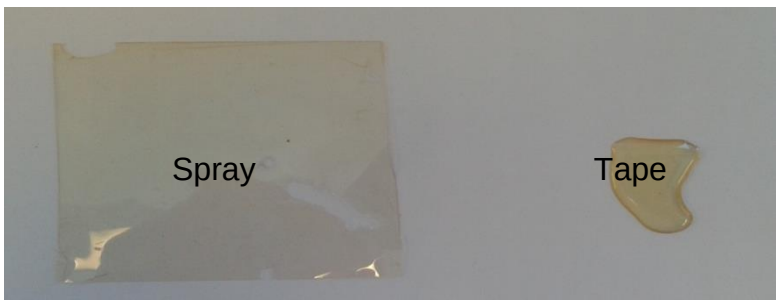

Figure 4.19 – Comparison of films removed from PTFE sprayed substrate and from PTFE taped substrate.

After heating at 60°C for 18 hours, DSC results (Figure 4.20) for both the samples show an endotherm at 88°C which could be due to melting or aging of the polymer. There is also an exotherm for both at 135°C (with 52.94 Jg^{-1}) for the spray and 130°C (with 61.61 Jg^{-1}) for the tape which could correspond to residual

polymerisation, fully cross-linking the polymer. The T_g's for are also similar with the spray having a T_g of 127°C and the tape 125°C. This is similar to what was previously found in the kinetic study performed and unlike the results that were obtained using the a clean glass substarte.

Table 4.2 – Effect of changing substrate on glass transition temperature for polymers from RDGE and L-PACM

Experiment	Cure Temp (°C)	Time (h)	T_g 1st run (°C)	T_g 2nd run (°C)
Spray	60	18	N/A	127
	140	2	124	126
Tape	60	18	N/A	125
	140	2	128	129

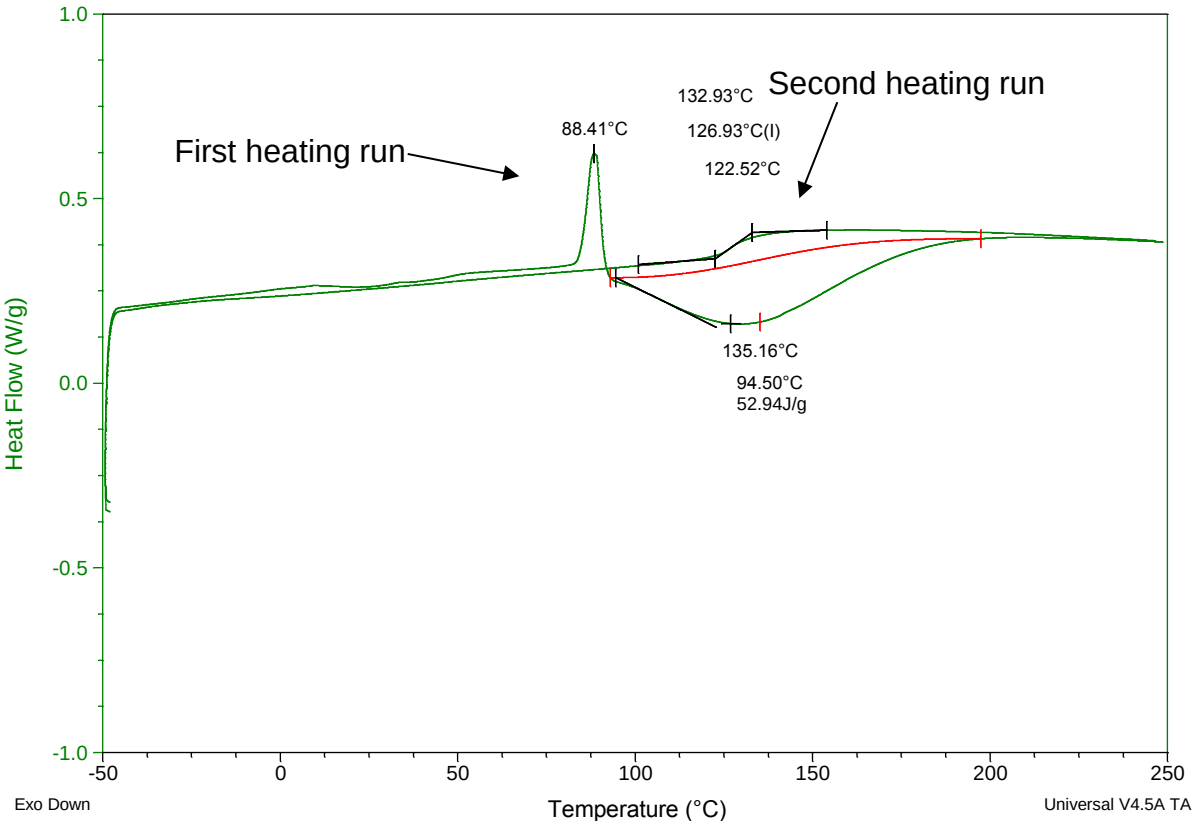

Figure 4.20 – DSC graph for after 60°C cure.

After heating for 2 hours at 140°C, both of the coatings appear to have been fully cured. The sprayed substrate sample has an increase of T_g of 2°C with the first run being 124°C and the second 126°C. The tape sample also has an increase of 1°C with the first heating run T_g of 128°C and the second 129°C. The reason why

the tape sample has a lower difference could be due to the exotherm of the polymer occurring in more concentrated area as they were in globules instead of a film.

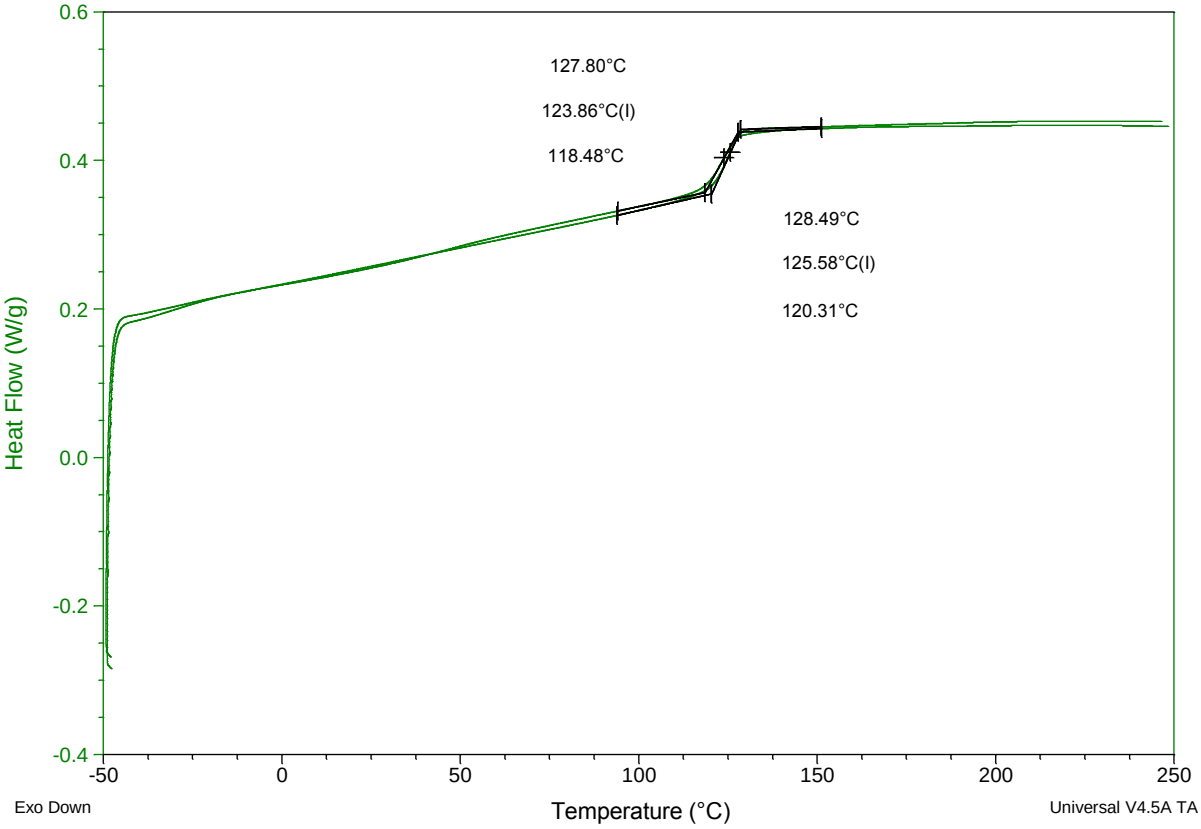

Figure 4.21 – DSC graph for after 140°C post cure.

4.4.2 – Development of curing method for HDGE

As the melting point of hydroquinone is quoted to be 118-119°C[218] a different method than that used for the curing of RDGE with PACM was researched. Therefore as there is a higher melting temperature, a mixture of HDGE and L-PACM was prepared before heating and then heated under stirring until there was a homogenous mixture. This occurred at a temperature of 110°C therefore this temperature was used for the curing of the mixture as this would keep the mixture in the liquid state.

4.4.2.1 – Initial Curing of HDGE using liquid PACM at 110°C

The procedure used in this report for the curing of HDGE with L-PACM appears to have been successful. The polymeric material that has been produced has a clear dark brown colour to it but appears to have no solid material present. The DSC results show however that the reaction has not gone to completion with the T_g of the first heating cycle being 126°C but on the second heating run it appears to be 149°C (Figure 4.22). What seems to be an exotherm appears after the T_g during the first heating run with a mid-peak temperature of 156°C at 5.79 Jg^{-1}. There is also a problem with removing the polymer from the substrate as it has adhered to the glass panel.

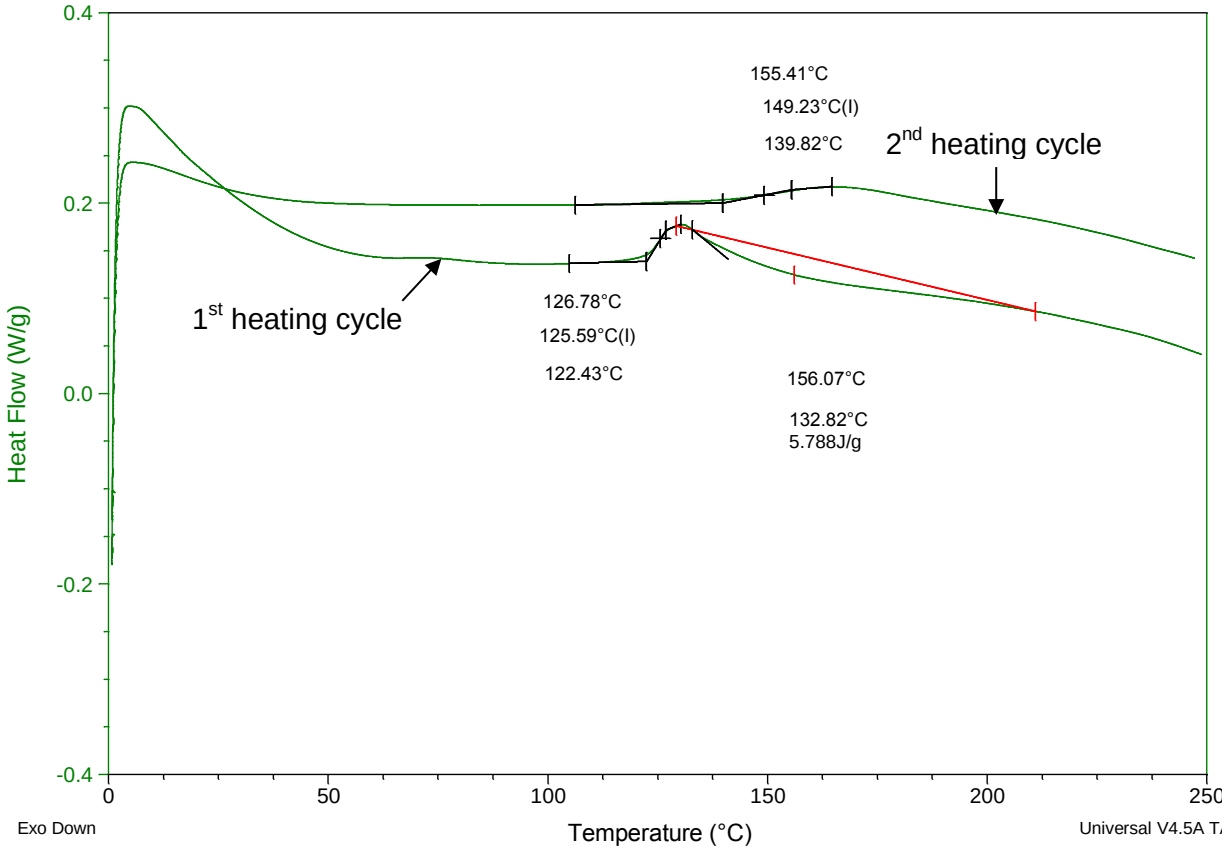

Figure 4.22 – DSC graph for the initial cure of HDGE at 110°C

4.4.2.2 – Kinetic study of HDGE using liquid PACM

As the polymer did not go to full cure after reacting the film at 110°C over-night a test to determine the best cure temperature based on the T_g was performed

in the same manner as previous. The DSC results (Figure 4.23) show that there is an endotherm on the first heating ramp at approximately 60°C which could be due to an initial melt of the system or ageing of the polymer. After this there is an exotherm that starts at 70°C and finishes at approximately 170°C. This could be due to the cure reaction that takes place with this polymer as it is highly exothermic. There is also a slight endotherm at 100°C during the exotherm which could relate to some melting of the polymer after possibly solidifying at the lower temperatures before reaction. On the second heating run there is a transition that begins at 107°C and finishes at 143°C with a mid-point of 118°C which relates to the glass transition temperature. This is slightly lower than that achieved previously which had a T_g of approximately 150°C. However it is difficult to decipher a T_g from the kinetic run as there is only a slight change in the heat capacity which restricts the ability to determine and accurate reading.

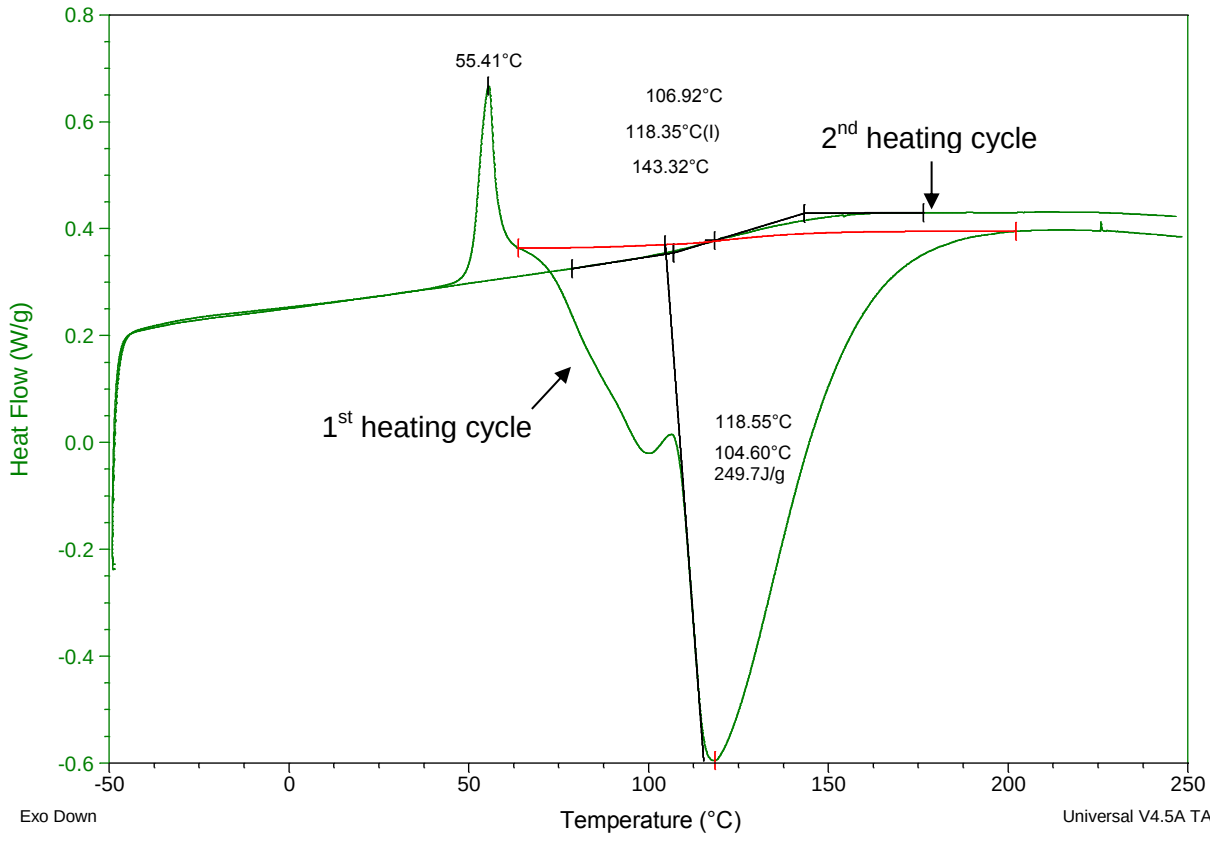

Fig 4.23 – DSC graph for kinetic study of HDGE with L-PACM

4.4.2.3 – Initial cure of 110°C with post cure of 150°C

As the previous T_g obtained was approximately 150°C it was decided that this would be a good temperature to react the polymer in an attempt to obtain full cure. As the RDGE sample was difficult to remove after it had been cured at just the higher temperature a lower temperature was used for the initial cure. With the previous data collected showing that the system was a liquid above 110°C this initial temperature was used to keep the entire sample in the liquid state. However even after this initial cure a perfect film was not removed however a partial film was able to be recovered. The colour of this polymer sample was significantly darker then the RDGE sample as can be seen in Figure 4.24. As can be seen from the DSC results in Figure 4.25 it is still difficult to determine a T_g for the sample as there is only a slight change in the heat flow. This could be due to a change in crystallinity in the sample which has been shown to have a decrease in the heat capacity (C_p) at the T_g as shown by Lappalainen e*t al*[219]. This is due to the decrease in the amorphous phase in the polymer material which gives rise to the T_g as described earlier. However it is possible to determine a slight T_g from the cure at both 110 and 140°C as summarised in Table 4.3. In both DSC results there appears to be a slight exotherm after the T_g on the first run which suggests that the reaction did not go to completion even after the post-curing at 140°C. However instead of this appearing as a peak it looks to be more of a step change with the C_p not levelling out again as with RDGE samples. This could be due to possible crystallisation of the sample which would suggest that this polymer is more crystalline than the others. As can be seen in Table 4.3 there is a dramatic increase in the T_g for the polymer after curing at 110°C of over 40°C with the T_g after the second run being 150°C. This is higher than that after the reaction is pushed to a higher temperature of 150°C which has a second run temperature of 10°C lower. The difference is lower between the first run and the second run of less than 20°C which suggests further cure.

Table 4.3 – Variations in the T_g of HDGE determined from DSC.

Experiment	Temperature (°C)	Time (h)	T_g 1st run (°C)	T_g 2nd run (°C)
4.4.2.3	110	20	102	150
	150	18	124	141

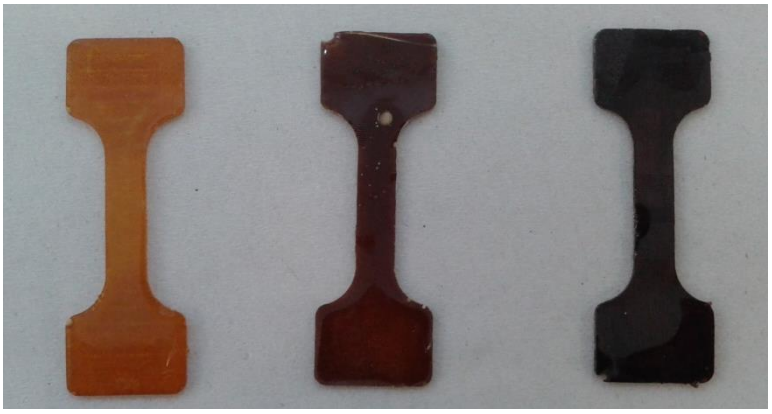

Figure 4.24 – Difference between polymers from RDGE (left), HDGE (centre) and CDGE (right).

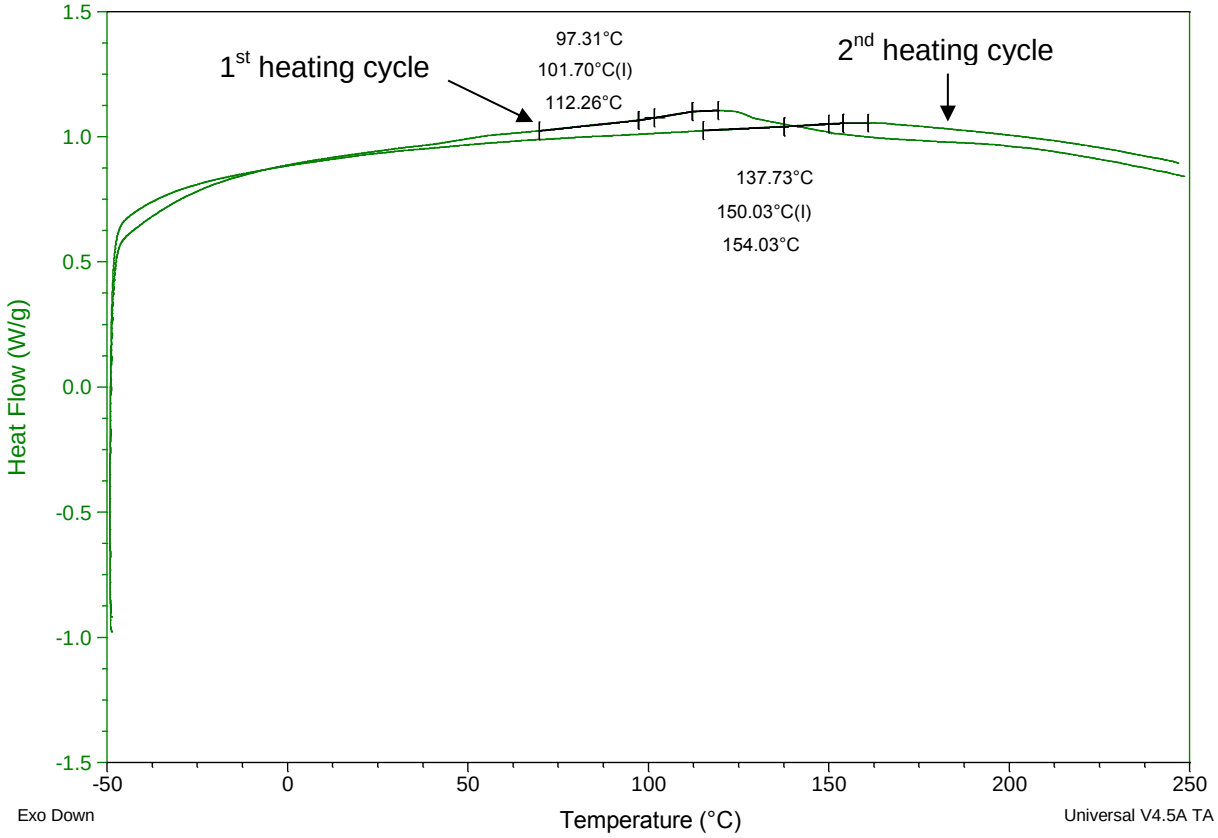

Figure 4.25 – DSC graph for HDGE with L-PACM cured at 110°C for 20 hours.

4.4.3 – Development of curing temperature for CDGE

This sample appears to have a lower melting point of approximately 30°C which means that the same method of polymerisation as used for RDGE could be used with this epoxide too. By melting the CDGE and adding L-PACM a

homogeneous mixture was able to be produced which was then added to the PTFE sprayed glass panel.

4.4.3.1 – Kinetic study of CDGE using liquid PACM

The analysis of this polymer shows to endothermic peaks that occur before the exotherm in the first heating run as shown in Figure 4.26. This could relate to melting of the starting materials and or oligomers and or the aging of the polymer. The exotherm could show the curing of the reaction which starts at 63°C and has a change in energy of 85.33 Jg^{-1} and a mid-point of 113°C. The T_g on the second heating run is the only result that is observed which appears at 104°C which shows that this is the temperature that is required for curing.

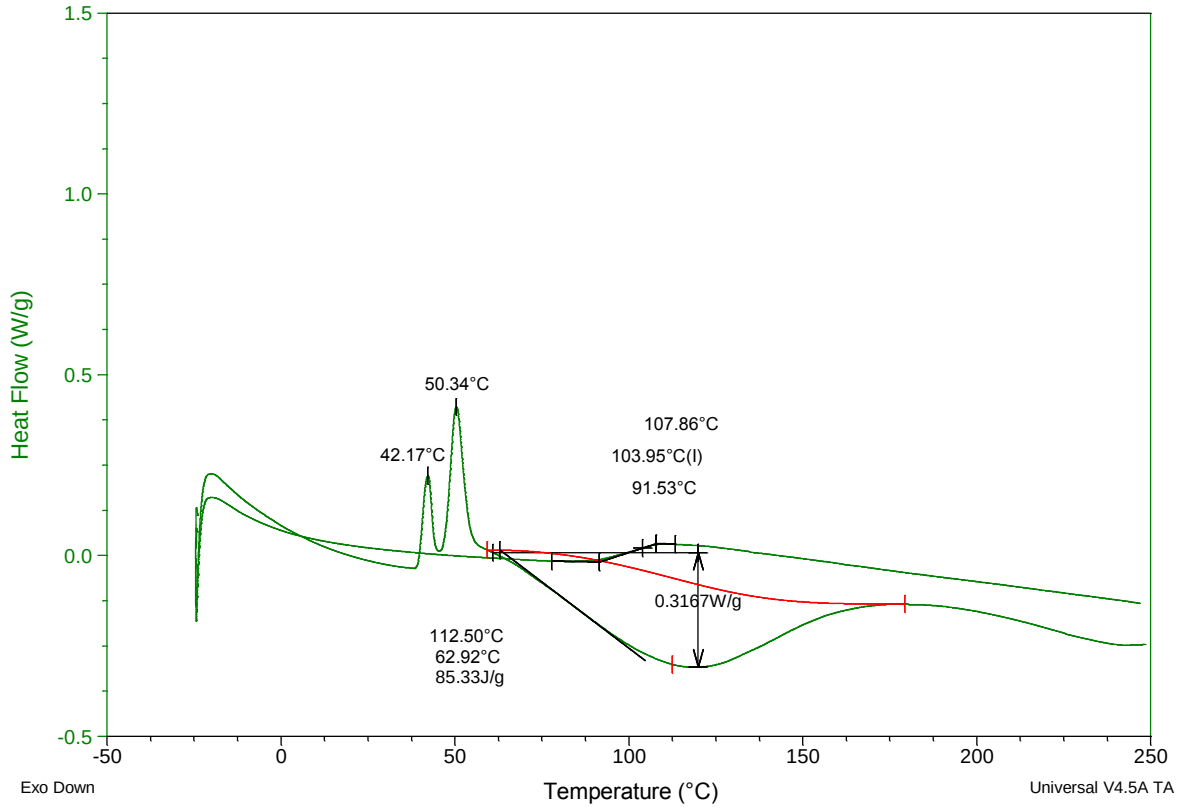

Figure 4.26 – DSC graph for kinetic study of CDGE with L-PACM

4.4.3.2 – Initial cure of 60°C with post cure of 120°C

As the kinetic study shows the T_g of the polymer is roughly 100°C but due to possible difficulties in removing the polymer from the substrate, therefore, a lower cure temperature was initially used in the hope that this would be easier to remove due to not being fully cured and therefore more flexible. However this polymer was still difficult to remove and as can be seen from the DSC (Figure 4.27) after curing at 60°C there appears to be a large endotherm at 82°C which does not return to the initial heat capacity. This could be due to a change from the glassy to the rubbery state which suggests that the T_g occurs under this peak. This could be due to this temperature physically ageing the polymer and therefore a higher temperature is needed to complete the cure. On the second heating run in the DSC the T_g occurs at 101°C. The peak at 82°C does not occur in the second heating run which suggests that it could be physical ageing of the polymer. After taking it approximately 40°C above the T_g rejuvenates the polymer after annealing at this temperature or above. The physical aging process occurs when a polymer is held below the T_g for extended periods which rotate the polymer chains and also decreases the free volume of the polymer[220]. The rejuvenation appears to have occurred as in the DSC graph for the polymer cured at 100°C there does not appear to be any endothermic peak that would relate to this. However the T_g for the first heating run is still lower than what is expected being only 75°C which is over 25°C lower than that after the second heating run. This suggests that the polymer is not fully cured as the T_g on the second heat cycle was 99°C.

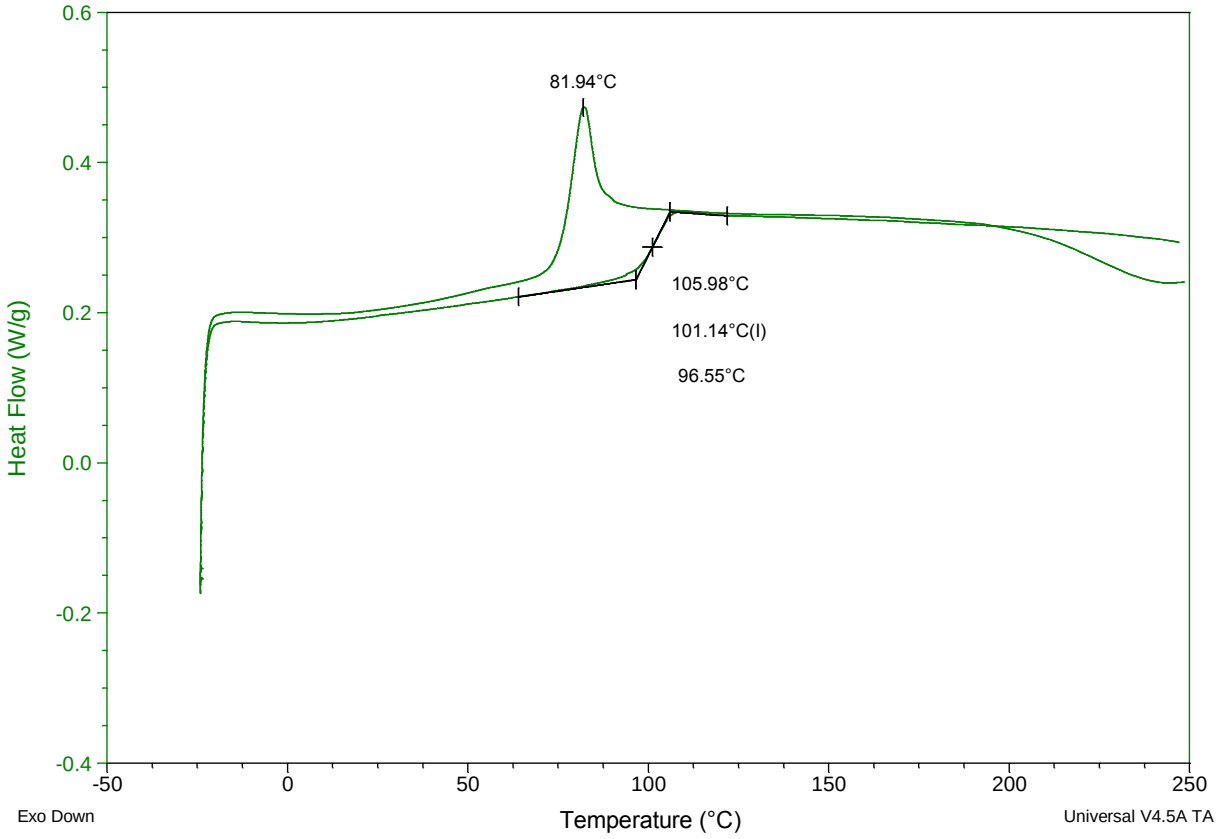

Figure 4.27 – DSC graph for CDGE with L-PACM cured at 60°C for 18 hours

4.5 – Preparation of polymer networks of 1 mm thickness

Some of the analysis on the polymers require the samples to be about 1 mm thick which requires a different method of polymerisation due to the film being impossible to be removed using a 1 mm draw-down bar. Also some of the samples require to be shaped and the polymers that are made are brittle which means that they are impossible to form into the shapes that are required. Therefore another method was required to produce the required polymers. As the PTFE spray made the samples slightly easier to use, PTFE moulds of approximately 1 mm were used as they could be made into different shapes for the analysis required. As can be seen in Figure 4.28 there are two main PTFE moulds used, the square one for making samples for most analysis and the bone shaped mould for samples for thermo-mechanical analysis.

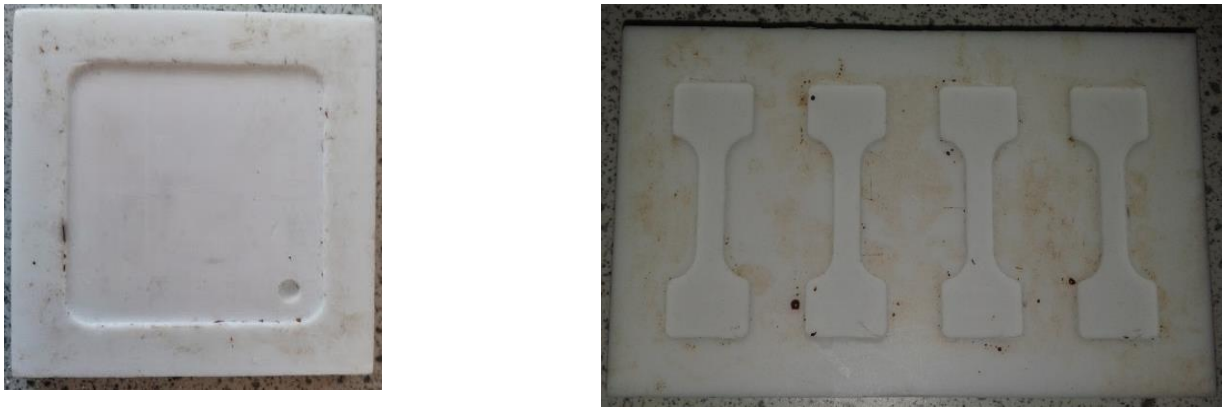

Figure 4.28 – PTFE moulds for producing samples of approximately 1 mm. (Left) mould for most analysis; (Right) mould for thermo mechanical analysis.

All of the epoxides were melted before addition of L-PACM and then put into the mould and smoothed over until the polymer covered the mould. For HDGE the mould was preheated to the cure temperature so that there would be less chance of the polymer coming out of the liquid state.

4.5.1 – Determining a cure system to use on each system at higher temperature

As the cure cycles for each of the polymers appears to have pushed the reaction to almost full conversion a uniform cure system for the polymers was required. Therefore the polymers were submitted for thermogravametric analysis (TGA) to determine at which temperature they start to degrade and therefore what would be a safe temperature for the cure. As can be seen from the results in Figure 4.29 most of the polymers appear to start to degrade at approximately 275°C with the CDGE degrading the fastest. However with the CDGE there is also a decrease over the temperatures 50°C to 275°C of 5% which could be due to moisture in the film (obtained during curing). Therefore the temperature at the mid-point of this curve was used as only less than 3% loss in the CDGE.

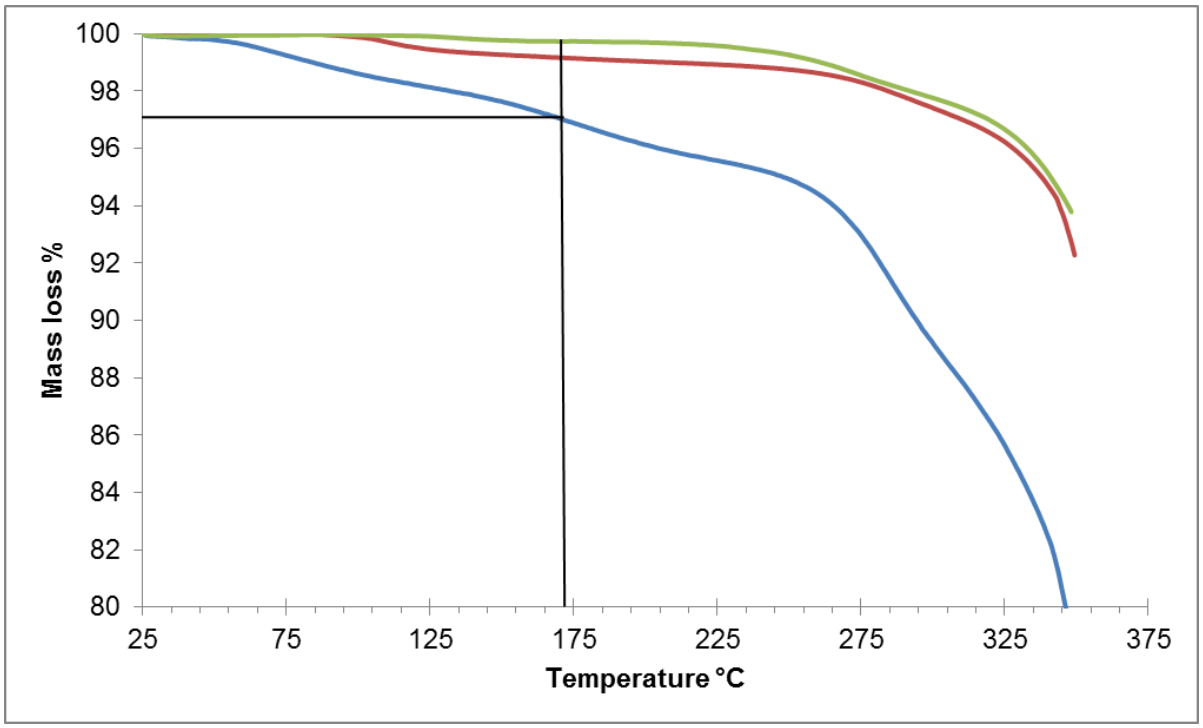

Figure 4.29 – TGA results for all of the epoxides to determine a cure temperature that does not degrade the polymers. – RDGE; – HDGE and – CDGE, the line relates to less than 3% degradation of CDGE.

From this data we can see that at 170°C the samples are all stable and therefore as a post-cure temperature this would be the best. However initial

polymerisations at this temperature might affect the polymer cure therefore a lower temperature of 100°C was chosen as an initial cure as it would keep all of the polymers in the melt state and also not physically age the CDGE as was found to have happened at 60°C.

4.5.2 – Polymerisation of RDGE using PTFE mould at 100°C, post cure at 170°C

Curing at this new temperature does not change the T_g of the sample as compared to experiment 4.4.1.5 as can be seen in Figure 4.30 which shows that the T_g of the polymer for the first heating run is 129°C which is only slightly increased on the second heating run to 130°C. This is consistent with the previous T_g's, obtained using 140°C as the cure temperature which were only slightly lower at 126°C. This could be due to the sample being pushed to further completion at the higher temperature.

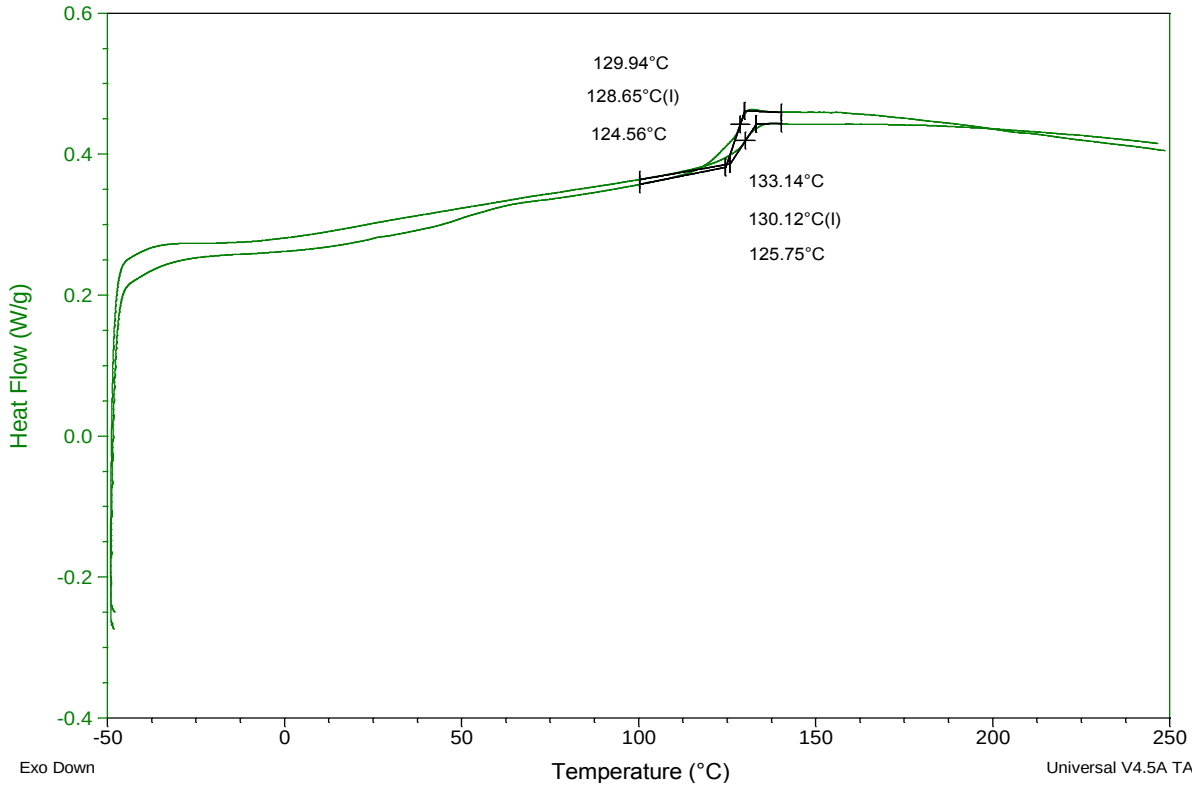

Figure 4.30 – DSC graph for RDGE with L-PACM cured at 100°C for 16 hours and post cured at 170°C using PTFE mould

4.5.3 – Polymerisation of HDGE using PTFE mould at 100°C, post cure at 170°C

The DSC results (Figure 4.31) for this polymer show that there is an increase in the T_g from 107°C (previously obtained in section 4.4.2.3) to 124°C on the first heating cycle. However in using the higher temperature the transition appears have a stronger change in the C_p which makes analysis easier[221]. This could be due to a change in the cross-linking as it has been reported that a change in the amount of cross-linking in a polymer will change the ΔC_p[222]. There also appears to be a transition which occurs at a lower temperature of 53°C which does not appear in the second heating run. This could be due to low molecular weight oligomers which react at higher temperatures in the DSC. The second heating run appears to only have the T_g occurring at 147°C which is slightly higher than that of the previous method in section 4.4.2.3 by 7°C. Again there is an increase in the change of the C_p which also suggests that there is a change in the cross-linking. There is a smaller increase in the T_g between the two heating runs which suggests that the polymer has undergone a higher cure at this temperature as compared to previously.

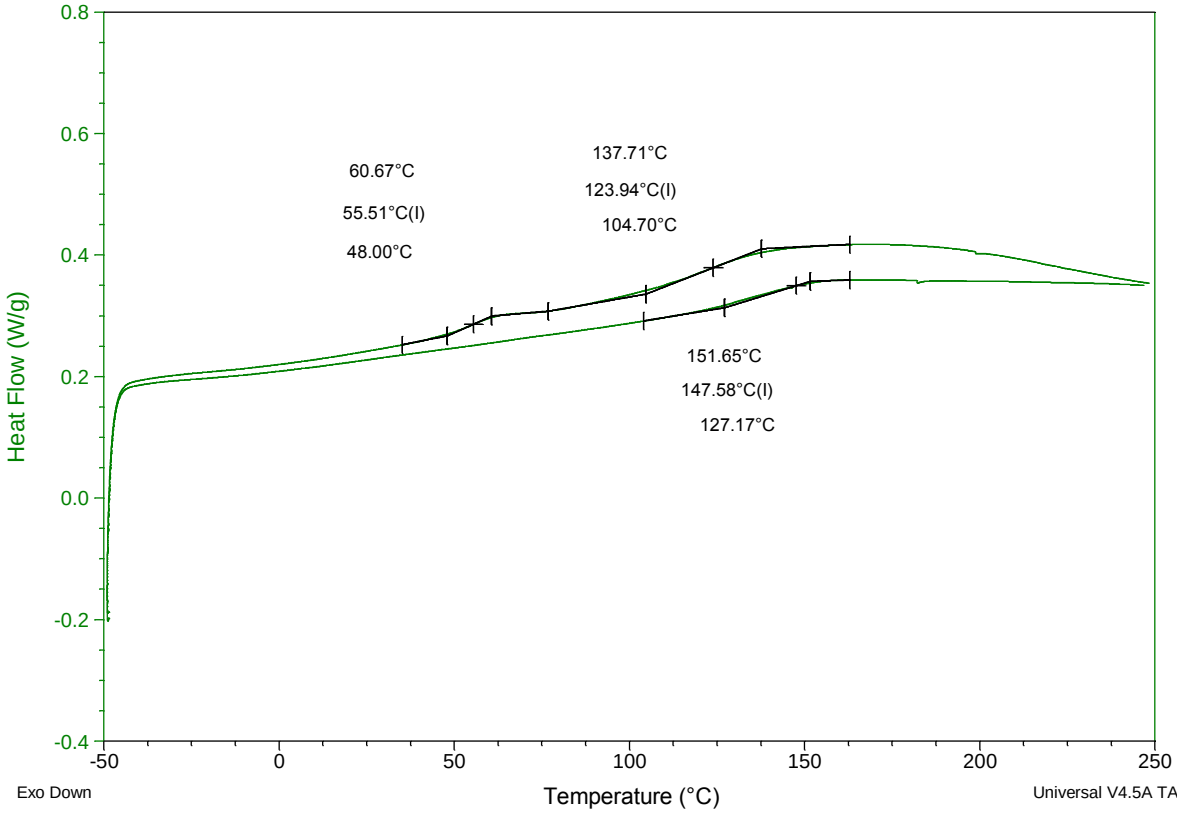

Figure 4.31 – DSC graph for HDGE with L-PACM cured at 100°C for 16 hours and post cured at 170°C using PTFE mould

4.5.4 – Polymerisation of CDGE using PTFE mould at 100°C, post cure at 170°C

With the CDGE sample, the DSC (Figure 4.32) shows an increase in the T_g between the first and second heating runs of circa 11°C. Comparing to the previous results obtained (section 4.4.3.2) the first heating run does not contain evidence of aging in the polymer. There also appears to be an exotherm occurring after 200°C which could be due to further cross-linking of the film. The second run however is very similar to that previously found with only a change from 101°C to 105°C which shows that the thermal properties of the sample are similar. This suggests that the reaction time at 120°C is run for long enough to produce full conversion of the polymer.

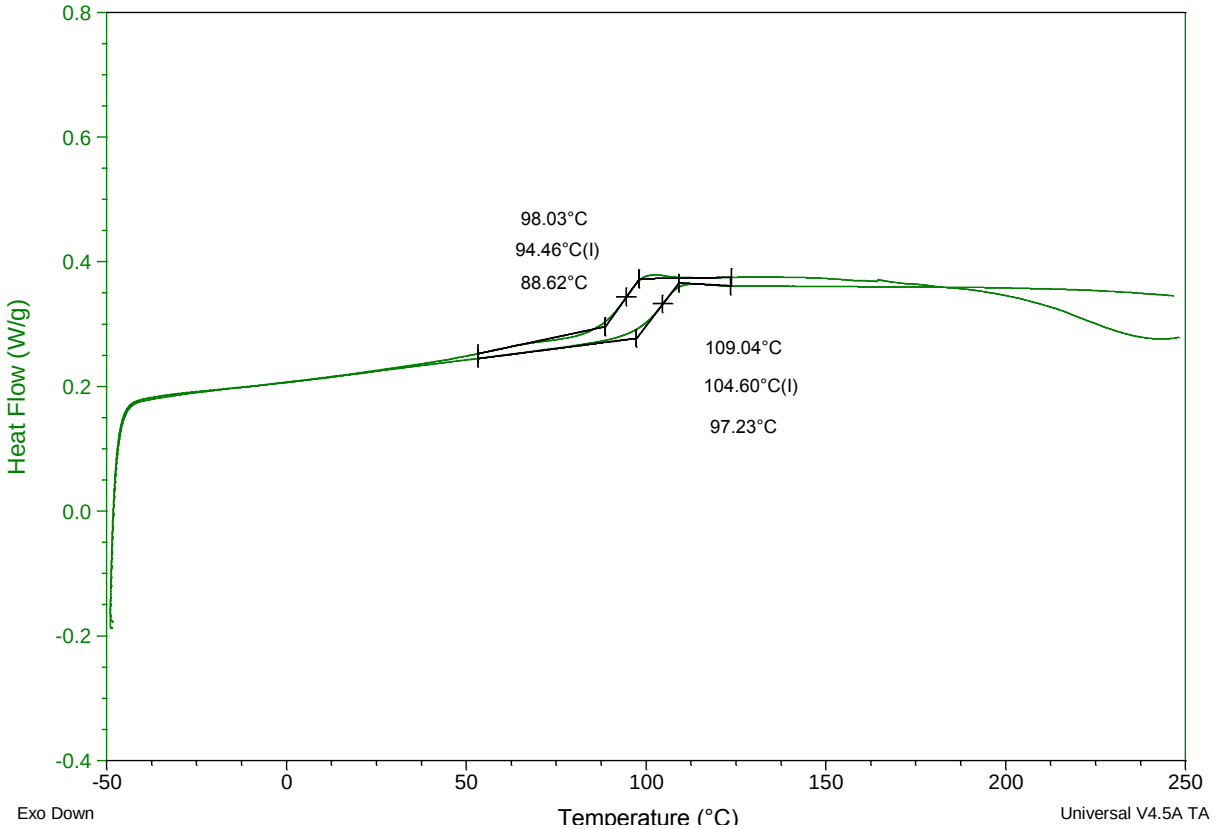

Fig 4.32 – DSC graph for CDGE with L-PACM cured at 100°C for 16 hours and post cured at 170°C using PTFE mould

4.6 – Conclusion

As can be seen the epoxides were all purified to above 95% which is acceptable for the polymerisations. As can be seen from the NMR spectra and GC-MS the samples contain no oligomers and only pure epoxide and some residual molecules containing some alkene groups from the synthesised epoxides.

The differences between the two types of amine curing agent used shows that there is a difference in the isomer content. As the 4,4'-methylenebis(cyclohexyl) amine contains two cyclohexane rings gives rise to three different configurations. Sigma Aldrich's PACM is mainly the trans-trans sample as this is the most readily available isomer with several papers suggesting that this is the most stable isomer[214], and also more crystalline. The Air Products PACM however is in the form of a liquid which initially suggests that it has less of the trans-trans isomer present. Analysis of this shows there is mainly one isomer with a potential second isomer. However it is difficult to determine which isomer this is. After time however the sample became more crystalline which, when analysed showed the appearance of another isomer which occurs where the trans-trans isomer appears in the GC trace.

Using the different amines to cure the epoxides showed that there was difficulty in producing good removable films using the Sigma Aldrich PACM. This could be due to the crystallinity of the amine. Even utilising different substrates the Sigma Aldrich PACM produced films that were not readily removable. However switching to the Air Products L-PACM the films produced for each of the epoxides were more readily removed for analysis.

By changing time and temperature and curing agent it is possible to obtain a good polymerisation technique for all of the isomers. As they all have different melting points different temperatures close to that of the T_g of the polymers were used to produce the polymer films. By changing the reaction time it is possible to produce a higher degree of curing as measured by the change in the T_g determined by DSC. If the sample was not fully cured the T_g's would increase due to vitrification

of the sample at the temperature of cure. Upon heating in the DSC to a temperature above the cure temperature used, the sample softens; gains mobility and reactions start again, therefore conversion increases and so does T_g.[223, 224]

With a good initial curing method and using a draw-down bar and PTFE sprayed glass panel for the substrate for 300µm films were able to be made. However most analysis required a thicker film of approximately 1 mm which when using a draw-down bar proved impossible to remove from the substrate. Therefore a new method using PTFE moulds were used which produced readily removed films that were shaped using the different moulds. A uniform temperature of cure was also developed so that all of the polymers received the same treatment to produce good model systems.

Chapter 5 – Physical Properties of Polymer Films

5.1 – Aims and approach

The aim of the work described in this chapter is to investigate the properties of the polymer films prepared as described in the previous chapter. A range of analytical techniques have been used to determine the structural characteristics of the different polymers. By testing different physical properties it is hoped that these could be related to the chemical resistance of the polymer. From this the structure of the different polymers is related to their thermodynamics and chemical resistance. These will then be used to determine which structural effect plays the biggest role in the chemical resistance of the polymers.

Structural analysis of the polymers was performed to determine their structure so that the results obtained from other analyses could be related to the presence of epoxide moieties in the polymers. Analysis was performed using both IR and solid state NMR spectroscopy to determine the functional groups present in the polymers. Also, this provided an insight in to the presence of any small molecule 'impurities' such as unreacted epoxides or amines remaining after cure, which would suggest the polymers were not fully cross-linked.

Thermo-mechanical analysis based on results obtained by DMTA was performed to determine how the structure of the polymers relates to the performance of the polymers and subsequently how these relate to chemical resistance. Positron annihilation lifetime spectroscopy PALS was able to be used to probe the intermolecular properties of the polymers such as average hole volume of the free volume. These can then be compared to the transport properties of the polymers, determined by swelling of the polymers in different solvents. Taken together this data will provide insights into the effects of the epoxide isomer on the chemical resistance of the polymer films.

5.2 – Structural analysis

Each of the polymers were analysed by FTIR spectroscopy and ^{13}C solid state NMR spectroscopy. This was used to determine the chemical structure of these polymers.

5.2.1 – FTIR spectroscopy

FTIR spectroscopy was performed on the polymer films and on precursor monomers to identify peaks and comparison of these spectra was used to determine the conversion of the epoxide groups that appear circa 900 cm^{-1} for each of the polymers.

5.2.1.1 – IR analysis of RDGE and L-PACM polymer

Using FTIR spectroscopy, RDGE, L-PACM and the corresponding polymer formed by their polymerization were compared (Figure 5.1). From this it is possible to identify characteristic peaks of the monomers and how these are converted to those of the polymers as the degree of error is low being between 0.1 and 1%.

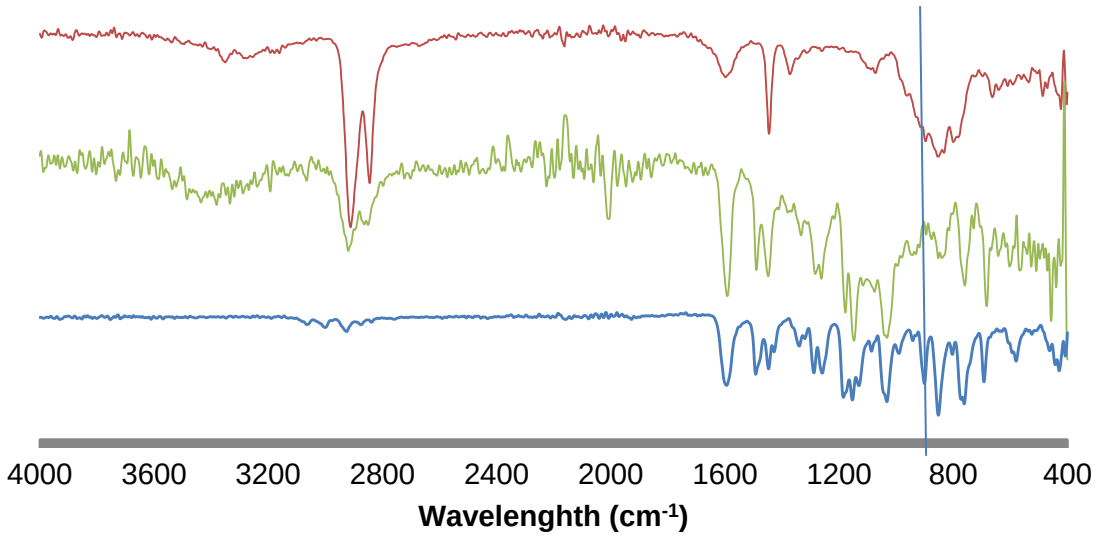

Figure 5.1 – FTIR spectrum for RDGE/ L-PACM polymer and monomers. – L-PACM, – polymer and – RDGE monomer.

As can be seen in Figure 5.1 in the polymer spectra shows a disappearance of the epoxide monomer absorbance 906 cm^{-1} (as shown by the blue line across the spectra) and an appearance of an OH stretch at 3700 – 3200 cm^{-1}. There are also peaks at 1266 and 1144 cm^{-1} which relate to the amine linkage with C-N and C-N-C respectively. The peaks at 842, 762 and 680 cm^{-1} are indicative of the out of plane bending of the C-H on the 1,3-disubstituted aromatic ring.

5.2.1.2 – FTIR analysis of HDGE and L-PACM polymer

FTIR spectroscopy was used as before to investigate the reaction between HDGE and L-PACM.

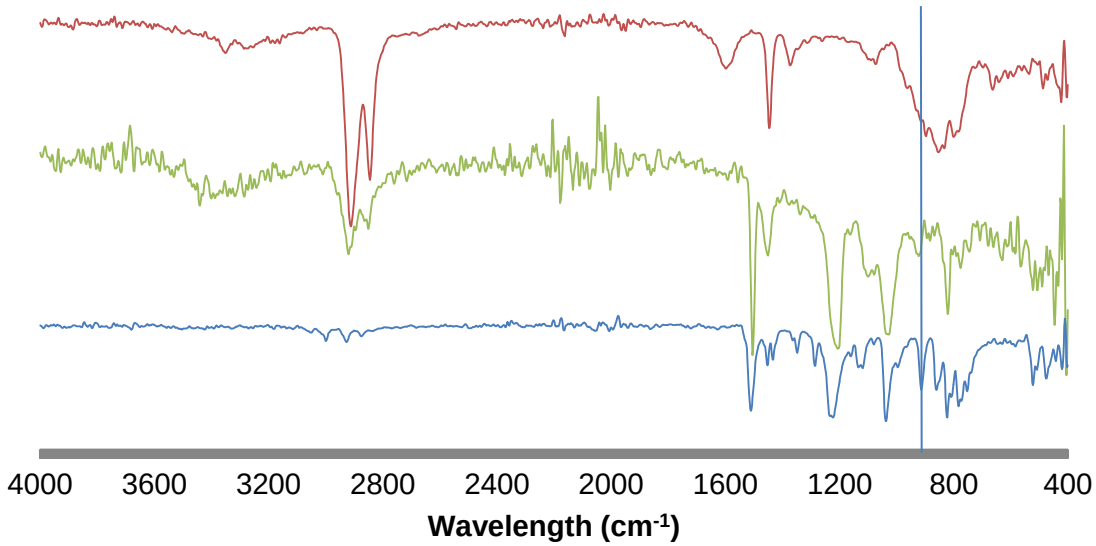

Figure 5.2 – IR spectrum for HDGE/ L-PACM polymer and monomers. – L-PACM, – polymer and – HDGE monomer.

The peak at 916 cm^{-1} (as shown by the blue line in the spectra) corresponds to the oxirane ring, is removed after polymerisation. This suggests that the reaction has converted all of the epoxides and the polymer is fully cured. The polymer spectrum peak that occurs at 3700 to 3100 cm^{-1} correlates to the -OH which is formed upon ring opening of the epoxide. There is also evidence of high conversion of the amine in the peak occurring at 1102 cm^{-1} which relates to the -C-N-C- bond after polymerisation. However, it cannot be confirmed if there is total conversion of

the amines as the peak that occurs for primary and secondary amines is overlaid by the peak relating to the -OH. The peak at 822 cm^{-1} is indicative of the 1,4-disubstitution on the aromatic ring.

5.2.1.3 – FTIR analysis of CDGE and L-PACM polymer

FTIR spectroscopy was also used to show the reaction between CDGE and L-PACM and compared to the monomers.

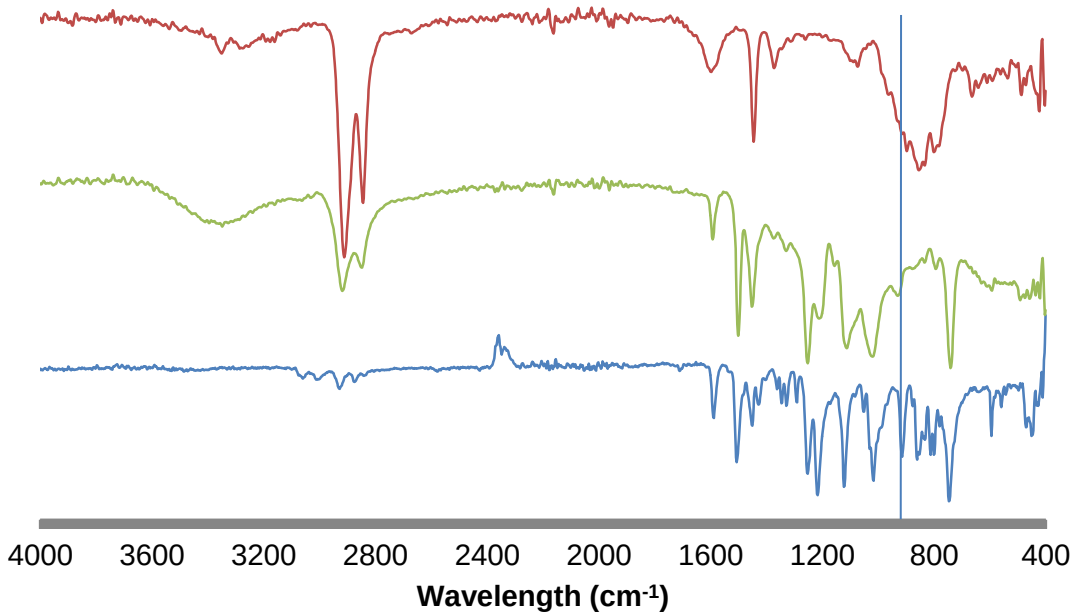

Figure 5.3 – IR spectrum for CDGE/ L-PACM polymer and monomers. – L-PACM, – polymer and – CDGE monomer.

Again as before there is evidence that there is full conversion from the epoxide to the polymer as the peak at 920 cm^{-1} (as shown by the blue line in the spectra) in the CDGE monomer spectra, disappears in the spectra for the polymer. It also shows that there is formation of the –OH group as there is a peak at 3700 to 3100 cm^{-1} which shows that there has been ring opening of the epoxide by the amine. Again it shows that there are –C-N-C- groups in the polymer as shown by the peak at 1252 cm^{-1}. The peak at 742 cm^{-1} relates to the 1,2-disubstitution effects on the aromatic ring.

5.2.1.4 – FTIR conclusion

The FTIR spectra show that there is consumption of the epoxides as with formation of –OH groups and -C-N-C- bonds. These suggest that the monomers are converted to polymers which suggest that there is full cure within the detection limits of the analytical technique.

5.2.2 – Solid State NMR Spectroscopy

^{13}C solid state NMR spectroscopy was used to attempt to identify the polymer end groups in particular epoxide or free amine groups. The peaks in the spectrum were compared to those of the starting material to aid characterisation of the polymers.

5.2.2.1 – Solid State NMR Analysis of polymer from RDGE and L-PACM

Figure 5.4 shows several peaks which relate to the presence of the monomeric species. However it is impossible to determine the amount of remaining end groups as these peaks would occur at 50.82 ppm for the $-NH_2$ and 50.10 ppm for the -CH of the epoxide and are obscured by overlaying peaks due to the broad peaks at 68.56 and 29.80 ppm.

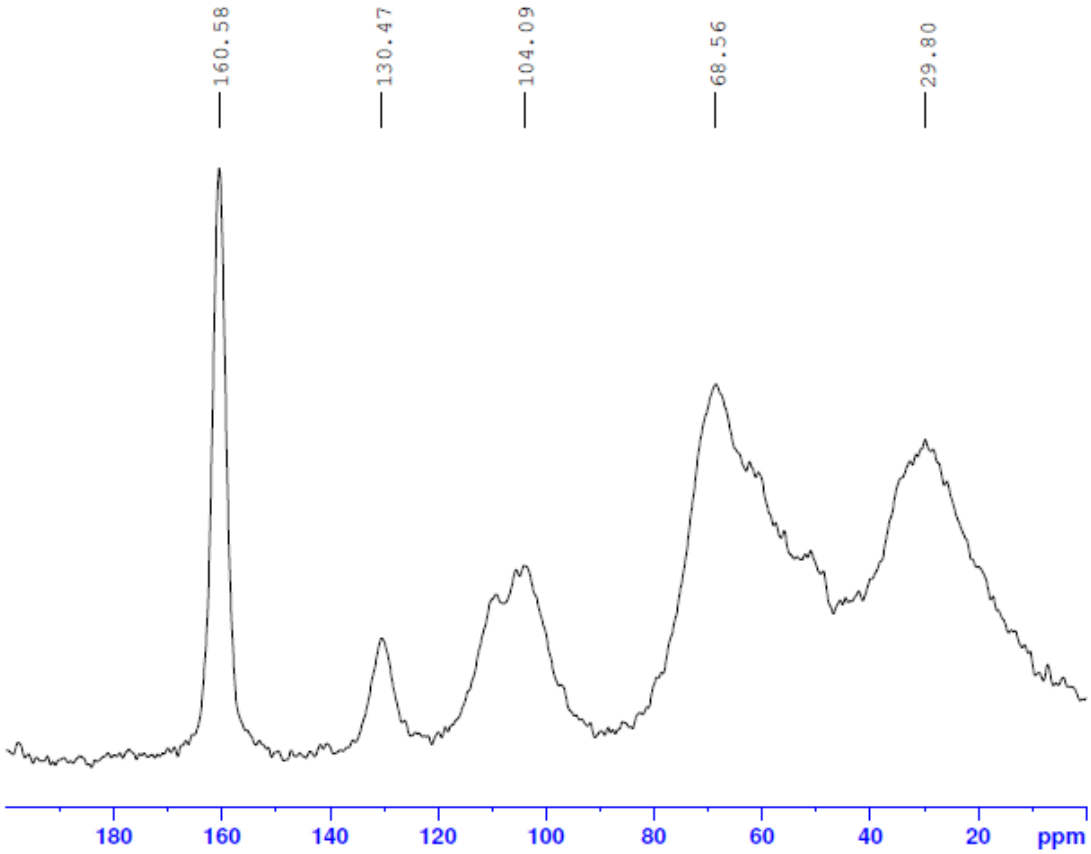

Figure 5.4 – ^{13}C NMR spectrum of the polymer network from RDGE and L-PACM

All of the peaks in the spectrum in Figure 5.4 relate to peaks of either RDGE or L-PACM which shows that there are probably few reactions occurring during polymerization. The peak at 68.56 ppm relates to the C-OH that is formed upon ring-opening of the epoxide. The peaks at 29.80 ppm relate to L-PACM but it is impossible to resolve each peak. The peaks of 160.58 (Ar, C), 130.47 (Ar, CH *meta*) and 104.09 (Ar, CH *ortho*) ppm relate towards RDGE.

For the polymer from RDGE and L-PACM, ^{15}N NMR spectroscopy was also performed in an attempt to identify remaining free amine species. However from this analysis it is impossible to deduce if there are any free amines due to there being little difference in the two spectra.

5.2.2.2 – Solid State NMR Analysis of polymer from HDGE and L-PACM

Figure 5.5 shows that it is impossible to determine the amount of remaining end groups. The end group peaks would occur at 50.82 ppm for the -NH_2 and 50.25 ppm for the -CH of the epoxide but would be obscured by the broad peaks at 68.25 and 31.76 ppm.

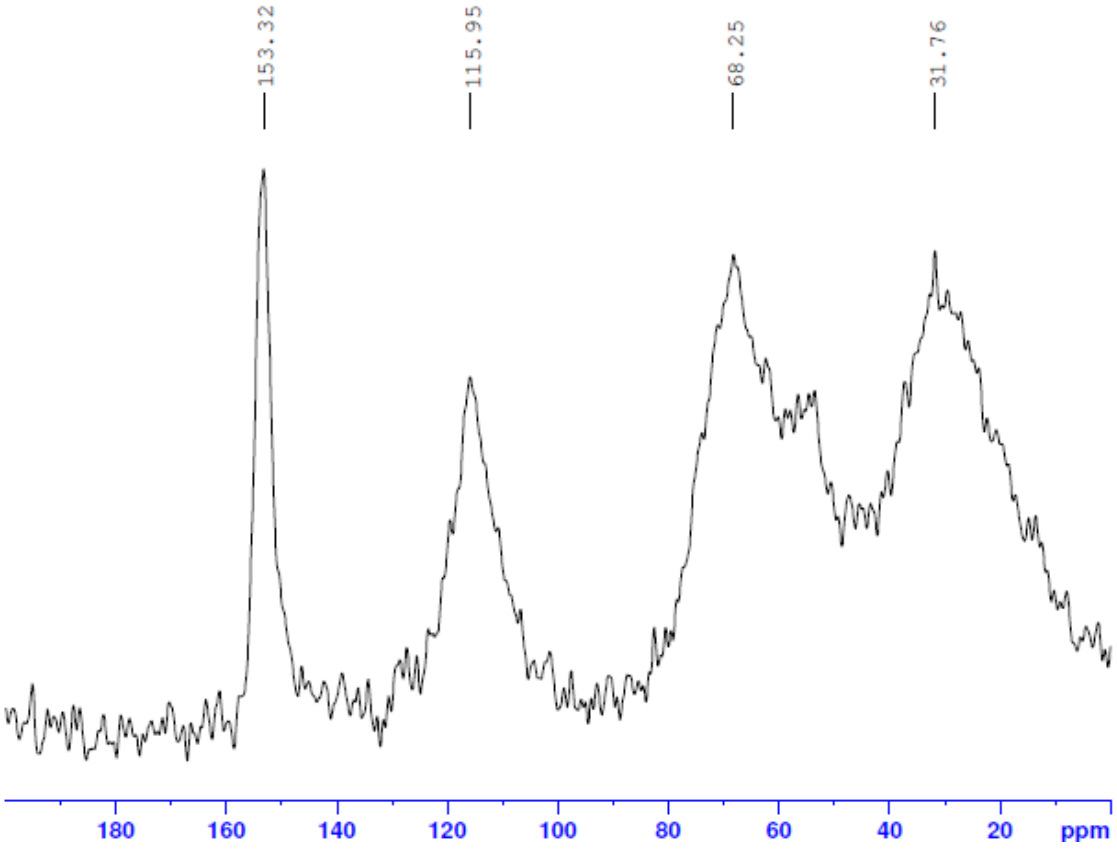

Figure 5.5 – ^{13}C NMR spectrum of the polymer network from HDGE and L-PACM

The peak at 68.25 ppm relates to the C-OH that is formed upon ring opening of the epoxide. The peaks at 31.76 ppm relate to L-PACM but it is impossible to resolve each peak. The peaks of 153.32 (Ar, C) and 115.95 (Ar, CH) ppm relate to HDGE.

5.2.2.3 – Solid State NMR Analysis of polymer from CDGE and L-PACM

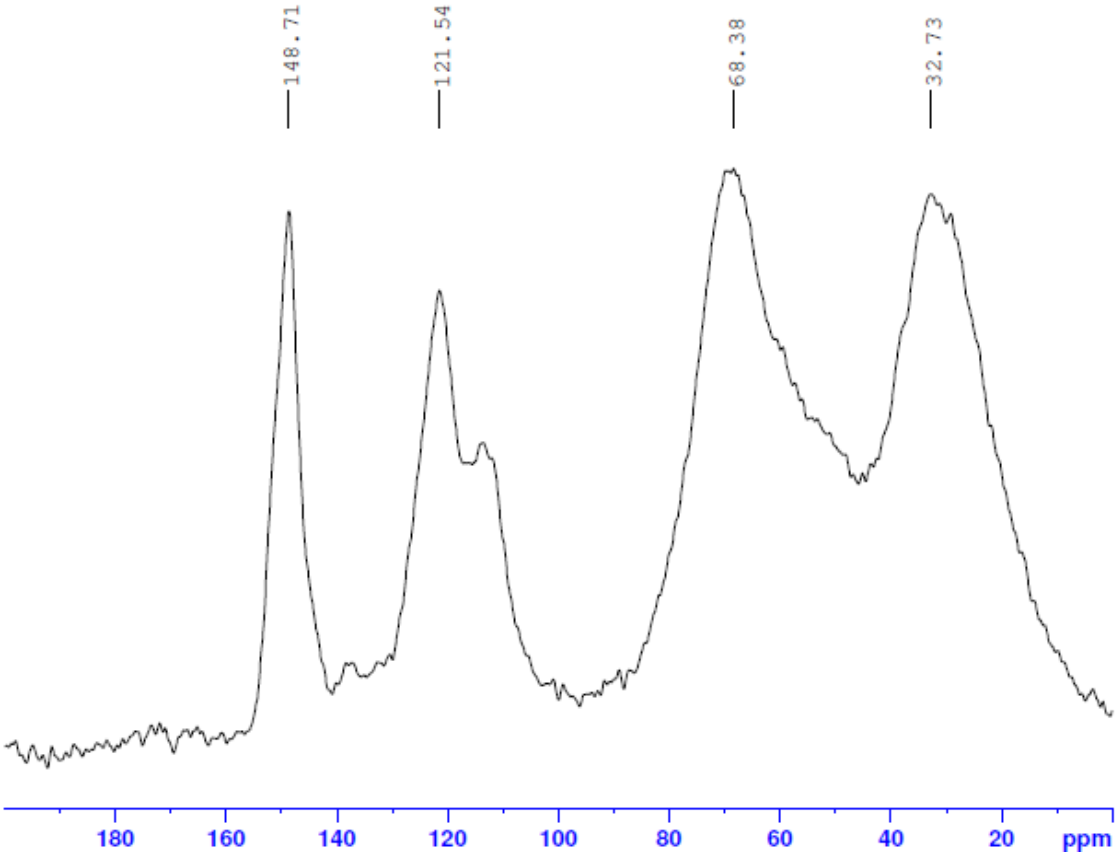

Figure 5.6 – ^{13}C NMR spectrum for CDGE and L-PACM polymer network

Once again it is impossible to determine the amount of conversion in the polymer as the peaks of the free amine and epoxide are hidden under the overlap caused by the peaks at 68.38 and 32.73 ppm, which relate to the C-OH from the ring opened epoxide and CH_2 from L-PACM respectively. The peaks at 148.71 (Ar, C), 121.54 (Ar, CH *meta*) and 112.60 (Ar, CH *ortho*) ppm relate to the carbons of the aromatic ring of the catechol moiety.

5.2.3 – Conclusions for structural analysis

As can be seen from the FTIR and NMR analysis, the polymers appear to contain the functional groups that are expected from a fully cross-linked epoxy-amine polymer. As far as can be deciphered from the analysis there are no remaining free

amines or epoxides which suggests that there is almost full conversion for each of the polymers. There also does not appear to be any sign of homopolymerisation of the epoxide which could occur when the hydroxyl group that is formed from the epoxide, attacks another epoxide. From this we can surmise that the structures of the polymers are as shown in Figure 5.7.

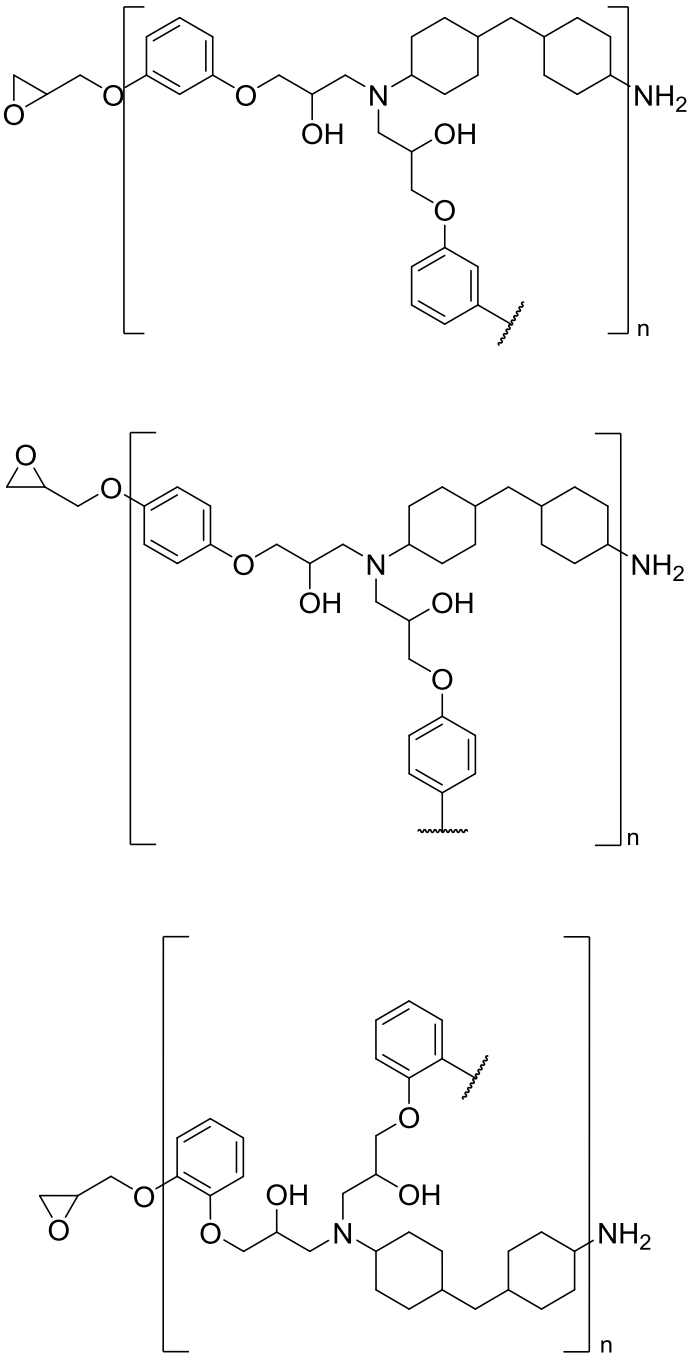

Figure 5.7 – Structure of epoxy-amine polymer formed by RDGE and L-PACM (top), HDGE and L-PACM (middle) and CDGE and L-PACM (bottom).

5.3 – Thermo-mechanical analysis

A range of analytical techniques were used to determine the thermal and mechanical properties of the polymers. As differential scanning calorimetry (DSC) and thermos-gravimetric analysis (TGA) were previously discussed in Chapter 4 only a brief account will be given for reference compared to the other thermal analytical techniques used. The thermo-mechanical properties of the polymers were measured by dynamic mechanical thermal analysis (DMTA) specifically the: storage modulus (E'), loss modulus (E'') and tan delta (tan δ) were analysed. The information that is obtained from these parameters can be used to determine several characteristics of the polymer including the glass transition (T_g)[225], the cross-link density[226] and the molecular weight between cross-links[227].

5.3.1 – DMTA analysis of polymer from RDGE and L-PACM

Experiments were done in triplicate to check the reproducibility of results with the heating rate of 3°C and a frequency of 1.00 Hz. The values were taken from the traces as shown in Figure 5.8, and tabulated in Table 5.1. The E' value is taken from the onset of the curve, E'' is taken from the apex of the peak as is Tan δ. The values relate to T_g in different ways; E' relates to the lower temperature of the T_g which is the most subjective in the analytical interpretation; the E'' the mid temperature which is related more to the physical property changes of the polymer; and tan δ is the T_g value quoted with the height and shape of the peak relating to the amorphous content of the polymer.

Table 5.1 – Results from the DMTA analysis of RDGE and L-PACM polymers[a]

Sample	T_g E' (°C)	T_g E'' (°C)	T_g tan δ (°C)
1	131.2	136.3	150.3
2	131.0	135.4	149.8
3	130.9	135.8	150.5
Average	131.3	135.8	150.2
Standard deviation	0.42	0.34	0.29

[a] T_g obtained from DSC analysis 130°C.

The DMTA T_g values are higher than that observed from the DSC analysis which gave the T_g of the fully cured polymer film as 130°C. This is expected with the different analytical techniques with temperature differences of ± 10-20°C being quoted[225]. The results show that the lower temperature for the T_g is 131 ± 0.42°C as taken from the E', the middle temperature is 136 ± 0.34°C and the higher temperature from tan δ is 150 ± 0.29°C. This is within 20°C of the results obtained by DSC.

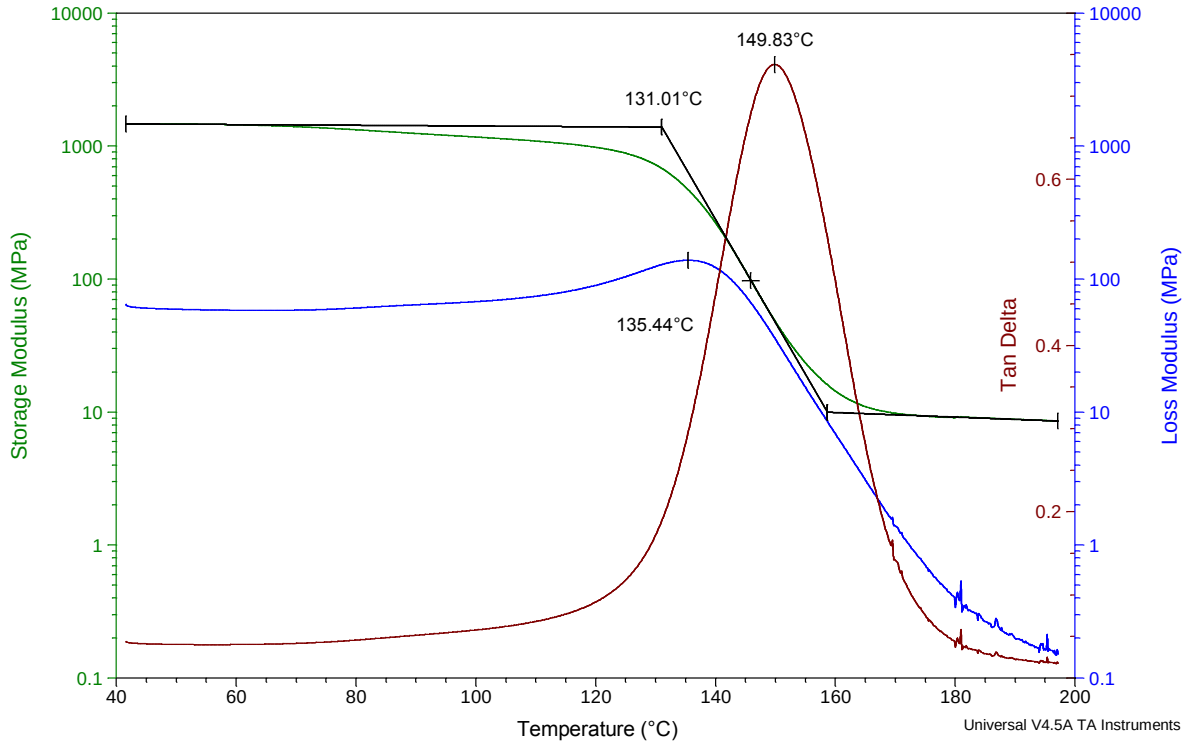

Figure 5.8 – DMTA plot for RDGE and L-PACM polymer films (sequence 2).

As can be seen in Figure 5.8 the storage modulus (E') contains three parts, the initial area before the onset of the slope, which relates to the glassy region; the area where there is a slope in the E', and the E'' and tan delta reach their peaks, which relates to the transition area where the T_g occurs; and the area after the slope which is the rubbery plateau region. This region can be used to determine the cross-link density and the molecular weight between cross-links.

To determine the cross-link density a reading of the storage modulus (E') in the rubbery plateau region at a specific temperature is required. For this analysis a

temperature of 180.08°C (453.23K) was used on each of the three DMTA graphs obtained as this temperature is on the plateau for each result. These were then used in the following equation:

$$\vartheta_e = \frac{E'}{3RT} \quad (5.1)$$

where ϑ_e is the cross-link density, E' is the storage modulus, R is the gas constant and T is the temperature at which the storage modulus reading was taken at in K.

The storage modulus at 180°C was determined as a temperature of 453.23K which gives an average cross-link density of 8.72 x 10^{-4} mol cm^{-3}. The full set of cross-link densities are tabulated in Table 5.2.

Table 5.2 – Cross-link density of RDGE and L-PACM polymers as determined by DMTA[a]

Sample	E' (MPa)	Cross-link density ϑ_e (mol cm^{-3})
1	10.460	9.25E-04
2	9.133	8.08E-04
3	9.982	8.83E-04
Average	9.858	8.72E-04
Standard deviation	0.549	4.85E-05

[a] Temperature E' value taken at 180.08°C (453.23K)

Upon finding the cross-link density it is then possible to determine the molecular weight between cross-links M_c by using equation 5.2:

$$M_c = \frac{\rho}{\vartheta_e} \quad (5.2)$$

where ρ is the density of the polymer and ϑ_e is the cross-link density as calculated from equation 5.1.

The density of the polymers was determined by accurately weighing a sample measured with a pair of digital callipers to determine the accurate dimensions. The sample that was chosen had the following dimensions: 21.24 x 16.53 x 1.07 mm giving a volume of 0.3757 cm^3 and a mass of 0.411 g which using equation 5.3 gives the density of 1.094 g cm^{-3}.

$$\rho = \frac{Mass}{Volume} \tag{5.3}$$

Inputting the density value into equation 5.2 gives the results shown in table 5.3.

Table 5.3 – Molecular weight between cross-links for polymer from of RDGE and L-PACM[a]

Sample	ϑ_e (mol cm^{-3})	Molecular weight between cross-links (g mol^{-1})	Average no of repeat units
1	9.25E-04	1182	2.3
2	8.08E-04	1354	2.6
3	8.83E-04	1239	2.4
Average	8.72E-04	1255	2.4
Standard deviation	4.85E-05	71	0.14

[a] Density of sample 1.094 g cm^{-3}

Using the probable structure of the repeat units as shown in section 5.2.3 suggests that the average number of repeat units is 2.4 throughout the sample.

5.3.2 – DMTA analysis of polymers from HDGE and L-PACM

Again using the same techniques the T_g was able to be determined using DMTA with E', E'' and tan delta as shown in Table 5.4.

Table 5.4 – Results from the DMTA analysis of HDGE and L-PACM polymers[a]

Sample	T_g E' (°C)	T_g E'' (°C)	T_g tan δ (°C)
1	116.3	120.8	145.4
2	117.9	119.9	148.6
3	114.3	118.8	141.4
Average	116.2	119.8	145.1
Standard deviation	1.47	0.84	2.94

[a] T_g obtained from DSC analysis 147°C

These DMTA results give a lower T_g than that obtained from the DSC analysis. What can be seen in the DSC graphs is that there is a very small change in the heat capacity which shows that the DSC has low sensitivity in this system. This could be a reason as to why the T_g is lower in the DMTA results compare to the DSC results as the DMTA gives a clearer reading with the two techniques measuring different values. As has been previously discussed a change in the ΔC_p is caused by a change in the cross-link density, with an increase in the cross-link density reducing the change in the C_p[228]. To determine if this is the reason why there is a different result in the DMTA compared to the DSC, determination of the cross-link density can be calculated as in equation 5.1.

Again, by using the rubbery plateau in Figure 5.9 it is possible to determine the cross-link density and the molecular weight between cross-links. The temperature that was selected for this polymer was 180.00°C.

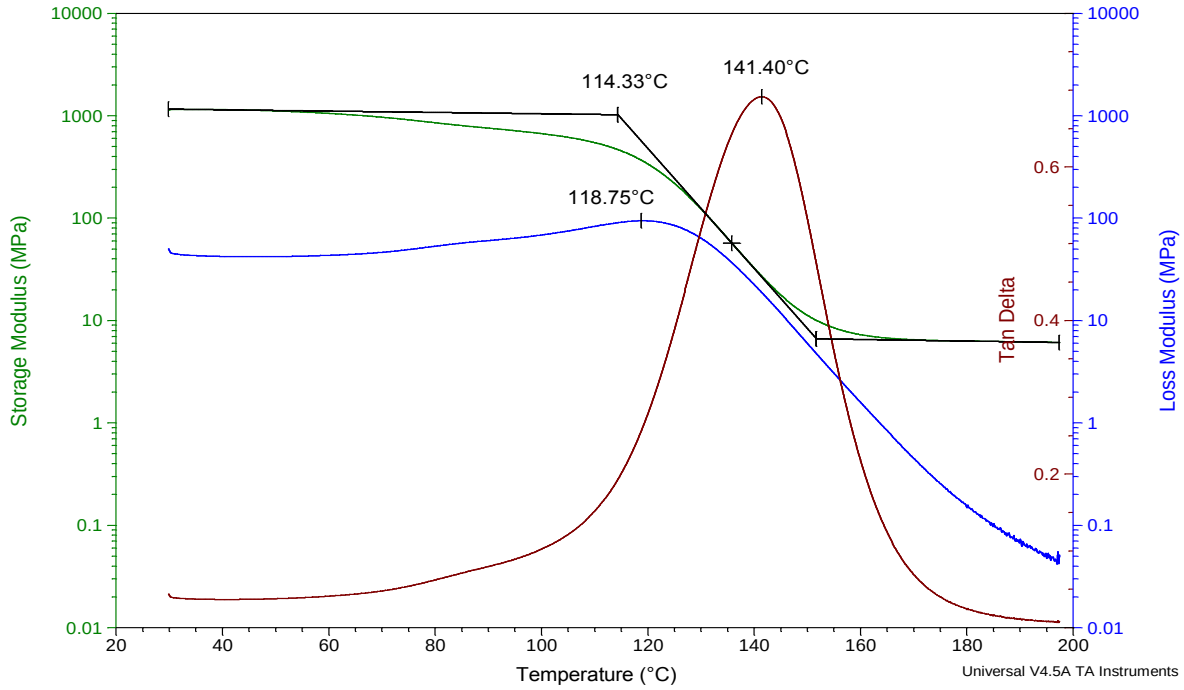

Figure 5.9 – DMTA plot for HDGE and L-PACM polymer films.

Table 5.5 shows the results obtained from the rubbery plateau portion of the E' trace for HDGE and L-PACM polymer which suggests that there is a lower cross-link density in this polymer network compared to that observed from RDGE and L-PACM.

Table 5.5 – Cross-link density of HDGE and L-PACM polymers as determined by DMTA[a]

Sample	E' (MPa)	Cross-link density ϑ_e (mol cm^{-3})
1	4.679	4.14E-04
2	3.910	3.46E-04
3	6.309	5.58E-04
Average	4.966	4.39E-04
Standard deviation	1.000	8.85E-05

[a] Temperature E' value taken at 180.00°C (453.15K)

There is also evidence that there is a large variation in cross-link density between the samples. This could be due to the packing of the polymer changing throughout the polymer which could decrease the ability of the polymer to cross-link during curing. Using the results obtained from Table 5.5 it is possible to use equation 5.2 to determine the average molecular weight between the cross-links.

The density of the polymer can be determined by the same method as described previously which gives dimensions of 50.56 x 50.46 x 0.96 mm giving a volume of 2.44 cm^{-3} and a mass of 2.59 g. When inputted into equation 5.3 this gives a density of 1.064 g m^{-3} which again is lower than that of the RDGE polymer. This data can then be used in equation 5.2 to give the results shown in table 5.6.

Table 5.6 – Molecular weight between cross-links for polymers from HDGE and L-PACM[a]

Sample	ϑ_e (mol cm^{-3})	Molecular weight between cross-links (g mol^{-1})	Average no of repeat units
1	4.14E-04	2570	4.9
2	3.46E-04	3075	5.9
3	5.58E-04	1906	3.6
Average	4.39E-04	2421	4.6
Standard deviation	8.85E-05	479	0.91

[a] Density of sample 1.064 g cm^{-3}

The structure as described in 5.2.3 suggests that the average number of repeat units is variable with the average being 4.6 repeat units.

These results are higher than those of the RDGE polymer which is consistent with the previous results as a higher molecular weigh between cross-links gives a lower cross-link density. This also agrees with the lower T_g from the DMTA results which relate to the cross-link density[229]. There is a linear relationship between the cross-link density and the glass transition temperature as shown in equation 5.4[230].

$$\frac{T_g - T_{g_0}}{T_{g_0}} = \frac{\left(\frac{\varepsilon\infty}{\varepsilon_0} - \frac{c\infty}{c_0}\right)\vartheta_e}{1 - \left(1 - \frac{c\infty}{c_0}\right)\vartheta_e} \qquad (5.4)$$

Where ε is the lattice energy, *c* is the segment mobility and the sub-indices 0 and ∞ are the uncross-linked and fully cross-linked polymers respectively and ϑ_e is the cross-link density.

This suggests that the T_g values determined by DMTA are the most reliable results as the trends observed agree with the results obtained for the cross-link density and the molecular weight between cross-links.

5.3.3 – DMTA analysis of CDGE and L-PACM polymer

Using the same analysis techniques the CDGE and L-PACM polymer networks were analysed and the results are shown in Table 5.7.

Table 5.7 – Results from the DMTA analysis of polymers from CDGE and L-PACM[a]

Sample	T_g E' (°C)	T_g E'' (°C)	T_g tan δ (°C)
1	116.7	120.7	133.5
2	116.4	121.0	133.2
3	115.9	120.2	133.9
Average	116.4	120.7	133.5
Standard deviation	0.31	0.33	0.28

[a] T_g obtained from DSC analysis 105°C

These results are in a better agreement with the DSC results that those for the HDGE and L-PACM polymer. However as can be seen in Figure 5.10 there is a secondary peak or shoulder in the tan delta peak after the T_g, at 154°C

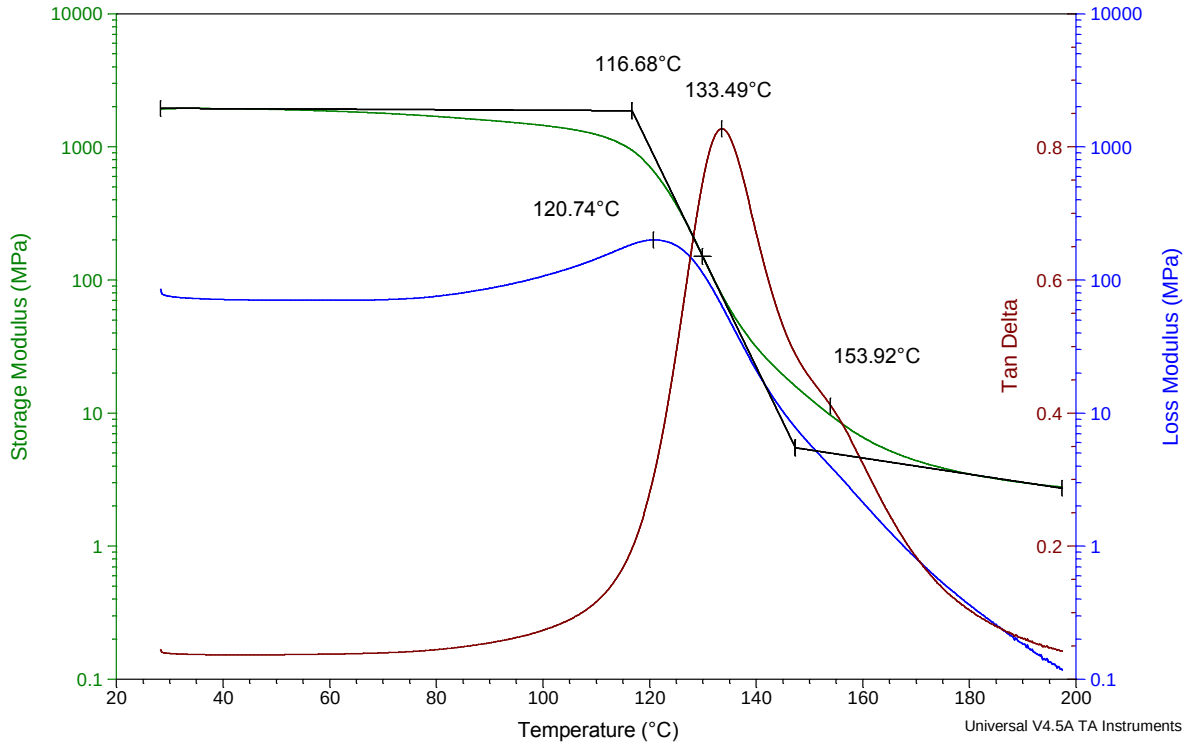

Figure 5.10 – DMTA graph for HDGE and L-PACM polymer films..

This extra peak suggests the presence of two polymeric species in the sample. Due to previous spectral analysis this would have to be a species similar to that of the main polymer as the FTIR and NMR results suggest that only one species is present. One possible reason could be due to cyclization of some parts of the polymer chain if two epoxide groups react with the same amine forming a structure as shown in Scheme 5.1[231]. This can then be further reacted to form a second ether linkage which could give rise to the secondary peak if some portions of the polymer contain this cyclized ether linkage.

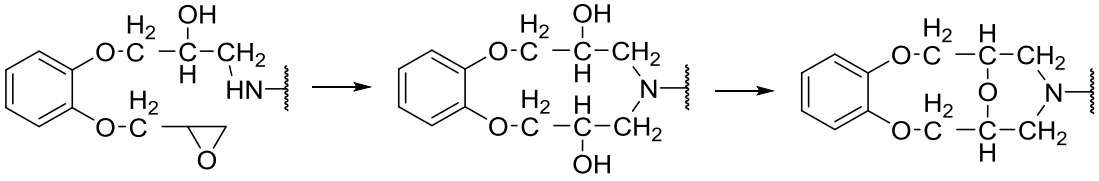

Scheme 5.1 – Formation of cyclized ether with ring opening of neighbouring epoxides by the same amine.

The cross-link density can again be determined using the rubbery plateau although in this instance a constant E' value has not been reached. Using data from the storage modulus taken at 180.03°C (453.18K) and inputting into equation 5.1 gives the results shown in table 5.8.

Table 5.8 – Cross-link density of CDGE and L-PACM polymers as determined by DMTA

Sample	E' (MPa)	Cross-link density ϑ_e (mol cm^{-3})
1	3.486	3.08E-04
2	6.829	6.04E-04
3	4.098	3.63E-04
Average	4.804	4.25E-04
Standard deviation	1.453	1.29E-04

[a] Temperature E' value taken at 180.03°C (453.18K)

There is a large fluctuation in the cross-link density result which again suggests there is the possibility of another polymer species in the sample. This is also consistent with the T_g data as the lower T_g is consistent with a lower cross-link density. Using the data shown in Table 5.8, equation 5.2 can now be used to determine the molecular weight between cross-links. The density of the polymer was found using equation 5.3 with the sample dimensions 50.19 x 50.10 x 0.98 mm which gives a volume of 2.46 cm^3, which with a mass of 2.66 g gives a density of 1.084 g m^{-3}.

Table 5.9 – Molecular weight between cross-links for polymers from CDGE and L-PACM[a]

Sample	ϑ_e (mol cm^{-3})	Molecular weight between cross-links (g mol^{-1})	Average no of repeat units
1	3.08E-04	3516	6.7
2	6.04E-04	1795	3.4
3	3.63E-04	2991	5.7
Average	4.25E-04	2551	4.8
Standard deviation	1.29E-04	882	1.37

[a] Density of sample 1.084 g cm^{-3}

These results are consistent with the cross-link density and T_g results which suggests that there is the possibility of another molecular structure within the polymer. Using the structure from section 5.3.1 also suggests that there is a range of repeat units which could again suggest another molecular structure.

5.3.4 – Conclusions for thermo-mechanical analysis

The results suggest that there is a difference in the T_g value determined by DMTA and DSC measurements. This is due the DMTA applying oscillatory deformation to the sample while DSC is a static measurement. The T_g results are consistent with the other data obtained from the DMTA analysis with the cross-link density and molecular weight between cross-links giving consistent results. The average results are tabulated below in table 5.10.

Table 5.10 – Average results obtained from thermal analysis

Sample	Tan δ (°C)	DSC (°C)	Density (g m^{-3})	Cross-link density ϑ_e (mol cm^{-3})	Molecular weight between cross-links (g mol^{-1})	Average no of repeat units
RDGE	150	130	1.094	8.72E-04	1255	2.4
HDGE	145	147	1.064	4.39E-04	2421	4.6
CDGE	134	105	1.084	4.25E-04	2551	4.9

5.4 – Positron Annihilation Lifetime Spectroscopy

To develop an understanding of the internal properties of the polymers formed positron annihilation lifetime spectroscopy (PALS) was performed. A positron is the anti-particle of an electron having the same mass and spin but opposing charge with the positron being positively charged and the electron being negatively charged. Although positrons do not readily exist in the natural world it can be formed by from a radioactive source for example the decay of the radioisotope of ^{22}Na from ^{22}NaCl. When one or more electrons surround a positron there is the possibility of both of the particles to annihilate which destroys both of the particles and emits energy as γ-quanta, controlled by quantum electrodynamics. Before annihilation the proton and electron can bond to form a positronium atom (Ps), these can account for 20-70% of all the positrons injected into the molecular system. There are three possible particles that can be formed in samples where positroniums are able to exist with varying annihilation lifetimes. The first, *para*-positroniums (*p*-Ps), have the shortest lifetime with annihilation occurring over 125 picoseconds and is independent of the environment. The second is free positrons which annihilate after 100-500 picoseconds. The final species, *ortho*-positronium (*o*-Ps) has a lifetime of approximately 10^3 picoseconds. This difference in lifetime between the positroniums is due to the relationship of spin between the electron and the positron with the *p*-Ps having anti-parallel spins and *o*-Ps having parallel spins. This causes the decay of the positroniums to occur differently with *p*-Ps decaying by 2-γ annihilation and the *o*-Ps decaying to 3-γ annihilation. Positron annihilation lifetime spectroscopy measures the initial emmision and consequent annihilation of a positron via the formation and annihilation of positroniums. The most probably positronium formed in polymeric materials is the *ortho*-positronium which can form and annihilate in the amorphous region. The annihilation of the *o*-Ps can give information on the size and number of cavities within a sample. The lifetime of the positronium (τ_3) can be used to measure the size of the vacancy due to the repulsion between the electrons in the sample and the electron in the positronium which means that areas that have a lower electron density (such as free volume holes) will trap the *o*-Ps more readily. The intensity (I_3) corresponds to the amount of annihilations that occur in the sample at

one time. This can then be related to the number density of the free volume holes. Therefore the size and amount of free volume holes can be determined by the formation of *o*-Ps[232-234].

5.4.1 – Results

In this study PALS was used to determine the free volume of the samples to determine whether this parameter has an influence on the data from the other analysis techniques. PALS measurements were kindly performed and data analysed by Dr Mina Roussenova at Bristol University. The analysis performed gives the *o*-Ps lifetime, which can related to the average hole volume for the free volume, and the dispersion of the *o*-Ps which shows the size dispersion of volume hole sizes. The data for the *o*-Ps lifetime and dispersion as converted to hole volume is shown in Figure 5.11.

The results the RDGE polymer has an average hole volume 3-4 $Å^3$ smaller than the CDGE and HDGE polymers. HDGE and CDGE polymers have similar results with overlapping with the error bars which suggests that these samples have very similar hole volumes. However, there is a higher distribution of hole volume in the RDGE polymer of over twice as much of the other two polymers. This suggests that although the RDGE polymer has a lower average hole volume there is a wider range of hole volumes. All the results were obtained at room temperature.

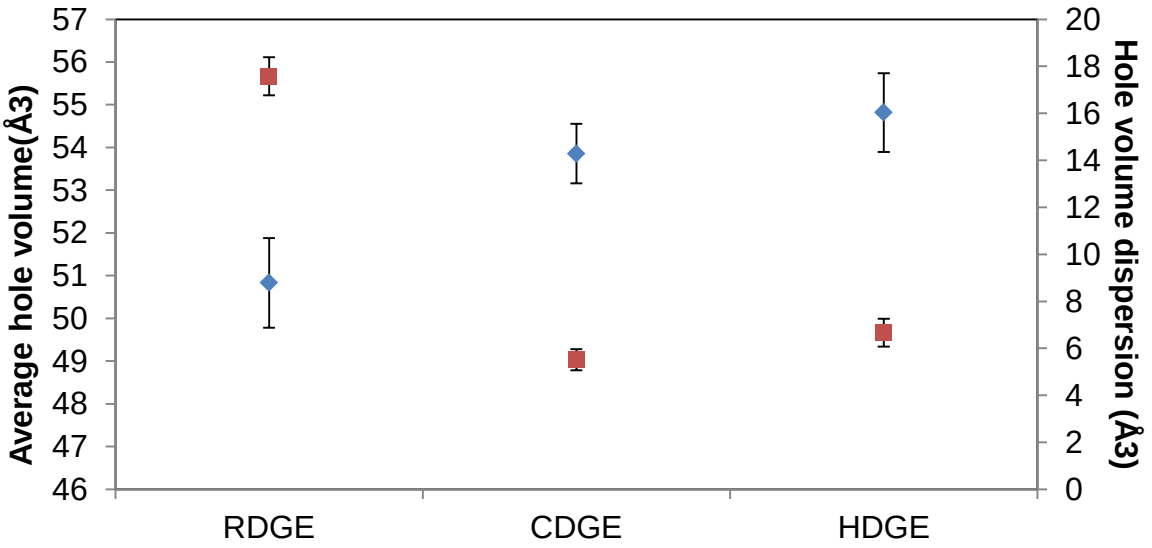

Figure 5.11 – Graphic representation of results from positron annihilation spectroscopy: ♦ is average hole volume; ■ is hole volume dispersion.

5.4.2 – Comparison with DMTA results

PALS and DMTA results are expected to be related since free volume hole size should influence thermo-mechanical behaviour. Consequently the obtained results have been compared to see if there is any relationship between them.

5.4.2.1 – Comparison of glass transition temperature with averaging hole volume

Comparing these PALS to the T_g as obtained by DSC and DMTA (as shown in figure 5.12) there does not appear to be an obvious relationship with the average void size with DSC and Tan δ results. Between RDGE and CDGE there is a drop in the T_g and an increase in the average hole size (Å) which is expected. However, using DSC and tan δ, there is an increase in the T_g and an increase in the average void size comparing HDGE polymer to CDGE polymer. However as previously discussed there is an overlap in the average void sizes between CDGE and HDGE polymers which could show there is a slight relationship. When compared to the E' and E'' results there appears to be an almost inverse linear relationship between the T_g and average void size. This appears to be consistent with what is expected with the relationship between void sizes and T_g as discussed in the introduction.

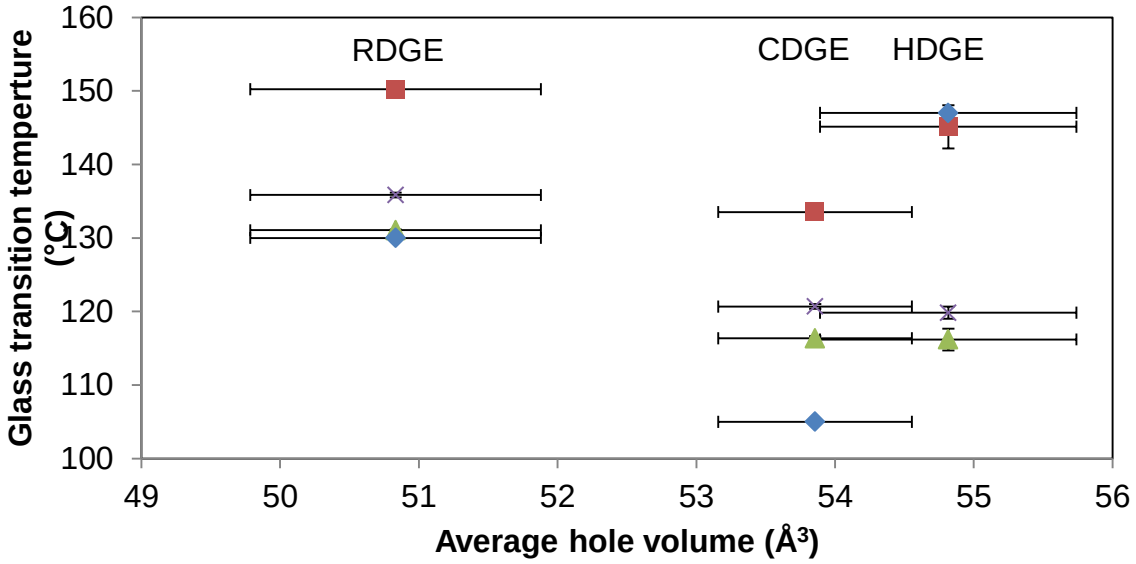

Figure 5.12 – Graphic representation of results from positron annihilation spectroscopy compared to DMTA results. ♦ T_g from DSC; ■ is T_g from Tan δ; ▲ is T_g from E' and X is T_g from E''.

5.4.2.2 – Comparison of cross-link density and molecular weight between cross-links with average hole volume

The average hole volume values were plotted against cross-link density and molecular weight between cross-links (Figure 5.13).

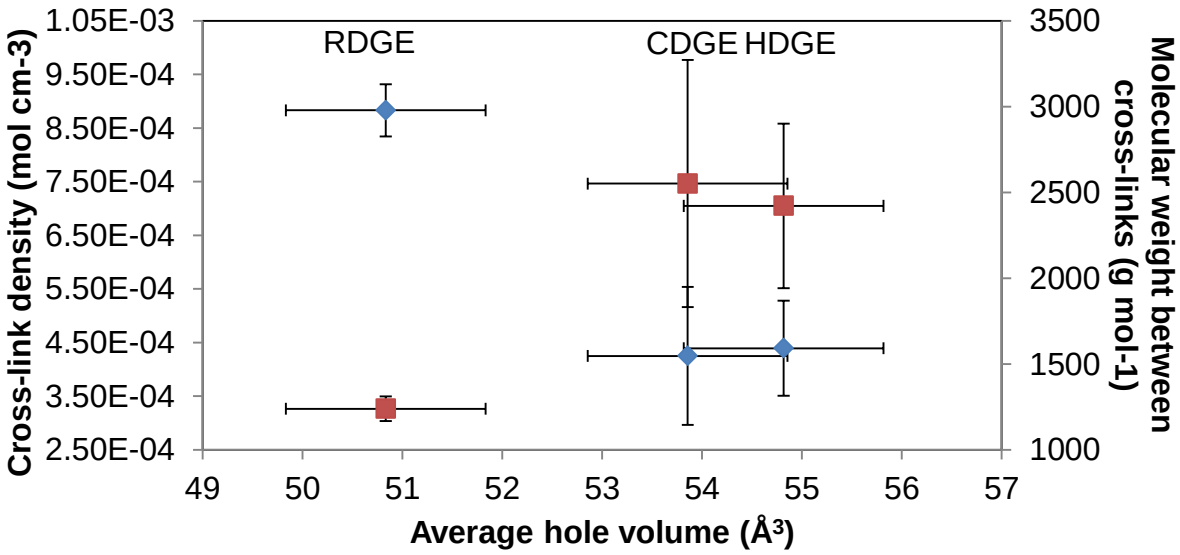

Figure 5.13 – Graphic comparison of results from positron annihilation spectroscopy and DMTA results: ♦ cross-link density; ■ molecular weight between cross-links

These results show that taking into account the error bars the results for HDGE and CDHE show similarities between the cross-link density and the average hole volume and between the average molecular weight between cross-links and the average hole volume. There is a relationship between the RDGE polymer with the other polymers shows what is expected that the smaller the hole volume the higher the cross-link density and lower the molecular weight between cross-links.

5.4.3 – Conclusions for PALS

The results obtained have some relationships that are expected with the RDGE polymers having the smallest average hole size and the highest DMTA T_g. However CDGE and HDGE have too similar results to determine a useful relationship between the DMTA results and the PALS results.

5.5 – Solvent transport properties

To determine the chemical resistance of the polymers their solvent swelling behaviour was investigated. Swellability can then be used to determine the permeability and diffusivity of the polymers which is related to their chemical resistance of the polymers. By determining the sorption coefficient, and the relationship this has with the DMTA and PALS data we will determine how the structure of the polymer affects its chemical resistance.

A homologous series of alcohols with varying van der Waals volumes was used to determine the ability of different sized molecules to permeate into the polymer film. The series that was used was: water (18Å^3)[235]; methanol (37Å^3); ethanol (52Å^3), propan-2-ol (69Å^3)[236] and *tert*-butanol (89Å^3)[237] due to the chemistries of the solvents being the same and the sizes known to determine the ability of these alcohols to be able to swell the polymers.

5.5.1 – Swelling profile for polymers from RDGE and L-PACM polymer

Square samples of the RDGE and L-PACM polymer (1 cm x 1 cm x 1 mm) were submerged in 1 cm^3 of solvent in a seal container and results collected over several months at room temperature. By measuring the mass increase of the polymers the percentage mass increase was calculated using equation (5.5):

$$Q(t) = \frac{M_t - M_i}{M_i} 100 \qquad (5.5)$$

Where Q(t) is the percentage mass increase at a certain time, M_t is the mass of the swollen polymer at a certain time and M_i is the initial mass of the polymer.

As can be seen in Figure 5.10 the only molecules that are taken up to any effect are methanol and water which have results in a mass change at equilibrium of 16.6 and 2.4% respectively. The water uptake is low based on the molecules size which suggests that other factors such as hydrophobicity are present. Using the

data obtained it was possible to determine the sorption equilibrium parameter using equation 5.6:

$$S = \frac{M_s}{M_i} \tag{5.6}$$

where M_s is the mass of solvent uptaken, M_i is the mass of the initial polymer

The mass of methanol at equilibrium was 15.03 mg and the initial mass of the polymer was 86.9 mg giving a sorption equilibrium parameter (S) of 0.173 mg of solvent per mg of polymer By determining the initial slope of the methanol data from Figure 5.14 it was possible to determine the diffusion coefficient (D) using the following equation[238]:

$$D = \pi \left(\frac{h\theta}{4Q_\infty}\right)^2 \tag{5.7}$$

where *h* is the initial thickness of the sample, Q_∞ is mass change at equilibrium and θ is the initial slope of the uptake.

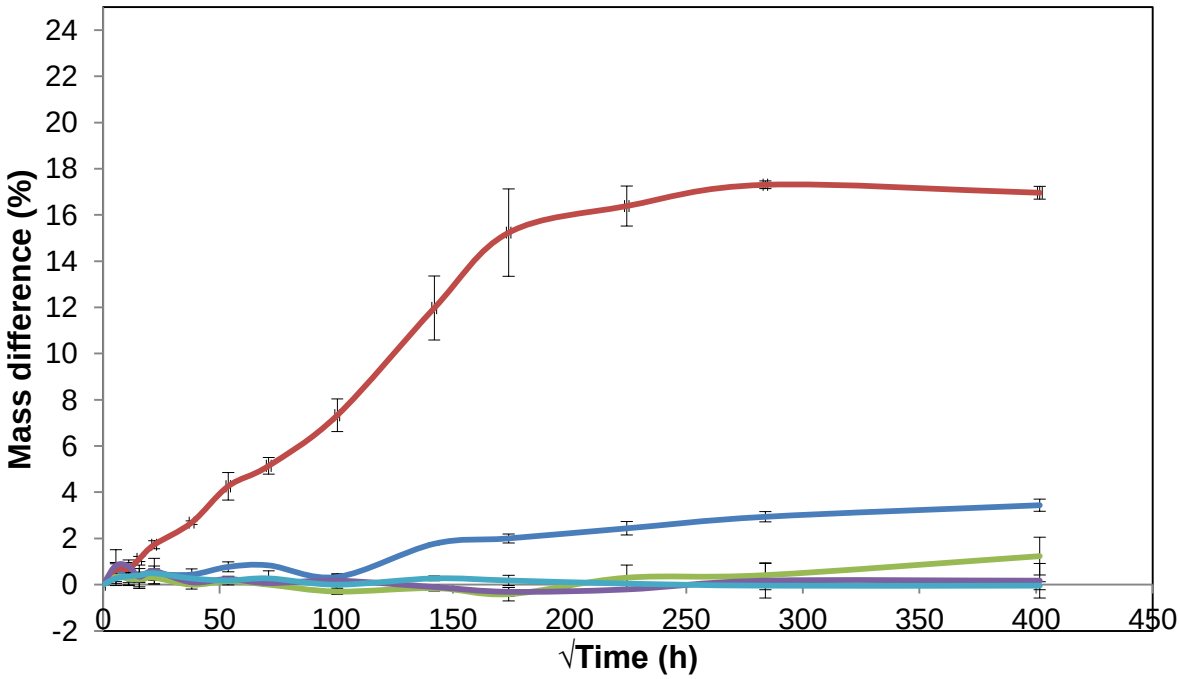

Figure 5.14 – Uptake of solvent in RDGE and L-PACM polymers. – water; – methanol; – ethanol; – propan-2-ol and – *tert*-butanol.

The data in figure 5.14 shows a methanol uptake at equilibrium of 16.6%, the initial slope is 0.085% h^{-1} and the sample thickness is 1.07mm. Inputting this into equation 5.7 gives the following:

$$D = \pi \left(\frac{1.07\ x\ 0.0852}{4\ x\ 16.569} \right)^2$$

This gives the diffusion coefficient (D) as 5.944 x 10^{-6} mm^2 h^{-1}. This can then be used to determine the permeability coefficient using the relationship shown below:

$$P = D.S \tag{5.8}$$

Using previously calculated values of diffusion coefficient (D) and the sorption equilibrium parameter (S) value gives the following:

$$P = 5.944 \times 10^{-6} \times 0.173$$

This gives a permeability coefficient of 1.029 x 10^{-6} mm^2 h^{-1}. The same process can be performed for the uptake of water into the polymer with the following S=0.029 mg/mg, D= π((1.07 x 0.009)/(4 x 2.436))^2 giving 2.934 x 10^{-6} mm^2 h^{-1} and P = 8.615 x 10^{-8} mm^2 h^{-1}.

Table 5.11 – Swellability results for polymers from RGDE and L-PACM

Solvent	Mass uptake (%)	Sorption Equilibrium parameter (mg/mg)	Diffusion Coefficient (mm^2 h^{-1})	Permeability Coefficient (mm^2 h^{-1})
Methanol	16.6	0.17	5.94E-06	1.03E-06
Water	2.4	0.03	2.93E-06	8.62E-08

5.5.2 – Swelling profile of polymers from HDGE and L-PACM

The analysis of the polymer from HDGE and L-PACM is plotted in Figure 5.15. As can be seen there is a dramatic increase in the mass uptake of methanol which reaches 21.2% after a short period (168 hours) compared to the RDGE

polymer which took 1344 hours to reach equilibrium. There is also a greater uptake of water as well with the swelling reaching equilibrium at 6.3%. There is also a small uptake of ethanol which does not reach equilibrium in the experimental time frame.

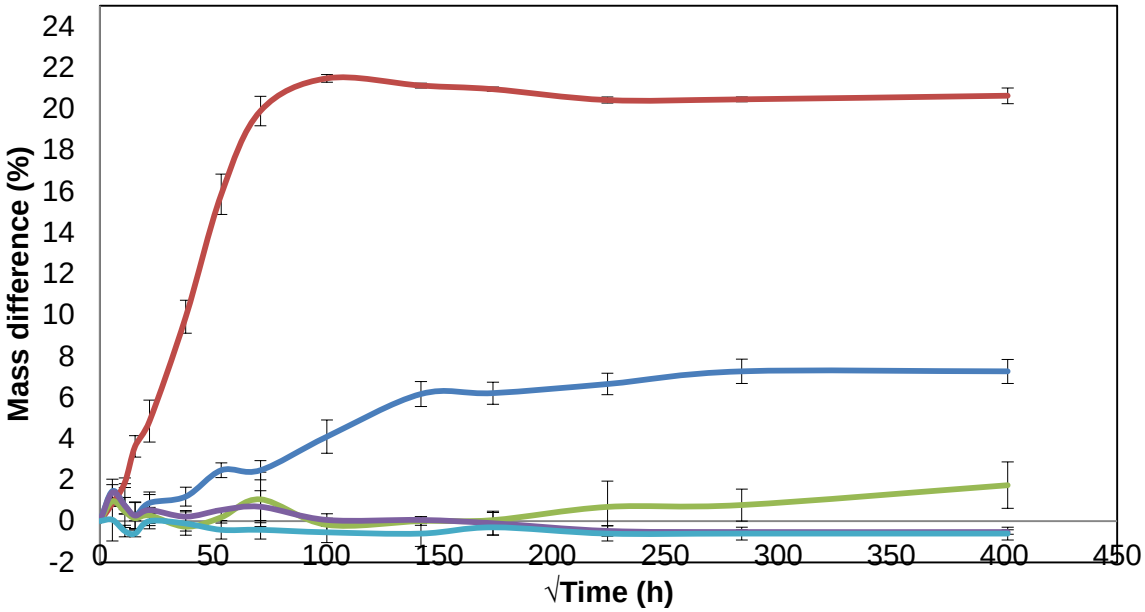

Figure 5.15 – Uptake of solvent in HDGE and L-PACM polymers. – water; – methanol; – ethanol; – propan-2-ol and – *tert*-butanol.

Using the data obtained for methanol, it is possible to determine the sorption equilibrium parameter, diffusion coefficient and permeability coefficient. The sorption equilibrium parameter is calculated using the mass of solvent uptake (19.57 mg) and the initial mass of the polymer (94.83) mg giving 0.205 mg/mg. Using equation 5.7 the diffusion coefficient is determined using the mass difference at equilibrium of 21.2%, the slope of 0.295 % h^{-1} and the sample thickness of 0.956 mm. This gives the diffusion coefficient of 3.474 x 10^{-5} mm^2 h^{-1}. Inputting these results into equation 5.8 gives a permeability coefficient of 7.123 x 10^{-6} mm^2 h^{-1} for methanol uptake. The same analysis was performed on water uptake which gave the following S=0.058 mg/mg, D= $\pi((0.95 \times 0.017)/(4 \times 6.262))^2$ giving 7.242 x 10^{-6} mm^2 h^{-1} and P = 4.208 x 10^{-7} mm^2 h^{-1}.

Table 5.12 – Swellability results for polymers from HGDE and L-PACM

Solvent	Mass uptake (%)	Sorption Equilibrium parameter (mg/mg)	Diffusion Coefficient ($mm^2\ h^{-1}$)	Permeability Coefficient ($mm^2\ h^{-1}$)
Methanol	21.2	0.21	3.47E-05	7.12E-06
Water	6.3	0.06	7.24E-06	4.21E-08

5.5.3 – Swelling profile of polymer from CDGE and L-PACM

The analysis for the polymer from CDGE and L-PACM is plotted in Figure 5.16. These results show that there is again a dramatic increase in the mass uptake of methanol of which is similar to that of HDGE polymer of 21.2% over 168 hours to equilibrium and higher than the RDGE polymer which took 1344 hours to reach equilibrium. There is also a greater increase in the uptake of water as well with the swelling reaching equilibrium at 6.3 %. There is also a large increase in the uptake of ethanol which does not reach equilibrium, however the error for these results is large (as seen in Figure 5.16). This may suggest that the ring formation as describe in section 5.3.3 is present in the sample where there is an increase as this could have an effect on the hole sizes in the free volume which could increase swelling. Although as can be seen the error in the last result is too large to have any significance for the determination of the sorption equilibrium parameter and the diffusion and permeability coefficients.

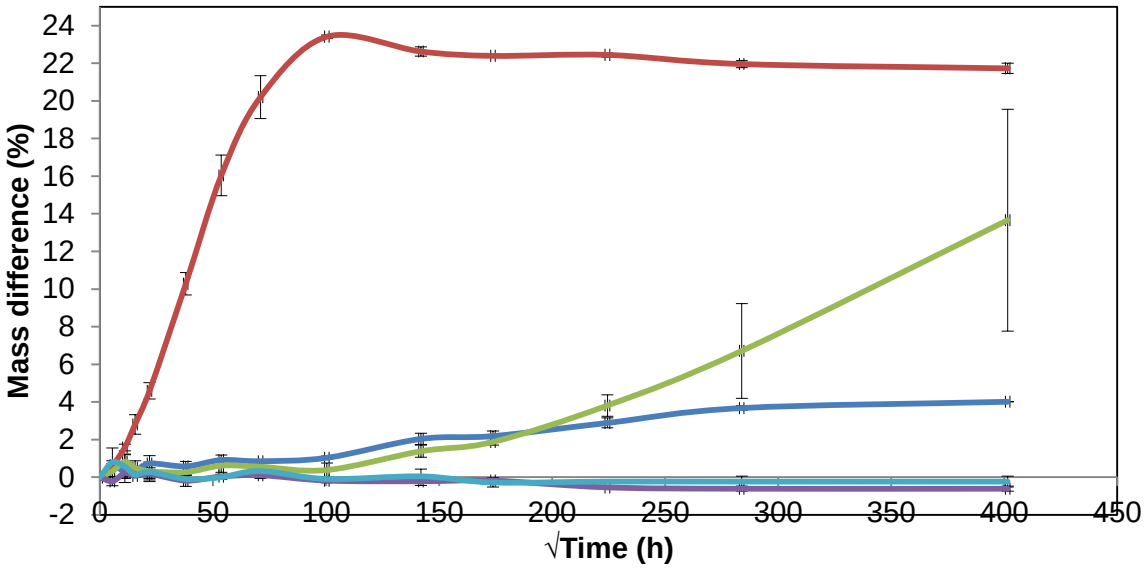

Figure 5.16 – Uptake of solvent in CDGE and L-PACM polymers. – water; – methanol; – ethanol; – propan-2-ol and – *tert*-butanol.

The methanol data was used to determine the sorption equilibrium parameter, diffusion coefficient and permeability coefficient. The mass of solvent uptake is 30.60 mg and the initial mass of the polymer of 131.50 mg giving a sorption equilibrium parameter of 0.234 mg of solvent per mg of polymer. The diffusion coefficient was determined using equation 5.7: the mass difference at equilibrium of 22.5%; the slope 0.304 % h^{-1} and the sample thickness of 0.976 mm giving the diffusion coefficient of 3.413 x 10^{-5} mm^2 h^{-1}. Using equation 5.8 gives a permeability coefficient of 7.99 x 10^{-6} cm^2 s^{-1} for methanol uptake. The same analysis was performed on water uptake which gave the following S=0.040 mg/mg, D= 2.375 x10^{-6} mm^2 h^{-1} and P = 9.522 x 10^{-8} cm^2 s^{-1}.

Table 5.13 – Swellability results for polymer from CGDE and L-PACM

Solvent	Mass uptake (%)	Sorption Equilibrium parameter (mg/mg)	Diffusion Coefficient (mm^2 h^{-1})	Permeability Coefficient (mm^2 h^{-1})
Methanol	22.5	0.23	3.41E-05	7.99E-06
Water	3.3	0.04	1.14E-06	4.55E-09

5.5.4 – Conclusions for transport properties

Of the solvents studies significant uptake was only observed with water and methanol. As can be seen in Table 5.14 there is an increase in the mass uptake of solvent in RDGE to HDGE and CDGE, which is predicted from the T_g from the DMTA results. Specifically the RDGE polymer has a permeability coefficient significantly lower than both HDGE and CDGE which appear to have similar properties. The diffusion coefficient for the RDGE polymer is an order of magnitude higher than that of bother HDGE and CDGE polymers. This suggests that RDGE has a better chemical resistance and HDGE and CDGE polymers have similar chemical resistances.

Table 5.14 – Swellability for each polymer in methanol

Polymer	Mass uptake (%)	Sorption Equilibrium Parameter (mg solvent /mg polymer)	Diffusion Coefficient ($mm^2\ h^{-1}$)	Permeability Coefficient ($mm^2\ h^{-1}$)
RDGE	16.6	0.17	5.94E-06	1.03E-06
HDGE	21.2	0.21	3.47E-05	7.10E-06
CDGE	22.5	0.23	3.41E-05	7.99E-06

For the water uptake results have a different relationship. Here the water uptake in HDGE polymer is twice that of the other two polymers and CDGE polymer uptake is only slightly higher than that of RDGE polymer. However, the diffusion coefficient is much lower for RDGE compared to the two other polymers with HDGE and CDGE polymers having similar diffusion coefficients. The permeability coefficient however is lower for the CDGE polymer which is an unexpected result.

Table 5.15 – Swellability for each polymer in water

Polymer	Mass uptake (%)	Sorption Equilibrium Parameter (g solvent /g polymer)	Diffusion Coefficient ($cm^2\ s^{-1}$)	Permeability Coefficient ($cm^2\ s^{-1}$)
RDGE	2.44	0.03	2.93E-06	8.62E-08
HDGE	6.26	0.06	7.24E-06	4.21E-08
CDGE	3.34	0.04	1.14E-06	4.55E-09

5.6 – Interpretation of results and comparisons

Comparison of the transport properties of the polymers studied in the chapters provides an insight in to which facts determine chemical resistance. As has previously been discussed the glass transition temperature obtained by DSC for the HDGE polymer is not a consistent result and will therefore be ignored from these comparisons.

5.6.1 – Comparison of thermal analysis results with solvent transport properties

5.6.1.1 – Comparison of glass transition temperature

To determine the relationship between the glass transition temperature of the polymers and their solvent transport properties, each glass transition value was plotted against the solvent uptake at equilibrium for both methanol and water.

As can be seen in figure 5.17 there is a trend between methanol uptake and the T_g as shown by the tan delta values. For both E' and E'' measured T_g's there appears be a slight relationship with a decrease from RDGE polymer to HDGE and CDGE polymer where there is a plateau. With the DSC results obtained in Chapter 4, however, no relationship between the solvent uptake and the glass transition temperature which is due to the result obtained from the HDGE polymer as described earlier.

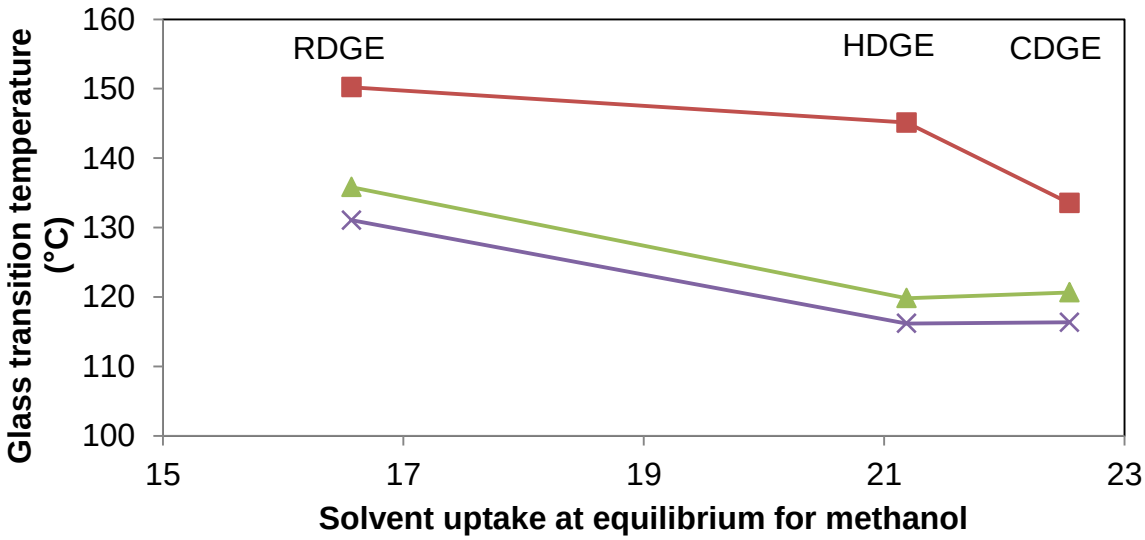

Figure 5.17 – Graphic representation of solvent uptake of methanol versus glass transition temperature. ■ is T_g from tan δ; ▲ is T_g from E'' and X is T_g from E'.

With the water uptake results however there appears to be no trend between the percentage uptake at equilibrium compared to the T_g of the polymers as recorded by DMTA (Figure 5.18).

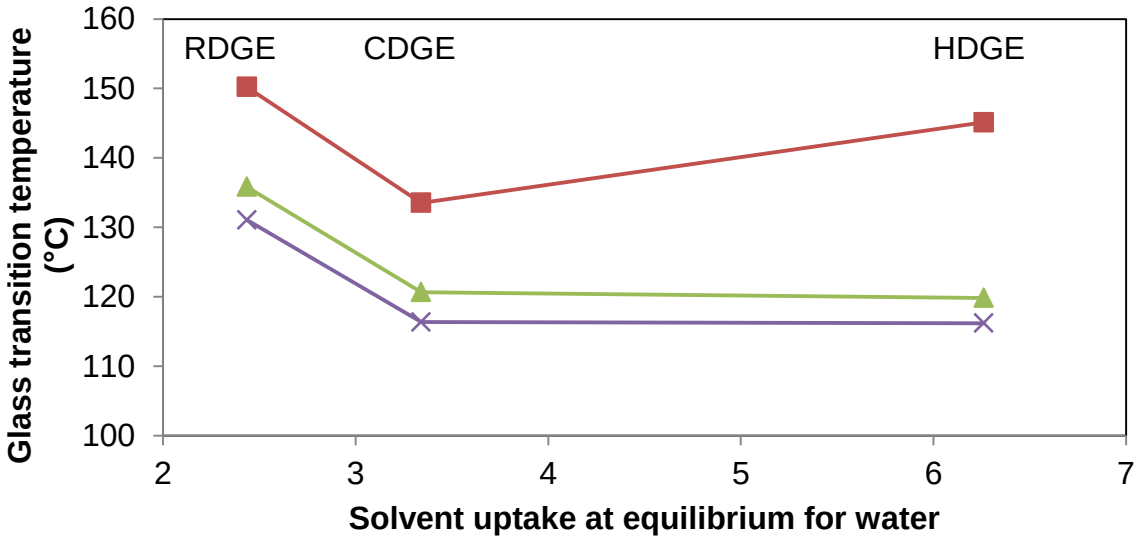

Figure 5.18 – Graphic representation of solvent uptake of water versus glass transition temperature. ■ is T_g from Tan δ; ▲ is T_g from E'' and X is T_g from E'.

However, there is a decrease in the T_g with an increase in the water uptake at equilibrium using T_g values from E' and E''. This is similar as discovered between the average hole volume discussed in section 5.4.2.1.

5.6.1.2 – Comparison of cross-link density and molecular weight between cross-links

As the cross-link density and molecular weight between cross-links have previously been shown to have a loose relationship with the average hole volume, the effect of these parameters on the solvent uptake at equilibrium for methanol and water was examined. Figure 5.19a shows that there is an almost linear relationship between the solvent uptake at equilibrium for methanol compared to both ϑ_e and Mc. This suggests that the cross-link density affects the free volume as has already been discussed.

In contrast there does not appear to be any significant relationship between water up take at equilibrium and the cross-link density and molecular weight between cross-links as shown in Figure 19b.

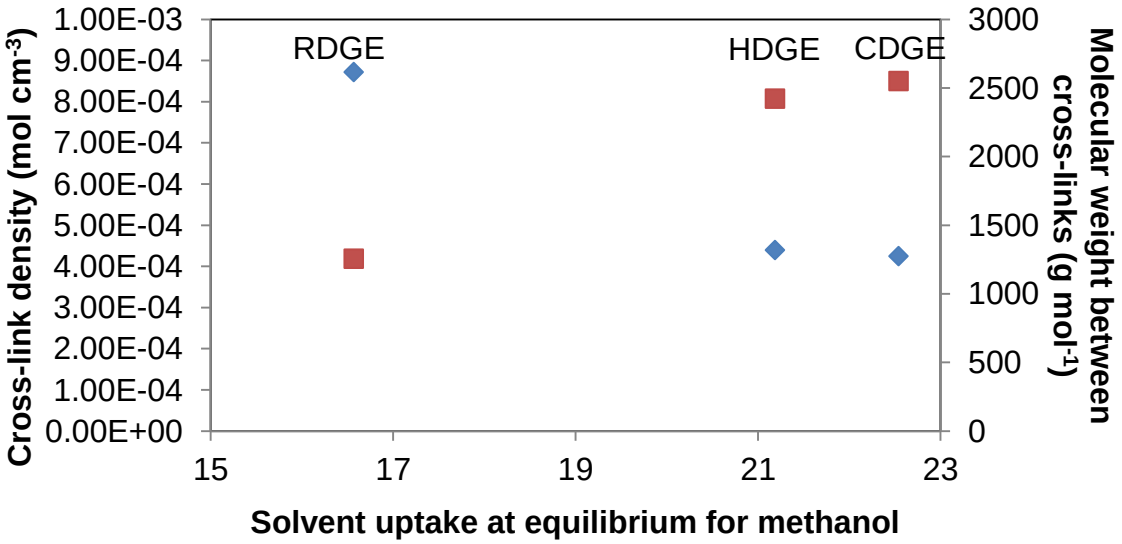

Figure 5.19a – Plot of methanol uptake versus ϑ_e and M_c. ♦ ϑ_e; ■ M_c

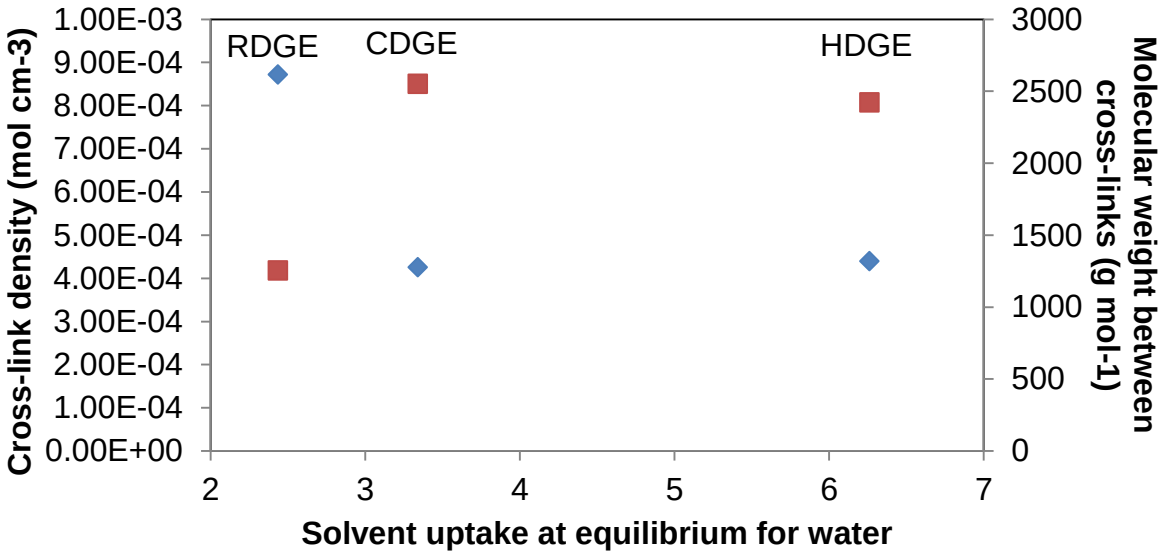

Figure 5.19b – Plot of methanol uptake versus ϑ_e and M_c. ♦ ϑ_e; ■ M_c

5.6.2 – Comparison of PALS results against solvent transport properties

To see how the average hole volume affects the uptake of the different solvents the data obtained from PALS plotted against solvent uptake experiments. As can be seen in Figure 5.20 there is a relationship between the average hole volume and water uptake but with the statistical error there is an overlap with the results for the average hole volume between CDGE and HDGE which limits the significance of the results.

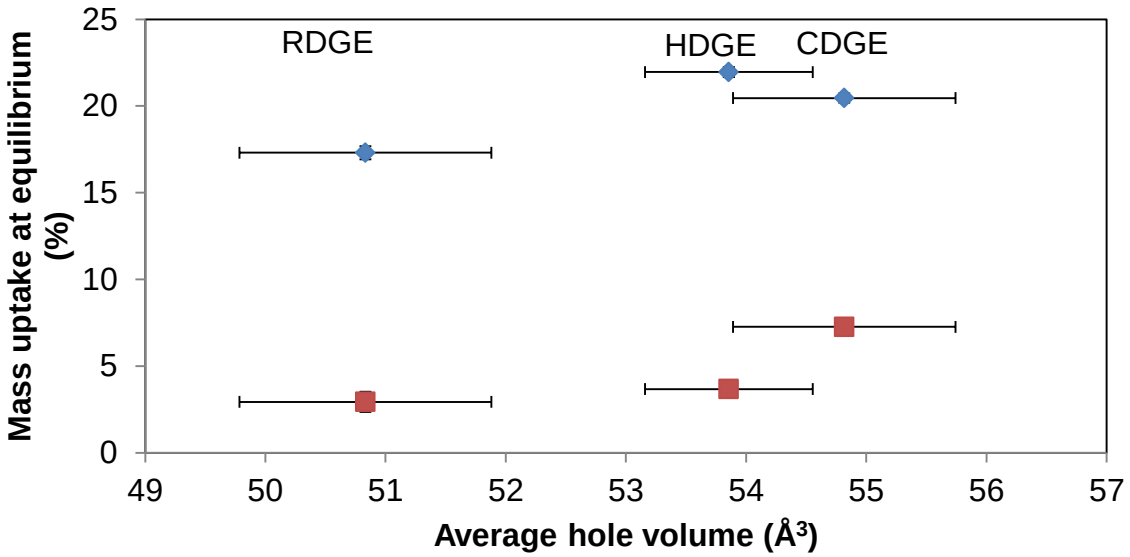

Figure 5.20 – Graphic representation of solvent uptake versus average hole volume. ♦ Methanol; ■ Water

From this it is possible to determine that the HDGE and CDGE polymers have similar properties. The RDGE polymer however, appears to have a higher chemical resistance with lower solvent uptake at equilibrium for both water and methanol.

The average hole volume data shows that on average, the size of the holes are smaller than both propan-2-ol and *tert*-butanol molecules. As a result, these solvents are unable to penetrate into the polymers. The average hole volume for RDGE is lower than the size of an ethanol molecule which would explain why there is no uptake of ethanol in the RDGE polymer. In HDGE polymer however the volumes are similar with HDGE having an average hole volume of 53.9Å^3 and ethanol being 52Å^3, which limits the penetration of the solvent into the polymer. CDGE polymer however has a higher average hole volume of 54.8Å^3 which could be why there is a large uptake of ethanol shown in figure 5.13, but with large errors in the solvent uptake which could be due to errors in the average hole volume.

5.7 – Conclusions

Structural analysis of the polymers show that the expected polymers have been formed with limited evidence of homopolymerisation of the epoxide groups. This suggests that they are viable model systems for testing chemical resistance. However, as the DMTA results suggest there is possible contamination or cyclization within the catechol derivative, as there is a possibility of two epoxides on CDGE being able to react with the same free amine of L-PACM. However, it was not possible to detect this product by NMR or FTIR as the peaks that would occur for the cyclized product would occur at a similar position as the non-cyclized product. However, as the polymer does not dissolve in a range of solvents this suggests that there is a limited amount of the cyclized product in the polymer network.

The results obtained from the comprehensive analysis of the polymers suggest that there are discrepancies between the different methods of determining the glass transition temperature. In particular the HDGE T_g is higher when measured by DSC compared with DMTA, whereas generally DMTA is expected to give a higher T_g. This may be due to the symmetry of hydroquinone (para isomer). The is possible that the more symmetrical HDGE polymer has a greater degree of freedom when there is no applied stress. When force is applied it is possible that polymer is able to respond to the stress more readily than CDGE and RDGE thereby lowering the T_g as measured by DMTA.

Comparing the results of mass of solvent uptake there is an apparent relationship between chemical resistance and epoxide isomer. This is due to nature of the network formed by each of the polymers. For example the average hole volume is inversely proportional to the cross-link density. This affects the swelling of the polymer and restricts the ability of solvents to penetrate the polymers. The results are summarised in Table 5.16 which clearly shows that RDGE has the best overall chemical resistance due to having the lowest of all the parameters analysed. The relative performance for HDGE and CDGE varies depending on the solvent with the former being more resistant to methanol and the latter more resistant to water. This suggests that the results for these two systems are similar. However, the glass

transition temperature, uptake and diffusion coefficients, and permeability coefficient for CDGE show that, for methanol, this system is predicted to have the lowest chemical resistance.

Table 5.16 – Tabulated results obtained for each polymer

	E' T_g (°C)	E'' T_g (°C)	Tan δ T_g (°C)	DSC T_g (°C)	Mass uptake at equilibrium (%) Methanol	Cross-link density ϑ_e (mol cm^{-3})	Molecular weight between cross-links (g mol^{-1})	Average number of repeat units	Density (g m^{-3})	S (mg solvent/ mg polymer)	D (mm^2 h^{-1})	P (mm^2 h^{-1})	Average hole volume ($Å^3$)	Hole volume disp. ($Å^3$)
CDGE	116.4	120.7	133.5	105	22.5	4.39E-04	2421	4.8	1.08	0.234	3.41E-05	7.99E-06	53.86	5.51
HDGE	116.3	119.8	145.1	147	21.2	4.25E-04	2551	4.6	1.06	0.205	3.47E-05	7.12E-06	54.82	6.66
RDGE	131.1	135.8	150.2	130	16.6	8.72E-04	1255	2.4	1.09	0.173	5.94E-06	1.03E-06	50.83	17.58

Chapter 6 - Experimental

6.1 – General

6.1.1 – Solution State NMR Spectroscopy

Proton, carbon and fluorine nuclear magnetic resonance spectra (^{1}H NMR, ^{13}C NMR and ^{17}F NMR) were recorded on either a Bruker Advance 400 (^{1}H NMR, 400 MHz; ^{13}C NMR, 100 MHz; ^{17}F NMR 376 MHz) or a Varian VNMRS-700 (^{1}H NMR, 700 MHz; ^{13}C NMR, 126 MHz) spectrometer with solvent resonance as the internal standard (^{1}H NMR, $CDCl_3$ at 7.26 ppm or D_2O at 4.79 ppm; ^{13}C NMR, $CDCl_3$ at 77.36 ppm). ^{1}H, ^{13}C and ^{17}F spectroscopic data are reported as follows: chemical shift, integration, multiplicity (s= singlet, d= doublet, dd= doublet of doublets, dt= doublet of triplets, dq= doublet of quartets, ddd= doublet of doublets of doublets, ddt=doublet of doublets of triplets, dddd= doublet of doublets of doublets of doublets, m = multiplet), coupling constant (Hz) and assignment.

6.1.2 – Mass Spectroscopy

GC-MS analysis was performed on a Trace GC-MS device (Thermo-Finnigan Corporation) operating in electron impact ionization (EI) mode with 70 eV electron energy. LC-MS analysis was performed on a TQD mass spectrometer equipped with an Acquity UPLC (Waters Ltd, UK) operating electron spray ionization (ESI).

6.1.3 – Elemental Analysis:

C, H, and N analysis was collected with an Exeter Analytical CE-440 Elemental Analyser.

6.1.4 – Infra Red Analysis

Infra-red (IR) spectra were recorded on a Perkin Elmer 1600 Series FTIR using a golden gate attachment, scanning in a range from 400 to 4000 cm^{-1}.

6.1.5 – Differential Scanning Calorimetry

Differential scanning calorimetry was carried out on a DSC Q1000 (TA instruments) using approximately 10 mg of sample. This was performed using a dual heating system of -50 to 250 °C at a heating and cooling rate of 10 °C per minute. The interpretation was performed on TA Universal Analysis using the half height as the T_g.

6.1.6 – Dynamic Mechanical Analysis

Dynamic mechanical analysis was performed on a DMA Q800 (TA Instruments) using dual cantilever of 8 mm size. The samples were prepared using the “dog bone” shape with the analysis section approximately 5 mm width and 1 mm thickness. The analysis performed was temperature ramp method set with multi-frequency sweep against strain. The amplitude was set to 20 µm and the frequency at 1.00 Hz, the temperature was set from room temperature up to 200°C with an increase of 3°C per minute.

6.1.7 – Thermogravimetric Analysis

Thermogravimetric analysis (TGA) was executed using a Pyris 1 TGA (Perkin Elmer) at a heating rate of 10°C a minute under a flow of helium of 40 mL min^{-1}. Sample masses ranged between 10µg to 30µg and were analysed using ceramic pans.

6.1.8 – Solid State NMR Spectroscopy

^{13}C NMR spectroscopy was performed on a Varian NMRS 400 using a frequency of 100 MHz over a period of 40s with 1320 repetitions using a 4 mm magic angle spinning probe.

6.1.9 – Positron Annihilation Lifetime Spectroscopy

Positron annihilation lifetime spectroscopy (PALs) was kindly performed by Professor Ashraf Alam's group at Bristol University.

6.1.10 – Swellability Studies

An accurately weighed sample of polymer (of 1 x 1 cm x 1 mm dimensions) was placed in a sample vial with 1 cm^3 of solvent. The mass was then measured periodically at time intervals of: 0.5, 2, 4, 8, 24, 48, 84, 168, 336, 504, 840, 1344 and 2688 hours. After this the mass difference (Q(t)) was determined using the following equation as discussed in Chapter 1:

$$Q(t) = \frac{M_t - M_i}{M_i} 100 \quad (6.1)$$

6.1.11 – Materials

Unless stated all materials and solvents were used as received without further purification. Drying of materials was performed using a gentle vacuum under heating.

6.2 – Allylation of dihydroxybenzenes

6.2.1 – Williamson ether synthesis

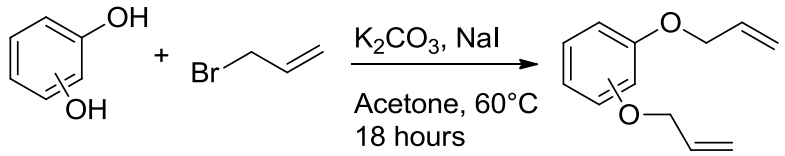

1a	1,4-di substituted benzene	**2a**
1b	1,2-di substituted benzene	**2b**
1c	1,3-di substituted benzene	**2c**

Scheme 6.1 – General Williamson ether reaction

6.2.1.1 – Synthesis of 1,4-diallyl benzene ether

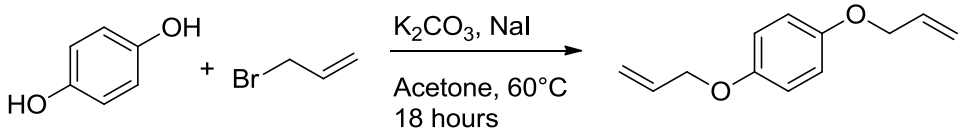

1a **2a**

Scheme 6.2 – Reaction of hydroquinone with allyl bromide to yield hydroquinone diallyl ether

A mixture of acetone (~30 mL), potassium carbonate (18.16 g, 0.13 mol) and hydroquinone (5.79 g, 52.57 mmol) was heated at 55 °C under nitrogen for ~30 min with stirring. Dry sodium iodide (0.40 g, 2.63 mmol) was added to the mixture. In a pressure equalising dropping funnel, allyl bromide (13.99 g, 0.12 mol) in acetone (4 mL) was added drop wise to the reaction vessel over 30 min. The mixture was then refluxed for 18 hours at 55 °C. After this period a sample was extracted and washed with dilute hydrochloric acid and extracted with dichloromethane and subsequently analysed by ^{1}H NMR spectroscopy. The remainder of the mixture was filtered and the solvent evaporated. The residual oil was dissolved in dichloromethane (~20mL) and washed with 2M sodium hydroxide (4 x 20 mL). The organic material was dried ($MgSO_4$) and evaporated. The residue was dried under high vacuum for to give a hydroquinone diallyl ether as a crystalline solid.

Yield- 8.88 g (87%); TLC (1:4 EtOAc: hexane) – product (hydroquinone diallyl ether) 0.80; ^{1}H NMR spectroscopy (400 MHz, $CDCl_3$) δ 6.86 (s, 4H, Ar-**H**), 6.06 (ddt, 2H, *J* = 17.2, 10.6, 5.3 Hz, R-C**H**-R_1), 5.42 (dq, 2H, *J* = 17.3, 1.6 Hz, trans R=C$\mathbf{H}_2$), 5.29 (dq, 2H, *J* = 10.5, 1.4 Hz, cis R=C$\mathbf{H}_2$), 4.49 (dt, 4H, *J* = 5.3, 1.5 Hz, RO-C$\mathbf{H}_2$-R_1); ^{13}C NMR spectroscopy (100 MHz, $CDCl_3$) δ152.91 (Ar, C), 133.63 (-**CH**=), 117.49 (=$\mathbf{CH_2}$), 115.66 (Ar, CH), 69.46 (O-$\mathbf{CH_2}$-); Elemental analysis, Calculated- C: 75.76, H: 7.42, Found- C: 75.17, H: 7.39; GC-MS m/z (EI^+) 190.1 ([M^+] 88%) expected m/z 190.1.

The reaction was repeated in a larger scale with hydroquinone (57.88 g), allyl bromide (139.90 mL), sodium iodide (3.94 g) and potassium carbonate (181.62 g) to give 90 g of product at a 90% yield.

6.2.1.2 – Synthesis of Catechol Diallyl Ether

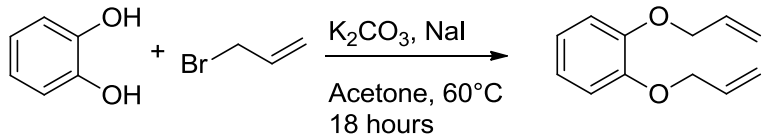

1b **2b**

Scheme 6.3 – Reaction of catechol with allyl bromide to yield catechol diallyl ether

Following the process described above, allyl bromide (13.99 g, 0.12 mol), potassium carbonate (18.16 g, 0.13 mol) and catechol (5.80 g, 52.57 mmol) gave catechol diallyl ether as a viscous oil. Yield- 8.15 g (82%); TLC (1:4 EtOAc: hexane) – product (catechol diallyl ether) 0.64; ^{1}H NMR spectroscopy (400 MHz, $CDCl_3$) δ 6.93 (m, 4H, Ar-**H**), 6.12 (ddt, 2H, *J* = 17.2, 10.6, 5.3 Hz, R-C**H**-R_1), 5.45 (dq, 2H, *J* = 17.3, 1.6 Hz, trans R=C$\mathbf{H}_2$), 5.30 (ddd, 2H, *J* = 10.5, 2.9, 1.4 Hz, cis R=C$\mathbf{H}_2$), 4.64 (dt, 4H, *J* = 5.3, 1.5 Hz, RO-C$\mathbf{H}_2$-R_1); ^{13}C NMR spectroscopy (100 MHz, $CDCl_3$) δ 148.62(Ar, C), 133.61 (-**CH**=), 121.29 (Ar *meta*, CH), 117.50 (=$\mathbf{CH_2}$), 114.34 (Ar *ortho*, CH), 69.93 (O-$\mathbf{CH_2}$-); Elemental analysis, Calculated- C: 75.76, H: 7.42, Found- C: 75.24, H: 7.36; GC-MS m/z (EI^+) 190.1 ([M^+], 98%) expected m/z 190.1.

The reaction was repeated at a larger scale with catechol (57.88 g), allyl bromide (139.90 mL), sodium iodide (3.94 g) and potassium carbonate (181.62 g) to give 95 g of product at a 95% yield.

6.2.1.3 – Synthesis of Resorcinol Diallyl Ether

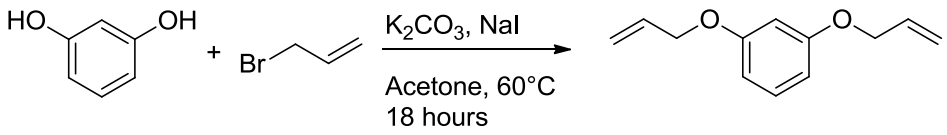

1c **2c**

Scheme 6.4 – Reaction of resorcinol with allyl bromide

Following the process described above, allyl bromide (13.99 g, 0.12 mol), potassium carbonate (18.16 g, 0.13 mol) and resorcinol (5.80 g, 52.57 mmol) gave mixture of products in the form of a viscous oil. Crude yield of 8.91 g (88%); TLC (1:2 EtOAc: hexane) - products 0.91, 0.76 and 0.58; ^{1}H NMR spectroscopy (400 MHz, $CDCl_3$) δ 7.29 – 7.17 (m, 1H, Ar-**H**), 6.59 (d, 1H, *J* = 2.3 Hz, Ar-**H**), 6.58 (d, 2H, *J* = 1.4 Hz, Ar-**H**), 6.11 (ddt, 2H, *J* = 17.3, 10.5, 5.3 Hz, R-C**H**-R_1), 5.47 (dq, 2H, *J* = 17.3, 1.6 Hz, trans R=C**H**$_2$), 5.34 (dq, 2H, *J* = 10.5, 1.5 Hz, cis R=C**H**$_2$), 4.56 (dt, 4H, *J* = 5.3, 1.6 Hz, RO-C**H**$_2$-R_1); ^{13}C NMR spectroscopy (100 MHz, $CDCl_3$) δ 159.82 (Ar, C), 133.28 (R-**CH**=), 129.85 (Ar, **C**-H), 117.69 (R=**CH$_2$**), 107.15 (Ar, **C**-H), 101.98 (Ar, **C**-H), 68.82 (O-**CH$_2$**-); GC-MS m/z (EI^+) 190.1, ([M^+], 85%) for the desired product and ^{1}H NMR spectroscopy (400 MHz, $CDCl_3$) δ 7.09 (d, *J* = 8.2 Hz), 6.56 – 6.47 (m), 6.05 – 5.99 (m), 5.19 – 5.03 (m), 3.42 (dq, J = 6.8, 1.7 Hz); ^{13}C NMR spectroscopy (100 MHz, $CDCl_3$) δ 158.22, 157.02, 133.45, 133.38, 129.98, 116.96, 115.07, 105.26, 100.40, 68.97, 68.73; GC-MS m/z (EI^+) 230.2 ([M^+], 45%) for the impurities.

6.2.2 – Allylation of resorcinol using potassium *tert*-butoxide

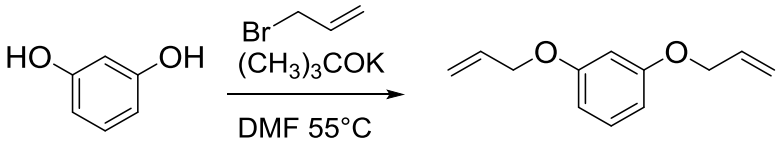

1c **2c**

Scheme 6.5 – Reaction of resorcinol with allyl bromide using potassium tert-butoxide as the base

A mixture of DMF (~30mL), dried potassium tert-butoxide (13.27 g, 0. 13mol) and dried resorcinol (5.80 g, 52.57 mmol) were heated to 55 °C for 30 minutes with stirring under nitrogen. Allyl bromide (14.00 g, 0.12 mol) in DMF (4 mL) was added drop wise over 30 minutes. The mixture was then refluxed for 18 hours. After this period the mixture was filtered and solvent evaporated. The residual oil was dissolved in dichloromethane (~20mL) and washed with 2M sodium hydroxide (4 x 20mL). The organic material was dried ($MgSO_4$) and evaporated to give a viscous oil. ^{1}H NMR spectroscopy shows a mixture of desired product 2c of 87% and by-product of 13%, spectral data as above.

6.2.3 – Synthesis of diallyl ethers by microwave heating

6.2.3.1 – General procedure

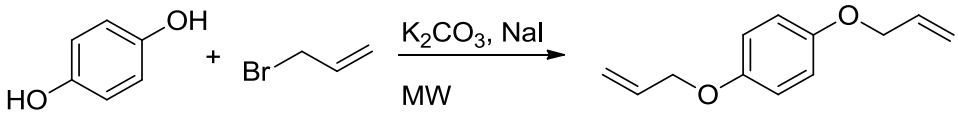

1a **2a**

Scheme 6.6 – Microwave allylation of hydroquinone

Potassium carbonate (1.82 g, 13.14 mmol), hydroquinone (0.58 g, 5.26 mmol) and sodium iodide (0.04 g, 0.26 mmol) were placed into a 10-20 mL microwave vial (Biotage) sealed and purged with nitrogen for 5 minutes. Acetone (~8 mL) with allyl

bromide (1.40 g, 0.12 mol) were added. This was placed into the microwave reactor (Biotage Initiator) and heated at 55 °C for at 900rpm and high intensity. The resulting mixture was filtered and the solvent evaporated. The residual oil was dissolved in dichloromethane (20 mL) and washed with 2M sodium hydroxide solution (18.90 mL), dried ($MgSO_4$) (2.30 g) and evaporated giving hydroquinone diallyl ether as a crystalline solid. Analysis conforms with previous analysis. The reaction was repeated using other solvents and conditions, yields are tabulated in Table 6.1.

Table 6.1 – Solvent conditions used for allylation of hydroquinone by microwave heating

Diol	Solvent	Time (min)	Temperature (°C)	Yield Product (%)
Hydroquinone	DMA	20	150	96
	NMP	20	150	79
	Acetone	20	55	99

6.2.4.2 – Synthesis of diallyl resorcinol ether (2c) – optimisation of reaction conditions

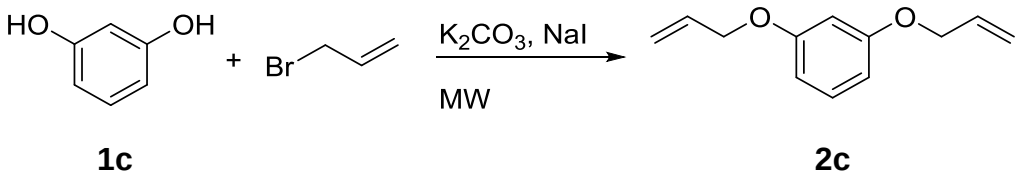

1c **2c**

Scheme 6.7 – Allylation of resorcinol under microwave heating

Following the process described above, resorcinol (0.58g, 5.26 mmol), allyl bromide (1.40 g, 0.12 mol), potassium carbonate (1.82 g, 13.14 mmol) and sodium iodide (0.04 g, 0.26 mmol) in a solvent at the desired temperatures gave viscous oils. ^{1}H NMR analysis confirms the presence of 2c as discussed previously with yields shown in Table 6.2.

Table 6.2 – Conditions used for allylation of resorcinol by microwave heating.

Solvent	Time (min)	Temperature (°C)	Allyl bromide Eq	Yield Product 2c (%)	Yield By-product 3 (%)
DMA	15	150	2.2	66	34
NMP	15	150	2.2	-	-
DMF	20	150	2.2	65	35
DMF	40	70	2.2	79	21
Acetone	40	100	2.2	79	21
Acetone	40	70	2.2	81	19
Acetone	15	70	2.2	36	64
Acetone	30	70	2.2	62	38
Acetone	60	70	2.2	63	37
Acetone	30	70	1.5	88	12
Acetone	30	70	4.0	85	15

6.3 Epoxidation using trichloroisocyanuric acid

6.3.1 – Synthesis of chlorohydrins: general procedure

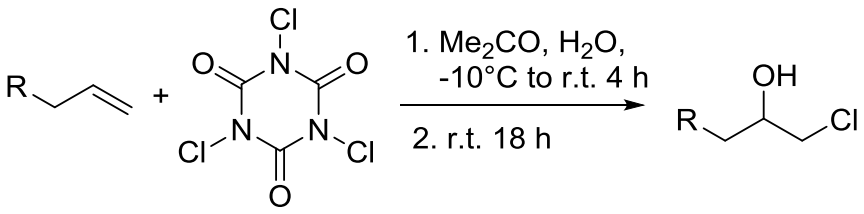

2a	R= O-Ar-OR (p)	**4a**
2b	R= O-Ar-OR (o)	**4b**

Scheme 6.8 – General reaction for the synthesis of chlorohydrin

In a round bottomed flask, 2g of diallyl ether was added to a mixture of 5:1 acetone and water (28 mL). The mixture was stirred and cooled to 0 - 5°C and trichloroisocyanuric acid (0.8 mol eq, 1.96g) was added slowly to ensure no exotherm was created. The reaction mixture was stirred at a temperature below 10°C for four hours after which it was allowed to warm up to r.t. and stirred for a further 16 hours. The white precipitate was filtered and the acetone evaporated. The residual oil was dissolved in 50 mL of dichloromethane and washed with 50 mL of sodium thiosulfate and evaporated to give a product which was analysed via ^{1}H NMR spectroscopy and GC-MS.

6.3.1.1 – Synthesis of hydroquinone dichlorohydrin ether

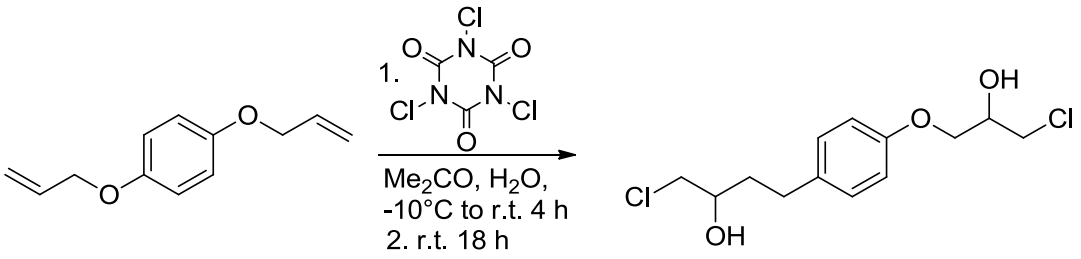

2a **4b**

Scheme 6.9 – Synthesis of hydroquinone dichlorohydrin ether

Using the procedure described above, hydroquinone diallyl ether (2.00g, 10mmol) and trichloroisocyanuric acid (1.96g, 8mmol) gave hydroquinone dichlorohydrin ether as a viscous liquid with the following results: ^{1}H NMR spectroscopy (400 MHz, $CDCl_3$) δ 6.82 (d, 4H, *J* = 2.0 Hz, Ar-**H**), 4.28 – 4.16 (m, 2H, -C**H**OH-), 4.16 – 4.12 (m, 2H, -O-C**H$_2$**-), 4.01 – 3.99 (m, 2H, -O-C**H$_2$**-), 3.93 (ddt, 2H, *J* = 9.8, 5.4, 1.3 Hz, -C**H$_2$**Cl), 3.76 – 3.64 (m, 2H, -C**H$_2$**Cl), m/z (EI)$^+$ 293.99. The product was used without further purification.

6.3.1.2 – Synthesis of catechol dichlorohydrin ether

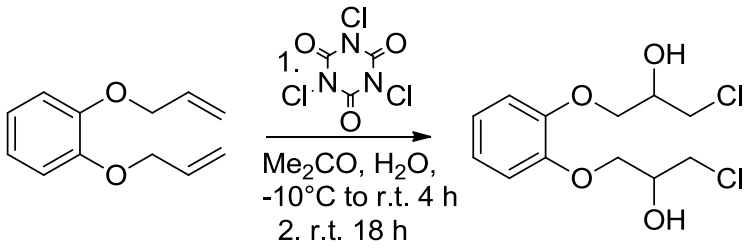

2b **4b**

Scheme 6.10 – Synthesis of catechol dichlorohydrin ether

Catechol diallyl ether (2.00g, 10mmol) was reacted with 0.8 mol equivalence of trichloroisocyanuric acid (1.96g, 8mmol) gave the following results: ^{1}H NMR spectroscopy (400 MHz, $CDCl_3$) δ 7.02 – 6.63 (m, 4H, Ar-**H**), 4.31 – 4.25 (m, 2H, -C**H**OH-), 4.22 – 4.13 (m, 2H, -O-C**H$_2$**-), 4.04 (ddd, 2H, 5.1, 4.5, 1.2 Hz,-O-C**H$_2$**-), 4.02 – 3.90 (m, 2H, -C**H$_2$**Cl), 3.81 – 3.68 (m, 2H, -C**H$_2$**Cl), m/z (EI)$^+$ 294.018 (54%), 327.982 (46%).

6.3.2 – Epoxide formation: general procedure[167]

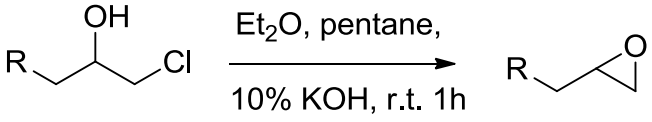

4a R= O-Ar-OR (p) **5a**
4b R= O-Ar-OR (o) **5b**

Scheme 6.11 – General formation of epoxides via ring closing of chlorohydrins

The crude chlorohydrins were dissolved in a mixture of diethyl ether (50 mL), pentane (50 mL) and aqueous potassium hydroxide (10% by weight in 10 mL of water) and stirred for 1 hour at room temperature. The organic layer was separated and washed with water, dried ($MgSO_4$) and solvent evaporated.

6.3.2.1 – Epoxide formation hydroquinone dichlorohydrin ether

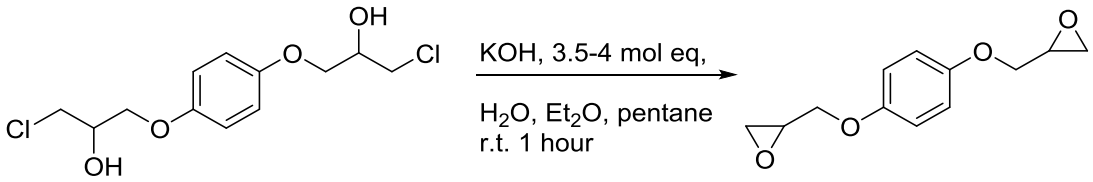

4a **5a**

Scheme 6.12 – synthesis of hydroquinone diglycidyl ether

Hydroquinone dichlorohydrin ether (3.06g, 10mmol) and potassium hydroxide (1.51g, 38mmol) were reacted together as described above. After work up gave a residual solid of hydroquinone diglycidyl ether with the following results: (96% Yield) ^{1}H NMR spectroscopy (400 MHz, Chloroform-d) δ 6.85 (s, 4H, Ar-**H**), 4.17 (dd, 2H, *J* = 11.0, 3.2 Hz, RO-C**H$_2$**-R), 3.90 (dd, 2H, *J* = 11.0, 5.7 Hz, RO-C**H$_2$**-R), 3.33 (ddt, 2H, *J* = 5.7, 4.1, 2.9 Hz, R-C**H**-R$_1$), 2.89 (ddd, 2H, *J* = 4.9, 4.1, 1.7 Hz, R-(O)-C**H$_2$**), 2.73 (dd, 2H, *J* = 4.9, 2.7 Hz, R-(O)-C**H$_2$**), GC-MS m/z (EI)$^+$ 221.977,

6.3.2.2 – Epoxide formation of catechol dichlorohydrin ether

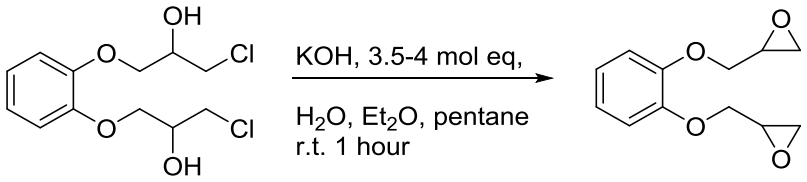

4b **5b**

Scheme 6.13 – synthesis of hydroquinone diglycidyl ether

Catechol dichlorohydrin ether (3.06g, 10mmol) and potassium hydroxide (1.51g, 38mmol) were reacted together as described above. After work up gave a residual oil of catechol diglycidyl ether, catechol dichlorohydrin ether and the ring

chlorinated derivatives the following results: ^{1}H NMR spectroscopy – a mixture of products as discussed in section 2.3.2.2; GC-MS m/z $(EI)^{+}$ 222.10 (5b, 29%), 258.07 (ring chlorinated 5b, 36%), 292.06 (4b, 26%), 328.02 (ring chlorinated 4b, 9%).

6.4 Epoxidation using HOF.MeCN

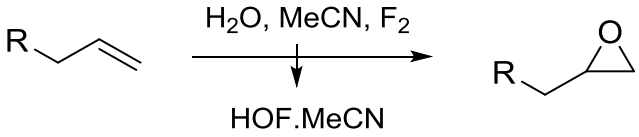

6	R= C_9H_{10}	**8**
7	R= O-Ar	**9**
2a	R= O-Ar-OR	**5a**
2b	R= O-Ar-OR	**5b**
2c	R= O-Ar-OR	**5c**

Scheme 6.14 – General reaction for epoxidation of alkenes using HOF.MeCN

6.4.1 Batch epoxidation: general procedure

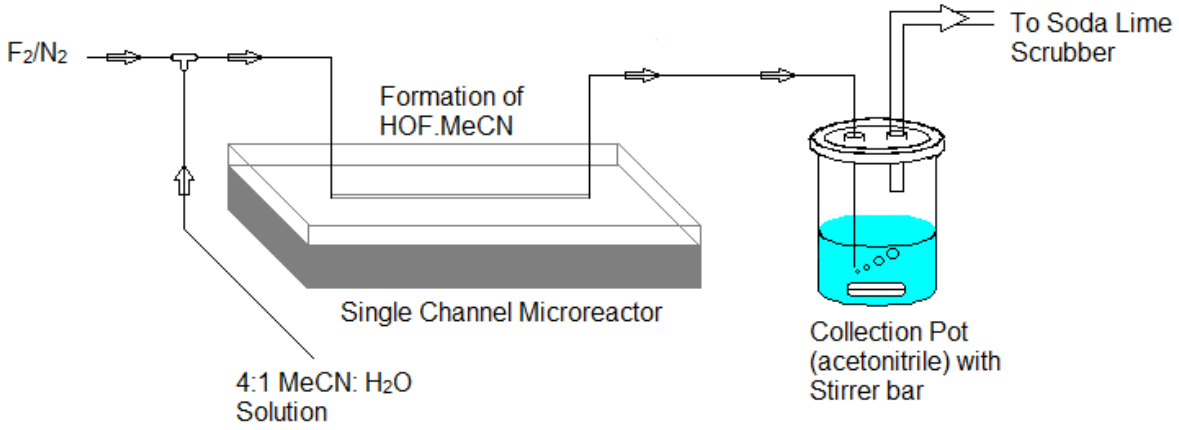

Figure 6.1 – Reaction set up for batch reactions with HOF.MeCN

Fluorine (10% in nitrogen) was passed at a prescribed flow rate, calibrated to 2 mmol h^{-1}, into the micro-reactor channel via a t-piece and simultaneously, acetonitrile and water in a ratio of 4:1 (10mL) was added via a syringe pump into the channel at a flow rate of 9.90mL h^{-1} (110.0mmol h^{-1}). After passage through the micro-reactor system, all reaction fluids were collected in a vessel containing water (50 mL). After purging the apparatus with nitrogen, the reaction mixture was added to $NaHCO_3$ solution (25 mL), extracted with CH_2Cl_2 (3 x 75 mL), dried ($MgSO_4$) and filtered. The solvent was removed under reduced pressure to yield the product, with no further purification required[196].

6.4.1.1 Calibration using dodec-1-ene

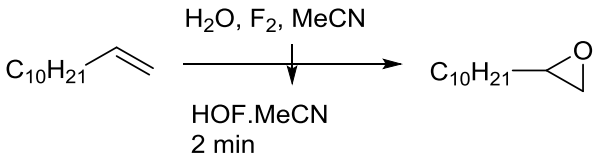

6 **8**

Scheme 6.15 – Epoxidation of dodec-1-ene

Dodec-1-ene (0.17g, 2 mmol) and HOF.MeCN solution as prepared above (10% F_2 in N_2 (2 mmol h^{-1}, 14 mL min^{-1} for 30 minutes) and 1:4 mixture of H_2O and MeCN (110 mmol h^{-1}, 9.90 mL h^{-1})) gave 2-decyloxirane (14 mL min^{-1} – 0.33g 90%) as a clear oil which gave the following results: ^{1}H NMR spectroscopy (200 MHz, $CDCl_3$) δ 2.92 – 2.80 (m, 1H, R-C**H**-(O)-R), 2.69 (dd, 1H, *J* = 5.1, 4.0 Hz, R-(O)-C**H$_2$**), 2.41 (dd, 1H, *J* = 5.1, 2.7 Hz, R-(O)-C**H$_2$**), 1.55 – 1.15 (m, 18H, -C**H$_2$-**), 0.91 – 0.76 (m, 3H, -C**H$_3$**) corresponding to the literature data[196].

6.4.1.2 Calibration using phenol allyl ether

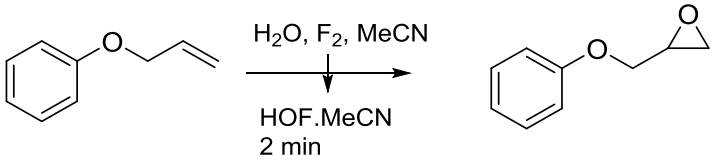

7 **9**

Scheme 6.16 – epoxidation of phenol allyl ether

Phenol allyl ether (Sigma, 0.13 g, 2.0 mmol) and HOF.MeCN mixture as prepared above (2 mmol h^{-1}, 14 mL min^{-1} for 30 minutes) and 1:4 mixture of H_2O and MeCN (110 mmol h^{-1}, 9.90 mL h^{-1})) gave phenol glycidyl ether in a yield of 97% giving the results; ^{1}H NMR spectroscopy (400 MHz, $CDCl_3$) δ 7.40 – 7.23 (m, 2H, Ar-**H** *meta*), 7.05 – 6.89 (m, 3H, Ar-**H** *ortho* and *para*), 4.24 (dd, 1H, *J* = 11.0, 3.2 Hz, R-O-C**H$_2$**-R), 3.99 (dd, 1H, *J* = 11.0, 5.6 Hz, R-O-C**H$_2$**-R), 3.38 (dddd, 1H, *J* = 5.7, 4.1, 3.2, 2.7 Hz, 1H, R-C**H**-(O)-R), 2.93 (dd, 1H, *J* = 4.9, 4.1 Hz, R-(O)-C**H$_2$**), 2.78

(dd, 1H, *J* = 4.9, 2.7 Hz, R-(O)-C**H$_2$**); m/z (EI)$^+$ 150 ([M]$^+$, 95%) as compared to that in the literature[239].

6.4.1.3 Epoxidation of hydroquinone diallyl ether

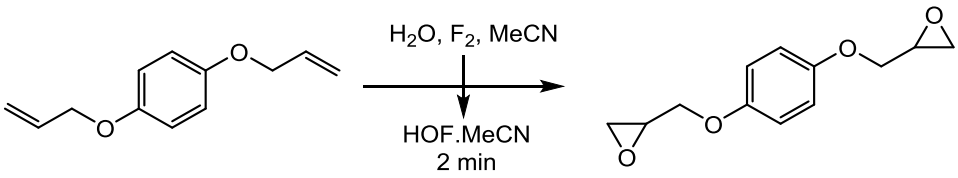

2a **5a**

Scheme 6.17 - epoxidation of hydroquinone diallyl ether

Hydroquinone diallyl ether (0.19 g, 2 mmol) and HOF.MeCN mixture as prepared above (2 mmol h^{-1}, 14 mL min^{-1} for 60 minutes) and 1:4 mixture of H_2O and MeCN (110 mmol h^{-1}, 9.90 mL h^{-1})) gave hydroquinone diglycidyl ether as a white crystalline solid with the following results: Yield= 82%, ^{1}H NMR spectroscopy (400 MHz, $CDCl_3$) δ 6.79 (s, 4H, Ar-**H**), 4.11 (dd, 2H, *J* = 11.0, 3.2 Hz, R-O-C**H$_2$**-R), 3.84 (dd, 2H, *J* = 11.0, 5.7 Hz, R-O-C**H$_2$**-R), 3.27 (ddt, 2H, *J* = 5.8, 4.1, 3.0 Hz, R-C**H**-(O)-R), 2.83 (dd, 2H, *J* = 4.9, 4.2 Hz, R-(O)-C**H$_2$**), 2.68 (dd, 2H, *J* = 4.9, 2.7 Hz, R-(O)-C**H$_2$**).

6.4.1.4 Epoxidation of Catechol diallyl ether

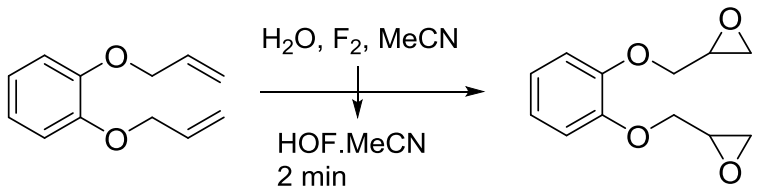

2b **5b**

Scheme 6.18 - epoxidation of catechol diallyl ether

Catechol diallyl ether (0.19 g, 2 mmol) was added to HOF.MeCN mixture, prepared at 15 mL min^{-1} over 1 hour. The residual liquid was analysed with the following results: ^{1}H NMR spectroscopy (400 MHz, $CDCl_3$) δ 6.94 (d, *J* = 1.4 Hz, Ar-

H (di)), 6.92 (d, *J* = 2.0 Hz, Ar-**H** (mono)), 4.33 – 4.18 (m, R-O-C**H₂**-R), 4.11 – 3.95 (m, R-O-C**H₂**-R), 3.47 – 3.30 (m, R-C**H**-(O)-R), 2.89 (ddd, *J* = 4.9, 4.2, 2.9 Hz, R-(O)-C**H₂**), 2.76 (dt, *J* = 5.0, 2.6 Hz, R-(O)-C**H₂**) for the epoxy and 6.90 (q, *J* = 1.8 Hz), 6.08 (ddtd, *J* = 16.8, 10.5, 5.3, 0.8 Hz), 5.42 (ddt, *J* = 17.3, 2.9, 1.5 Hz, trans R=CH_2), 5.27 (ddd, *J* = 10.5, 3.2, 1.5 Hz), 4.60 (ddt, *J* = 5.4, 4.0, 1.5 Hz) for unreacted alkene.

6.4.2 – Continuous flow: general procedure

Fluorine (10% in nitrogen) was passed at prescribed flow rate, calibrated to 2 mmol h^{-1}, into the micro-reactor channel via a t-piece and simultaneously, acetonitrile and water at a ratio of 4:1 (10mL) was added via a syringe pump into at a flow rate of 9.90mL h^{-1} (110.0mmol h^{-1}). The alkene (2mmol), in CH_2Cl_2 (10 mL), was added via syringe pump at a flow rate of 9.90 mL h^{-1}. After passage through the micro-reactor system, all reaction fluids were collected in a vessel containing water (50 mL). After purging the apparatus with nitrogen, the reaction mixture was added to $NaHCO_3$ solution (25 mL), extracted with CH_2Cl_2 (3 x 75 mL), dried ($MgSO_4$) and filtered. The solvent was removed under reduced pressure to yield the product, with no further purification required.

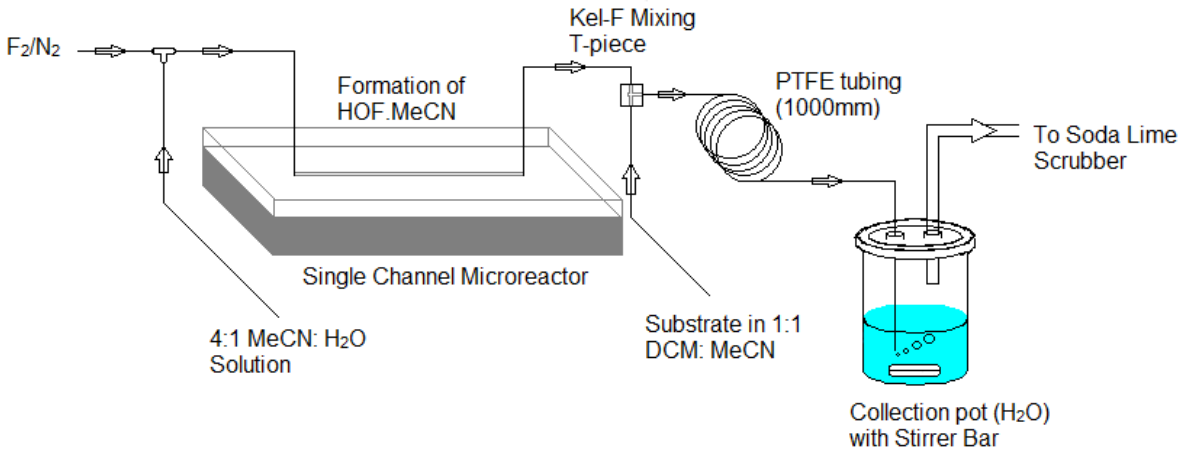

Figure 6.2 – Reaction set up for continuous flow HOF.MeCN reactions

6.4.2.1 – Calibration using dodec-1-ene

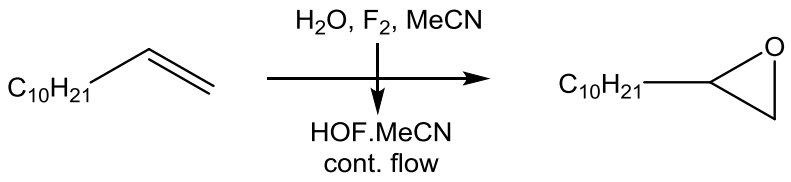

6 **8**

Scheme 6.19 – Epoxidation of dodec-1-ene in continuous flow

Using the procedure described above, dodec-1-ene (0.34g, 2 mmol h^{-1}) was reacted with HOF.MeCN for 15 minutes prepared at flow rates of 10% F_2 of 7.5, 10, 12.5, 15, 17.5 and 20 mL min^{-1} with MeCN and water mixture at 9.90 mL h^{-1} (110.0 mmol h^{-1}). This gave 2-decyloxirane as a clear oil with the following results: ^{1}H NMR spectroscopy (200 MHz, $CDCl_3$) δ 2.92 – 2.80 (m, 1H, R-C**H**-(O)-R), 2.69 (dd, 1H, *J* = 5.1, 4.0 H, R-(O)-C**H$_2$**z), 2.41 (dd, 1H, *J* = 5.1, 2.7 Hz, R-(O)-C**H$_2$**), 1.55 – 1.15 (m, 18H, R-C**H$_2$**-R), 0.91 – 0.76 (m, 3H, -C**H$_3$**) consistent with the literature data[196]. The different conversions are given in Table 6.3 for each flow rate.

Table 6.3 – Calibration table for dodec-1-ene in continuous flow

Flow rate of F_2 mL min^{-1} (mmol h^{-1})	MeCN: H_2O flow rate mL h^{-1}	dodec-1-ene		Conversion % from ^{1}H NMR*
		mmol	Flow rate (mL h^{-1})	
7.5 (1.8)	9.90	2	9.90	9
10 (2.4)	9.90	2	9.90	17
12.5 (3.1)	9.90	2	9.90	43
15 (3.7)	9.90	2	9.90	55
20 (4.9)	9.90	2	9.90	91

*conversion of alkene to epoxide by measured by integration of resonances of 5.80 ppm of the alkene and 2.89 ppm of the epoxide.

6.4.2.2 – Epoxidation of phenol allyl ether

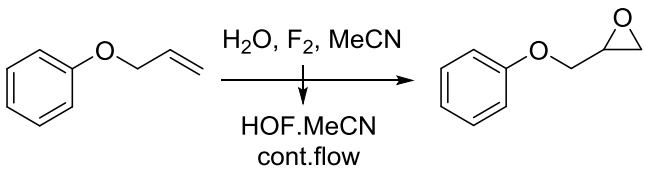

7 **9**

Scheme 6.20 – Epoxidation phenol allyl ether in continuous flow

Using the procedure described above phenol allyl ether (0.27g, 2 mmol h^{-1}) was reacted in continuous flow with HOF.MeCN for 30 minutes prepared at flow rates of 10% F_2 of 20 and 25 mL min^{-1} with MeCN and water mixture at 9.90 mL h^{-1} (110.0 mmol h^{-1}). This gave phenol allyl ether as a clear oil with the following results: ^{1}H NMR spectroscopy (400 MHz, $CDCl_3$) δ 7.40 – 7.23 (m, 2H, Ar-**H** *meta*), 7.05 – 6.89 (m, 3H, Ar-**H** *ortho* and *para*), 4.24 (dd, 1H, *J* = 11.0, 3.2 Hz, R-O-C**H$_2$**-R), 3.99 (dd, 1H, *J* = 11.0, 5.6 Hz, R-O-C**H$_2$**-R), 3.38 (dddd, 1H, *J* = 5.7, 4.1, 3.2, 2.7 Hz, R-C**H**-(O)-R), 2.93 (dd, 1H, *J* = 4.9, 4.1 Hz, R-(O)-C**H$_2$**), 2.78 (dd, 1H, *J* = 4.9, 2.7 Hz, R-(O)-C**H$_2$**).

Table 6.4 – Calibration table for phenol allyl ether in continuous flow

Flow rate of F_2 mL min^{-1} (mmol h^{-1})	MeCN: H_2O flow rate mL h^{-1}	dodec-1-ene		Conversion % from ^{1}H NMR*
		mmol	Flow rate (mL h^{-1})	
20 (4.9)	9.90	2	9.90	93
25 (6.1)	9.90	2	9.90	97

*conversion of alkene to epoxide by measured by integration of resonances of 6.10 ppm of the alkene and 3.37 ppm of the epoxide.

6.4.2.3 – Optimisation of epoxidation of hydroquinone diallyl ether by continuous flow

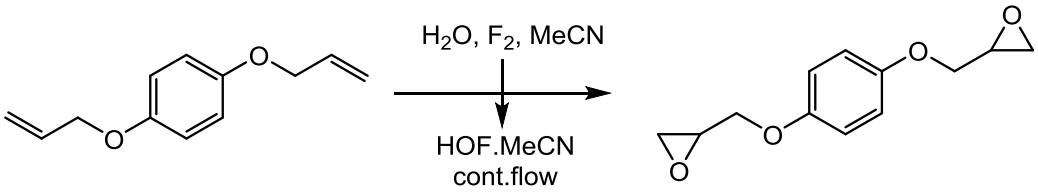

2a **5a**

Scheme 6.21 – Epoxidation of hydroquinone diallyl ether by continuous flow

Using the procedure described above hydroquinone diallyl ether (0.38g, 2 mmol) was reacted in continuous flow with HOF.MeCN for 30 minutes prepared using different parameters as described below. This gave a mixture of hydroquinone diallyl ether, hydroquinone monoepoxide ether and hydroquinone diglycidyl ether as a crystalline solid with the following results: ^{1}H NMR spectroscopy (400 MHz, $CDCl_3$) δ 6.79 (s, 4H, Ar-**H**), 4.11 (dd, 2H, *J* = 11.0, 3.2 Hz, R-O-C**H$_2$**-R), 3.84 (dd, 2H, *J* = 11.0, 5.7 Hz, R-O-C**H$_2$**-R), 3.27 (ddt, 2H, *J* = 5.8, 4.1, 3.0 Hz, R-C**H**-(O)-R), 2.83 (dd, 2H, *J* = 4.9, 4.2 Hz, R-(O)-C**H$_2$**), 2.68 (dd, 2H, *J* = 4.9, 2.7 Hz, R-(O)-C**H$_2$**) for the bisepoxide, with 6.69 (Ar-H) for the monoepoxide and 6.62 (Ar-H) for the alkene (as described in section 6.2.1.1).

6.4.2.3.1 – Collection solvent

Following the procedure described above hydroquinone diallyl ether was reacted with HOF.MeCN using different solvents in the collection vessel and conversions to 5a are given in Table 6.5.

Table 6.5 – Variation of collection solvents in reactions with HDGE

Flow rate of F_2 mL min^{-1} (mmol h^{-1})	MeCN: H_2O flow rate mL h^{-1}	Collection solvent	Hydroquinone diallyl ether		Conversion % from ^1H NMR*
			mmol	Flow rate (mL h^{-1})	
25 (6.1)	9.90	H_2O	2	9.90	61
25 (6.1)	9.90	MeCN	2	9.90	56
25 (6.1)	9.90	$NaHCO_3$	2	9.90	51

*conversion of alkene and monoepoxide to bisepoxide by measured by integration of resonances of 6.62 ppm of the alkene, 6.69 ppm of the monoepoxide and 6.79 ppm of the bisepoxide.

6.4.2.3.2 – Optimisation using 1:1 DCM. MeCN solvent system

Following the procedure described above hydroquinone diallyl ether was dissolved in a mixture of 1:1 DCM: MeCN and reacted with HOF.MeCN using different flow rates of F_2 with the conversions shown in Table 6.6.

Table 6.6 – Epoxidation of HDGE using 1:1 substrate DCM. MeCN solvent mixture

Flow rate of F_2 mL min^{-1} (mmol h^{-1})	Substrate solvent solution	Hydroquinone diallyl ether		Conversion % from ^1H NMR*
		mmol	Flow rate (mL h^{-1})	
20 (4.9)	1:1 DCM:MeCN	2	9.90	79
25 (6.1)	1:1 DCM:MeCN	2	9.90	92
30 (7.3)	1:1 DCM:MeCN	2	9.90	92

*conversion of alkene and monoepoxide to bisepoxide by measured by integration of resonances of 6.62 ppm of the alkene, 6.69 ppm of the monoepoxide and 6.78 ppm of the bisepoxide.

6.4.2.3.3 – Changing flow rate of acetonitrile: water mixture and 10% F_2 in N_2

Following the procedure above, different flow rates of MeCN: H_2O and F_2 were utilized for the epoxidation of HDGE with the results tabulated in Table 6.7.

Table 6.7 – Variations of flow rates of MeCN: H_2O and 10% F_2 in epoxidations of HDGE in continuous flow

Flow rate of F_2 mL min^{-1} (mmol h^{-1})	MeCN: H_2O flow rate mL h^{-1}	Time (min)	Hydroquinone diallyl ether		Conversion % from ^1H NMR*
			mmol	Flow rate (mL h^{-1})	
20 (4.9)	10	30	2	14	72
20 (4.9)	15	30	2	13	74
25 (6.1)	10	30	2	11	80
25 (6.1)	15	30	2	11	83
25 (6.1)	10	60	2	15	77
25 (6.1)	15	60	2	10	86
25 (6.1)	20	60	2	7	88

*conversion of alkene and monoepoxide to bisepoxide by measured by integration of resonances of 6.62 ppm of the alkene, 6.69 ppm of the monoepoxide and 6.78 ppm of the bisepoxide.

6.4.2.3.4 – Test for hydrolysis product in HDGE

Fluorine (10% in nitrogen) was passed at prescribed flow rate, calibrated to 2 mmol h^{-1}, into the micro-reactor channel via a t-piece and simultaneously, acetonitrile and deuterium oxide at a ratio of 4:1 (5 mL) was added via a syringe pump into at a flow rate of 9.90mL h^{-1} (110.0mmol h^{-1}). Hydroquinone diallyl ether (0.36g, 2mmol), in a mixture of CH_2Cl_2 (5 mL) and MeCN (5 mL), was added via syringe pump at a flow rate of 9.90 mL h^{-1}. After passage through the micro-reactor system, all reaction fluids were collected in a vessel containing acetonitrile (20 mL). After purging the apparatus with nitrogen, the reaction mixture was washed with 5 drops of sodium deuteroxide in 5 mL of deuterium oxide and extracted with CH_2Cl_2 (10 mL). The organic and aqueous layers were analysed using ^1H NMR analysis

being discussed in section 3.4.3.4. After analysis the NMR tube was doped with a small amount of hydroquinone and re-analysed.

6.4.2.4 – Optimisation of epoxidation of catechol diglycidyl ether by continuous flow

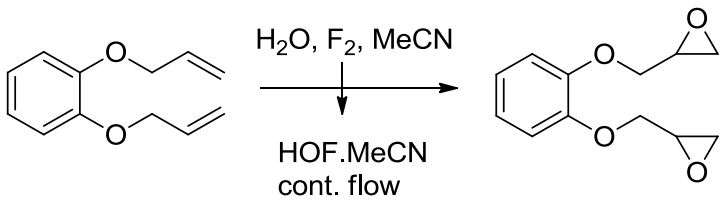

2b **5b**

Scheme 6.22 – Epoxidation of catechol diallyl ether using HOF.MeCN

Using the procedure described above catechol diallyl ether (0.38g, 2 mmol) was reacted in continuous flow with HOF.MeCN for 30 minutes prepared at flow rates of 10% F_2 of 20, 25 and 30 mL min^{-1} with MeCN and water mixture at 20 mL h^{-1} (220.0 mmol h^{-1}). This gave a mixture of catechol diallyl ether, catechol allylglycidyl ether and catechol diglycidyl ether as a clear viscous liquid with the following results: ^{1}H NMR spectroscopy (400 MHz, $CDCl_3$) δ 6.95 (d, 4H, *J* = 1.4 Hz, Ar-**H**), 4.27 (ddd, 2H, *J* = 11.3, 3.2, 1.6 Hz, R-O-C**H$_2$**-R), 4.02 (ddd, 2H, *J* = 11.3, 5.5, 4.6 Hz, R-O-C**H$_2$**-R), 3.39 (ddt, 2H, *J* = 6.6, 5.5, 2.5 Hz, R-C**H**-(O)-R), 2.90 (ddd, 2H, *J* = 4.9, 4.1, 0.6 Hz, R-(O)-C**H$_2$**), 2.77 (dt, 2H, *J* = 4.9, 2.4 Hz, R-(O)-C**H$_2$**) for the bisepoxide, with 6.94 (Ar-H) for the monoepoxide and 6.93 (Ar-H) for the alkene (as described in section 6.2.1.2). The conversions for each flow rate are given below in Table 6.8.

Table 6.8 – Variations of 10% F_2 flow rate in epoxidations of CDGE in continuous flow

Flow rate of F_2 mL min^{-1} (mmol h^{-1})	MeCN: H_2O flow rate mL h^{-1}	Catechol diallyl ether		Conversion % from ^1H NMR*
		mmol	Flow rate (mL h^{-1})	
20 (4.9)	20	2	9.90	79
25 (6.1)	20	2	9.90	90
30 (7.3)	20	2	9.90	98

*conversion of alkene and monoepoxide to bisepoxide by measured by integration of resonances of 6.93 ppm of the alkene, 6.94 ppm of the monoepoxide and 6.95 ppm of the bisepoxide.

6.4.3 – Scaling up of synthesis

6.4.3.1 – Utilization of HPLC pumps

Two Gilson HPLC pumps (one 305 and one 306 both using 25SC heads) were used to replace the syringe pumps as utilised previously. The HPLC pumps were set up in tandem with the Gilson 305 HPLC pump being the control pump and the Gilson 306 HPLC pump being the secondary pump as seen in Figure 6.3. The HPLC pumps were calibrated flow rates of 20.301 mL h^{-1} of MeCN: H_2O and 9.99 mL h^{-1} of substrate. This was achieved by first priming the heads by pressing prime on the controller and allowing solvent to pass through the head until no air bubbles were in the tubing. After this the pump was programmed by selecting Mode » Prog » Cond and setting the flow ramp as Flow 0 – 0.338 mL min^{-1} and Mixt100% A and clocking Next. Then setting the Flow as 0.505 and the Mixt as 67% A and saving the programme. Once the programme was prepared the selection of Mode » Prog » Run was required to perform the flow.

Figure 6.3 – HPLC pump set up. Bottom is a Gilson 305 pump with system control set for aqueous solvent. Top is a Gilson 306 as the secondary pump set for organic solvent.

6.4.3.2 – Extended reaction time for synthesis of hydroquinone diglycidyl ether

Following the procedure described in section 6.3.2 using HPLC injector pumps, hydroquinone diallyl ether was reacted with HOF.MeCN prepared at flow rates of 10% F_2 of 25 mL min^{-1} by continuous flow for different reaction times. The yield and conversion to hydroquinone diglycidyl ether are collected in Table 6.9.

Table 6.9 – Effect of time on the conversion of hydroquinone diglycidyl ether

MeCN: H_2O flow rate mL h^{-1}	Catechol diallyl ether		Reaction time (h)	Yield (%)	Conversion % from ^1H NMR*
	mmol	Flow rate (mL h^{-1})			
20.3	2	9.90	2.5	44	95
20.3	2	9.90	21	44	95
20.3	2	9.90	23	33	91

*conversion of alkene and monoepoxide to bisepoxide by measured by integration of resonances of 6.62 ppm of the alkene, 6.69 ppm of the monoepoxide and 6.78 ppm of the bisepoxide.

6.4.3.3 – Effect of time on catechol diglycidyl ether

Following the procedure described in section 6.3.2 using HPLC injector pumps, catechol diallyl ether was reacted with HOF.MeCN prepared at flow rates of 10% F_2 of 30 mL min^{-1} by continuous flow for different reaction times. The conversion to catechol diglycidyl ether are collected in Table 6.10.

Table 6.10 – Effect of time on the conversion of catechol diglycidyl ether

MeCN: H_2O flow rate mL h^{-1}	Catechol diallyl ether		Reaction time (h)	Conversion % from ^1H NMR*
	mmol	Flow rate (mL h^{-1})		
20.3	2	9.90	2	98
20.3	2	9.90	18	94
20.3	2	9.90	24	92

*conversion of alkene and monoepoxide to bisepoxide by measured by integration of resonances of 6.93 ppm of the alkene, 6.94 ppm of the monoepoxide and 6.95 ppm of the bisepoxide.

6.4.3.4 – Effect of concentration on hydroquinone diglycidyl ether

Following the procedure described in section 6.3.2 using HPLC injector pumps, hydroquinone diallyl ether was reacted with HOF.MeCN prepared at different flow rates of F_2 and H_2O: MeCN and different concentrations of substrate and F_2, by continuous flow for 1 hour. The yield and conversion to hydroquinone diglycidyl ether are collected in Table 6.11.

Table 6.11 – Effect of changing HOF.MeCN concentration on hydroquinone diglycidyl ether

HOF.MeCN/ HDGE conc. (mmol h^{-1})	F_2 %	Flow F_2 mL min^{-1} (mmol)	Flow of H_2O MeCN: substrate (mL h^{-1})	Yield (%)	Conversion % from ^1H NMR*
1	10	20 (4.9)	10:10	62	89
2	10	25 (6.1)	20:10	49	97
4	20	25 (12.2)	40:10	0	0
8	20	50 (24.5)	80:10	0	0

*conversion of alkene and monoepoxide to bisepoxide by measured by integration of resonances of 6.62 ppm of the alkene, 6.69 ppm of the monoepoxide and 6.78 ppm of the bisepoxide.

6.4.3.5 – Effect of concentration on hydroquinone diglycidyl ether

Following the procedure described in section 6.3.2 using HPLC injector pumps, catechol diallyl ether was reacted with HOF.MeCN prepared at different flow rates of F_2 and H_2O: MeCN and different concentrations of substrate and F_2, by continuous flow for 1 hour. The yield and conversion to hydroquinone diglycidyl ether are collected in Table 6.12.

Table 6.12 – Effect of changing HOF.MeCN concentration on catechol diglycidyl ether for 2 hours

HOF.MeCN/ HDGE conc. (mmol h^{-1})	F_2 %	Flow F_2 mL min^{-1} (mmol)	Flow of H_2O MeCN: substrate (mL h^{-1})	Yield (%)	Conversion % from ^1H NMR*
2	10	30 (7.3)	20:10	93	97
4	20	30 (14.7)	40:10	61	86
8	20	60 (29.4)	80:10	53	86

6.5 Polymerisation

6.5.1 – Calculations

6.5.1.1 – Determination of epoxide equivalent weight[211]

The epoxide equivalent weight (EEW) was determined using the following equation:

$$EEW = \frac{1}{2}Mw(repeat\,unit) \times n + \frac{1}{2}Mw(pure\,compound) \tag{6.1}$$

$$\text{Where } n = \frac{\left(\frac{Ar\ protons}{Epoxide\ protons}actual\right) - \left(\frac{Ar\ protons}{Epoxide\ protons}theoretical\right)}{\frac{Ar\ protons}{Epoxide\ protons}theoretical} \tag{6.2}$$

The actual ratio was taken from ^{1}H NMR analysis from comparing the aromatic integrals compared to the epoxide integrals.

6.5.1.2 – Determination of stoichiometric ratios

Using the calculated EEW it is possible to determine accurately the amounts of epoxide from a predetermined mass of amine for 100% stoichiometry using the following equation:

$$Mass\,epoxide = \frac{functional\,eq \times EEW}{stoichiometry} \tag{6.3}$$

Where the functional eq is:

$$funtional\,eq = \frac{mass\,amine}{AHEW} \tag{6.4}$$

Where the active hydrogen equivalent weight:

$$AHEW = \frac{Mw}{N^o\ active\ hydrogens} \qquad (6.5)$$

6.5.2 – Preparation of monomers

6.5.2.1 – Preparation of pure HDGE and CDGE

All synthesised epoxides were re-crystallised using a 1:1 mixture of ethoxyethyl ether ethyl isobutyl ketone prior to use. The samples were then analysed with the following results:

Hydroquinone diglycidyl ether: ^{1}H NMR spectroscopy (400 MHz, $CDCl_3$) δ 6.79 (s, 4H, Ar-**H**), 4.11 (dd, 2H, *J* = 11.0, 3.2 Hz, R-O-C**H$_2$**-R), 3.84 (dd, 2H, *J* = 11.0, 5.7 Hz, R-O-C**H$_2$**-R), 3.27 (ddt, 2H, *J* = 5.8, 4.1, 3.0 Hz, R-C**H**-(O)-R), 2.83 (dd, 2H, *J* = 4.9, 4.2 Hz, R-(O)-C**H$_2$**), 2.68 (dd, 2H, *J* = 4.9, 2.7 Hz, R-(O)-C**H$_2$**); ^{13}C NMR spectroscopy (100 MHz, $CDCl_3$) δ 153.09 (Ar C), 115.78 (Ar CH), 69.94 (R-(O)-**C**H$_2$), 50.25 (R-**C**H-(O)-R), 44.73 (R-O-**C**H$_2$-R); GC-MS: - RT 19.62 min m/z 222.017.

Catechol diglycidyl ether: ^{1}H NMR spectroscopy (400 MHz, $CDCl_3$) δ 6.95 (d, *J* = 1.4 Hz, Ar-**H**), 4.27 (ddd, 2H, *J* = 11.3, 3.2, 1.6 Hz, R-O-C**H$_2$**-R), 4.02 (ddd, 2H, *J* = 11.3, 5.5, 4.6 Hz, R-O-C**H$_2$**-R), 3.39 (ddt, 2H, *J* = 6.6, 5.5, 2.5 Hz), R-C**H**-(O)-R, 2.90 (ddd, 2H, *J* = 4.9, 4.1, 0.6 Hz, R-(O)-C**H$_2$**), 2.77 (dt, 2H, *J* = 4.9, 2.4 Hz, R-(O)-C**H$_2$**); ^{13}C NMR spectroscopy (100 MHz, $CDCl_3$) δ 147.78 (Ar C), 122.14 (Ar CH), 115.22 (Ar CH), 70.35 (R-(O)-**C**H$_2$), 50.30 (R-**C**H-(O)-R), 44.80 (R-O-**C**H$_2$-R); GC-MS: - RT 5.02 min m/z 222.100.

6.5.2.2 – Preparation of pure RDGE

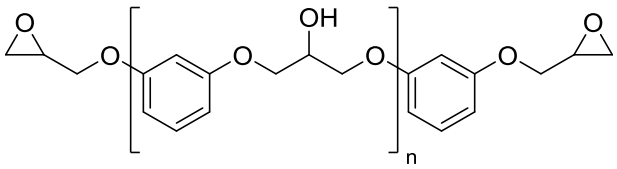

Figure 6.3 – Structure of resorcinol diglycidyl ether (RDGE)

RDGE (CVC Speciality Chemicals) was transferred into a round bottomed flask and distilled under vacuum (2 mbar) until the pure RDGE was collected at about 180°C. The collected creamy white crystalline solid was then analysed via giving the following results: TLC (1:2 EtOAc: hexane) - starting material (impure RDGE) 0.58, 0.40, 0.33, product (pure RDGE) 0.65; ^{1}H NMR spectroscopy (400 MHz, $CDCl_3$) δ 7.23 – 7.10 (m, 1H, Ar-**H**), 6.54 (d, 1H, *J* = 2.4 Hz, Ar-**H**), 6.52 (q, 2H, *J* = 1.4 Hz, Ar-**H**), 4.21 (dd, 2H, *J* = 11.0, 3.0 Hz, R-O-C**H$_2$**-R), 3.90 (dd, 2H, *J* = 11.0, 5.8 Hz, R-O-C**H$_2$**-R), 3.34 (ddt, 2H, *J* = 5.7, 4.1, 2.9 Hz, R-C**H**-(O)-R), 2.89 (dd, 2H, *J* = 4.8, 4.3 Hz, R-(O)-C**H$_2$**), 2.74 (dd, 2H, *J* = 4.9, 2.7 Hz, R-(O)-C**H$_2$**); ^{13}C NMR spectroscopy (100 MHz $CDCl_3$) δ 159.69 (Ar C), 130.03 (Ar CH), 107.34 (Ar CH), 101.83 (Ar CH), 68.79 (R-(O)-**C**H_2), 50.10 (R-**C**H-(O)-R), 44.67(R-O-**C**H_2-R); GC-MS: - RT 19.25 min m/z 222.172.

6.5.2.3 – Characterisation of PACM

A sample of PACM (Sigma Aldrich) was taken and analysed using ^{1}H NMR spectroscopy (400 MHz, $CDCl_3$), ^{13}C NMR spectroscopy (100 MHz, $CDCl_3$), HSQC (^{1}H - 700 MHz, ^{13}C – 176 MHz, $CDCl_3$) and COSY (400 MHz, $CDCl_3$) NMR spectroscopy GC-MS (EI) as discussed in section 4.3.

6.5.3 – General preparation of polymers

In a sample vial the epoxide (2.11g) was heated until fully melted. To this liquid state PACM (1.00g) was added and stirred vigorously for 2 minutes and cured in two ways.

The first, using a 300µm stainless steel draw down bar (as shown in Figure 6.4) onto a preheated, prepared glass panel (by cleaning, PTFE spray or PTFE film) the mixture was applied and placed in an oven at various temperatures under nitrogen for 18 hours, with a small sample being used for a DSC analysis. After this time the samples were heated at a higher temperature to 10°C above their glass transition temperature, as obtained by DSC.

The second, using a preheated 1mm thick PTFE mould (as shown in Figure 6.5) the mixture was applied and spread around evenly to try and remove any air bubbles. This was then heated in an oven under nitrogen at 100°C for 18 hours and then cured at an elevated temperature of 170°C for 5 hours. These samples were then removed and tested. By using different moulds it was possible to get the shapes that were required for analysis (Figure 6.5).

Figure 6.4 – (Left) Draw down bar onto a glass substrate and (right) removed film

Figure 6.5 – (Left) Standard PTFE mould, (right) mould for DMA

Chapter 7 – Conclusions and Future Work

7.1 – Conclusions

The aim of this work as described at the beginning of chapter 2 was to produce polymer films based on bisepoxides and bisamines with different structural symmetry and to fully characterise these polymers with regards to their chemical resistance and how the structure effects the chemical resistance. For the polymer films to be produced different synthetic routes were used to synthesise to epoxide monomers from starting diols as described in chapter 2.

Using the synthetic routes shown in Chapter 2, we have successfully shown the synthesis and purification of both hydroquinone and catechol diglycidyl ethers but not for resorcinol diglycidyl ether. Using the initial Williamson ether reaction we were able to synthesise hydroquinone and catechol diallyl ether, however, attempts to follow the same procedure with resorcinol produced significant by-products formed by an electrophilic substitution process via the activation of the 2, 4 and 6 positions of the aromatic ring. All attempts to remove the by-products by purification and changing reaction set ups were futile deeming the synthetic approach for the resorcinol derivative redundant. However, resorcinol diglycidyl ethers are commercially available and readily purified by vacuum distillation. Subsequent epoxidation of the bisallyls by a more conventional synthetic route using trichloroisocyanuric acid showed varied results. Hydrochlorination of the bisallyl of hydroquinone gave a conversion of 96% whereas the hydrochlorination of the bisallyl catechol system gave a mixture of products due to ring chlorination at a 1:1 ratio. Studies to attempt to limit the ring chlorination of the catechol derivative were unsuccessful with lower reaction times and equivalents of TCA still producing the ring chlorinated product. Consequently this synthetic route was viable for the formation of hydroquinone epoxides with the desired bis product being the major component with only small amounts of mono- epoxide present. In contrast catechol product contained a mixture of bis and mono epoxides which could not be separated.

Small scale synthesis showed that it was possible to epoxidise both hydroquinone diglycidyl ether and catechol diglycidyl ether using HOF.MeCN as the oxidising agent, however, with the catechol derivative limited conversion was found.

Using the HOF.MeCN reaction in a continuous method demonstrated effective conversions in the epoxidation of both the hydroquinone and catechol isomers. With the hydroquinone isomer substrate, however, there is evidence of acid catalysed hydrolysis as a competing process which accounted for half of the yield. This was seen in the ^{1}H NMR spectra at 6.71 ppm which was able to be removed by washing with 2M NaOH solution which became the preferred method for workup. From the initial synthesis using continuous flow the best synthesis parameters were found to be a F_2 flow rate of 25 mL min^{-1} (6.1 mmol h^{-1} F_2); collecting in water; with a substrate solvent mixture of 1:1 acetonitrile to dichloromethane; a flow rate ratio of 20:10 mL h^{-1} of acetonitrile/ water mix to substrate and then working the reaction up with 2 M sodium hydroxide. In contrast the catechol isomer substrate undergoes no apparent hydrolysis nor was any other by-products observed to form although higher flow rates of F_2 were required to push the reaction to completion. The best parameters found for the synthesis of catechol diglycidyl ether were found to be a fluorine flow rate of30 mL min^{-1} (7.3 mmol h^{-1} F_2) for the catechol, collecting the mixture in water, with the substrate dissolved in a mixture of 1:1 acetonitrile to dichloromethane. This mixtures were injected into the system at a flow rate ratio of 20:10 mL h^{-1} of acetonitrile/ water mix to substrate and then working the reaction up with 2 M sodium hydroxide.

Scaling up of the synthesis was also possible using the continuous flow set up, changing the syringe pumps for HPLC pumps to provide more continuous reactions. Once calibrated the HPLC pumps provided conversions that were comparable to previous reactions using syringe pumps. As described in section 3.5 there were different parameters researched to scale up the reactions with time and concentration being researched in this work. Due to the acid catalysed hydrolysis found in the hydroquinone derivative reaction, increasing the concentration of the HOF.MeCN and substrate had a detrimental effect on the synthesis of the desired product. Using concentrations of 4 and 8 mmol h^{-1} showed no evidence of product formed while reducing the concentration increased the crude yield but with a decrease in the conversion. Increasing the time of the reaction was shown to have no detrimental effect on either the conversion or the yield and was therefore shown to be a suitable means of scaling up the hydroquinone diglycidyl ether reaction. As

the catechol derivative does not undergo hydrolysis both increasing time and increasing concentration were shown to have positive effects on the amount of product produced without having a detrimental effect on the yield or conversion. This shows that both of the epoxides can be synthesised in usable amounts using HOF.MeCN over longer reaction periods with the limiting factors being the size of the storage cylinder and substrate containers. Purification of the monomers was readily performed using recrystallization and the analysis shows no evidence oligomers, starting materials or by-products.

Utilising different substrates and different samples of PACM which contain different ratios of isomers produce different films and different degrees of ease for removal. The results showed that the use of the predominantly trans-trans isomer containing Sigma Aldrich PACM produced good films that were however difficult to remove from a variety of substrates such as PTFE sprayed glass and PTFE taped glass. The best cross-linked polymer film that could be readily removed was shown produced using Air Products L-PACM which contains little or none of the trans-trans isomer that when applied using a draw down bar onto different substrates of PTFE sprayed glass and cleaned glass produced films that were readily removed. However for thicker samples that were required for analysis a draw down bar of 1mm did not produce suitable films. Therefore the best substrate was the PTFE moulds which good consistent films for each of the epoxides which could be moulded and were readily removed for analysis. Through variation in both polymerization time and temperature it was possible to optimize the conditions for all three isomers with RDGE being cured at 60°C and post curing at 140°C, HDGE was cured at 110°C due to the higher melting point of HDGE and post cured at 150°C and CDGE was cured at 60°C and post cured at 120°C. To produce a uniform cure system that could be used for each of the polymers, DSC analysis and TGA was performed to determine which temperatures would be appropriate. An isothermal cure of 100°C for 18 hours followed by 170°C isotherm (as determined from the TGA with none of the polymers degrading at this temperature) for 4 hours post-cure gave structurally stable polymer films which DSC appeared to indicate as being fully converted.

Structural analysis of the polymers showed that the expected polymerization amine nucleophilic addition reaction was followed, with limited homopolymerisation of epoxide rings present. The FTIR analysis shows that there are the peaks relating to the functional groups of the expected polymers with the appearance of the peaks relating to the OH stretch and the peaks relating to the amide linkages. There is also disappearance of the free epoxide peaks in all of the spectra which suggests that full conversion has occurred. ^{13}C solid state NMR spectroscopy shows the expected peaks as compared from the liquid state NMR spectra of the starting materials, however, as is discussed it is difficult to determine the end groups. Further analysis that could be undertaken could be XPS which would be able to give information into the difference between the amine and amide groups. DMTA analysis suggests that there is possibility of either contamination or cyclization within the catechol derivative with a hump on the tan δ peak. The cyclization mechanism could result from reaction of two epoxide moieties on the catechol diglycidyl ether with a single diamine. There is however no evidence of cyclization from spectral analysis, but it should be noted that the cyclization products peaks may reasonably be expected to be obscured by the main product peaks.

Analysis of the polymers using DMTA and DSC gave contradicting results with regards to the behaviour of the glass transition temperatures for the polymers. With DSC results the polymer with the highest T_g was HDGE (147°C) followed by RDGE (130°C) and CDGE having the lowest (105°C), however, with DMTA results the RDGE polymer has a higher T_g than that of the HDGE polymer while the CDGE polymer has the lowest again. This could be due to the different methods of the measurements as DSC is static and DMTA applies oscillatory deformation. Other data from the DMTA results gives information on the cross-link density and the molecular weight between cross-links. What is seen is that there is a higher cross-link density in the RDGE polymer followed by the HDGE and finally the CDGE which as discussed in the introduction is expected from the T_g results from the DMTA. The molecular weight between cross-links can be used to determine the average number of repeat units which shows that RDGE has 2.4 repeat units (a repeat unit containing one PACM and 2 RDGE molecules). The HDGE polymer has almost double the number of repeat units with 4.6 and the CDGE being higher still with 4.9. There

does not appear to be a relationship with the T_g results obtained by DSC and tan δ with the positron annihilation spectroscopy with the PALS data showing that the average hole volume is lower in the CDGE polymer compared to the HDGE polymer, with RDGE being lower still. There is however a large variation in the errors for the average hole volume which could be attributed to this results. For the results of the T_g from E' and E'' there could arguably be an almost linear relationship but again the error for the PALS limit the reliability of this interpretation. The same is seen when comparing the PALS data with the results for the cross-link density and the molecular weight between cross-links, however in this interpretation there is cross over with the error bars observed. The results obtained from methanol in the transport properties show that the RDGE polymer has the lowest sorption equilibrium, diffusion coefficient and permeability coefficient of all of the polymers. The HDGE polymer has slightly lower parameters than CDGE but both of the results are of the same magnitude. The results for water transport properties however show a different result with CDGE having the lowest diffusion and permeability coefficients as compared to the RDGE polymer with HDGE having the highest results. These results relate to the T_g obtained from tan δ with an increase in the methanol uptake against a lower glass transition temperature. This shows that the effect of the polymer structure has an effect on the polymer properties and therefore the chemical resistance as shown from the results obtained.

The results are consistent with the literature[31] as described in the introduction which suggested that the 1,3-isomer has higher barrier properties. This is shown in this work with the RDGE polymer demonstrating the best chemical resistance with the relative performance of HDGE and CDGE appear to be similar. However, the glass transition temperatures and coefficients of uptake, diffusion and permeability would suggest the CDGE methanol has the lowest chemical resistance. This shows that the 1,3-isomer has the highest chemical resistance the 1,4-isomer has the second and the 1,2-isomer has the worst chemical resistance.

7.2 – Future work

- Full scale up of the HOF.MeCN would be viable for epoxide synthesis. This could be performed using multichannel micro-reactors to produce HOF.MeCN. Alternatively a modular microreactor device such as that developed by Chambers *et al*[240]. could be used. This has been shown to support a continuous reaction via a 60 channel reactor (figure 7.1). This can be used to produce *circa* 300g per day.

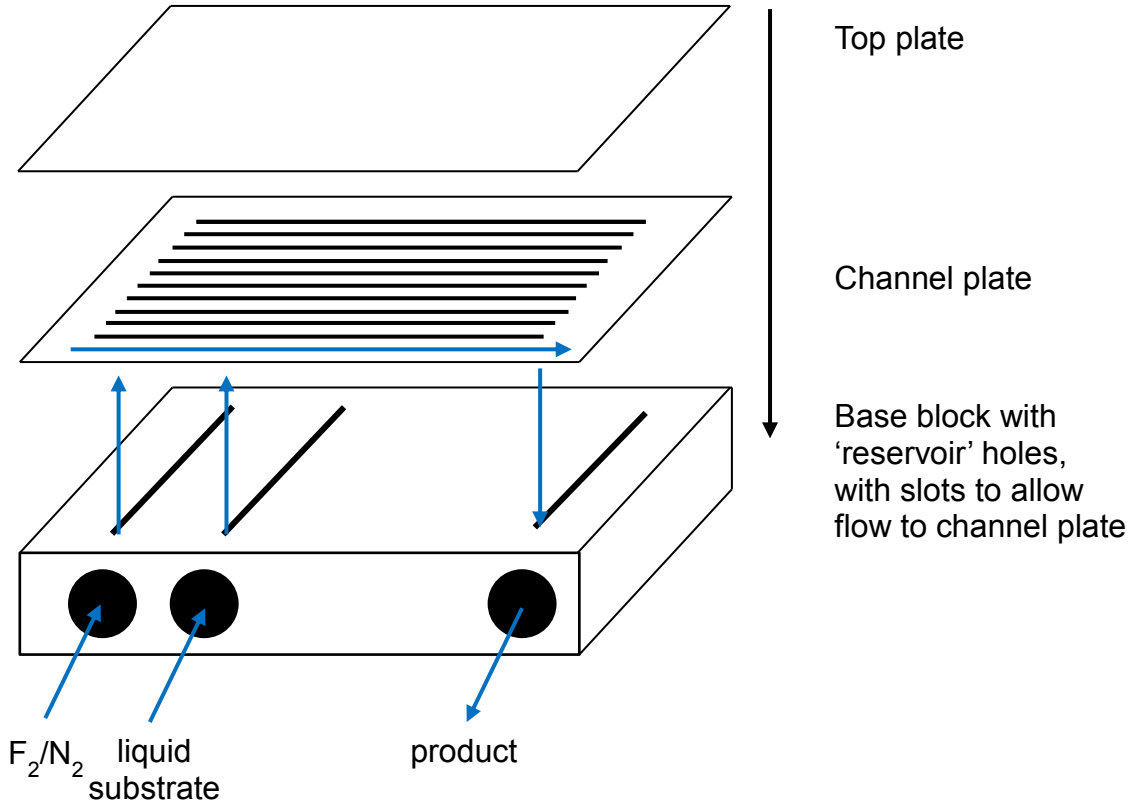

Figure 7.1 – Multi-channel reactor for the synthesis of HOF.MeCN as developed by Chambers *et al*.

- Research into other multi-functional epoxy monomers such as tri-functional and tert-functional aromatic glycidyl ethers as shown in figure 7.2. These would be able to increase the cross-links density within the polymers.

- Determining the transport properties of a different homologous series of solvents to determine the solvent interactions with the polymers.

- Using industrial curing methods and the incorporation ‘catalysts’, solvents and pigments to determine how the polymers would affect the chemical resistance in a ‘real’ world setting.

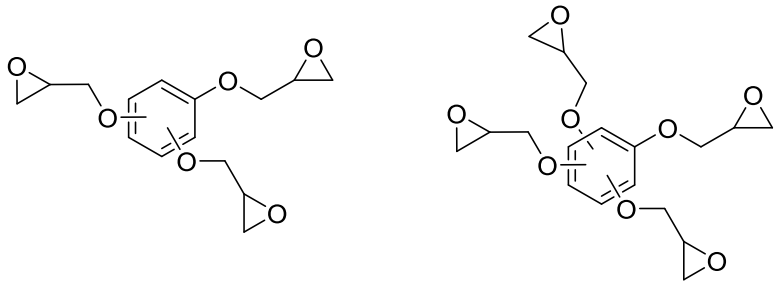

Figure 7.2 – tri and tert- functional glycidyl ethers.

Chapter 8 – References

1. R. A. McCarthy, *Vinyl plastics: a world view of the industry and market*, M. Dekker, New York, 1985.
2. A. Marrion, A. B. Port, C. Cameron, J. Warnon, P. A. Reynolds, W. A. E. Dunk, A. G. Guy and A. Milne, *The chemistry and physics of coatings*, Royal Society of Chemistry, Cambridge, 2nd edn, 2007.
3. D. o. S.-C. C. Rilem Technical Committee Tc 205-Dsc, G. De Schutter and K. Audenaert, *Durability of self-compacting concrete*, RILEM, Bagneux, France, 2007.
4. F. A. Pfaff and B. Moyer, NACE International, 2003.
5. T. D. Klingner and M. F. Boeniger, *Appl Occup Environ Hyg*, 2002, **17**, 360-367.
6. Y. Ikeda, K. Shudo and Y. Aoyagi, US20100138978 A1, 2010.
7. J. Skarelius, US4614208 A, 1986.
8. E. D. Sheets, D. Holowka and B. Baird, *J Cell Biol*, 1999, **145**, 877-887.
9. J. Y. Jia, S. Lamer, M. Schümann, M. R. Schmidt, E. Krause and V. Haucke, *Mol Cell Proteomics*, 2006, **5**, 2060-2071.
10. J. Baõos, R. Baõos and V. Baõos, US20120100360, 2012.
11. J. Escarsega, *Amptiac Quarterly*, 2004, **8**, 96-100.
12. K. Marsh and B. Bugusu, *J Food Sci*, 2007, **72**, R39-R55.
13. M. Chiodo, US5934495, 1997.
14. R. H. Evans, J. Niederst, R. M. O'brien, B. Prouvost, K. Romagnoli, G. Schutte, P. Stenson, K. Tom Van, WO2011130671A2, 2011.
15. J. Jang and H. Ishida, *Corrosion Science*, 1992, **33**, 1053-1066.
16. C. R. Hegedus, S. J. Spadafora, A. T. Eng, D. F. Pulley and D. J. Hirst, *Paint and Coating Testing Manual: Fifteenth Edition of the Gardner-Sward Handbook*, 2012, 739-750.
17. M. Li, K. D. Lokkesmoe, G. J. Wei, US6427826 B1, 2002.
18. T. Zhang and D. Tang, *Recent Pat. Corros. Sci.*, 2009, **1**, 1-5.
19. S. B. Harogoppad and T. M. Aminabhavi, *Macromolecules*, 1991, **24**, 2598-2605.
20. Y. Sato, T. Takikawa, A. Sorakubo, S. Takishima, H. Masuoka and M. Imaizumi, *Industrial & Engineering Chemistry Research*, 2000, **39**, 4813-4819.
21. S. C. George and S. Thomas, *Progress in Polymer Science*, 2001, **26**, 985-1017.
22. H. L. Frisch, *Journal of Applied Polymer Science*, 1970, **14**, 1657-1657.
23. *Journal of Membrane Science*, 1978, **3**, 97 - 115.
24. U. S. Aithal, T. M. Aminabhavi and S. S. Shukla, *Journal of Chemical & Engineering Data*, 1990, **35**, 298-303.
25. J. Crank, *The mathematics of diffusion*, 2nd edn., Clarendon Press, Oxford, 1975.
26. L. N. Britton, R. B. Ashman, T. M. Aminahhavi and P. E. Cassidy, *Journal of Chemical Education*, 1988, **65**, 368.
27. A. Eckelt, J. Eckelt and B. Wolf, in *Encyclopedia of Polymer Science and Technology*, John Wiley & Sons, Inc., 2002.
28. D. W. v. Krevelen and K. t. Nijenhuis, *Properties of polymers : their correlation with chemical structure, their numerical estimation and prediction from additive group contributions*, 4th edn., Elsevier Science, Oxford, 2009.
29. W. D. Callister, W. D. M. s. Callister and engineering, *Fundamentals of materials science and engineering: an interactive e.text*, 5th edn., Wiley, New York; Chichester, 2001.

30. V. R. Gowariker, N. V. Viswanathan and J. Sreedhar, *Polymer science*, Wiley, New York; Chichester, 1986.
31. C. L. Aitken, W. J. Koros and D. R. Paul, *Macromolecules*, 1992, **25**, 3424-3434.
32. X. Wang, P. Intveld, Y. Lu, B. Freeman and I. Sanchez, *Polymer*, 2005, **46**, 9155-9161.
33. A. Y. Alentev, I. A. Ronova, B. V. Shchukin and Y. P. Yampolskii, *Polymer Science Series A*, 2007, **49**, 217-226.
34. D. Pavel, R. Shanks, S. Sangari, S. Alazaroaie and N. Hurduc, *Macromolecular Theory and Simulations*, 2003, **12**, 127-141.
35. K. Tanaka, H. Kita, K. Okamoto, A. Nakamura and Y. Kusuki, *J Membrane Sci*, 1989, **47**, 203-215.
36. M. Salame, *Polym Eng Sci*, 1986, **26**, 1543-1546.
37. L. Cui, W. Qiu, D. R. Paul and W. J. Koros, *Polymer*, 2011, **52**, 5528-5537.
38. C. Nagel, K. Günther-Schade, D. Fritsch, T. Strunskus and F. Faupel, *Macromolecules*, 2002, **35**, 2071-2077.
39. M. R. Pixton and D. R. Paul, *Macromolecules*, 1995, **28**, 8277-8286.
40. I. A. Ronova, E. A. Sokolova and M. Bruma, *J Polym Sci Pol Phys*, 2008, **46**, 1868-1877.
41. A. Kausar, S. Zulfiqar, C. T. Yavuz and M. I. Sarwar, *Polym Degrad Stabil*, 2011, **96**, 1333-1341.
42. G. Tillet, B. Boutevin and B. Ameduri, *Prog Polym Sci*, 2011, **36**, 191-217.
43. M. J. McClure, S. A. Sell, C. P. Barnes, W. C. Bowen and G. L. Bowlin, *J Eng Fiber Fabr*, 2008, **3**, 1-10.
44. A. Dimopoulos, A. A. Skordos and I. K. Partridge, *J Appl Polym Sci*, 2012, **124**, 1899-1905.
45. B. X. Fu, M. Namani and A. Lee, *Polymer*, 2003, **44**, 7739-7747.
46. C. G. Robertson and X. R. Wang, *Macromolecules*, 2004, **37**, 4266-4270.
47. P. N. Patil, S. K. Rath, K. Sudarshan, D. Dutta, M. Patri and P. K. Pujari, *International Conference on Physics of Emerging Functional Materials (Pefm-2010)*, 2010, **1313**, 298-300.
48. A. Shefer and M. Gottlieb, *Macromolecules*, 1992, **25**, 4036-4042.
49. J. A. Brydson, *Plastics materials*, 7th edn., Butterworth-Heinemann, Boston, 1999.
50. H. W. Sung, D. M. Huang, W. H. Chang, R. N. Huang and J. C. Hsu, *J Biomed Mater Res*, 1999, **46**, 520-530.
51. Z. Rappoport, *The chemistry of peroxides*, John Wiley & Sons, Chichester, 2006.
52. S. H. Goodman, *Handbook of thermoset plastics*, 2nd ed. edn., Noyes Publications, Westwood, N.J., 1998.
53. H. H. Pham and M. A. Winnik, *Macromolecules*, 2006, **39**, 1425-1435.
54. J. W. Gooch, *Encyclopedic dictionary of polymers*, 2nd edn., Springer, New York; [London], 2011.
55. K. Sung, P.-M. Huang and C.-H. Zhou, *Journal of Fluorescence*, 2007, **17**, 492-499.
56. D. J. Kim, W. S. Kim, D. H. Lee, K. E. Min, L. S. Park, I. K. Kang, I. R. Jeon and K. H. Seo, *J Appl Polym Sci*, 2001, **81**, 1115-1124.
57. C. Y. Han, X. H. Ran, X. Su, K. Y. Zhang, N. N. Liu and L. S. Dong, *Polym Int*, 2007, **56**, 593-600.

58. I. Mironi-Harpaz, M. Narkis and A. Siegmann, *J Appl Polym Sci*, 2007, **105**, 885-892.
59. D. Klempner, V. Sendijarevi\02B9c and R. M. Aseeva, *Handbook of polymeric foams and foam technology*, 2nd edn. edited by Daniel Klempner and Vahid Sendijarevic, Hanser, Munich, 2004.
60. D. Bogdal, J. Pielichowski, P. Penczek, J. Gorczyk and G. Kowalski, *Polimery*, 2002, **47**, 842-844.
61. D. Braun, *Polymer synthesis : theory and practice: fundamentals, methods, experiments*, 4th edn., Springer, Berlin, 2005.
62. Z. W. Wicks, *Organic coatings: science and technology*, 3rd edn., Wiley-Interscience, Hoboken, N.J., 2007.
63. C. L. Liu, Q. G. Guo, J. L. Shi and L. Liu, *Mater Chem Phys*, 2005, **90**, 315-321.
64. T. A. Morley, R. Karunakaran, C. L. O'Connell, N. Shields, N. K. E. Verghese, M. F. Reimers, WO2013003202A1, 2013.
65. E. E. Cole, G. G. Eagle, S. Feng, R. D. Froese, M. R. Golden, G. L. Jialanella, Y-F. Liu, A. Lutz, M. Ming, WO2012006001A2, 2012.
66. J. Puig, C. E. Hoppe, L. A. Fasce, C. J. Perez, Y. Pineiro-Redondo, M. Banobre-Lopez, M. A. Lopez-Quintela, J. Rivas and R. J. J. Williams, *J Phys Chem C*, 2012, **116**, 13421-13428.
67. M. Morell, X. Fernández-Francos, X. Ramis and A. Serra, *Macromolecular Chemistry and Physics*, 2010, **211**, 1879-1889.
68. K. Makuuchi and S. Cheng, *Radiation processing of polymer materials and its industrial applications*, Wiley, Oxford, 2012.
69. D. W. Johnson, C. Sherborne, M. P. Didsbury, C. Pateman, N. R. Cameron and F. Claeyssens, *Adv Mater*, 2013.
70. S. D. Kimmins, P. Wyman and N. R. Cameron, *React. Funct. Polym.*, 2012, **72**, 947-954.
71. S. Kanehashi, T. Nagasawa, M. Kobayashi, S. L. Lee, M. Nakamura, S. Sato, M. F. Beristain, T. Ogawa, T. Miyakoshi and K. Nagai, *J. Appl. Polym. Sci.*, Ahead of Print.
72. R. Parthasarathy, A. Misra, J. Park, Q. Ye and P. Spencer, *J Mater Sci-Mater M*, 2012, **23**, 1157-1172.
73. D. L. Safranski and K. Gall, *Polymer*, 2008, **49**, 4446-4455.
74. J. V. Koleske, *Paint and coating testing manual: fourteenth edition of the Gardner-Sward handbook*, 14th edn., ASTM, Philadelphia, Pa., 1995.
75. D. Stoye, W. Freitag and G. n. Beuschel, *Resins for coatings : chemistry, properties, and applications*, Hanser, Munich, 1996.
76. S. Desai, I. M. Thakore and S. Devi, *Polym Int*, 1998, **47**, 172-178.
77. D. Santiago, X. Fernández-Francos, X. Ramis, J. M. Salla and M. Sangermano, *Thermochim Acta*, 2011, **526**, 9-21.
78. J. S. Nakka, K. M. B. Jansen and L. J. Ernst, *J Polym Res*, 2011, **18**, 1879-1888.
79. U. Gedde, *Polymer physics*, Chapman & Hall, 1995.
80. M. S. M. Alger, *Polymer science dictionary*, Chapman & Hall, London, 1997.
81. J. Comyn, *Polymer permeability*, Chapman & Hall, London, 1985.
82. A. J. Hill, S. Weinhold, G. M. Stack and M. R. Tant, *Eur Polym J*, 1996, **32**, 843-849.
83. M. Jackson, M. Kaushik, S. Nazarenko, S. Ward, R. Maskell and J. Wiggins, *Polymer*, 2011, **52**, 4528-4535.

84. Y. J. Fu, C. C. Hu, K. R. Lee, H. A. Tsai, R. C. Ruaan and J. Y. Lai, *Eur Polym J*, 2007, **43**, 959-967.
85. F. l. e. Mantia, *Handbook of plastics recycling*, Rapra Technology, Shrewsbury, 2002.
86. J. K. Fink, *High performance polymers*, William Andrew; Oxford: Elsevier Science [distributor], Norwich, N.Y., 2008.
87. M.-H. Kim, J. Lee, M.-S. Cho and H.-G. Woo, in *Advanced Functional Materials*, Springer Berlin Heidelberg, 2011, pp. 65-101.
88. V. Mittal, in *High Performance Polymers and Engineering Plastics*, John Wiley & Sons, Inc., 2011
89. Z. K. Xu, M. Bohning, J. Springer, F. P. Glatz and R. Mulhaupt, *Journal of Polymer Science Part B-Polymer Physics*, 1997, **35**, 1855-1868.
90. S. Miyata, S. Sato, K. Nagai, T. Nakagawa and K. Kudo, *J Appl Polym Sci*, 2008, **107**, 3933-3944.
91. X. Y. Wang, R. D. Raharjo, H. J. Lee, Y. Lu, B. D. Freeman and I. C. Sanchez, *J Phys Chem B*, 2006, **110**, 12666-12672.
92. H. Y. Jeon, S. H. Cho, M. S. Mok, Y. M. Park and J. W. Jang, *Polymer Testing*, 2005, **24**, 339-345.
93. J. F. Dezern and C. I. Croall, *Advances in Polyimide Science and Technology, Proc. 4th Int'l. Con*, 1993.
94. Z. Y. Wang and C. Zhang, *Macromolecules*, 1992, **25**, 5851-5854.
95. J. W. Martin, *Concise encyclopedia of the structure of materials*, Elsevier, Oxford, 2007.
96. C. D. Craver and C. E. Carraher, Jr., *Applied polymer science: 21st century*, Elsevier, Amsterdam; London, 2000.
97. T. Imae, *Current Opinion in Colloid & Interface Science*, 2003, **8**, 307-314.
98. R. D. van de Grampel, W. Ming, A. Gildenpfennig, W. J. van Gennip, J. Laven, J. W. Niemantsverdriet, H. H. Brongersma, G. de With and R. van der Linde, *Langmuir*, 2004, **20**, 6344-6351.
99. M. Sadat-Shojai and A. Ershad-Langroudi, *J Appl Polym Sci*, 2009, **112**, 2535-2551.
100. S. Park, J. W. Lee and B. N. Popov, *Int J Hydrogen Energ*, 2012, **37**, 5850-5865.
101. M. Miyamoto, K. Aoi and T. Saegusa, *Macromolecules*, 1989, **22**, 3540-3543.
102. D. K. Kim, S. B. Lee, K. S. Doh and Y. W. Nam, *J Appl Polym Sci*, 1999, **74**, 1917-1926.
103. Q. H. Yang, T. Y. Zhang and Z. J. Li, *J Soc Leath Tech Ch*, 2010, **94**, 106-110.
104. J. K. Seydel and M. D. Wiese, *Drug-membrane interactions: analysis, drug distribution, modeling*, Wiley-VCH, Weinheim ; [Great Britain], 2002.
105. S. Gaboury, K. A. Wood, M. Zheng, WO2006078425A2, 2006
106. M. Uyanik, E. Arpac, H. Schmidt, M. Akarsu, F. Sayilkan and H. Sayilkan, *J Appl Polym Sci*, 2006, **100**, 2386-2392.
107. A. P. Kharitonov and L. N. Kharitonova, *Pure Appl Chem*, 2009, **81**, 451-471.
108. G. Buxbaum, *Industrial inorganic pigments*, 2nd edn., Wiley-VCH, Weinheim; Chichester, 1998.
109. L. Edwards and J. Lawless, *The natural paint book: [a complete guide to natural paints, recipes, and finishes]*, 1st American edn., Rodale, Emmaus, Pa.; Great Britain, 2002.

110. H. S. Katz and J. V. Milewski, *Handbook of fillers for plastics*, Van Nostrand Reinhold, 1987.
111. S. C. Jana and S. Jain, *Polymer*, 2001, **42**, 6897-6905.
112. C. M. Sahagun and S. E. Morgan, *ACS Appl Mater Interfaces*, 2012, **4**, 564-572.
113. A. Kalendova and J. Snuparek, *Macromol Symp*, 2002, **187**, 97-107.
114. A, Hayashi, T. Iimura, WO2012091178A1, 2012
115. G. O. Brown, X. Meng, WO2011150147A1, 2011.
116. S. Pilotek, D. Burgard, M. Herold and K. Steingrover, *Nanotech Conference & Expo 2009, Vol 3, Technical Proceedings*, 2009, 244-247.
117. J. A. Orlicki, US20130018144A1, 2013.
118. S. Simone, A. Figoli, S. Santoro, F. Galiano, S. M. Alfadul, O. A. Al-Harbi and E. Drioli, *Sep Purif Technol*, 2012, **90**, 147-161.
119. D. D. L. Chung, *Composite materials : science and applications*, 2nd ed. edn., Springer, New York ; London, 2010.
120. A. K. Kulshreshtha and C. Vasile, *Handbook of polymer blends and composites*, Rapra Technology Ltd., Shrewsbury, 2002.
121. A. A. Moslemi, *Adv Perform Mater*, 1999, **6**, 161-179.
122. T. Hanemann and D. V. Szabo, *Materials*, 2010, **3**, 3468-3517.
123. H. Patel and V. Shah, *Polymer-Plastics Technology and Engineering*, 1995, **34**, 511-516.
124. S. N. Monteiro, V. Calado, R. J. S. Rodriguez and F. M. Margem, *Materials Science and Engineering: A*, 2012, **557**, 17-28.
125. K. Momose, S. Takayama, E. Hata and Y. Tomita, *Opt Lett*, 2012, **37**, 2250-2252.
126. T. K. Pavlushkina and O. A. Gladushko, *Glass Ceram+*, 2000, **57**, 310-313.
127. K. M. Nam, Y. J. Lee, S. R. Kim, W. T. Kwon, H. Kim and Y. Kim, *Mater. Sci. Forum*, 2012, **724**, 107-110.
128. M. Helou, G. Moriceau, Z. W. Huang, S. Cammas-Marion and S. M. Guillaume, *Polymer Chemistry*, 2011, **2**, 840-850.
129. K. Raghu, P. N. Khanam and S. V. Naidu, *J. Reinf. Plast. Compos.*, 2010, **29**, 343-345.
130. B. R. Guduri, A. V. Rajulu and A. S. Luyt, *J Appl Polym Sci*, 2007, **106**, 3945-3951.
131. J. K. Fink, *Reactive Polymers Fundamentals and Applications: A Concise Guide to Industrial Polymers*, William Andrew Publishing, 2005.
132. S. Schliemann and P. Elsner, *Skin protection: practical applications in the occupational setting*, Karger, Basel; New York, 2007.
133. J. S. Amstock, *Handbook of adhesives and sealants in construction*, McGraw-Hill, New York; London, 2001.
134. I. Hamerton, *Recent developments in epoxy resins*, Rapra Technology Limited, 1996.
135. E. C. Dearborn, R. M. Fuoss, A. K. Mackenzie and R. G. Shepherd, *Ind Eng Chem*, 1953, **45**, 2715-2721.
136. R. A. Veselovskii and V. N. Kestel, *Adhesion of polymers*, McGraw-Hill, New York; London, 2002.
137. Z. G. Liu, G. Zhang, Z. Liu, H. C. Sun, C. J. Zhao, S. Wang, G. B. Li and H. Na, *Polym Degrad Stabil*, 2012, **97**, 691-697.
138. D. Cattell, *Rapra Rev. Rep.*, 1990, **4**, 1-105.

139. J. J. Wang, J. Gong, Z. L. Gong, X. L. Yan, B. Wang, Q. L. Wu and S. J. Li, *Nucl Instrum Meth B*, 2010, **268**, 2355-2361.
140. H. M. Wang, Y. C. Zhang, L. R. Zhu, Z. J. Du, B. L. Zhang and Y. Y. Zhang, *Thermochim Acta*, 2011, **521**, 18-25.
141. R. K. Bregg, *Frontal polymer research*, Nova Science Publishers, New York, 2006.
142. K. Strzelec, N. Bączek, S. Ostrowska, K. Wąsikowska, M. I. Szynkowska and J. Grams, *Comptes Rendus Chimie*, 2012, **15**, 1065-1071.
143. D. Feldman and A. Barbalata, *Synthetic polymers: technology, properties, applications*, Chapman & Hall, London, 1996.
144. J. M. Espana, L. Sanchez-Nacher, T. Boronat, V. Fombuena and R. Balart, *J. Am. Oil Chem. Soc.*, 2012, **89**, 2067-2075.
145. E. M. Petrie, *Epoxy adhesive formulations*, McGraw-Hill Professional; London: McGraw-Hill [distributor], New York, 2006.
146. R. E. R. Williams, EP1980542A2, 2008
147. S. Sato, R. C. Bueno, A. A. Shigueru, A. Ferreira, EP2123689A1, 2009..
148. J.-P. Pascault and R. J. J. Williams, *Epoxy polymers : new materials and innovations*, Wiley-VCH, Weinheim, 2010.
149. N. Sbirrazzuoli, A. Mititelu-Mija, L. Vincent and C. Alzina, *Thermochim Acta*, 2006, **447**, 167-177.
150. K. C. Cole, *Macromolecules*, 1991, **24**, 3093-3097.
151. K. C. Cole, J. J. Hechler and D. Noel, *Macromolecules*, 1991, **24**, 3098-3110.
152. B. A. Rozenberg, *Advances in Polymer Science*, 1986, **75**, 113-165.
153. E. Raidma, *Oil Shale*, 1995, **12**, 259-269.
154. A. Wegmann, *Progress in Organic Coatings*, 1997, **32**, 231-239.
155. E. V. Shinkareva and V. D. Koshevar, *Russ J Appl Chem+*, 2011, **84**, 479-485.
156. C.-F. Dai, C.-J. Weng, P.-R. Li and J.-M. Yeh, *Polym Degrad Stabil*, 2010, **95**, 600-609.
157. R. G. Neville, J. W. Mahoney and K. R. Mcdowall, *J Appl Polym Sci*, 1968, **12**, 607-&.
158. J. E. White, H. C. Silvis, M. N. Mang, S. L. Kram, R. E. Hefner, US5686551A, 1997.
159. D. J. Brennan, H. C. Silvis, J. E. White and C. N. Brown, *Macromolecules*, 1995, **28**, 6694-6696.
160. P. Castan, Google Patents, Editon edn., 1948.
161. H. C. Kolb and B. K. Sharpless, *Tetrahedron*, 1992, **48**, 10515 - 10530.
162. F. E. Bentley and W. J. Peppel, US3268561, 1966.
163. Z. Wang, in *Comprehensive Organic Name Reactions and Reagents*, John Wiley & Sons, Inc., Editon edn., 2010.
164. I. Sakurada, S. Yamasaki, R. Göttlich, T. Iida, M. Kanai and M. Shibasaki, *Journal of the American Chemical Society*, 2000, **122**, 1245-1246.
165. R. H. V. Nishimura, F. T. Toledo, J. L. C. Lopes and G. C. Clososki, *Tetrahedron Letters*, 2013, **54**, 287 - 290.
166. E. Santacesaria, R. Vitiello, R. Tesser, V. Russo, R. Turco and M. Di Serio, *Industrial & Engineering Chemistry Research*, 2013.
167. M. Wengert, A. M. Sanseverino and M. C. S. de Mattos, *Journal of the Brazilian Chemical Society*, 2002, **13**.
168. R. D. Bach, C. Canepa, J. E. Winter and P. E. Blanchette, *The Journal of Organic Chemistry*, 1997, **62**, 5191-5197.

169. A. H. Hoveyda, D. A. Evans and G. C. Fu, *Chemical Reviews*, 1993, **93**, 1307-1370.
170. H. Moissan, *Compt. rend.*, 1886, **103**, 202-205, and 256-208.
171. R. E. Krebs, *The history and use of our earth's chemical elements: a reference guide*, 2nd ed. edn., Greenwood, Westport, Conn.; London, 2006.
172. R. E. Banks, B. E. Smart and J. C. Tatlow, *Organofluorine chemistry: principles and commercial applications*, Plenum, New York; London, 1994.
173. J. Fried and E. F. Sabo, *J Am Chem Soc*, 1954, **76**, 1455-1456.
174. I. Ojima, *Fluorine in medicinal chemistry and chemical biology*, Wiley-Blackwell, Oxford, 2009.
175. M. M. Boudakian, *J Fluorine Chem*, 1981, **18**, 497-506.
176. G. A. Olah and S. J. Kuhn, *J Org Chem*, 1961, **26**, 237-&.
177. J. Mizukado, Y. Matsukawa, H. D. Quan, M. Tamura and A. Sekiya, *J Fluorine Chem*, 2006, **127**, 79-84.
178. S. Rozen and M. Brand, *Angewandte Chemie International Edition in English*, 1986, **25**, 554-555.
179. S. Rozen, Y. Bareket and M. Kol, *Tetrahedron*, 1993, **49**, 8169-8178.
180. S. Rozen, *European Journal of Organic Chemistry*, 2005, **2005**, 2433-2447.
181. S. Rozen, *Pure and Applied Chemistry*, 1999, **71**, 481–487.
182. S. Rozen and M. Kol, *The Journal of Organic Chemistry*, 1990, **55**, 5155-5159.
183. E. Golan, A. Hagooly and S. Rozen, *Tetrahedron Letters*, 2004, **45**, 3397-3399.
184. S. Rozen, Y. Bareket and J. Blum, *Tetrahedron Letters*, 1997, **38**, 2333-2334.
185. E. M. Sanford, C. C. Lis and N. R. McPherson, *Journal of Chemical Education*, 2009, **86**, 1422-1423.
186. M. Hayashida, M. Ishizaki and H. Hara, *Chemical and Pharmaceutical Bulletin*, 2006, **54**, 1299-1303.
187. C. D. Hurd, H. Greengard and F. D. Pilgrim, *Journal of the American Chemical Society*, 1930, **52**, 1700-1706.
188. S. Ibrahimi, G. Sauvé and E. Essassi, *International Journal of Molecular Sciences*, 2003, **4**, 371-378.
189. D. Astruc, L. Djankovitch and J. R. Aranzaes, *Arkivoc*, 2006, 173-188.
190. J. Zukerman-Schpector, I. Caracelli, C. C. Carvalho, M. L. de Faria, F. C. Silva, L. G. D. Matias and T. J. Brocksom, *Journal of the Brazilian Chemical Society*, 2001, **12**, 154-158.
191. R. B. Durairaj, *Resorcinol: chemistry, technology and applications*, Springer, Berlin; London, 2005.
192. J. A. van Rijn, M. Lutz, L. S. von Chrzanowski, A. L. Spek, E. Bouwman and E. Drent, *Advanced Synthesis & Catalysis*, 2009, **351**, 1637-1647.
193. J. D. Moseley, *Chimica Oggi-Chemistry Today*, 2009, **27**, 6-10.
194. E. Kolvari, A. Ghorbani-Choghamarani, P. Salehi, F. Shirini and M. A. Zolfigol, *Journal of the Iranian Chemical Society*, 2007, **4**, 126-174.
195. B. V. Silva, P. M. Esteves and A. C. Pinto, *Journal of the Brazilian Chemical Society*, 2011, **22**, 257-263.
196. C. B. McPake, C. B. Murray and G. Sandford, *Tetrahedron Letters*, 2009, **50**, 1674-1676.
197. A. Eisenberg, *Physical properties of polymers*, 1984.

198. L. National Research Council Committee on Acute Exposure Guideline, in *Acute Exposure Guideline Levels for Selected Airborne Chemicals: Volume 8*, National Academies Press (US)., Washington (DC), 2010. 214
199. J. Schmedt auf der Günne, M. Mangstl and F. Kraus, *Angewandte Chemie International Edition*, 2012, **51**, 7847-7849.
200. C. B. McPake, *New Continuous Flow Oxidation Methodology.* Doctoral thesis, Durham University, 2011.
201. E. H. Appelman, *Accounts of Chemical Research*, 1973, **6**, 113-117.
202. E. H. Appelman and A. W. Jache, *Journal of the American Chemical Society*, 1987, **109**, 1754-1757.
203. D. A. Johnson, *Some thermodynamic aspects of inorganic chemistry*, 2nd edn., CUP, 1982.
204. S. Elliott, *Atmospheric Environment (1967)*, 1983, **17**, 759-761.
205. M. Srnec, M. Ončák and R. Zahradník, *The Journal of Physical Chemistry A*, 2008, **112**, 3631-3637.
206. R. D. Chambers, D. Holling, R. C. H. Spink and G. Sandford, *Lab on a Chip*, 2001, **1**, 132-137.
207. R. D. Chambers, D. Holling, A. J. Rees and G. Sandford, *Journal of Fluorine Chemistry*, 2003, **119**, 81-82.
208. C. B. McPake, C. B. Murray and G. Sandford, *Chimica Oggi-Chemistry Today*, 2010, **28**, 6-7.
209. C. J. Brinker, *Journal of Non-Crystalline Solids*, 1988, **100**, 31-50.
210. S. Garea, A. Corbu, C. Deleanu and H. Iovu, *Polymer Testing*, 2006, **25**, 107-113.
211. F. G. Garcia and B. G. Soares, *Polymer Testing*, 2003, **22**, 51-56.
212. T. Oshima, H. Asahara, T. Koizumi and S. Miyamoto, *Chemical Communications*, 2008, 1804-1806.
213. E. Marand, K. R. Baker and J. D. Graybeal, *Macromolecules*, 1992, **25**, 2243-2252.
214. F. R. Prince and E. M. Pearce, *Macromolecules*, 1971, **4**, 347-&.
215. A. E. Barkdoll, H. W. Gray, W. Kirk, D. C. Pease and R. S. Schreiber, *J Am Chem Soc*, 1953, **75**, 1238-1239.
216. A. E. Barkdoll, H. W. Gray and W. Kirk, *J Am Chem Soc*, 1951, **73**, 741-746.
217. H. van Brederode, Delft University of Technology, 1971.
218. E. G. G. Werner and E. Farenhorst, *Recl. Trav. Chim. Pays-Bas Belg.*, 1948, **67**, 438-441.
219. M. Lappalainen and M. Karppinen, *J Therm Anal Calorim*, 2010, **102**, 171-180.
220. G. M. Odegard and A. Bandyopadhyay, *J Polym Sci Pol Phys*, 2011, **49**, 1695-1716.
221. S. Z. D. Cheng, M. Y. Cao and B. Wunderlich, *Macromolecules*, 1986, **19**, 1868-1876.
222. H. J. Chung, K. S. Woo and S. T. Lim, *Carbohyd Polym*, 2004, **55**, 9-15.
223. K. Dušek, M. Bleha and S. Luňák, *J. Polym. Sci. Polym. Chem. Ed.*, 2003, **15**, 2393-2400.
224. G. a. G. J. K. Wisanrakkit, *Journal of Applied Polymer Science*, 1990, **41**, 2885--2929.
225. H. Lobo and J. V. Bonilla, *Handbook of plastics analysis*, Marcel Dekker, New York, N.Y., 2003.
226. L. W. Hill, *Progress in Organic Coatings*, 1997, **31**, 235-243.

227. J. P. Bell, *Journal of Applied Polymer Science*, 1970, **14**, 1901-1906.
228. S. Montserrat, *Polymer*, 1995, **36**, 435-436.
229. G. Levita, S. De Petris, A. Marchetti and A. Lazzeri, *Journal of Materials Science*, 1991, **26**, 2348-2352.
230. P. K. Gallagher, M. E. Brown and R. B. Kemp, *Handbook of thermal analysis and calorimetry*, Amsterdam; Oxford: Elsevier, 1998.
231. L. Matějka, P. Špaček and K. Dušek, *Polymer*, 1991, **32**, 3190-3194.
232. A. Seide. *Properties and behavior of polymers*, Wiley; [Chichester]: John Wiley [distributor], Hoboken, N.J., 2011.
233. A. E. Dupasquier and A. P. E. Mills, *Positron spectroscopy of solids: Course: Papers*, Ohmsha, IOS, 1995.
234. D. W. Gidley, H.-G. Peng and R. S. Vallery, *Annual Review of Materials Research*, 2006, **36**, 49-79.
235. F. Franks, *Water : a matrix of life*, 2nd edn., Royal Society of Chemistry, Cambridge, 2000.
236. Y. H. Zhao, M. H. Abraham and A. M. Zissimos, *The Journal of Organic Chemistry*, 2003, **68**, 7368-7373.
237. J. T. Edward and P. G. Farrell, *Canadian Journal of Chemistry*, 1975, **53**, 2965-2970.
238. T. M. Aminabhavi and H. G. Naik, *Journal of Hazardous Materials*, 1998, **60**, 175-203.
239. J. G. Dorsey, G. F. Dorsey, A. C. Rutenberg and L. A. Green, *Analytical Chemistry*, 1977, **49**, 1144-1145.
240. R. D. Chambers, M. A. Fox, D. Holling, T. Nakano, T. Okazoe and G. Sandford, *Lab on a Chip*, 2005, **5**, 191-198.